Statistical thermodynamics of charge-stabilized colloids

Statistical thermodynamics of charge-stabilized colloids
Aldemar Torres Valderrama
Ph. D. Thesis Utrecht University, June 2008
ISBN:978-90-6464-235-7

Statistical thermodynamics of charge-stabilized colloids

Statistische thermodynamica van geladen colloiden

(met een samenvatting in het Nederlands)

Proefschrift

ter verkrijging van de graad van doctor aan de Universiteit Utrecht op gezag van de rector magnificus, prof.dr. J.C. Stoof, in gevolge het besluit van het college voor promoties in het openbaar te verdedigen op maandag 9 juni 2008 des middags te 2.30 uur

door

Aldemar Torres Valderrama

geboren op 27 oktober 1977 te Málaga, Colombia.

Promotor: prof.dr. H. van Beijeren
Co-promotor: dr. R. van Roij

The work presented in this thesis is part of the research programme of the Foundation for Fundamental Research on Matter (FOM), which is financially supported by the Dutch Organization for the Advancement of Research (NWO).

– A man is only good as his tools –
Paul Gilbert's grandfather *

*Space ship one, *Shrapnel*, June 7, (2005).

– Physics is a sharp tool with strong handle –
A.T.

Samenvatting

Dit proefschrift richt zich op het deelgebied van de Statistische Mechanica dat zich bezig houdt met de bestudering van zogenaamde Coulomb Systemen (CS). Dit betreft systemen met electrische ladingen zodat de krachten tussen (sub)microscopische deeltjes een gevolg van de wet van Coulomb zijn. Bekende voorbeelden zijn plasma's, elektrolyten en colloïdale suspensies. Hoewel quantum-mechanica eigenlijk essentieel is om de stabiliteit van CS te kunnen begrijpen, kunnen CS vaak ook in goede benadering bestudeerd worden binnen de Klassieke Statistische Mechanica (KSM), waaruit de thermodynamische eigenschapen van CS te bestuderen zijn.

Het specifieke geval in dit proefschrift betreft suspensies van geladen colloïden. Dit zijn asymmetrische mengsels bestaande uit een moleculair oplosmiddel (vaak met cationen en anionen) waarin mesoscopische colloïdale deeltjes gesuspendeerd zijn. Vaak is het oppervlak van de colloïden zodanig dat een chemische reactie optreedt waarbij positief geladen ionen (de zgn. tegen-ionen) zich los maken van het oppervlak en daarbij een negatieve oppervlaktelading achterlaten. De interacties tussen de colloïden worden dus bepaald door deze oppervlaktelading in combinatie met de eigenschappen van het oplosmiddel en de daarin opgeloste tegenionen, cationen, en anionen, die alle met elkaar wisselwerken alsmede met het geladen oppervlak. Dit soort asymmetrische CS zijn van belang in veel wetenschapsgebieden binnen en buiten de fysica, o.a. de fysische chemie, de moleculaire biologie, en de biofysica.

De inhoud van dit proefschrift kan in drie stukken verdeel worden. Deel I, bestaande uit de hoofdstukken 3 en 4, behandelt parallelle membranen en colloïdale plaatjes. Een membraan of vlies is een dunne, vlakke structuur die twee ruimtes van elkaar scheidt. Zo vormen biologische membranen bijvoorbeeld een belangrijke basis van het leven, en worden cellen omgeven door een celmembraan om ze bij elkaar te houden en af te scheiden van de buitenwereld. Ook de organellen binnen een cel worden door membranen bij elkaar gehouden en van elkaar gescheiden. Membranen zijn vaak geladen en ze zijn in contact met elektrolyten. In hoofdstuk 3 bestuderen we de krachten tussen twee zwak geladen membranen in een zoutoplossing met behulp van lineaire screening theorie, waarbij we ons met name richten op het effect van de eindige dikte van de twee membranen. In hoofdstuk 4 bestuderen we sterk geladen membranen, waarvoor niet-lineaire elektrostatische verschijnselen moeten worden geïncorporeerd in de theorie. Deze modellen kunnen ook gebruikt worden om colloïdale plaatjes te bestuderen.

In deel II, te weten hoofdstukken 5 en 6, bestuderen we binaire mengsels van colloïden. In hoofdstuk 5 ontwikkelen we een model voor de theoretische beschrijving van ladingsrenormalisatie. Dit betreft een generalisatie van het zogenaamde cel model. Met dit model kunnen we de thermodynamische eigenschappen van colloïdale mengels berekenen, niet alleen voor laaggeladen maar ook voor hooggeladen colloïden waarvoor niet-lineaire screening op een efficiënte manier in rekening is gebracht. In hoofdstuk 6 bestuderen we effectieve elektrostatische interacties in een mengsel van verschillende type colloïden. We richten ons op lage zoutconcentraties, waar de zoutionwolken rondom de colloïdale deeltjes zo uitgestrekt zijn dat ze de de wolken van naburige deeltjes sterk gaan overlappen. We laten zien dat deze situatie niet beschreven kan worden met de traditionele DLVO theorie, en we presenteren een theorie voor de effectieve potentiaal tussen de colloïden die dit regime wel kan beschrijven.

In deel III, gevormd door de hoofdstukken 7 en 8, bestuderen we geladen colloïden in het externe aardse gravitatieveld. In hoofdstuk 7 laten we zien dat de aanwezigheid van zwaartekracht leidt tot een macroscopische ladingsscheiding van colloïden en de ionen, mits de concentratie van toegevoegd zout laag genoeg is. Dit mechanisme is het gevolg van een complex evenwicht van entropie van de colloïden en de ionen, de potentiële energie, en de elektrostatische energie. Hierdoor worden de colloïden opgetild tot veel grotere hoogte dan hun gravitatielengte en neemt men sedimentatieprofielen waar die sterk niet-barometrisch zijn. Door middel van de Ornstein-Zernike vergelijking met de zg. MSA-benadering berekenen we zulke sedimentatieprofielen voor een één-componentssysteem van colloïden die met paarsgewijze DLVO-potentiaal wisselwerken. Onze resultaten komen, voor experimenteel relevante zoutconcentraties, kwantitatief overeen met resultaten van simulaties van het het zgn. primitieve model, waarin zowel de colloïden als de cationen en de anionen expliciet worden meegenomen. In hoofdstuk 8 bestuderen we sedimentatie van binaire mengsels van geladen colloïden m.b.v. de theorie die in hoofdstuk 5 werd ontwikkeld. We vinden, voor zoutloze systemen, kwantitatieve overeenkomst met resultaten van simulaties van het primitieve model.

Acknowledgements

It is a pleasure to acknowledge the collaboration with my promotor Prof.dr. Henk van Beijeren and my co-promotor Dr. René van Roij, who contributed immensely to each part of this thesis with his profound physical insight and knowhow. Prof van Beijeren greatly contributed to the preparation of the manuscript, by critically reviewing each section and providing very useful feedback. Apart for his permanent assistance regarding the technical details of this work, Dr. van Roij also facilitated the cooperation with other scientific groups which turned out to be extremely fruitful. Other scientists contributed directly to the research presented in this thesis. I would like to thank to Dr. Gabriel Téllez Acosta, who, during his visits to the Institute for Theoretical Physics in 2005 and 2006, contributed enormously to the algorithms on which chapters 3 and 4 are sustained. I also want to express my gratitude to Prof.dr Marjolein Dijkstra and Dr. Alejandro Cuetos who performed extensive Monte Carlo simulations that allowed to test the theoretical models presented in part III. I own my gratitude to many other people who contributed less directly but importantly to this work. I would like to specially thank Prof.dr. Jan Dhont and Dr.ing. Ger Koper for useful discussions during the Han-sur-Lesse winter school on Physical Chemistry.

My scientific career has been greatly enriched through my interaction with the academic staff of the Institute for Theoretical Physics during the last years. I want to express my gratitude to all the staff of the ITF in particular to Prof.dr. Henk van Beijeren, Prof.dr. Henk Stoof and Prof.dr. Renate Loll, for their inspiring lectures on Non-equilibrium Statistical Mechanics, Statistical Field Theory and General Relativity respectively. I also want to thank Prof.dr. Gerard Barkema for making possible my participation in the prestigious 11^{th} international summer school Fundamental Problems in Statistical Physics, which greatly enhanced my understanding and interest in this field. I want to specially acknowledge the extremely valuable help in all kind of practical matters I received from the manager and secretaries of the ITF, Biene Meijerman, Geertje Speelman, Wilma van Egmond and from Maria Teuwissen (FOM bureau).

Aldemar Torres Valderrama
Zeist, March 2008

About the author

Aldemar Torres Valderrama was born in Málaga Santander, Colombia. He studied in the Colegio Nacional Custodio García Rovira, where he graduated with honors in 1994. He did his B.S. in Physics at the National University of Colombia and his M.S. in Physics at the Universidad de Los Andes, where he graduated cum laude in 2004. In September 2004 he travelled to The Netherlands to continue his studies at the Institute for Theoretical Physics in Utrecht. From August 2008 he will be working at the department of Neurosurgery of the Rudolf Magnus Institute of Neuroscience, where he will be developing statistical physics models for electro-corticography based brain-computer interfaces.

Foreword

This thesis is divided into three parts. Part I encompassing chapters 2 and 3, deals with finite-thickness effects in charged planar membranes and colloidal platelets. Part II, namely chapters 4 and 5, includes models for the study of charge-stabilized colloidal mixtures. In part III, comprising chapters 6 and 7, charge-stabilized colloidal dispersions in external fields are considered. An overview of the contents of each part is to be found at the end of the introduction. Chapters are self-contained. The reader is strongly advised to refer to the *corresponding* introductory sections (where all symbols used in a given chapter are defined) when studying material in a particular chapter.

Aldemar Torres Valderrama
Zeist, February 2008.

Publications related to this thesis

- Chapter 2:
  Finite-Thickness-Enhanced attractions in oppositely charged membranes and colloidal platelets.
  A. Torres and R. van Roij, *Langmuir* **24**, 1110 (2008).

- Chapter 3:
  Finite-Thickness and charge relaxation in double-layer interactions.
  A. Torres, R. van Roij and G. Téllez *J. Coll. Int. Sci.* **301**, 176 (2006).

- Chapter 4:
  The polydisperse cell model: non-linear screening and charge renormalization in colloidal mixtures.
  A. Torres, G. Téllez and R. van Roij *J. Chem. Phys.* **128**, 154906 (2008).

- Chapter 5:
  The role of ionic strength in the colloidal many-body problem, (in preparation).
  A. Torres, A. Cuetos, M. Dijkstra, R. van Roij

- Chapter 6:
  Sedimentation of charged colloids: the primitive model and the effective one-component approach.
  A. Torres, A. Cuetos, M. Dijkstra, R. van Roij, *Phys. Rev. E* **75**, 041405 (2007).

- Chapter 7:
  Breakdown of the Yukawa model in deionized colloidal suspensions.
  A. Torres, A. Cuetos, M. Dijkstra, R. van Roij, *Phys.Rev. E* **77**, 031402 (2008).

Other publications by the author

- General Considerations on the Finite-Size Corrections for Coulomb Systems in the Debye-Hückel Regime.
  A. Torres and G. Téllez, *J. Stat. Phys.* **118**, 735 (2005).

- Finite-Size Corrections for Coulomb Systems in the Debye-Hückel Regime,
  A. Torres and G. Téllez *J. Phys. A: Math. Gen.* **37**, 2121 (2004).

- Sine-Gordon field theory for the calculation of universal finite-size corrections in the free energy of Coulomb Systems in the Debye-Hückel regime.
  A. Torres, Master Thesis, Universidad de Los Andes, (2003).

- Propiedades universales de los sistemas de Coulomb: correcciones de talla finita para la energía libre en el régimen de Debye-Hückel.
  A. Torres and G. Téllez *Rev. Col. Fis.* **35:2**, 271 (2003).

- Mecánica estadística, topología y el sonido del tambor.
  A. Torres and G. Téllez *Revista HipOtesis, Facultad de Ciencias, Uniandes*, **3**, 18 (2004).

Contents

1

Introduction

In this introductory chapter we set the framework of this thesis. We stress the importance of electrostatic interactions in many-body systems, highlight the difficulty of a first-principles theoretical description, and the need for phenomenological theories. We introduce the different ranges of action of the Coulomb force and the phenomena of screening and electroneutrality as the most important features of electrostatic interactions in many-body systems. Charge-stabilized colloids are introduced as an example of many-body systems with electrostatic interactions and their soft and inhomogeneous character are discussed. Interfacial electrostatic phenomena are also treated. The objective here has not been to review the immense amount of literature on the subject, but to introduce the concepts required to understand the key references and the subsequent chapters of this thesis.

1.1 Fundamentals

Electrostatic interactions in many-body systems

In a many-body system of neutral particles, these move around freely without experiencing forces until a collision occurs. The latter are binary events in which short-range electrostatic forces operate only during the collision time. In a many-body system of charged particles on the other hand, the charged particles are subject to long-ranged Coulomb forces. As a consequence, the particles experience many "distant encounters" and exhibit more strongly collective behavior. Although the electrostatic force between two charged particles decays with the mutual distance ($\sim 1/r^2$), the combined effect of all charged particles may not even decay, since the interaction volume increases ($\sim r^3$). This is a typical collective effect exhibited by diverse systems in nature, e.g., plasmas, electrolytes and charge-stabilized colloids, which are known in general as Coulomb Systems (CS) [1, 2].

The collective behavior of CS is the result of the statistics of many charged particles, each moving in the field created by all the other particles. Charge-stabilized colloids, the type of systems studied in this thesis, are nothing but asymmetrical Coulomb Systems. The asymmetric character of colloids is twofold. The particles are asymmetric in size, i.e., some of the particles in the system are up to four orders of magnitude larger than others, those are known as colloidal particles. The other particles are sub-nanometer sized ions and solvent molecules. The second element of asymmetry refers to the charge, which is several orders of magnitude larger for the colloidal particles than for the ions. These elements, namely asymmetry in size, asymmetry in charge, and the collective behavior rendered by the Coulomb potential, shape the thermodynamic properties of colloidal systems. In addition, the second law of thermodynamics manifests itself through powerful entropic forces that often dominate the electrostatic ones. The combination of these effects is responsible for all phenomena in charge-stabilized colloids that do not involve chemical reactions* and is the leitmotif of this work.

Many-body systems of ionized atoms and/or (macro)-molecules can be studied by using the tools of Classical Electrodynamics as a result of the Hellmann-Feynman (HF) theorem [3]. The HF theorem states that once the spatial distribution of the charged particles (nuclei and electron clouds) has been determined by solving the Schrödinger equation, all the forces in the system can be calculated using *Classical* Electrostatics†. The HF theorem is valid within the Born-Oppenheimer (BO) approximation, in which the electrons can be regarded as particles that follow the nuclear motion adiabatically, meaning that they are "dragged" along with the nuclei without requiring a finite relaxation time. The nuclei, which can be several thousand times heavier than electrons, are spatially more localized than the electronic component of the wave function. The HF theorem states that in the BO approximation the forces on nuclei in molecules are those which would arise electrostatically if the electron probability density were treated as a static distribution of negative electric charge. The HF theorem allows to study statistical thermodynamics of charged molecules without concern for quantum electrodynamic effects, since in the classical limit, the nuclei are fully localized at single points representing classical point particles.

When neutral atoms come together to form a molecule covalent bonds are created. These bonds are characterized by electrons being shared between the atoms. The electron charge distributions change completely and merge, so that the discrete nature of atoms is lost. These bonds involve *short-range* electrostatic forces. They operate at distances of interatomic separations ($0.1 - 0.2$nm). Their strength depends on the type of other molecules nearby and is of the order of $100 - 300 k_B T$, where T is the temperature and k_B is the Boltzmann constant. Ionized atoms interact by long-range Coulomb forces and remain as separate entities. Their electron charge distribution during interaction is merely perturbed. Nevertheless, long-range Coulomb forces between pairs of ionized atoms can be as strong as covalent bonds, and even the weakest are strong enough to hold molecules together in solids and liquids at room temperature as well as to stabilize colloidal systems against flocculation. For instance, a straightforward calculation shows that the binding energy of two isolated ions, e.g. Na^+ and Cl^- in contact, i.e., at a separation distance equal to two ionic radii (0.27nm) is of the order of $200 k_B T$ per ion pair in vacuum. The Coulomb

*Remarkable exceptions are the electrochemical surface reactions which regulate colloidal charges discussed in chapter 2

†In the absence of magnetism.

energy falls below k_BT only at separation distances of the order of 56nm. These examples illustrate the fact that electrostatic forces can manifest themselves differently with respect to their strength, range and mode of action: short-range force fields arise around neutral atoms and molecules and rarely extend over more than one or two atomic distances. These short-range forces are traditionally studied in chemistry and biology. Long-range electrostatic forces operate between ionized atoms and/or (macro-)molecules and ultimately determine whether the latter are able to get close enough to interact by short-range electrostatic forces. These long-range forces are traditionally studied in physics, and in particular in this thesis.

Stability

Consistent statistical mechanical properties [‡] for a system of N particles with potential energy of the form $U_N(\mathbf{r}_1, ..., \mathbf{r}_N) = \sum_{i<j}^{N} v(\mathbf{r}_i - \mathbf{r}_j)$ can be obtained from a grand canonical description provided the pair interaction potential $v(\mathbf{r}_i - \mathbf{r}_j)$ satisfies the conditions:

$$\sum_{i<j}^{N} v(\mathbf{r}_i - \mathbf{r}_j) \geq -AN; \quad A \geq 0 \qquad \text{stability} \tag{1.1}$$

$$v(|\mathbf{r}_i - \mathbf{r}_j|) \leq B/|\mathbf{r}_i - \mathbf{r}_j|^{3+\epsilon}; \quad B \geq 0, \epsilon > 0, \; r \geq r_0 \quad \text{weak tempering} \tag{1.2}$$

where A, B, ϵ and r_0 are constants. The stability condition states that an extensive lower bound for the total potential energy should exist. The weak tempering condition demands that the potential cannot be too repulsive at long distances [1]. Short-ranged potentials with a repulsive core meet these conditions, however, both conditions are violated by the Coulomb potential

$$v_c(|\mathbf{r}_i - \mathbf{r}_j|) = \begin{cases} e^2 q_i q_j \ln(|\mathbf{r}_i - \mathbf{r}_j|/L)/\varepsilon & \text{for } d = 2 \\ e^2 q_i q_j |\mathbf{r}_i - \mathbf{r}_j|^{2-d}/\varepsilon(d-2) & \text{for } d \neq 2 \end{cases} \tag{1.3}$$

where eq_i are the charges, d is the spatial dimension, ε the dielectric constant of the medium in which the particles are immersed, and L is an arbitrary constant fixing the Gauge of the Coulomb potential in two dimensional systems. The stability problem can be traced back to the singularity of the Coulomb potential at short distances, and quantum mechanics has to be invoked in order to prove that matter is indeed stable, i.e., that many-body systems with electrostatic interactions do not collapse. In a classical picture short range terms, often in the form of a hard core, have to be added to stabilize the system. The weak tempering problem cannot be cured by quantum mechanics. However, a screening mechanism always present in CS, effectively shortens the range of the interactions and prevents matter from exploding.

Debye shielding

Electrostatic interactions in many-body systems always give rise to electroneutrality and screening [2]. A system in thermal equilibrium does not tolerate any charge inhomogeneity over more than a few intermolecular distances. Any excess charge will be expelled

[‡] In the sense that the thermodynamic limit exists and agrees with thermodynamics, and that the various ensembles are equivalent.

to the boundary of the system. This creates an external field whose effect is to shift the activities for all the particles, while the system remains electrically neutral inside. On the other hand, a screening cloud of opposite sign of charge forms around any charged particle inside the system. If the quantum mechanical nature of the particles is taken into account the screening is less efficient but still occurs [2]. These remarkable features of the Coulomb potential are common to both short-ranged and long-ranged electrostatic forces. Thus, for instance, in a system of neutral atoms or molecules, each charge belongs to a neutral entity that has an extension of the order of the atomic or molecular diameter. On the other hand, a charge in an electrolyte, such as sodium chloride, carries a neutralizing cloud. The size of such a screening cloud can be characterized by the Debye length λ_D which is proportional to $\sqrt{T/n}$ with n the number density of ions and T the temperature.

Screening and electroneutrality manifest themselves in the form of specific constraints on the static correlations between the charged particles. These constraints are expressed by exact sum rules which can be obtained relatively easily in the framework of statistical mechanics. In contrast, full correlation functions are more laborious to calculate. Therefore, sum rules are important since they provide exact relations involving the correlation functions which serve as guiding constraints in building phenomenological schemes. Some of the most fundamental sum rules are the Carnie-Chan rule [7], the Stillinger-Lovett rule [5, 6] and the Contact Theorem [3, 8]. The latter is the classical counterpart of the Hellman-Feynman theorem. The Carnie-Chan sum rule expresses the fact that each ion is surrounded by a cloud of ions bearing a net opposite charge. It provides a constraint on the sums of the zeroth moments of the total correlation functions of ion pairs. The Stillinger-Lovett rule provides a constraint on the total sum of the second-moments of the ion-ion pair correlation functions, but does not determine the individual second moments. Thus, for an $s-$component system, there are s Carnie-Chan sum rules but only one Stillinger-Lovett sum rule. It is worth to stress the fact that these rules are universal and independent of any short range interaction between the ions. They are consequences of the screening and electroneutrality phenomena rendered by the Coulomb potential in many-body systems.

Typical systems and parameters

Examples of Coulomb Systems are plasmas (man-made and astrophysical), electrolytes, ionic liquids, and charge-stabilized colloids. A set of parameters, which can be conveniently combined to have dimensions of length, characterize Coulomb Systems [11]. All excess thermodynamic properties, that is, thermodynamic properties inherited from the presence of charged species interacting through Coulomb forces, will depend on these parameters. A first convenient length scale is the ion sphere radius l, defined by the relation:

$$n = \frac{3}{4\pi l^3} \quad l\text{: ion-sphere radius,} \tag{1.4}$$

with $n = N/V$ where N is the number of point ions and V is the volume. The ion-sphere radius, is the radius of a sphere containing on the average one ion, i.e., l is roughly the average distance between ions. A second important parameter is the Landau length, also known as Bjerrum length in the context of electrolytes:

$$\lambda_B = \frac{Z^2 e^2}{\varepsilon k_B T} \quad \text{Bjerrum length,} \tag{1.5}$$

with Ze the charge of the ions and ε the dielectric constant of the medium. The Bjerrum length is the distance at which the potential electrostatic energy between two ions equals the thermal energy. A third parameter is the de Broglie wave length:

$$\Lambda = \frac{h}{\sqrt{2\pi m k_B T}} \quad \text{de Broglie wave length.} \tag{1.6}$$

Quantum diffraction effects at short distances will only be negligible if $\Lambda/l \ll 1$, a low density or high temperature requirement. Another important parameter is the Debye length, which represents the size of the screening sphere surrounding each ion:

$$\lambda_D = \sqrt{\frac{\varepsilon k_B T}{4\pi n Z^2 e^2}} \quad \text{Debye length.} \tag{1.7}$$

Notice that, in order for statistical considerations involving this length scale to be valid for individual systems, many particles have to be present in the Debye sphere, i.e., $N_D \equiv 4\pi\lambda_D^3 n/3 \gg 1$ which is again a *low* density or high temperature requirement. Some values of the parameters corresponding to typical Coulomb systems are given in table I (see also Ref. [1]).

	Interstellar gas	Thermonuclear plasma	Electrolyte
Z	1(H)	1(H)	1(NaCl)
n(particles/m^3)	10^6	10^{21}	10^{26}
l(m)	$6 \cdot 10^{-3}$	$6 \cdot 10^{-8}$	$7 \cdot 10^{-10}$
T(eV)	1	10^4	$1/40$
Λ/l	$2 \cdot 10^{-11}$	$5 \cdot 10^{-9}$	$5 \cdot 10^{-3}$
λ_D(m)	7	$2 \cdot 10^{-5}$	$3 \cdot 10^{-10}$
λ_B	10^{-8}	10^{-13}	$7 \cdot 10^{-10}$
a(m)	$8 \cdot 10^{-11}$	$8 \cdot 10^{-11}$	10^{-10}

Table I: order of magnitude of typical Coulomb System parameters.

1.2 Charge-stabilized colloids

Charge-stabilized colloids, the systems under study in this thesis, are extremely asymmetric mixtures of mesoscopic colloidal particles, which are micron-sized in at least one dimension, and sub-nanometer sized neutral solvent molecules and ions. The size of the colloidal particles and the typically large values of their charges, make charge stabilized colloidal suspensions a very special type of Coulomb system, and some of their properties differ from those of other CS systems, such as those mentioned in table I.

Size

The size range of colloidal particles is bounded from above and below. In general, colloidal particles must be large with respect to the solvent molecules but still small enough

to display thermal motion [12]. The minimum size is set by the requirement that the solvent molecules interact with the colloidal particle only in an averaged way, that is, many solvent molecules are supposed to interact with a single colloidal particle. For common systems this restricts the lowest size of the colloidal particles to 1nm. The maximum size of a colloidal particle is set by the condition that it behaves as a molecule in the sense that it should display Brownian motion. This means that its displacements in a time scale corresponding to the Brownian time, which for colloidal particles of is of the order of seconds, should be comparable to their colloidal linear dimension. For common systems this sets the upper size at 10μm, i.e., several orders of magnitude larger than the size of the particles in table I. Particles in solution which are smaller than the approximate lower bound of 1nm, such as sugar or salt dissolved in water, can be separated from other substances, such as gelatin or starch, by selective diffusion through a semipermeable membrane, e.g., parchment or cellophane. The Scottish chemist Thomas Graham (1805-1869) gave the name colloid, meaning gluelike, to the sticky substances that do not diffuse through the semipermeable membrane due to the size of their macromolecular constituents, and the name crystalloid to those that do diffuse such as sodium chloride.

Charge

The charge of colloidal particles typically ranges between $100e$ and $10000e$. The surface of a colloidal particle in solution can be charged due to several mechanisms. One example of such mechanism is the preferential adsorption of ions from a solution on an initially uncharged surface. Another possible mechanism is the dissociation of surface groups, which usually leaves the surface of the colloidal particles with a negative charge, releasing positive ions into the solvent. Additional ions can be present in the solvent as a consequence of adding an ionic solute (e.g. sodium chloride) to the suspension. The surface charge acquired depends not only on the chemical compositions of the two phases but also on the structure of the electrostatic fields they cause, leading to a self consistency problem (See Sec. 1.5 and Chap. 2).

The behavior of the ions about a charged colloidal particle is similar to that of a CS in bulk. All charges are screened, and the correlations between them decay exponentially with distance. All charge-stabilized colloids are electro-neutral. The counterion charge screens the colloidal charge and the ion density profiles are exponentially decaying at the same rate as in a bulk electrolyte. An estimate of the screening (Debye) length for colloidal particles suspended in pure water at room temperature, with monovalent positive and negative ions with total number density $2\rho_s$ expressed in Mol per liter, is given by the useful relation

$$\lambda_D = \sqrt{\frac{\varepsilon k_B T}{8\pi e^2 \rho_s}} \approx \frac{0.3[\text{nm}]}{\sqrt{\rho_s[\text{M/l}]}}. \tag{1.8}$$

As a consequence of the screening of the colloidal particle charges by the charge of the mobile ions, one can treat the colloids as having an effective charge such that the long distance interaction between two colloids is determined by their effective charge and by the bulk decay length of the electrolyte [4].

Softness

Colloidal suspensions are an example of so-called soft matter. The softness of soft materials is necessarily linked to their intrinsic inhomogeneity, which persists at mesoscopic scales [13]. Softness can be better understood when contrasted with its counterpart. Hard matter refers to matter in the solid phase that exhibits high resistance to various kinds of shape change when force is applied, and is generally characterized by strong intermolecular bonds. Hard matter generally exhibits three types of responses after the application of a force depending on the magnitude of the force and the type of material. It can respond elastically, temporarily changing shape but returning to the original shape when the force is removed, it can respond plastically by changing shape but remaining in one piece or it can fracture, i.e., break into two or more pieces. Examples of hard matter are ceramics, composites, metals and semiconductors. When hard materials are studied with a microscope with a resolution of 0.1nm, their microscopic constituents become "visible" and the piece of hard matter appears inhomogeneous. When the resolution decreases to about 1nm, the microscopic building blocks are no longer detectable and the system appears homogeneous.

In contrast, typical soft materials under the microscope, appear completely inhomogeneous even when observed with a resolution of up to 1000nm. The reason for this is that the building blocks of soft materials are objects with dimensions of the order of up to 10μm. The softness of soft materials can be illustrated by comparing the shear modulus of hard and soft matter [13]. The shear modulus is one of several quantities for measuring the strength of materials. It describes the material response to shearing strains, which are stresses parallel or tangential to a face of the material. The shear modulus ν of a crystal of linear size L is defined by the relationship

$$\frac{F}{L^2} = \nu \frac{\Delta L}{L} \tag{1.9}$$

where F is the shearing force and ΔL is the deformation. ν has the dimensions of $[energy]/[length]^3$. The energy scales of interest for the study of soft materials are of the order of the room temperature thermal energy $k_B T = (1/40)eV$. Here the length scale is proportional to the lattice constant L, the characteristic length scale of the crystal. Therefore, if we compare the shear modulus of a hard-matter crystal with that of a soft-matter crystal, consisting of large macro-molecules and a lattice constant which is about ten thousand times bigger than that of a hard-matter crystal, we conclude that the shear modulus of say, a colloidal crystal, is about 12 orders of magnitude smaller than that of a hard-matter crystal, thus, soft materials are indeed very easily deformable. This property is of extreme importance, e.g., in biological matter, since many of the functions of membranes and cells depend on their softness.

Inhomogeneity

Colloids are mixtures with properties intermediate between those of a homogeneous mixture and those of an inhomogeneous mixture. The homogeneous mixture character of colloids means that they have definite composition and properties which are the same for any part of a bulk system when observed with a resolution much larger than the particles' size. The inhomogeneous mixture character refers to the fact that colloids consist of at least two phases that can be mechanically separated from each other. As we have seen,

one of these phases consist of large molecules or crystallites, the colloidal particles, with typical sizes between 1nm and 10μm, and the other phase consists of solvent molecules with typical sizes of 0.1nm [12].

Non-locality

A system is non-local if a given property of the system at a point $\mathbf{r}$ depends not only on the local density $\rho(\mathbf{r})$ and local thermodynamic fields $X(\mathbf{r})$ such as pressure, temperature, etc..., also on the properties of the fluid *in the vicinity* of $\mathbf{r}$. The range of this vicinity is determined by the correlation length of the fluid, which is often a measure of the range of the intermolecular forces. In some cases, such as in the case of long-range interaction potentials, e.g., the Coulomb potential, and/or in the vicinity of a critical point, the correlation length may exceed the molecular size by several orders of magnitude. The non-locality of inhomogeneous fluids, and in particular of colloids, can be treated at several levels of approximation. The simplest approach treats the non-local character of the fluid, so that thermodynamic potentials, say the free energy density f, are determined locally by a relation of the form $f = f(\rho(\mathbf{r}), X(\mathbf{r}))$. In a second level of approximation, the gradient of the local density is also considered, which leads to a relation of the form $f = f(\rho(\mathbf{r}), \nabla\rho(\mathbf{r}), X(\mathbf{r}))$. A more elaborate treatment takes into account the direct correlations with other molecules located at a generic point $\mathbf{r}'$ by a relation of the form $f = f(\{\rho(\mathbf{r}), \rho(\mathbf{r}'), X(\mathbf{r}), c^{(2)}(\mathbf{r}, \mathbf{r}')\})$, with $c^{(2)}(\mathbf{r}, \mathbf{r}')$ the two-point direct correlation function. The techniques and models proposed in this thesis are based on these sort of approximations. The choice of the level of description varies depending on the particular problem.

Mean-field approach

In theoretical studies of charge-stabilized colloids, models and techniques are introduced to account explicitly for their collective behavior, and for their inhomogeneous and non-local character. In order to make progress in the theoretical description of these systems, phenomenological approaches often have to be adopted. For instance, when screening is expected, it is common practice to invoke mean field theories to replace the Coulomb potential by a screened potential. Likewise, when charged particles are in a medium, it is common to modify this screening potential by introducing a dielectric constant[¶]. This approach is a sensible attitude if one is determined to make some progress. In this section we briefly mention some of the theoretical methods used in this thesis.

The collective behavior of Coulomb systems can be described reasonably well, at least at low couplings, by a mean-field approach. The free energy of a system of many particles in equilibrium can be obtained within the canonical formalism from the definition $F \equiv \langle U \rangle - TS$, where $\langle U \rangle = \mathbf{tr}[p_N(\mathbf{r}_{1,\ldots,}\mathbf{r}_N)U(\mathbf{r}_{1,\ldots,}\mathbf{r}_N)]$ is the expectation value of the potential energy U averaged over the distribution

$$p_N(\mathbf{r}_{1,\ldots,}\mathbf{r}_N) = \frac{e^{-\beta U(\mathbf{r}_{1,\ldots,}\mathbf{r}_N)}}{\mathbf{tr}\big[e^{-\beta U(\mathbf{r}_{1,\ldots,}\mathbf{r}_N)}\big]} \tag{1.10}$$

[¶]In spite of the fact that there is no first principles theory of the dielectric constant which does not presuppose the existence of atoms and molecules, i.e., which does not take the thermodynamic stability of a system of many charged particles for granted.

and $S = -k_B \mathbf{tr}\{p_N(\mathbf{r}_{1,...,}\mathbf{r}_N) \ln p_N(\mathbf{r}_{1,...,}\mathbf{r}_N)\}$ is the entropy resulting from that distribution with $\mathbf{tr}$ the classical canonical trace, which involves integrals over all the ion-coordinates. The calculation of these averages amounts to the calculation of the partition function of the system of N interacting particles and it is a formidable task. In order to circumvent such difficulty we introduce the mean-field approximation, which consists of replacing the $N-$particle distribution function by a product of N (identical) one-particle distribution functions $p_1(\mathbf{r}_1) = \rho(\mathbf{r})/N$ with $\rho(\mathbf{r})$ the number density of particles at position $\mathbf{r}$, namely:

$$p_N(\mathbf{r}_{1,...,}\mathbf{r}_N) = p_1(\mathbf{r}_1)p_1(\mathbf{r}_2)\cdots p_1(\mathbf{r}_N) \quad \text{mean field approximation.}$$

As a consequence of the mean field approximation, the entropy and the energy of the system can be written as $S = -Nk_B \int d\mathbf{r} p_1(\mathbf{r}) \ln p_1(\mathbf{r})$ and $\langle U \rangle = N \int d\mathbf{r} p_1(\mathbf{r})\phi(\mathbf{r})$, where $\phi(\mathbf{r})$ is the mean field at position $\mathbf{r}$ generated by the charges on the particles. The system of N interacting ions thus reduces to a system of N non-interacting particles in the presence of the mean field generated by each others charges.

A common feature of mean-field theories is the identification of at least one order parameter. One approach is to express an approximate free energy functional in terms of this parameter and minimize the former with respect to the order parameter, usually under one or more constraints dictated by conservation laws, to obtain the free energy of the system. Another approach is to approximate an interacting system by a non-interacting system in a self-consistent external field expressed in terms of the order parameter. We will use both approaches in this thesis. The most serious fault in mean-field theories lies in the neglect of long-range fluctuations of the order parameter, i.e., ionic fluctuations and ion-ion correlations are neglected. This limitation manifests itself in different ways depending on the dimension of the system and may lead to qualitatively wrong results. In the case of monovalent electrolytes and charge-stabilized colloids at low coupling, results from mean-field theoretical approaches are in excellent agreement with experiments and simulations, as we will find later in chapters 6 and 7 of this thesis.

Poisson-Boltzmann theory

Poisson-Boltzmann theory is a mean field theory which combines Boltzmann statistics with Poisson's equation, in order to obtain an equation for the order parameters, i.e., the mobile charges density profiles, in the presence of inhomogeneities due to external fields, e.g. generated by a fixed distribution of charge. Consider a system consisting of a fixed charge density $eq(\mathbf{r})$ and one species of N point-like mobile counterions of charge Ze and mass m within a volume V in the presence of the field generated by $eq(\mathbf{r})$ (the generalization to several species of mobile charges can be trivially performed along the same lines). The fixed charge density can be due to the presence of charged colloids or in general to a charged interface with surface charge σ. The equilibrium distribution of the mobile counterions $\rho(\mathbf{r})$ at point $\mathbf{r}$ is given by the Boltzmann factor $\rho(\mathbf{r}) = \rho_0 e^{-\phi(\mathbf{r})}$ with $\phi(\mathbf{r})$ the (dimensionless) mean field, and ρ_0 is fixed by the relation $\int d\mathbf{r}\rho(\mathbf{r}) = N$. Combining this result with Poisson's equation: $\Delta\phi(\mathbf{r}) = -4\pi\lambda_B(\rho(\mathbf{r}) + q(\mathbf{r}))$ we obtain the celebrated Poisson-Boltzmann (PB) equation

$$\Delta\phi(\mathbf{r}) = -4\pi\lambda_B(\rho_0 \exp[-\phi(\mathbf{r})] + q(\mathbf{r})/Z) \tag{1.11}$$

which is an equation for the mean field from which the ion density profile (order parameter) can be obtained. Notice that the PB equation is a non-linear second order differential equation for the mean field, and therefore two boundary conditions (BCs) are required for a unique solution. The most common BCs are formulated by assuming that the fixed charge $q(\mathbf{r})$ is spread over a surface, which acquires a homogeneous surface charge σ localized at the interface between two phases, one of which is not penetrated by the moving charges and is characterized by a dielectric constant ε_{ext}. This corresponds to the boundary value problem

$$\Delta\phi(\mathbf{r}) = \begin{cases} -4\pi\lambda_B\rho_0 \exp\left[-\phi(\mathbf{r})\right] & \mathbf{r} \in \text{fluid} \\ 0 & \text{otherwise} \end{cases} \tag{1.12}$$

with BCs such that $\phi(\mathbf{r}) = 0$ far away from the interface and

$$\varepsilon_{int}\nabla_n\phi_{int}(\mathbf{r}) - \varepsilon_{ext}\nabla_n\phi_{ext}(\mathbf{r}) = -4\pi\varepsilon_{int}\lambda_B(\sigma/e) \tag{1.13}$$

for any position $\mathbf{r}$ on the interface, where $\lambda_B = e^2Z^2/\varepsilon_{int}k_BT$ is the (solvent) Bjerrum length with ε_{int} the dielectric constant of the phase where ions are present. Here $\phi_{int}(\mathbf{r}) = \phi(\mathbf{r}) \mid \mathbf{r} \in$ fluid, and $\phi_{ext}(\mathbf{r})$ is the mean field at the other side of the interface, which is assumed to be a dielectric medium characterized by ε_{ext}, and ∇_n is the spatial derivative in the direction perpendicular to the interface. The linear PB equation (Debye-Hückel limit) can be obtained by linearization with respect to the potential inside the fluid containing the charged particles, which is justified as long as $\phi(\mathbf{r}) \ll 1$, i.e., as long as the average potential felt by a charged particle, due to its interaction with all the other charged particles and the presence of any external charges, is much smaller than the thermal energy.

1.3 Colloidal interactions

Short-range forces

Colloidal interactions are dominated by surface effects because the interface between the solvent and the colloidal particles is large [12]. For instance, in one liter of colloidal suspension at a concentration of 0.1 volume fraction**, the interface area is of the order of 1500m^2. Different types of surface forces operate. Forces that are always present between colloidal particles are Van der Waals forces and repulsive hard-core interactions. Van der Waals forces are due to the interaction between electrical dipoles which are either permanent or induced. Even if the particles do not have a permanent dipole moment, distortions of the electron density give rise to a temporary electrical dipole which induces a dipole in particles nearby. The temporary dipole and the induced dipoles are then attracted to each other, therefore, Van der Waals forces are attractive and short range. This corresponds approximately to a pair-wise interaction radially-symmetric potential which behaves as r^{-6}. The strength of these forces is related to the refractive index difference between the particle cores and the solvent. In colloidal suspensions, the refractive index difference

**The volume or packing fraction of a colloidal suspension is defined as $\eta = NV_0/V$, where N is the number of colloidal particles, V_0 is the volume occupied by one particle and V the total volume occupied by the solution.

can be chosen to be small in order to minimize the attractive Van der Waals forces ("index matching")[12]. In addition, a repulsive hard-core force, due to the large increase in energy when the cores of two particles overlap, is always present. This can be described by a potential which is virtually infinite for separation distances between the centers of two colloidal particles smaller than twice their radius, and zero for larger separations. The surface of colloidal particles can also be coated with polymers which are chemically attached or physically adsorbed to the surface [13]. When the solvent is a good solvent for the polymers, the colloid-colloid interaction is repulsive since the polymers prefer to dissolve in the solvent rather than in their own melt. This kind of interaction is known as steric repulsion. If the solvent is a poor solvent for the polymers, the more favorable situation of overlapping polymers leads to an effective attraction between the colloidal particles. The fact that colloids exhibit these types of highly tunable effective pair interactions is one of their most interesting features both for theoretical and experimental studies.

Entropic and Hydrodynamic forces

In addition to the previous surface related interactions, which may exist in non-colloidal systems as well, there are two types of interactions which are specially important in colloidal systems namely entropic and hydrodynamic interactions. Entropic forces emerge as a consequence of the large size difference between the Brownian colloidal particles and the solvent molecules [13]. This difference in size implies that the time scale on which the colloidal particles move is much larger than that during which the solvent molecules move, where movement has to be understood as a change in position of the particles by a distance comparable to their own size. Due to this separation of scales, the solvent molecules can be considered in a state of equilibrium in the force field produced by the colloidal particles during their displacement. When the colloidal particles move, they perform a certain amount of work on the solvent which is equal to the change of the Helmholtz free energy of the total system, namely, the solvent and the colloidal particles. The change in free energy has two contributions. The first one is due to the change in potential energy of the colloidal particles and the solvent (ions, polymer etc...). The second is due to the change in entropy of the solvent. According to the second law of thermodynamics, an isolated system progresses to a state in which entropy is maximized. This manifests itself as effective forces of entropic origin between the macromolecules. Therefore, the free energy rather than the energy is the most relevant thermodynamic quantity in the study of colloidal interactions [3]. Hydrodynamic interactions arise from the fact that as a colloidal particle translates or rotates inside the solvent, it induces a fluid flow which affects the motion of other colloidal particles. Since the colloidal particles are much larger than the solvent molecules, this flow leads to a macroscopic hydrodynamic problem which can be studied in first approximation by using the theory of fluid dynamics [16]. Such hydrodynamic interactions will not be considered in this thesis.

Long-range forces

As we have seen, long-range forces are electrostatic in origin and render in the system a collective behavior. Electrostatic forces manifest themselves in the form of electroneutrality and screening. The resulting effective electrostatic interactions differ in many im-

portant aspects from other types of potentials. For example, the electrostatic potential of an electroneutral macromolecule with an internal charge distribution has generally the same long-range behavior as the potential of an ion. This long-range behavior operating between ions and/or macromolecules gives the potential a many-body character. It can only be split into separate pair contributions if the density of colloidal particles is low, or if the particles are highly screened, i.e., if their Debye length is small and they behave essentially as hard-spheres. Another consequence of screening, is that in charge-stabilized colloidal suspensions there are at least three different length scales[**]: the nanoscale of the ions, the microscale of the screening cloud formed by the counterions and the mesoscale of the colloidal particles. Treating all these scales on an equal footing is often impractical, if not impossible. In simulations, for instance, one would then spend most of the time updating the screening ions instead of the colloids, and in theoretical approaches, like those discussed in Sec 1.3, one would, e.g., need a sophisticated theory to describe the ions density profiles even if the colloidal particles were dilute. Let us proceed by describing some theoretical alternatives to study the effect of long-range electrostatic forces in charge-stabilized colloids.

McMillan-Mayer theory

Experimental observations with, e.g., video-microscopy, confocal microscopy or light scattering only concern the mesoscopic scales, leaving the microscopic degrees of freedom invisible. It is therefore natural and often necessary to regard charge-stabilized colloids as effective systems consisting of mesoscopic species only, interacting through an effective potential that takes into account possible effects due to the microscopic species, i.e., the ions within the PM. The rigorous procedure to calculate such effective potentials is based on the McMillan-Mayer (MM) theory and is briefly discussed below (see, e.g., [17–19]). Let us consider a typical charge-stabilized colloidal system consisting of N mesoscopic particles, the colloidal particles, with a diameter σ (which ranges between 1nm and 10μm), immersed in a solvent consisting of molecules which are much smaller than the colloids, and considered as a structureless medium characterized by a dielectric constant ε. The interior of the colloids is assumed to be a medium of the same permittivity in order to avoid image charge effects. In addition, there are N_+ positive and N_- negative mobile point-like ions. It is convenient to describe such a system as being in equilibrium with a bulk electrolyte reservoir, separated from the system by a membrane permeable for everything but the colloids. The system is thus open with respect to the ions. The pair distribution functions of the different components are statistical averages over this ensemble. The potential energy of such a system can be written as a pairwise sum of *direct interaction pair potentials* v_{cc}, v_{ii} and v_{ci} respectively involving colloid-colloid, ion-ion and colloid-ion interactions, namely

$$U = U_{cc}(\mathbf{R}^N) + U_{ii}(\mathbf{r}^{N_+}, \mathbf{r}^{N_-}) + U_{ci}(\mathbf{R}^N, \mathbf{r}^{N_\pm}), \tag{1.14}$$

where $\mathbf{R}$ and $\mathbf{r}$ refer to the colloids and ions coordinates respectively. Within the primitive model, U consists of bare Coulomb interactions between the different species and hard sphere like contributions that account for their finite size.

[**]Within the so called primitive model (PM), which considers the solvent as a structureless dielectric medium characterized by a dielectric constant.

Due to the large difference in length scales, the calculation of the free energy of such a system can be regarded as a two step thermal average. In the first step we calculate the average over the ion coordinates in the presence of (the field due to) a fixed random configuration of colloids. After this step the remaining distribution function is independent of the ion coordinates, and one can define an effective interaction potential between the colloidal particles, which is in general different from $U_{cc}(\mathbf{R}^N)$. In order to perform this first thermal average, we calculate the classical trace with respect to the ion coordinates of the Boltzmann factor with potential energy (1.14):

$$\begin{aligned} e^{-\beta U} &= e^{-\beta U_{cc}(\mathbf{R}^N)} \mathbf{tr}_+ \mathbf{tr}_- e^{-\beta U_{ii}(\mathbf{r}^{N_+}, \mathbf{r}^{N_-}) - \beta U_{ci}(\mathbf{R}^N, \mathbf{r}^{N_\pm})} \\ &\equiv e^{-\beta U_{cc}(\mathbf{R}^N)} e^{-\beta \Omega(\mathbf{R}^N)} \\ &\equiv e^{-\beta W_N(\mathbf{R}^N)} \end{aligned} \tag{1.15}$$

with $\mathbf{tr}_\pm$ the grand canonical classical trace w.r.t. the positive $(+)$ and negative $(-)$ ion coordinates. Notice that after integrating out the ion coordinates, we obtain by definition the Grand Potential of the ions $\Omega(\mathbf{R}^N)$ in the presence of the random configuration $\mathbf{R}^N$ of colloidal particles. Together with $U_{cc}(\mathbf{R}^N)$, the colloid-colloid interaction potential, $\Omega(\mathbf{R}^N)$ defines the $N-$body colloidal potential of mean force $W_N(\mathbf{R}^N)$.

The colloidal many-body problem

The $N-$body colloidal potential of mean force, referred to by some authors as an "effective" Hamiltonian[††], is in general not pairwise additive. $W_N(\mathbf{R}^N)$ can be expressed though a cluster expansion as a sum of one body terms $V_N^{(0)}$, pairs $v_2(\mathbf{R}_i, \mathbf{R}_j)$, triplets $v_3(\mathbf{R}_i, \mathbf{R}_j, \mathbf{R}_k)$ etc..., namely

$$W_N(\mathbf{R}^N) = V_N^{(0)} + \sum_{i \leq j}^{N} v_2(\mathbf{R}_i, \mathbf{R}_j) + \sum_{i \leq j \leq k}^{N} v_3(\mathbf{R}_i, \mathbf{R}_j, \mathbf{R}_k) + ... \tag{1.16}$$

Two important quantities, the potential of mean force between a colloidal particles pair and the free energy of the suspension, can be constructed from $W_N(\mathbf{R}^N)$ by integration over the colloidal particle coordinates (the second step of the thermal averaging procedure leading to thermodynamics). The potential of mean force between colloidal particles $\omega_{cc}(R_{ij})$, is defined by the relationship

$$\beta \omega_{cc}(R_{ij}) = -\ln g_{cc}(R_{ij}), \tag{1.17}$$

where $g_{cc}(R_{ij})$ corresponds to the *one-component* pair correlation function resulting from the effective interaction potential $W_N(\mathbf{R}^N)$, namely

$$g_{cc}(R_{ij}) = \frac{V^2 \int e^{-\beta W_N(\mathbf{R}^N)} d\mathbf{R}^{N-2}}{\int e^{-\beta W_N(\mathbf{R}^N)} d\mathbf{R}^N} \tag{1.18}$$

[††]The usage of such terminology should be avoided since no kinetic terms are involved in $W_N(\mathbf{R}^N)$. Besides, the $N-$body colloidal potential of mean force has a direct physical interpretation as a *potential*, since the force on a colloidal particle labelled j for a fixed configuration of the N colloidal particles is given by $\mathbf{F}_j = -\nabla_{\mathbf{R}_j} W_N(\mathbf{R}^N)$.

From $\omega_{cc}(R_{ij})$, the average force experienced by two colloidal particles at a separation distance $R_{ij} = |\mathbf{R}_i - \mathbf{R}_j|$ inside the suspension can be obtained as $F(R_{ij}) = -d\omega_{cc}(R_{ij})/dR_{ij}$. Notice that the potential of mean force $\omega_{cc}(R_{ij})$ is different from the N-body potential of mean force $W_N(\mathbf{R}^N)$. The latter is an (ion averaged) N-body quantity, whereas in the former $N-2$ colloidal degrees of freedom have been integrated out in addition, so that both $N-2$ colloidal particles and the $N = N_+ + N_-$ ions contribute to the average force experienced by two colloids as a function of their separation distance. In other words, the potential of mean force $\omega_{cc}(R_{ij})$ is a quantity averaged over *ions and colloids*. Notice that by construction the pair correlations $g_{cc}(R)$, i.e., the relative probability of finding a colloidal particle at a distance R from another colloidal particle, are identical to those in the original multi-component model. The importance of the potential of mean force resides in the fact that experimental measurements of $g_{cc}(R)$ are possible through techniques such as light scattering and confocal microscopy, and all the theoretical machinery available for the study of simple liquids can be used by treating the colloids as molecular constituents. We will find an example of such an approach in Chap. 6 of this thesis.

A second important quantity which can be constructed from the N-body potential of mean force, through thermal averaging over the colloidal coordinates, is the free energy F of the suspension. This quantity is obtained by calculating the classical trace of the Boltzmann factor corresponding to $W_N(\mathbf{R}^N)$, namely

$$e^{-\beta F} = \mathbf{Tr} e^{-\beta W_N(\mathbf{R}^N)}, \tag{1.19}$$

with $\mathbf{Tr}$ the classical canonical trace over the coordinates of the colloidal particles $\mathbf{R}^N$. Thermodynamic information is contained in the curvature of F, and can be extracted by studying the second order partial derivatives w.r.t. N, V and T, and by performing common tangent constructions.

Pairwise effective models

By neglecting three-body and higher order terms in (1.16), as well as position independent terms $V_N^{(0)}$, the $N-$body potential of mean force can be written in terms of an effective colloid-colloid pair potential as

$$W_N(\mathbf{R}^N) = \sum_{i<j}^{N} v_{cc}^{eff}(\mathbf{R}_i, \mathbf{R}_j). \tag{1.20}$$

The effective colloid-colloid pair potential $v_{cc}^{eff}(\mathbf{R}_i, \mathbf{R}_j)$ is thus identified with an *ion averaged* quantity. On the other hand, the colloid-colloid direct potential $U_{cc}(\mathbf{R}^N) = \sum_{i<j}^{N} v_{cc}(\mathbf{R}_i, \mathbf{R}_j)$ is by definition a sum of pairwise Coulomb interactions $v_{cc}(\mathbf{R}_i, \mathbf{R}_j)$ of the form (1.3) plus a hard core term. In general, those pair potentials are not equal, i.e.,

$$v_{cc}^{eff}(\mathbf{R}_i, \mathbf{R}_j) = v_2(\mathbf{R}_i, \mathbf{R}_j) \neq v_{cc}(\mathbf{R}_i, \mathbf{R}_j). \tag{1.21}$$

Nonetheless, from the definitions of the colloid-colloid potential of mean force $\omega_{cc}(R_{ij})$ it is clear that

$$\omega_{cc}(R_{ij}) \rightarrow \begin{cases} v_{cc}^{eff}(\mathbf{R}_i, \mathbf{R}_j) & \text{for low colloid concentration,} \\ v_{cc}(\mathbf{R}_i, \mathbf{R}_j) & \text{for low ion concentration.} \end{cases} \tag{1.22}$$

It will be shown later in chapters 5 and 7 that expression (1.20) is not entirely correct, and that a careful analysis based on the DFT formalism leads to an expression for the $N-$body potential of mean force of the form

$$W_N(\mathbf{R}^N) = W_1(\rho_c) + W_N(\{\mathbf{R}_i, \mathbf{R}_j\}) \tag{1.23}$$

with $\rho_c = N/V$ the colloid density. Further, $W_N(\{\mathbf{R}_i, \mathbf{R}_j\})$ consists of a sum of pairwise additive potentials, (with notation differing only in the argument from $W_N(\mathbf{R}^N)$, for the sake of economy in the use of symbols), and $W_1(\rho_c)$ is a coordinate independent term, which arises from a resummation of terms which are neglected in the pairwise approximation leading to (1.20). The position independent "volume term" $W_1(\rho_c)$ affects the phase behavior and the equation of state of the suspension. This can be understood by using (1.19) with $W_N(\mathbf{R}^N)$ from Eq. (1.23), which yields

$$F = W_1(\rho_c) - k_B T \ln \mathbf{Tr} e^{-\beta W_N(\{\mathbf{R}_i, \mathbf{R}_j\})}. \tag{1.24}$$

It will be shown later in this thesis that the second term on the r.h.s of (1.24) corresponds to the free energy of a Yukawa fluid with a screening length that depends on the colloidal particle density. The first term on the r.h.s. on the other hand, leads to a contribution to the free energy per volume of at least $O(\rho_c^2)$. The second term clearly contributes to the thermodynamic response functions, i.e., the second order partial derivatives or equivalently the curvature of F.

Yukawa model

From our previous discussion it is clear that $v_{cc}^{eff}(\mathbf{R}_i, \mathbf{R}_j)$ is the interaction potential between pairs of colloidal particles after averaging over the ionic species. If the solvent is treated "primitively", i.e., as a structureless medium, asymptotic forms for this effective one-component interaction potential $v_{cc}^{eff}(\mathbf{R}_i, \mathbf{R}_j)$ can be obtained in the limit of low colloidal particle concentrations from a number of statistical-mechanical approaches. Within linear Poison-Boltzmann theory, it can be shown that the effective pair potential takes the form

$$v_{cc}^{eff}(\mathbf{R}_i, \mathbf{R}_j) = \begin{cases} \infty & \text{for } |\mathbf{R}_i - \mathbf{R}_j| \leq \sigma \\ \frac{Z^2 \lambda_B \exp[\sigma/\lambda_D]}{(1+e^{\sigma/2\lambda_D})^2} \frac{\exp[-|\mathbf{R}_i - \mathbf{R}_j|/\lambda_D]}{|\mathbf{R}_i - \mathbf{R}_j|} & \text{for } |\mathbf{R}_i - \mathbf{R}_j| > \sigma, \end{cases} \tag{1.25}$$

where σ is the hard-core diameter and $\lambda_D = \kappa^{-1}$. In fact this interaction pair potential is only valid for situations where the electrostatic potential is small compared to $k_B T$, otherwise non-linear screening has to be taken into account. This rules out the possibility of an analytic treatment. On the other hand, in the derivation of Eq. (1.25) a constant surface charge of the colloidal particles independent of their separation has to be assumed. This is the case if all the surface chemical groups are ionized. Often the local electric field affects the degree of ionization and thereby the charge on the colloidal particle. If this is the case, conditions of constant surface potential and/or charge regulation have to be considered. These phenomena are discussed in more detail in the context of the next section where we consider charged planar interfaces.

In summary, the presence of mobile ions in the solvent is a factor affecting the interactions. One may first average over the ionic coordinates for the calculation of thermodynamic properties, which are then obtained on the basis $W_N(\mathbf{R}^N)$. The latter $N-$body

potential of mean force can be approximated by a sum of pairwise additive terms. These pairwise additive terms are not of the Coulomb form $v_{cc}(\mathbf{R}_i, \mathbf{R}_j) \sim R_{ij}^{-1}$ with R_{ij} the distance between the centers of the colloidal particles labelled i and j, but are effective potentials $v_{cc}^{eff}(\mathbf{R}_i, \mathbf{R}_j)$, mimicking the screening effect of the ions in the solvent. The asymptotic form of the latter at large separation distances between pairs of colloids, in case the potential energy is small compared to the thermal energy k_BT, is a Yukawa potential $v_{cc}^{eff}(\mathbf{R}_i, \mathbf{R}_j) \sim e^{-r/\lambda_D}/r$, where λ_D is a measure of the range of the screening, which is determined by the ion concentration and other parameters (see Eq. (1.7)). When the potential energy is large, the Yukawa approximation no longer holds and non-linear screening effects have to be taken into account. This problem will be studied in detail in chapter 4 in the context of colloidal mixtures. Another regime in which the Yukawa approximation is insufficient, is that in which the ion concentration is low. In that case the volume term $W_1(\rho_c)$ contributes non-trivially to the equation of state and expression (1.23) has to be used. This important regime will be discussed in detail in Chap. 7.

Cell model

Allow me to close this discussion on colloidal interactions by briefly mentioning a popular approach in which they are all but (completely) neglected, the so-called cell model [8]. The cell model allows to decouple a system of interacting colloids by ignoring their interactions. It rests on the assumption that equally charged colloids in suspension repel each other, and therefore organize themselves so as to stay as far as possible from each other. The solution then is partitioned by taking identical spherical cells, each containing one colloid in its center. By construction these cells are electrically neutral, therefore they don't interact with each other through electrostatic forces. Since the cells have the same volume, there exist correlations between them. These correlations are not taken into account in the model, which focuses on the ion-colloid and ion-ion correlations within a single cell. One advantage of the spherical symmetry is that these correlations can be studied within *non-linear* PB theory, by solving a one-dimensional problem. The PB equation for a spherical cell reads

$$\frac{1}{r^2}\frac{\partial}{\partial r}\left(r^2\frac{\partial \phi}{\partial r}\right) = \kappa^2 \sinh \phi(r) \tag{1.26}$$

with boundary conditions $\phi(r = a) = \phi_a$ and $\phi'(r = R) = 0$ where R is the radius of the cell. No analytical solution exists for (1.26), but it can be solved numerically in an $r-$grid. The osmotic pressure of a colloidal suspension within the cell model is determined by the number density of positive and negative ions at the cell boundary $\rho_+(R)$ and $\rho_-(R)$. These formalisms will be discussed in detail in chapter 4 in the more general context of colloidal mixtures.

1.4 Planar interfaces and surface phenomena

As we have seen, in describing many-body charged systems, a distinction is made between the fixed charge on the surfaces and the mobile counterions. For highly charged surfaces, most of the counterions reside close to the fixed charges in a thin layer of the order of few tenths of a nanometer. The remaining counterions are in solution with a

density that decreases as a function of the distance from the surface with fixed charge. These delocalized charges give rise to long-range interactions between the charged surfaces. Correlation effects between the mobile ions, i.e., deviations from the mean-field approach, can change the nature of the interactions between the surfaces, and may result in short-range *attractive* interactions between surfaces carrying charge of the same sign. In this section we will focus on simple geometries, namely isolated planar solutes and interacting charged walls, in order to illustrate several important concepts without need of computational complications. The concepts in this section will be used extensively later in this thesis in more general contexts.

Isolated planar wall with constant surface charge

Let us first consider a charged isolated planar interface in contact with a solution containing mobile charges, whose concentration far away from the surface is ρ_s, each for positive and negative ions, and focus on the study the density profiles of mobile positive $\rho_+(z)$ and negative $\rho_-(z)$ ions. Let z be the coordinate perpendicular to the surface. Since the $z = 0$ charged surface is infinite, the system is translationally invariant in the perpendicular x and y directions. Within Poisson-Boltzmann theory, the equilibrium density profiles of the ions are given by the expressions $\rho_\pm(z) = \rho_s \exp[\mp\phi(z)]$, where $\phi(z) = e\psi(z)/k_BT$ is the (dimensionless) mean field at a distance z from the wall where $\psi(z)$ is the electrostatic potential, which are related to the equilibrium local charge density $\rho(z) = \rho_+(z) - \rho_-(z)$ by Poisson's equation

$$\frac{d^2\phi(z)}{dz^2} = -\frac{4\pi e^2}{\varepsilon k_B T}\rho(z), \tag{1.27}$$

for the simple geometry under consideration, namely a single isolated charged interface. The presence of a fixed charge on the plane is introduced through the BCs $\phi'(z = 0) = -4\pi e\sigma/\varepsilon k_BT$ and $\phi'(z \to \infty) = 0$. It is useful to distinguish two cases: the case in which only counterions are present in the solution, i.e., $\rho_-(z) = 0$ for a negatively charged plane, and the case in which additional electrolyte is added to the system. In the former case the PB equation can be solved exactly, which leads to (see, e.g., [3, 8, 13])

$$\begin{aligned} \phi(z) &= 2\ln(z+b) + \phi_0 \quad \text{Counter-ion only} \\ \rho(z) &= \frac{1}{2\pi\lambda_B}\frac{1}{(z+b)^2} \end{aligned} \tag{1.28}$$

with $b = e/2\pi|\sigma|\lambda_B$ the so called Gouy-Chapman length and ϕ_0 a dimensionless reference potential. In the counter-ion only case the potential has a logarithmic divergence for $z \to \infty$. According to this solution, mobile charge is localized in a layer of thickness b close to the surface as to balance half of the surface charge. The other half is balanced by the reminder of counterions. For highly charged surfaces b is less that one nanometer, so that most of the counterions that effectively balance the surface charge are located at a sub-nanometer distance from the surface.

The second case is that in which the system is in osmotic contact with a 1:1 electrolyte reservoir with ions concentration $2\rho_s$, located far away from the surface, i.e., $\rho(z \to \infty) = 2\rho_s$. Integration of the PB equation with the same BC as in the case of counter-ions only

yields

$$\begin{aligned} \phi(z) &= 2\ln\frac{1-\gamma e^{-z/\lambda_D}}{1+\gamma e^{-z/\lambda_D}} = 2\ln\frac{1-e^{-z/\lambda_D}\tanh(\phi_s/4)}{1+e^{-z/\lambda_D}\tanh(\phi_s/4)} \\ \rho_\pm(z) &= \rho_s\left(\frac{1\pm\gamma e^{-z/\lambda_D}}{1\mp\gamma e^{-z/\lambda_D}}\right)^2 \quad \text{Added electrolyte} \end{aligned} \tag{1.29}$$

with $\gamma = -b/\lambda_D + \sqrt{(b/\lambda_D)^2+1}$ and ϕ_s the surface potential $\phi_s = \phi(z=0) = -4\arctan(\gamma)$. The exponential decay of $\phi(z)$ is reminiscent of the exponential screening of the correlation functions in bulk electrolytes.

Charge renormalization

In the case of highly charged walls, the strong electrostatic forces between the surface charge and the oppositely charged particles in solution induces the accumulation of the latter close to the walls [20, 21]. This non-linear condensation phenomenon cannot be described by a linearized Poisson-Boltzmann-like approach. However, the simplicity of the linear theories can be preserved by the use of the of notion of charge renormalization [20, 21, 76], which considers the colloid and its counterion shell as a single entity carrying a charge which is usually smaller than the bare charge of the colloid. This so called renormalized charge contains information on the long-distance behavior of the screened electric potential created by the colloid and its microion polarization cloud, taking into account non-linear effects. This concept has been successfully applied to calculate thermodynamic properties of highly charged monodisperse colloidal suspensions, in the regime where non-renormalized linear theories fail to correctly take into account the electrostatic interactions, and where other popular methods such as Monte Carlo simulations turn out to be computationally too expensive to be of any practical use. The notion of charge renormalization can be understood in the light of the previous discussion on the planar charged wall. In the limit of high surface potentials, the electrostatic potential $\phi(z)$ at a distance z from the interface, Eq. (1.29), becomes independent of ϕ_s. For separation distances larger than the Debye length we have

$$\phi(z) \approx 2\ln\frac{1-e^{-z/\lambda_D}}{1+e^{-z/\lambda_D}} \approx 4e^{-z/\lambda_D} \quad \text{for } \frac{1}{4}\phi_s \gg 1 \text{ and } z \gg \lambda_D. \tag{1.30}$$

The electrostatics away from the plane is thus completely insensitive to the surface charge density for surface potentials such that $\phi_s \gg 4$, which at room temperature is of the order of 100mV.

Consider now a single highly charged spherical colloidal particle of charge Z and radius a immersed in a symmetric 1:1 electrolyte. As we know from our discussion on colloidal interactions, for distances $r > a + \lambda_D$ the electrostatic potential becomes small and the PB equation can be linearized leading to a solution of the form

$$\phi(r) = A\frac{e^{-r/\lambda_D}}{r}, \tag{1.31}$$

with A a certain constant. Let us restrict the analysis to the case $\lambda_D \ll a$. For distances $a + \lambda_D < r < 2a$, curvature effects are negligible and the electrostatic potential is well approximated by that of a uniformly charged plane, Eq (1.30). Comparing Eqs. (1.31)

and (1.30), the value of the integration constant A can be determined and the potential at a distance $a + \lambda_D < r < 2a$ becomes

$$\phi(r) = 4a\frac{e^{-(r-a)/\lambda_D}}{r}. \tag{1.32}$$

Comparing to the solution of the linearized PB equation Eq. (1.25) it is clear that both coincide as long as the structural (bare) colloidal charge Z is replaced by a renormalized charge Z^{ren}. The renormalized charge shows in general a non-linear dependence on Z and for large values of the structural charge, it saturates to a certain value which depends on the other parameters characterizing the system. In the present example it can be shown that the saturation value equals $Z^{ren}_{sat} = 4a(1 + a/\lambda_D)/\lambda_B$ (see, e.g., [20]). The difficulty of defining the effective charge for suspensions including more than one colloidal particle, i.e., suspensions at non-zero concentrations, resides in the complexity of accounting for the consequences of colloidal interactions. One alternative is to use the cell model where those are neglected. We will use such formalism in chapter 4 of this thesis.

Charge regulation

In solving the PB equation in the previous example, the boundary condition $\phi'(z = 0) = -4\pi e\sigma/\varepsilon k_B T$ was used in order to fix the slope of the potential at contact with the charged surface. However, the surface charge of most colloids results from the dissociation of surface molecules and it is in general affected by the ionic environment, so that the condition of constant surface charge does not hold in general. In those dissociation processes, ionic compounds (complexes, molecules, or salts) separate into smaller molecules, ions, or radicals. This usually occurs in a reversible manner; the opposite process being known as association or recombination[‡‡]. Generally the dissociation is only partial, and the degree of dissociation is governed by the law of mass action, which depends on the local ionic environment. Any variation of the ion concentration or pH at the vicinity of such a charged surface, will lead to a fluctuation of the surface charge. Nevertheless, at thermal equilibrium it is possible to define some average structural charge. One has to calculate this bare charge self-consistently taking into account the local inhomogeneity it produces in the ionic environment. This is often a difficult task. Colloidal particles are often made of silica or are covered with an oxide surface. The principal mechanism by which silica acquires a charge in contact with water is the dissociation of silanol groups: $\mathrm{SiOH} \leftrightharpoons \mathrm{SiO^-} + \mathrm{H^+}$. Further protonation of the uncharged group is expected only under extremely acidic conditions. Oxide surfaces, on the other hand, can be charged positively or negatively by the dissociation of protons involving a two-step dissociation reaction: $\mathrm{AH_2^+} \leftrightharpoons \mathrm{AH} + \mathrm{H^+} \wedge \mathrm{AH} \leftrightharpoons \mathrm{A^-} + \mathrm{H^+}$ where AH refers to the neutral surface site of the oxide and $\mathrm{AH_2^+}$ and $\mathrm{A^-}$ are the positively and negatively charged surface sites respectively. These reactions are characterized by dissociation constants $\mathrm{K_+}$ and $\mathrm{K_-}$ according to the mass action equations: $\mathrm{K_+} = [\mathrm{AH}][\mathrm{H}]_b e^{-\phi_0}/[\mathrm{AH_2^+}], \quad \mathrm{K_-} = [\mathrm{A^-}][\mathrm{H}]_b e^{-\phi_0}/[\mathrm{AH}]$ where ϕ_0 is the potential at the surface and $[\mathrm{H}]_b = 10^{-\mathrm{pH}}$Mol/l is the bulk activity of protons.

The charge regulation mechanism for a single isolated charged wall leads to a Poisson-Boltzmann problem similar to that discussed above for the case of constant surface charge, with one BC given by $\phi'(z \to \infty) = 0$ but the other BC still undetermined. The slope of

[‡‡]This process is different from ionization where an atom or molecule is converted into an ion by changing the difference between the number of protons and electrons.

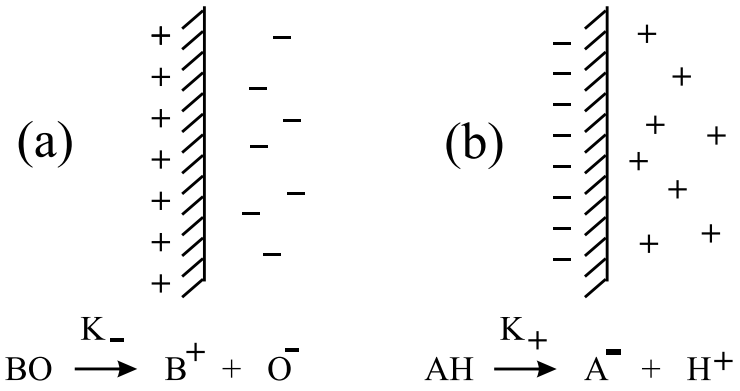

Figure 1.1: Illustration showing two possible dissociation processes leading to positive (a) and negative (b) surface charges.

the potential at contact with the plane, (which fixes one of the BC in the case of constant surface charge previously considered), is not necessarily $-4\pi e\sigma/\varepsilon k_B T$, because ionization of surface groups alters the value of σ through dissociation reactions depending on the potential at the surface $\phi_s = \phi(z = 0)$. The latter depends on the type of surface and on the type of dissociation reaction and si given by the law of mass action

$$\phi_s = \ln \frac{K_\pm}{\rho_s} - \ln\left(\frac{\alpha}{1-\alpha}\right), \tag{1.33}$$

where $\alpha = Z/M$ is the fraction of ionized sites on the surface with M the total number of ionizable sites, and Z number of ionized sites on the surface. $K_\pm$ are the dissociation constants governing the reaction. The sign is chosen depending on the sign of surface charge. The first dissociation constant K_+ in Eq. (1.33) characterizes a reaction which leads to a positively charged surface by releasing negatively charged surface groups into the solution whereas K_- leads to a negative surface charge by releasing positive groups (see fig 1.1). The area A per ionized site (A/M), depends on the chemical structure of the surfaces. Typical values range between $1e$ per $2 - 20\text{nm}^2$, thus charges are typically $1 - 5\text{nm}$ apart from each other on average. Equation (1.33) relates the value of the surface charge to the potential at that surface. Taking into account this relation, the boundary conditions become dependent on the potential at the surfaces. For a dissociation process leading to positive and negative surface charges we have

$$\phi'(0^-) - \phi'(0^+) = \frac{f}{1 + \rho_s e^{+\phi_s}/K_-}; \; + \text{ charged surface.} \tag{1.34}$$

$$\phi'(0^-) - \phi'(0^+) = \frac{f}{1 + \rho_s e^{-\phi_s}/K_+}; \; - \text{ charged surface.} \tag{1.35}$$

In contrast to the fixed surface charge case discussed before, now the surface charge on each plate has to be determined self-consistently from the solution of the PB equations which determine ϕ_s.

1.5 Overview

Many of the properties of colloids have common physicochemical origins, namely, a large number of internal degrees of freedom, weak (soft) interactions between structural elements, and a balance between energetic and entropic contributions to the free energy. Statistical mechanics provides a powerful theoretical framework to study this complex collective behavior, and many of its potential applications are still in their infancy. This thesis is a theoretical study of equilibrium statistical thermodynamic properties of colloidal systems in which electrostatic interactions play a dominant role, namely, charge-stabilized colloidal suspensions. As we have seen, such systems are fluids consisting of a mixture of a large number of mesoscopic particles and microscopic ions which interact via the Coulomb force, suspended in a molecular fluid. Quantum statistical mechanics is essential to fully understand the properties and stability of such systems. A less fundamental but for many purposes, sufficient description, is provided by classical statistical mechanics. In such approximation the system is considered as composed of a great number of charged classical particles with additional hard-core repulsions. The kinetic energy or momentum integrals become independent Gaussians, and hence their contribution to the free energy can be trivially evaluated. The contribution of the potential energy to the free energy on the other hand, depends upon the configuration of all the particles and becomes highly non-trivial due to the long-range character of the Coulomb force and the extremely different length scales involved in the problem. Using the microscopic model described above, we focus on the calculation of equilibrium thermodynamic properties (response functions), correlations (structure factors), and mechanical properties (forces and stresses), which can be measured in experiments and computed by Monte Carlo simulations.

This thesis is divided into three parts. In part I, comprising chapters 2 and 3, we focus on finite-thickness effects in colloidal platelets and rigid planar membranes. In chapter 2 we study electrolyte-mediated interactions between two of such colloidal objects. Several aspects of these interactions are considered including the nature (attractive or repulsive) of the force between the objects, the osmotic properties for different types of surfaces and image charge effects. We find that the interactions are affected by the thickness of the objects when the latter is of the order to the screening length of the electrolyte. The effect was found to be strongly dependent on the nature of the surfaces. In chapter 3 we focus on objects with the same sign of charge and calculate explicitly the solution of the non-linear Poisson-Boltzmann equation in terms of elliptic functions. Making use of this analytical laboratory we study in detail the role of non-linear screening, finite thickness and the phenomenon of "charge relaxation" in which charge can be transferred between the interfaces of each object. We find that this mobility of the surface charges manifests itself in the emergence of additional entropic forces, which have an effect on the disjoining pressure.

In part II, which includes chapters 4 and 5, we consider colloidal mixtures. In chapter 4 we propose a generalization of the cell model which allows the calculation of osmotic properties of polydisperse systems. The volume occupied by the suspension is filled with different spherical cells corresponding to the various colloidal species. An important difference with respect to the traditional cell model is that in the polydisperse case the radii of the cells are not fixed by the total packing fraction of the mixture, but must be calculated self-consistently within the solution of the non-linear Poisson-Boltzmann equation: the

cell radii play the role of parameters which guarantee that the total volume of the suspension is filled with cells. In chapter 5 we consider volume terms for colloidal mixtures. We calculate explicitly the effective interaction potential for a colloidal mixture that results after tracing out the ionic degrees of freedom. We find that the system can be effectively described by a Yukawa mixture, with screening parameter depending on the various colloidal particles densities, plus a volume term depending as well on the colloidal particles densities. This effective interaction potential effectively takes into account many-body interactions, and affects the thermodynamic properties of the mixture.

In part III, namely chapters 6 and 7, we study colloidal dispersions in external fields. In chapter 6 we focus on sedimentation of charge-stabilized colloids. We calculate sedimentation profiles by using a one-component model, which effectively treats the degrees of freedom associated with the ions, and compare the results with Monte Carlo simulations of the primitive model, which treats the ions explicitly. We find good agreement between both methods, which also reproduce recent experimental data. We find that in profiles calculated by Poisson-Boltzmann theory, a renormalized value of the colloidal charge has to be used in order to obtain good agreement with other models and the experiments considered. In chapter 7 we consider sedimentation of polydisperse systems. In particular we exploit the effective interaction potential calculated in chapter 5 to study the "colloidal Brazil nut effect". We focus on deionized systems and study the role of the volume term in the sedimentation profile. We find that in order to obtain good agreement with Monte Carlo simulations of the primitive model, the effect of the volume term must be taken into account in the calculation of the sedimentation profiles. This illustrates the breakdown of pairwise additivity in deionized colloidal interactions.

Part I

Membranes and colloidal platelets

2

Finite-thickness-enhanced attractions

In this chapter we study, within linearized Poisson-Boltzmann theory, the disjoining pressure of two oppositely charged parallel objects (membranes, colloidal platelets) in a 1:1 electrolyte, with a focus on effects of their finite thickness. This extension of the standard Gouy-Chapman model from an interacting *pair* of double layers to a *quartet* (one at each side of the two interacting objects), is shown to significantly enhance the regime of *attractive* interactions, in particular when the separation and the thickness are of the order of the Debye length of the solvent, provided the dielectric mismatch between objects and solvent is not too extreme. The enhancement of the attractions occurs for objects with a fixed charge as well as for those which exhibit charge regulation, but *not* for those with a constant surface potential. The underlying mechanism for this enhancement for thin objects is the transfer of net ionic charge from the electrolyte in between to the other sides. For biological membranes in water this effect is small, however, due to strong image charge effects.

2.1 Introduction

The interactions of charged surfaces across ionic solutions have been extensively studied for decades both theoretically and experimentally, for instance because of their relevance in soft and biological matter, see e.g. Ref.[3]. The key feature of a charged surface in contact with an electrolyte is the formation of a diffuse layer of co- and counterions. The typical thickness of this layer is of the order of the Debye length of the ionic solution, and the net total charge of this diffuse layer is exactly opposite to that of the charges bound to the surface. Whenever two charged surfaces are separated by a distance of the order of a few Debye lengths or less, their diffuse layers will overlap and restructure, giving rise to an effective surface-surface interaction of electrostatic origin [4, 12, 24, 25]. A particularly useful example is (described by) the Gouy-Chapman model, in which *two* parallel

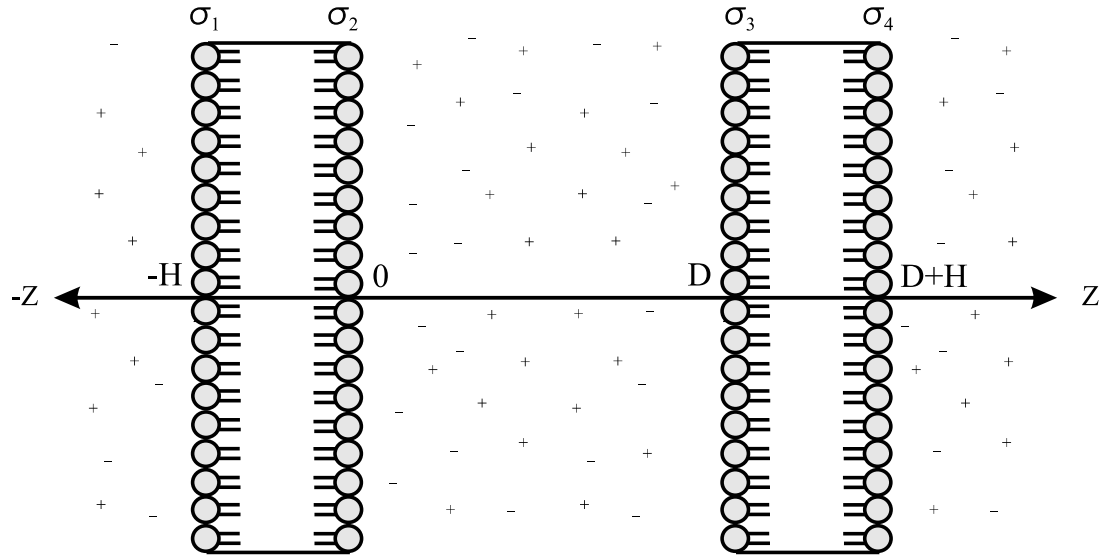

Figure 2.1: Schematic picture of two planar objects (e.g. membranes), each consisting of two charged layers of lipid molecules (a bilayer) of which the apolar tails are facing each other while the charged polar head groups (symbolized by the gray circles) are in contact with an electrolyte of screening length κ^{-1}. The membrane thickness is H, the membrane-membrane separation is D, and the normal cartesian coordinate is z. In this chapter we use the dimensionless thickness $h = \kappa H$, the dimensionless separation $d = \kappa D$, and the dimensionless coordinate $x = \kappa z$.

charged planes separated by distance D are considered, with an electrolyte in a dielectric continuum in the gap between the two planes [26, 27]. The disjoining pressure p, which is the D-dependent force per unit area exerted by one surface on the other, has been extensively studied for different types of surfaces, in particular surfaces with constant charge [28–30], surfaces at constant potential [4], and surfaces with ionizable surface groups that can dissociate [31–36]. Within Poisson-Boltzmann theory it was found that like-charged surfaces necessarily repel, i.e. $p > 0$ for all D, whereas oppositely charged surfaces may repel ($p > 0$) or attract ($p < 0$) each other depending on D and system parameters such as the ratio of the surface charges or the signs of the surface potentials [37, 38]. Apart form describing the interaction of planar surfaces through an intervening electrolyte, the Gouy-Chapman model has been used to study, for instance, the interaction of surfaces with different curvature [25], or to incorporate surface phenomena such as charge regulation involving multiple association-dissociation equilibria, taking into account the formation of Stern layers [39].

The Gouy-Chapman model has recently also been proposed to study the electrostatic interaction between charged membranes [40]. Membranes are structures consisting of a bilayer of amphiphilic lipid molecules with polar head groups and hydrophobic tails as schematically illustrated in Fig. 2.1. Biological membranes, for instance, separate cells or cell compartments with different chemical environments at both sides of the membrane [41–44]. Membranes are often not in isolation but interact with other structures [45–47]. One important example is the delivery of cationic vesicles to cells trough the cell membrane, during which membrane fusion or adhesion can occur [48–50]. As regards

the electrostatic forces, the interaction between planar membranes resembles that between charged colloidal surfaces as e.g. described by the afore mentioned Gouy-Chapman model [40].

Interestingly, however, there is a remarkable feature that has not received too much attention: many membranes and colloidal platelets have a typical thickness H of the order of a (few) nanometer, i.e. H is typically of the same order or even smaller than the Debye length at physiological conditions [41]. This implies that the interactions between two such objects (two membranes or two colloidal platelets) are not only determined by the properties of the two inner surfaces (with surface charges denoted by σ_2 and σ_3 in Fig.2.1) and the electrolyte in between them, but in principle also by the two outer surfaces (with charge densities σ_1 and σ_4 in Fig.2.1) and the electrolyte outside [51]. In other words, the interaction between two such objects involves a quartet rather than a pair of double layers. In this chapter we will show that the relatively small thickness of a membrane (compared to the Debye length), or equivalently that of a thin colloidal platelet, affects, in principle, the nature of the effective electrostatic pair interactions, depending on the dielectric mismatch between the interacting objects and the solvent. In particular we will find a significant enhancement of the surface-charge regimes that give rise to attractive interactions between thin colloidal platelets in an apolar solvent such as toluene, compared to thicker ones. This enhancement of attractive parameter regimes is not only quantitative, but also qualitative in the sense that the short-distance behavior of the disjoining pressure may change, under suitable but identical conditions, from strongly repulsive for thick platelets to attractive for thin ones. For parameters in the regime of biological membranes in water, however, we find that image charge effects give rise to a very weak dependence on the membrane thickness, i.e. the traditional Gouy-Chapman model gives results that are virtually indistinguishable from its extended version presented here.

An important underlying physical phenomenon for "thin" membranes or platelets, that is *not* taken into account in the classical Gouy-Chapman model (in which the charged surfaces are seen as the boundary of a half-space of infinite thickness), is that the net charge in the two overlapping diffuse layers in the vicinity of two surfaces is *not* necessarily exactly compensated by the two surface charges σ_2 and σ_3, as charge can migrate and repartition itself from the electrolyte in between the two membranes to the outer regions: left from the leftmost or right from the rightmost membrane in Fig.2.1. This additional ionic "relaxation mode", which is energetically too costly to be possible for sufficiently "thick" membranes, tends to lower the free energy (or grand potential) of the system, and thus favors less repulsive interactions while the total system remains charge neutral [51].

The focus of this chapter is on the effect of a finite thickness of the two interacting objects, for three types of membrane surfaces, namely those with (a) a constant surface charge, (b) a constant surface potential, and (c) a regulating surface charge based on association-dissociation equilibria at the surfaces. The difference in membrane surface properties manifests itself through different boundary conditions that accompany the Poisson-Boltzmann (PB) equation. For simplicity we work in the linear screening regime throughout, which is appropriate for low surface potentials [52–55], postponing extensions to nonlinear PB theory to the next chapter. The details of the theory and the boundary conditions for the index-matched case will be discussed in section 2.2, and the results for the electric potential and the disjoining pressure in section 2.3. We proceed with a few calculations for the case of a dielectric mismatch between the objects and the

solvent, followed by a conclusion.

2.2 Linear Poisson-Boltzmann Model for Charged Planar Objects

We consider two interacting objects, say membranes to be specific, of thickness H and closest surface-to-surface distance D, as depicted in Fig.2.1. The charged surface groups are modelled as surface charge densities in the planes located at $z_1 = -H$, $z_2 = 0$, $z_3 = D$ and $z_4 = H + D$, with surface charge densities σ_1, σ_2, σ_3, and σ_4, respectively. The region $z_1 < z < z_2$ corresponds to the interior of the left membrane, and $z_3 < z < z_4$ to the interior of the right membrane. The regions outside the membranes are filled with an electrolyte solution of dielectric constant ϵ at temperature T. In the interior of the membranes there is no electrolyte present, instead there is a medium that we consider, for simplicity, to be of the same dielectric constant as that of the electrolyte solution in order to avoid electrostatic image effects. The effects of a dielectric mismatch will be discussed later. The system is assumed to be in contact with a monovalent salt reservoir of salt density $2\rho_s$ such that the electrolyte has screening length $\kappa^{-1} = (8\pi\lambda_B\rho_s)^{-1/2}$, with $\lambda_B = e^2/(k_BT\varepsilon)$ the Bjerrum length. Here e is the elementary charge and k_B the Boltzmann constant. In what follows, all lengths will be conveniently given in units of the Debye length, namely $d = \kappa D$, $h = \kappa H$, and $x = \kappa z$. Within the present linear model, the dimensionless electrostatic potential $\phi = e\psi/(k_BT)$, with ψ the electrostatic potential, satisfies the linearized Poisson-Boltzmann equation

$$\phi''(x) = \begin{cases} \phi(x), & \text{within the electrolyte;} \\ 0, & \text{within the membranes,} \end{cases} \tag{2.1}$$

where a prime denotes a derivative with respect to the Cartesian coordinate x perpendicular to the surfaces.*. Imposing the boundary condition that $\phi(\pm\infty) = 0$ (which implies global charge neutrality) gives, for the geometry of Fig.2.1, a solution of the form

$$\phi(x) = \begin{cases} A_1 e^x & \text{for } x < -h \\ a_1 x + a_2 & \text{for } -h \le x < 0 \\ A_2 e^{-x} + A_3 e^x & \text{for } 0 \le x < d \\ a_3 x + a_4 & \text{for } d \le x < d + h \\ A_4 e^{-x} & \text{for } x \ge d + h \end{cases} \tag{2.2}$$

where the eight integration constants $\{A_i, a_i\}$ for $i = 1, ..., 4$ are to be fixed by eight boundary conditions (BC's) at the four surfaces located at $x = x_i = -h, 0, d, d + h$, for $i = 1, \cdots, 4$, respectively. Four out of eight BC's are obtained from the continuity of the potential at the four surfaces,

$$\phi(x_i^-) = \phi(x_i^+), \quad \text{continuity of } \phi(x), \tag{2.3}$$

for $i = 1, ..., 4$. Here $\phi(x_i^\pm)$ is short for $\lim_{\varepsilon\downarrow 0} \phi(x_i \pm \varepsilon)$. The remaining four BC's will be chosen such that either (a) the charge density σ_i at each surface is fixed, or (b) the

*Notice that $\phi(x) = 1 \Rightarrow \psi = 25mV$ at room temperature

potential φ_i at each surface is fixed, or (c) charge regulation takes place at each surface. In principle combinations of these BC's are possible, e.g. a fixed charge for some and charge regulation for other surfaces [38], but such cases will not be considered here.

In the case of a constant surface charge, the second set of four boundary conditions takes the form

$$\phi'(x_i^-) - \phi'(x_i^+) = f_i, \quad \text{constant surface charge,} \tag{2.4a}$$

where $f_i = 4\pi\lambda_B(\sigma_i/e)/\kappa$ is the dimensionless surface charge density of surface $i = 1, \cdots, 4$, or, equivalently, f_i is the ratio of the Debye length κ^{-1} and the Gouy-Chapman length $\Lambda_i = e/(4\pi\sigma_i\lambda_B)$. Note that f_i is also an estimate of the electrostatic energy compared to the characteristic energy of thermal fluctuations in the system. As a consequence, the present linear screening theory is limited to the regime $|f_i| \lesssim 1$. In order to study highly charged membranes, for which $|f_i| \gg 1$, non-linear screening has to be taken into account (See e.g. [51] and Chap. 3).

If the potential at the surfaces is kept fixed at values φ_i for $i = 1, \cdots, 4$, the second set of four BC's takes the form

$$\phi(x_i) = \varphi_i, \quad \text{constant potential} \tag{2.4b}$$

where it is understood that φ_i assumes small values in order for linear screening theory to be applicable [55]. We will see below that this constant-potential case is insensitive to the thickness of the membranes.

In the case of charge-regulating surfaces we presume that only a fraction α_i of the ionizable sites of surface i is actually ionized, with $0 \leq \alpha_i \leq 1$. Denoting the dimensionless maximum surface charge densities by f_i, analogous to the expression just below Eq.(2.4a), we can write the charge regulation BC's as

$$\phi'(x_i^-) - \phi'(x_i^+) = f_i\alpha_i, \quad \text{charge regulation.} \tag{2.4c}$$

The relation between the potential $\phi(x_i)$ and the surface charging parameter α_i follows from the law of mass action, which can be written as [39]

$$K_\pm = \frac{\alpha_i\rho_s \exp(\mp\phi(x_i))}{1-\alpha_i}, \tag{2.5}$$

where we introduced the reaction constants K_+ for desorbing cations (hence $f_i < 0$) and K_- for desorbing anions (hence $f_i > 0$). The mass action condition (2.5) describes the chemical equilibrium between the desorbed ions, which we assume here to be identical to the monovalent ions of the suspending electrolyte for simplicity, and the adsorbed ions which form neutral groups on the surfaces. Below we describe the equilibrium constants by the dimensionless combination $r_\pm = \rho_s/K_\pm$, and we expand Eq.(2.5) to linear order in $\phi(x_i)$ to be consistent with the linear screening theory.

For a given set of eight BC's, consisting of Eq.(2.3) and one out of the set of Eqs.(2.4a), (2.4b), and (2.4c), the integration constants $\{A_i, a_i\}$ can be determined straightforwardly by solving a system of eight coupled linear equations. Once the potential $\phi(x)$ is known, the disjoining pressure p between the two membranes, as e.g. given in Ref. [4] as

$$\frac{\beta p}{\rho_s} = -\left(\frac{d\phi(x)}{dx}\right)^2 + \phi^2(x), \tag{2.6}$$

is known explicitly, where p is to be evaluated for any $x \in (x_2, x_3)$ —that p is a constant independent of x in this interval is easily checked by considering its derivative with respect to x and using that $\phi(x)$ is a solution of Eq.(2.1).

We finish this section by noting that the BC's (2.4a) are slightly different from the equivalent ones in the standard Gouy-Chapman theory, in the sense that the *difference* of the electric fields at the two sides of the surface are here proportional to the surface charge density of the surface (as follows from the Maxwell equations). The standard Gouy-Chapman theory presumes a vanishing electric field inside the membrane, which corresponds, as we will see, to presuming the membrane to be much thicker than the the Debye length. An interesting consequence of Eq.(2.4a) is that the net charge of the "middle subsystem", defined here to consist of the two planes at $x_2 = 0$ and $x_3 = d$ together with the electrolyte in between them is not necessarily zero, as net charge can be transported to the outer regions $x < x_1$ and $x > x_4$. This can be made explicit by defining and calculating the dimensionless charge per unit surface area of the middle subsystem,

$$\Gamma = f_2 + f_3 - \int_{x_2}^{x_3} dx \phi(x) = \phi'(0^-) - \phi'(d^+), \tag{2.7}$$

where the integral represents the (dimensionless) electrolyte charge, and where we used the PB equation (2.1) and the BC's of Eq.(2.4a). Clearly, this reduces to $\Gamma = 0$ in the case of the usual Gouy-Chapman BC's, but generally $\Gamma \neq 0$ in the present case. In fact one sees that the middle subsystem is only charge neutral if the electric fields inside the two membranes are the same in sign and magnitude. The total system remains of course charge neutral.

2.3 Results and discussion

2.3.1 Fixed surface charges

Let us consider now the case of fixed surface charge for interacting dissimilar membranes. Here we focus on the particular case in which the surface charge on each side of a membrane is the same, i.e., $f_1 = f_2 = f_L$ and $f_3 = f_4 = f_R$, where the subscripts refer to the left and right positioned membrane. Fig. 2.2 shows the mean electrostatic potential $\phi(x)$, in each panel for three different membrane thicknesses $h = 1000$, $h = 5$, and $h = 1$, and in all cases for $f_L = 1$. In Figs. 2.2(a) and (b) the separation between the two membranes is three times the Debye length ($d = 3$), with $f_R = 0.5$ (like-charged) in (a) and $f_R = -0.5$ (oppositely charged) in (b). In Figs.2.2(c) and (d) the separation is half a Debye lenght ($d = 0.5$), with the same surface charge densities as in (a) and (b), respectively. A few global observations from Fig.2.2 are that the effect of the finite membrane thickness h on the potential in between the two membranes is relatively small for the larger separation $d = 3$ and significantly stronger for $d = 0.5$, that the slopes $\phi'(0^-)$ and $\phi'(d^+)$ inside the membranes are non-vanishing for $h = 5$ and especially for $h = 1$ such that a substantial charge migration from inside to outside (or vice versa) takes place on the basis of Eq.(2.7), and that $|\phi(x)| \lesssim 1$ in (a), (b), and (d) such that linear screening theory for these parameters is expected to be rather accurate, in contrast to the like-charged membranes at close contact in (c). In the remainder of this section we will focus on the case of oppositely charged membranes, such as in Fig.2.2(b) and (d).

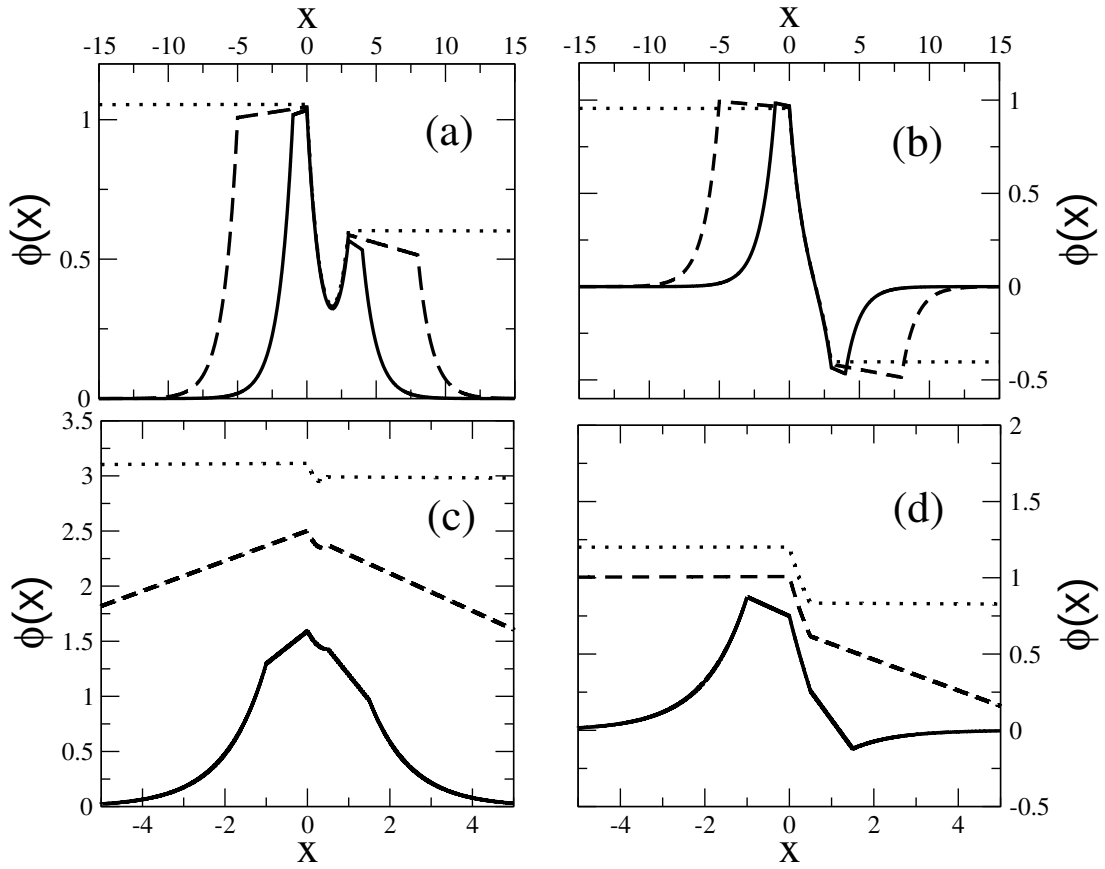

Figure 2.2: Mean dimensionless electrostatic potential $\phi(x)$ for two planar membranes in the geometry of Fig.2.1, in each panel for three thicknesses $h = 1000$ (dotted line), $h = 5$ (dashed line), and $h = 1$ (solid line), for a fixed left surface charge density $f_L = 1$ and for several combinations of surface-surface separation d and right surface charge f_R. In (a) and (b) we have a relatively large separation $d = 3$, and in (c) and (d) a small separation $d = 0.5$; in (a) and (c) we have two-like charged surfaces $f_R = 0.5$, and in (b) and (d) two oppositely charged surfaces $f_R = -0.5$. Note that all surface charges are small enough for the linear screening theory to apply, except for the small separation of the like-charged thick membranes in (c) [51].

In Fig.2.3 we plot the dimensionless disjoining pressure p as a function of the membrane-membrane separation d, as obtained from Eq.(2.6), for surface charge densities $f_L = 1$ and $f_R = -0.5$ as in Figs.2.2(b) and (d), for several membrane thicknesses $h = 1$, 5, 10, 1000. Interestingly, for the thinnest membrane, $h = 1$, the interaction is attractive ($p < 0$) for any separation d, whereas for thicker membranes the interaction is only attractive for sufficiently large separations $d \gtrsim 1$ and repulsive for separations smaller than about 1 Debye length. Evidently, the finite thickness of membranes has an effect on the nature of their interactions. It is also interesting to note from Figs.2.2 and 2.3 that for $d = 0.5$ and $h = 1, 5$, the surface potentials have the same sign and yet the interaction is attractive. For $d = 0.5$ and $h = 1000$ we find from Figs.2.2 and 2.3 that p, $\phi(0)$ and $\phi(d)$ are all positive. It turns out, as we will show below, that there are actually three regimes for oppositely charged membranes, (i) a regime where the interaction is repulsive with equal

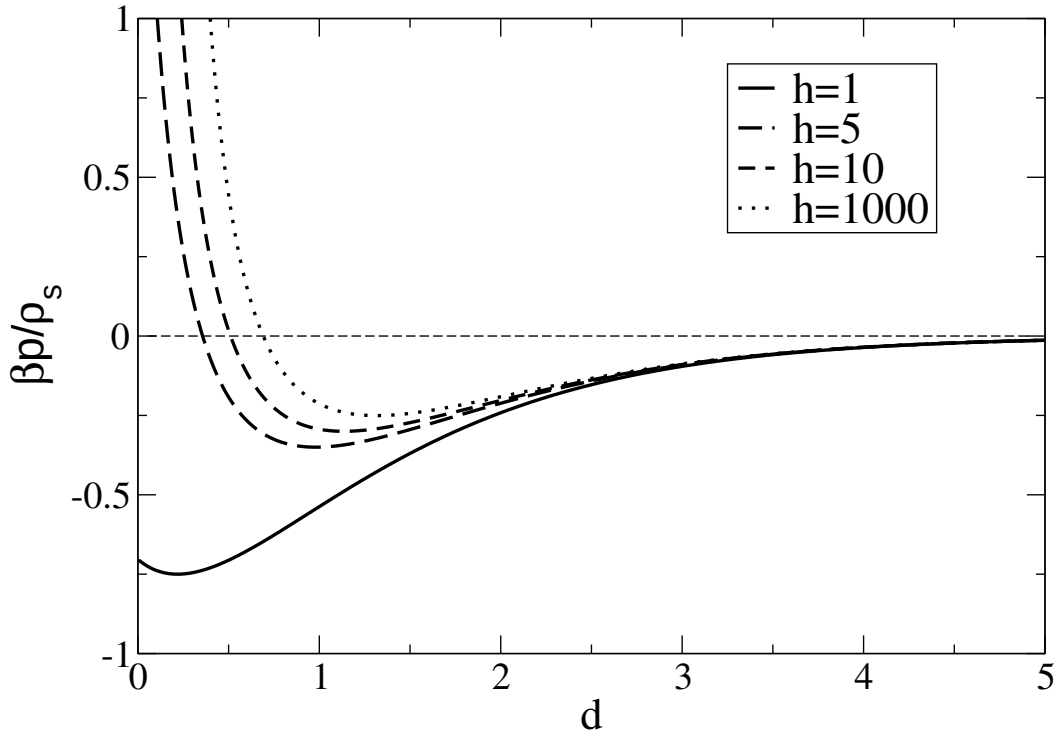

Figure 2.3: Reduced disjoining pressure as a function of the membrane-membrane separation d, for different membranes thicknesses, and oppositely charged membranes with reduced surface charge densities $f_L = 1$ and $f_R = -0.5$. Note that the finite thickness h enhances the attractive nature, $p < 0$, of the membrane-membrane interaction.

surface potential signs, (ii) an attractive regime with equal surface potential signs, and (iii) an attractive regime with opposite potential signs.

The charge ratio and the membrane separation d for which the crossover from repulsion to attraction occurs can be studied using the technique introduced by Parsegian and Gingell [37] and more recently by Russ *et al.* in Ref.[47] . After solving the PB equation, the condition of vanishing disjoining pressure i.e. $p = 0$ in equation (2.6), allows to find a relation between the surface charges and the geometrical parameters that separate the regions of negative (attraction) and positive (repulsion) pressure between the membranes. In the case of four dissimilar dimensionless surface charges f_i we obtain from the condition $p = 0$ a relation between the parameters f_1, f_2, f_3, f_4, h and d. This condition leads to two branches that we write as

$$\frac{\sigma_2}{\sigma_3} = -\frac{e^{-d}(2f_1e^d + f_1e^dh + f_3h + f_4h + f_3h^2}{f_3(1+h)(2+h)}; \tag{2.8a}$$

$$\frac{\sigma_2}{\sigma_3} = -\frac{f_1h + e^d(2+h)(f_3 + f_4 + f_3h)}{f_3h(1+h)}. \tag{2.8b}$$

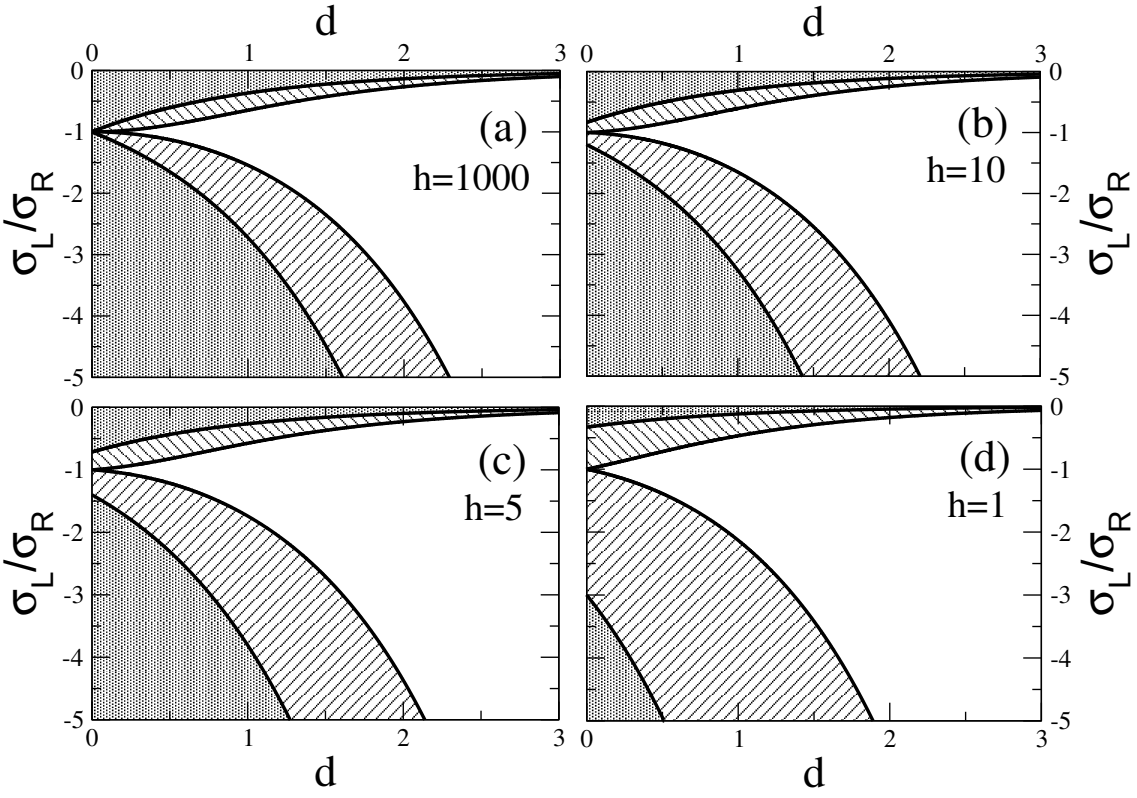

Figure 2.4: Diagrams indicating attractive (white and hatched) and repulsive (dark) regimes between oppositely charged membranes as a function of their separation d and the ratio of surface charge densities $\sigma_L/\sigma_R < 0$, for several membrane thicknesses h. The attractive regime consists of a part in which the two surface potentials have opposite signs (white), and two parts where they have the same sign (hatched). Note that the attractive parameter regime is enhanced considerably for thinner membranes.

In the limit $h \to \infty$ we recover the results by Parsegian and Gingell, $\sigma_2/\sigma_3 = -e^{\pm d}$ which is independent of the values of f_1 and f_4 [37]. In the particular case discussed above, $\sigma_1 = \sigma_2 = \sigma_L$ and $\sigma_3 = \sigma_4 = \sigma_R$, we obtain attractions provided

$$-\frac{h+2}{h}e^{d} < \frac{\sigma_L}{\sigma_R} < -\frac{h}{h+2}e^{-d}, \quad \text{attraction,} \tag{2.9}$$

and repulsions otherwise. The result of Eq.(2.9) shows explicitly that the attraction regime for oppositely charged membranes is enhanced, for any separation d, for smaller thickness h: the lower bound for σ_L/σ_R becomes more negative and the upper bound less negative with decreasing h.

In a similar fashion relations can be obtained to study the sign of the potential at the inner surfaces, $\phi(0)$ and $\phi(d)$, as a function of the geometrical parameters. In the particular case $\sigma_1 = \sigma_2 = \sigma_L$ and $\sigma_3 = \sigma_4 = \sigma_R$ we obtain that both $\phi(0) < 0$ and

$\phi(d) < 0$ provided

$$\frac{\sigma_L}{\sigma_R} < -\frac{1+h}{(1+h)\cosh(d)+\sinh(d)} \vee \phi(0) < 0; \tag{2.10a}$$

$$\frac{\sigma_L}{\sigma_R} < -\frac{(1+h)\cosh(d)+\sinh(d)}{1+h} \vee \phi(d) < 0, \tag{2.10b}$$

whereas at least one of the two surface potentials is positive otherwise. Again, in the limit $h \to \infty$ we recover Parsegian and Gingell's results [37].

In Fig.2.4 we plot diagrams, for several membrane thicknesses h, that indicate the attractive (white and hatched) and repulsive (dark) regimes, as a function of the separation d and the ratio of (negative) surface charge ratios σ_L/σ_R. The separation between the attractive and repulsive parameter regime (i.e. the boundary between hatched and dark in Fig.2.4) follows from the $p = 0$ conditions given by Eqs.(2.8a) and (2.8b). The attractive regime splits into a regime with opposite surface charges (white) and equal-signed ones (hatched) as follows from Eqs.(2.10a) and (2.10b). One global observation from Fig.2.4 is the smaller parameter regime for repulsions (i.e. a decreasing dark area) upon a decreasing membrane thickness h. Another observation is the relatively weak sensitivity of the white area on the parameter h, i.e. the main growth of the attractive regime with decreasing h is due to the growth of the regime with equal-signed surface potentials. Finally we conclude from Fig.2.4 that the effect of a finite membrane thickness on the attractive and repulsive nature of the membrane interactions is larger at short distances $d \lesssim 1$ than at larger distances. This is most evident from the $d = 0$ limit of the four diagrams shown in Fig.2.4, where attractions are only observed for exactly oppositely charged membranes ($\sigma_L/\sigma_R = -1$) in the thick membrane limit ($h = 1000$), whereas contact attractions occur for a whole regime $-3 \lesssim \sigma_L/\sigma_R \lesssim -0.4$ for membranes with a thickness of the Debye length ($h = 1$). In other words, it is only possible to bring two thick membranes in contact without experiencing any electrostatic repulsion by carefully adjusting $\sigma_L = -\sigma_R$, whereas for thin membranes no such fine tuning of the opposite surface charges is required since the region of attractions "opens" up.

It is interesting to correlate the finite-thickness induced enhancement of the parameter regime for attractive interactions between oppositely charged membranes to the (dimensionless) net charge Γ of the "middle subsystem" as defined in Eq.(2.7). For the case of present interest, $f_1 = f_2 = f_L$ and $f_3 = f_4 = f_R$, Eq.(2.7) takes the explicit form

$$\Gamma = \frac{2(f_L + f_R)}{e^d(2+h) - h}, \tag{2.11}$$

which shows that $\Gamma = 0$ for exactly oppositely charged membranes, $f_L = -f_R$, and that $\Gamma \to 0$ for $d, h \to \infty$, where the d-dependence is exponential and the h-dependence algebraic. For finite h and d one finds $\Gamma \neq 0$ provided $f_L \neq -f_R$. In Fig.2.5 we plot Γ for $f_L = 1$, in each panel for several membrane thicknesses $h = 1000$, 10, 5, and 1, where the case $h = 1000$ is hardly distinguishable from $\Gamma = 0$ on the scale of the plots. In panel (a) and (b) we plot Γ as a function of f_R for fixed separations $d = 1$ in (a) and $d = 5$ in (b), and in (c) and (d) as a function of d at fixed surface charge density $f_R = 0.5$ in (c) and $f_R = -0.5$ in (d). These numerical examples, and of course also Eq.(2.11), show that Γ takes the sign of the most highly charged one of the two approaching surfaces, such that the system has a tendency to "squeeze-out" counterions of the same charge of the most highly charged surface from the region in between the membranes to the exterior

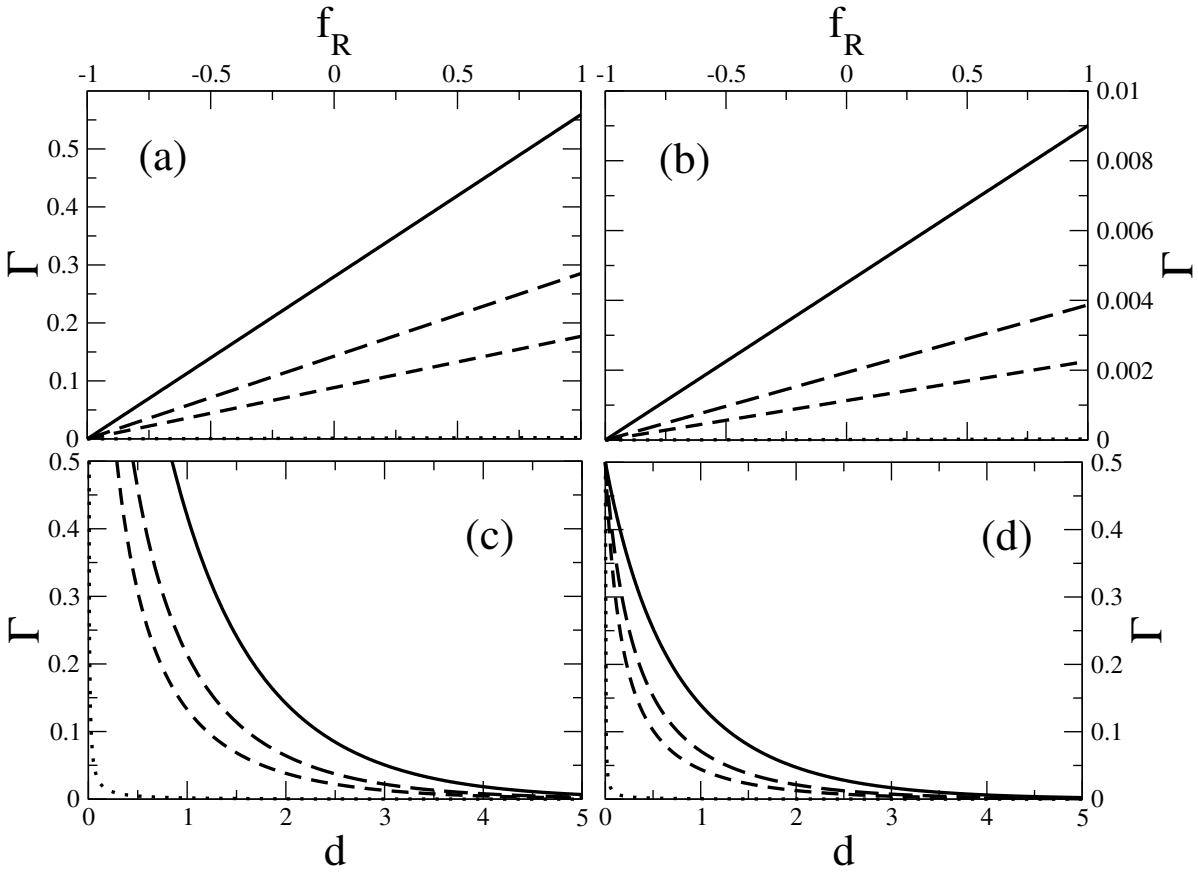

Figure 2.5: The dimensionless net charge Γ of the subsystem in between the two membranes (see text) for membranes of different thicknesses $h = 1000$ (dotted lines), $h = 10$ (long dashed lines), $h = 5$ (short dashed lines), and $h = 1$ (solid lines), in all cases for the left-membrane surface charge density $f_L = 1$. In (a) and (b) Γ is plotted as a function of the surface charge density f_R, with the separation fixed at $d = 1$ in (a) and $d = 5$ in (b). In (c) and (d) Γ is shown as a function of d, with $f_R = 0.5$ in (a) and $f_R = -0.5$ in (b).

electrolyte. Fig.2.5 also shows that in all cases $|\Gamma| \lesssim |f_2 + f_3|/10$ for $d \gtrsim 3$ and $h \geq 10$ or so. However, for $d \lesssim 2$ and $h \lesssim 5$, i.e. for nearby thin membranes, a substantial fraction of the membrane surface charge at $x_2 = 0$ and $x_3 = d$ is *not* balanced by the electrolyte in between x_2 and x_3 since Γ deviates substantially from zero in these regimes. For these parameters some of the compensating charge is squeezed-out to the electrolyte left of the left membrane and/or right of the right membrane. In other words, the parameter regime of nearby and thin membranes, say $d \lesssim 2$ and $h \lesssim 5$, is such that the "middle subsystem" is no longer charge neutral due to net charge being pushed away, more so for smaller thickness h. (Of course the system as a whole remains neutral.) As a consequence the pressure-distance curve between the two objects of interest depends substantially on their thickness, in this parameter regime.

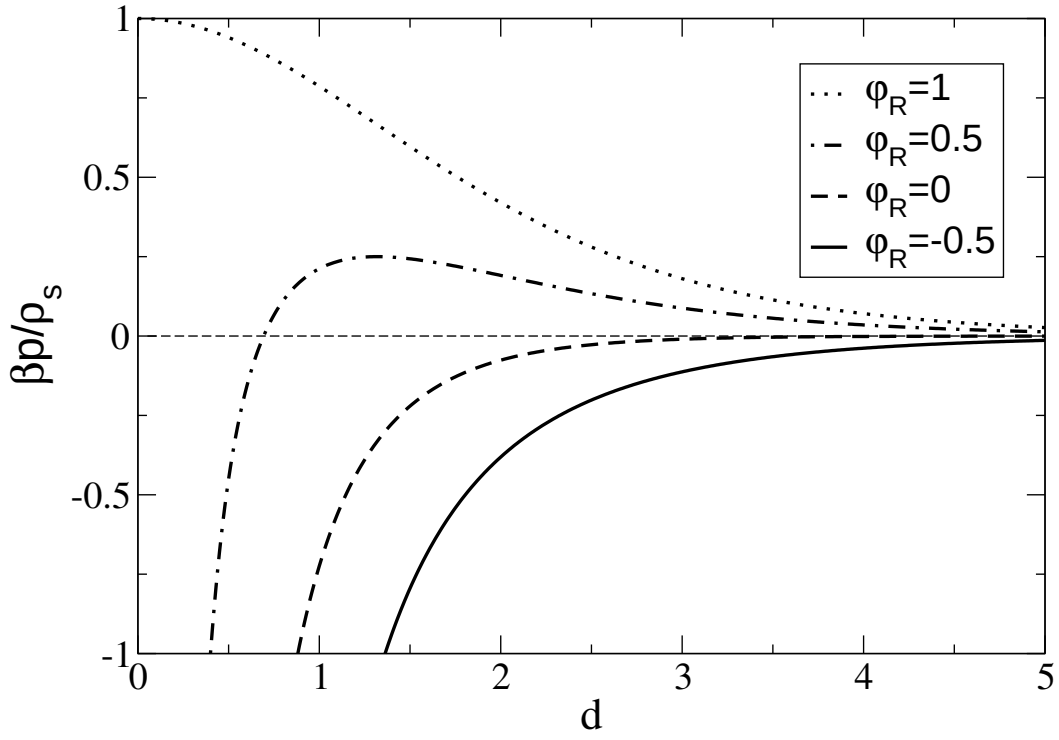

Figure 2.6: Disjoining pressure p as a function of the membrane separation d for fixed surface potential $\phi_L = 1$ of the left membrane, for several right-membrane potentials ϕ_R. In this constant-potential case the disjoining pressure is independent of the finite thickness of the membranes.

2.3.2 Fixed surface potential

In the case of fixed surface potentials the disjoining pressure turns out to be unaffected by the finite thickness of the two objects, say membranes. The reason is that the solution of Eq.(2.1) for $x_2 < x < x_3$, and hence also p from Eq.(2.6), is fully determined for fixed φ_2 and φ_3. Attraction or repulsion between the membranes can be observed depending on the value of the potential at the surfaces. In Fig.2.6 we plot the disjoining pressure p as a function of the separation d for a fixed potential $\varphi_1 = \varphi_2 = 1$ of the leftmost membrane for several potentials $\varphi_3 = \varphi_4 = \varphi_R$ of the rightmost one. We focus on small values of the potential where the present linear screening theory is applicable. The pressure changes from a purely repulsive character for all d at $\varphi_R = 1$ to purely attractive for $\varphi_R = -0.5$, with an interesting intermediate regime involving a repulsive barrier and an attractive close-contact force for $\varphi_R = 0.5$. Notice that it is possible to have (short-ranged) attractions between the membranes even though their surface potentials have the same sign.

2.3.3 Charge regulation

In the case of charge regulation boundary conditions, the finite size of the membranes does affect the disjoining pressure. This is illustrated in Fig.2.7 where we plot the reduced pressure as a function of the separation distance d between the membranes, in each panel for different membrane thicknesses $h = 1000$, 10, 5, and 1, and in all cases for a maximum surface charge density characterized by $f_1 = f_2 = f_L = 1$ and $f_3 = f_4 = f_R = -0.5$, i.e. the two membranes are oppositely charged. The dimensionless equilibrium constants are taken such that (a) $r_L = r_R = 0$, (b) $r_L = 0$ and $r_R = 3$, (c) $r_L = 3$ and $r_R = 0$, and (d) $r_L = r_R = 3$. Note that the choice $r_i = 0$ implies from Eq.(2.5) that membrane surface i is fully charged, $\alpha_i = 1$, while $r_i > 0$ implies that only a finite fraction of surface groups is charged, $0 < \alpha_i < 1$. One checks, therefore, that the disjoining pressure shown in Fig.2.7(a) is identical to that in Fig.2.3(a), and that the pressure becomes weaker in magnitude for the increasing r_i's from (a) through (d) as the surfaces carry a decreasing charge. We observe, nevertheless, that also in the charge-regulation case the parameter regime of attraction between the membranes is enhanced for membranes with a smaller thickness h. It is also interesting to compare Fig.2.7(b) and (c), for which the equilibrium constants are asymmetric, and where repulsions are more dominant in (b) than in (c), certainly for the thinnest membrane, with $h = 1$, that we considered. One checks that (b) is the more asymmetric case (with a fully positively charged left surface and a partially negatively charged right surface), for which one indeed expects a larger repulsive parameter regime on the basis of our findings for constant surface charges.

One interesting particularity of charge regulation boundary conditions of the present four-surface model is that both the potentials $\phi(x_i)$ and the charges $\alpha_i f_i$ on the surfaces $i = 1, \cdots, 4$ vary with the separation d depending on the membrane thickness h. This is illustrated in Fig.2.8, where we plot the four surface potentials (in (a) and (b)) and combinations of the effective charges of the two left (L) and the two right (R) membranes (in (c) and (d)), as a function of their separation d for two rather extreme thicknesses $h = 1000$ and $h = 1$. The combinations plotted in Fig.2.8(c) and (d) are the difference between the charge density of the inner and outer surface of both the left (L) and the right (R) membrane, i.e., $f_2\alpha_2 - f_1\alpha_1 = f_L\alpha_L^{in} - f_L\alpha_L^{out}$ and $f_3\alpha_3 - f_4\alpha_4 = f_R\alpha_R^{in} - f_R\alpha_R^{out}$. In all panels of Fig.2.8 we take for the left maximum surface charge densities $f_1 = f_2 = f_L = 1$, and all four equilibrium constants are identical such that $r_i = 1$. The right surface charges are $f_3 = f_4 \equiv f_R$, with the perfectly anti-symmetric case $f_R = -1$ in Fig.2.8(a) and (c), and $f_R = -0.5$ in (b) and (d). In (a) and (b) the branches with $|\phi(x_i)|$ closer to zero correspond to the inner surfaces, i.e. $i = 2, 3$, which are labelled explicitly in the figures (a) and (b) for clarity. The first observation from the surface potentials shown in (a) and (b) is that all membrane surfaces reach a well-defined limiting value when $d \gtrsim 5$, independent of the thickness h, i.e. for separations larger than, say, five Debye lengths the two membranes hardly affect each other and as a consequence both sides of each membrane have the same potential and carry the same charge (because of the symmetric parameter choice for both surfaces of a given membrane). Fig.2.8(a) and (b) show that for thick membranes, $h = 1000$, the state of the outer two surfaces $i = 1, 4$ does not vary with d whereas the absolute potentials of the inner membrane surfaces $i = 2, 3$ vary significantly with $d \lesssim 3$. Note that some variation of $\phi(x_2)$ and $\phi(x_3)$ with d is necessary, both for thin and thick membranes, since continuity of the potential imposes that $\phi(x_2) = \phi(x_3)$ if $d = 0$; this limit is satisfied for all cases in Fig.2.8. For

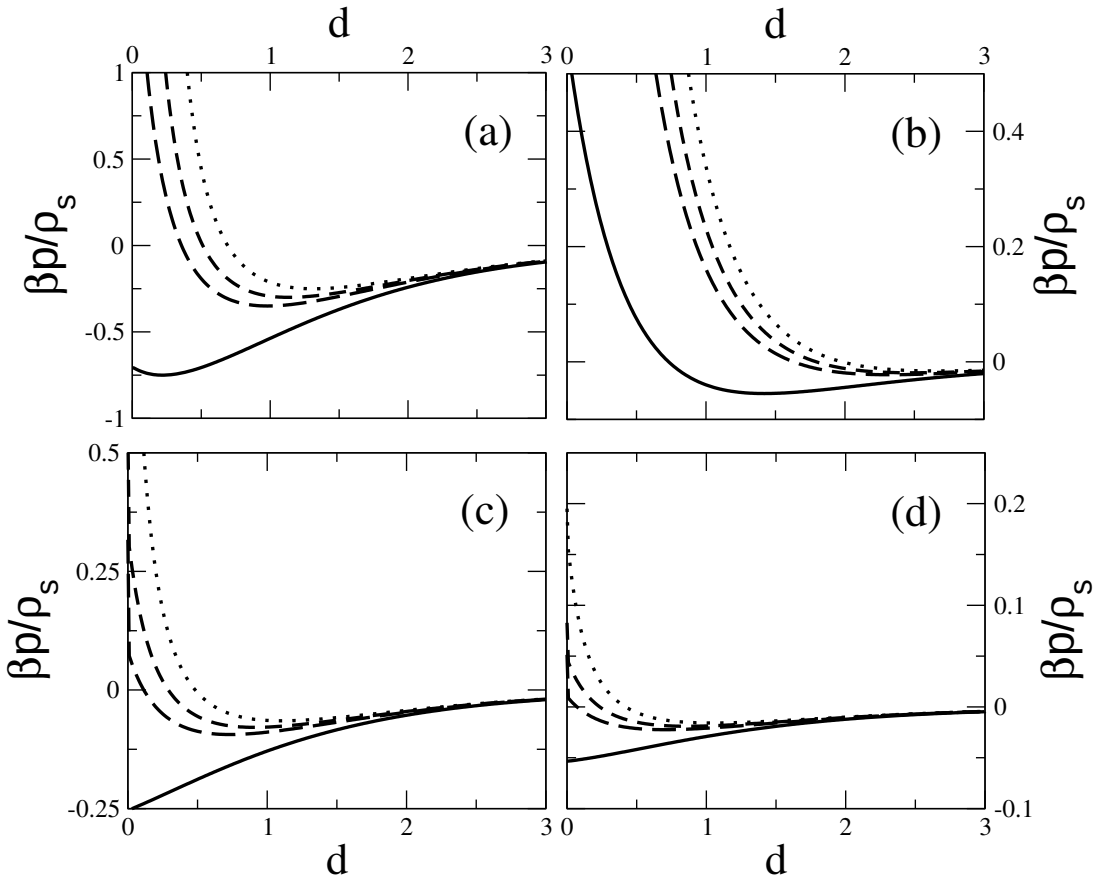

Figure 2.7: Reduced pressure as a function of the separation d for charge regulation boundary conditions, for maximum surface charge densities $f_L = 1$ and $f_R = -0.5$ for the left- and rightmost membrane, respectively, in each panel for several membrane thicknesses $h = 1000$ (dotted), $h = 10$ (long dashed), $h = 5$ (short dashed), and $h = 1$ (full curve). The different panels represent results for different surface reaction constants, (a) $r_L = r_R = 0$, (b) $r_L = 0$ and $r_R = 3$, (c) $r_L = 3$ and $r_R = 0$, and (d) $r_L = r_R = 3$.

the thinner membranes, $h = 1$, the variation with d of the inner surface potential is rather similar to the case $h = 1000$, certainly in (a), whereas for these thinner membranes also the outer surface potentials vary significantly with d, thereby changing the net charge of the outer surfaces. As regards the difference between the charge on the inner and outer surface of a membrane, as shown in Fig.2.8(c) and (d), we note (i) that the inner and outer surface carry the same charge for separations larger than several Debye lengths, regardless the thickness h, (ii) that this difference is no longer vanishingly small for separations smaller than a few Debye lengths, and (iii) that the difference between inner and outer surface charge tends to be more pronounced for thicker membranes. Generally we see that the inner surfaces carry, for the present parameter choices, a higher absolute net charge than the outer ones —in agreement with the law of mass action (2.5) and the information from Fig.2.8(a) and (b) that for fixed h and d we have $|\phi(x_{1(4)})| > |\phi(x_{2(3)})|$. This finding describes actually another mechanism with which the present system can "transport" charge towards or away from different sides of the membranes; in this case it

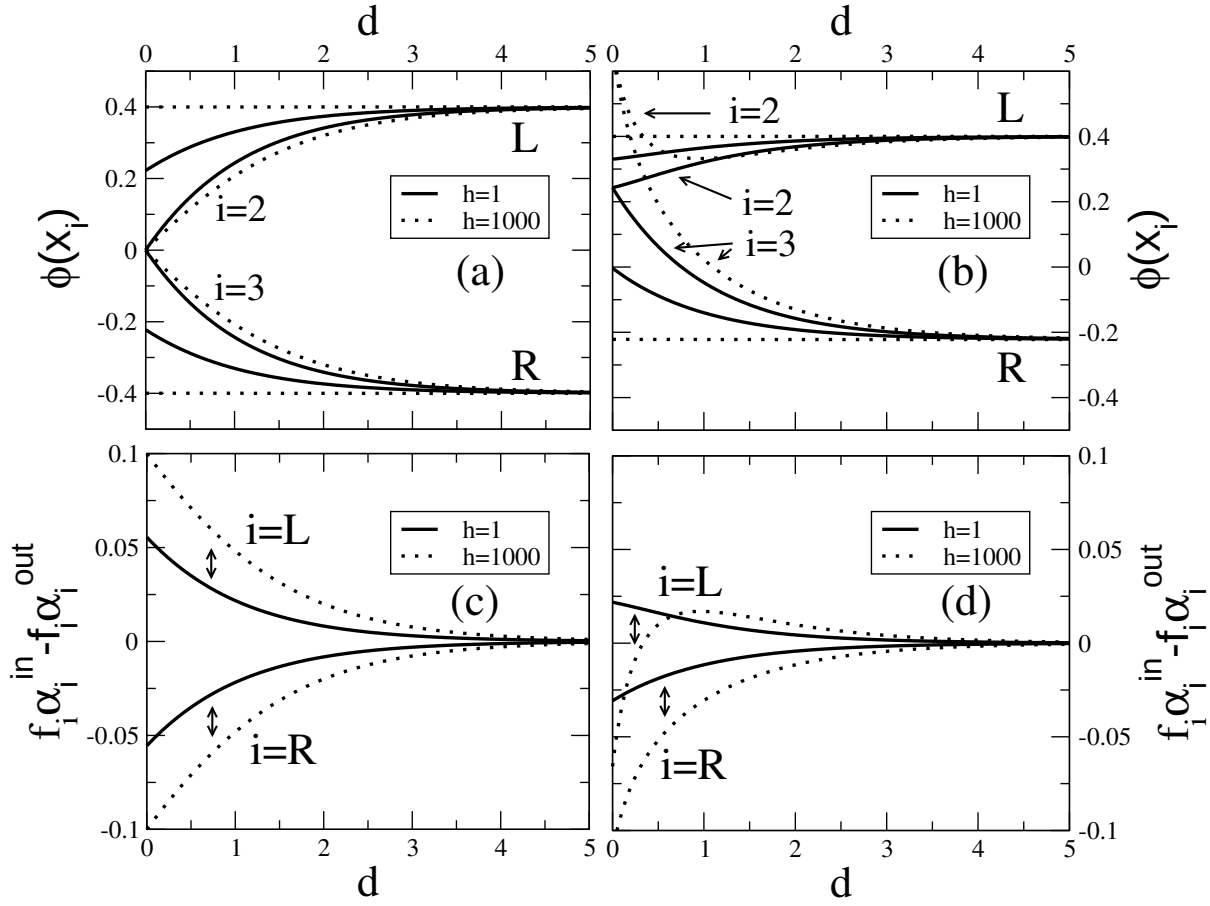

Figure 2.8: Surface potentials ((a) and (b)) and charge difference (see text) between the inner and outer side of the left (L) and right (R) membrane ((c) and (d)), as a function of the separation distance d between the membranes, for thick membranes ($h = 1000$, dotted) and thin ones ($h = 1$). In all cases the membranes are charge regulating, with a maximum charge density $f_L = 1$ and equilibrium constants $r_i = 1$ for all four surfaces $i = 1, \cdots, 4$ (see text), in (a) and (c) for $f_R = -1$ and in (b) and (d) for $f_R = -0.5$.

concerns surface charges in contrast to the ionic charges that can be placed at either side of the membrane surface in the case of a finite thickness h. It is, finally, interesting to observe from (c) and (d) that the charge difference between inner and outer surfaces tends to grow monotonically with decreasing d, except for the $h = 1000$ leftmost membrane in (d), for which the outer surface carries a higher charge than the inner one at separations $d \lesssim 0.5$.

2.4 Image charge effects

We have seen that the finite-thickness of *index-matched* oppositely charged membranes or colloidal platelets enhances their mutual attraction (or reduces their repulsion) due to the relocation of ions from the region between the interacting objects towards the outside regions: the larger ion-density in the outside regions affects the disjoining pressure in a

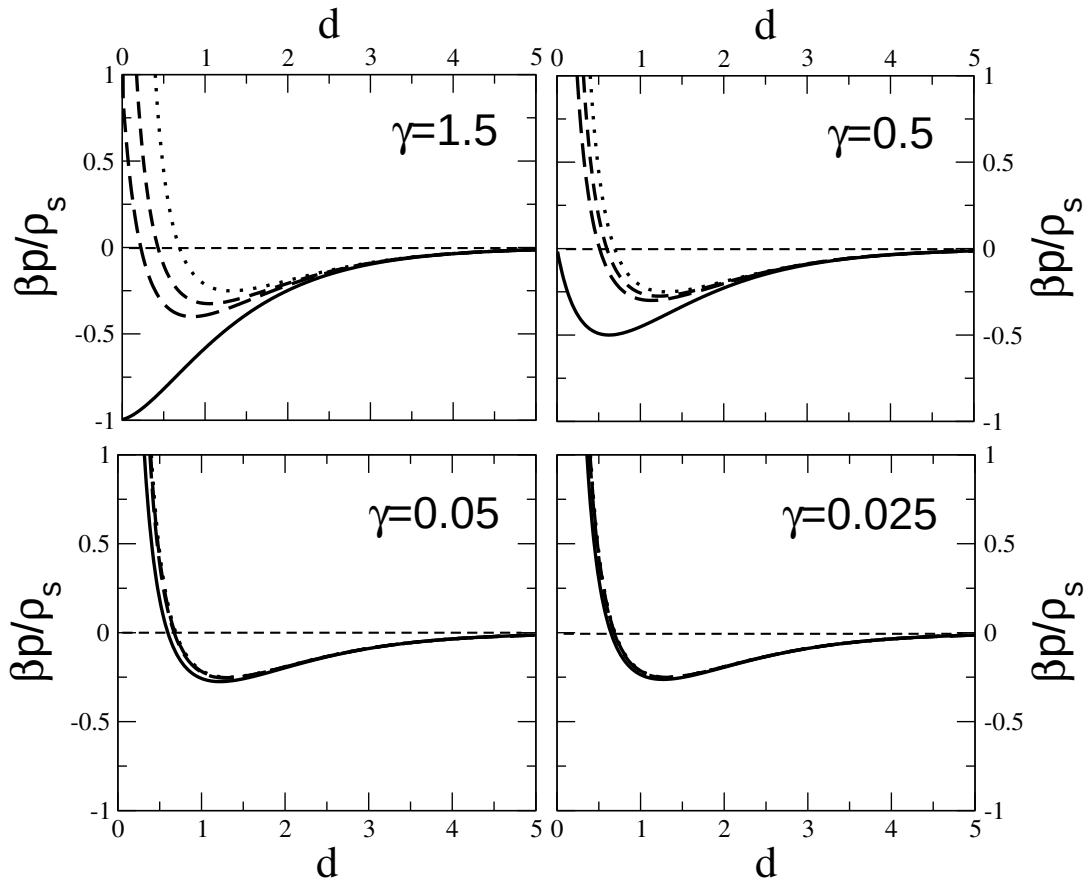

Figure 2.9: Reduced disjoining pressure as a function of the separation d for different values of the dielectric constant ratio γ (see text) for oppositely charged membranes with reduced surface charge densities $f_L = 1$ and $f_R = -0.5$ and membrane thickness $h = 1$ (solid line), $h = 5$ (long dashed line, $h = 10$ (short dashed line) and $h = 1000$ (dotted line).

way that depends on the boundary conditions and the geometric parameters (thickness and separation distance). It is interesting to enquire to what extent this mechanism is able to modify the interactions of actual membranes and colloidal platelets, which are often *not* index-matched such that image-charge effects are relevant. This can be studied by generalizing the second set of boundary conditions (which relate the differences in the electrostatic field at both sides of a charged layer) to the case where the dielectric constants at both sides are different. In the case of constant surface charges, one generalizes Eq.(2.4a) to

$$\phi'(x_i^-) - \gamma\phi'(x_i^+) = f_i \quad \text{for } i = 1, 3; \tag{2.12}$$

$$\gamma\phi'(x_i^-) - \phi'(x_i^+) = f_i \quad \text{for } i = 2, 4; \tag{2.13}$$

with $\gamma = \varepsilon^{obj}/\varepsilon^{solv}$, where ε^{obj} is the dielectric constant inside the object (membrane or colloidal platelet), and ε^{solv} is that of the solvent. As before we have $f_i = 4\pi\lambda_B(\sigma_i/e)/\kappa$ with the solvent Bjerrum length $\lambda_B = e^2/(k_B T\varepsilon^{solv})$, consistent with our previous notation. Similar equations can be written in the case of charge regulation boundary conditions Eq. (2.4c). Clearly the index-matched conditions are recovered for $\gamma = 1$.

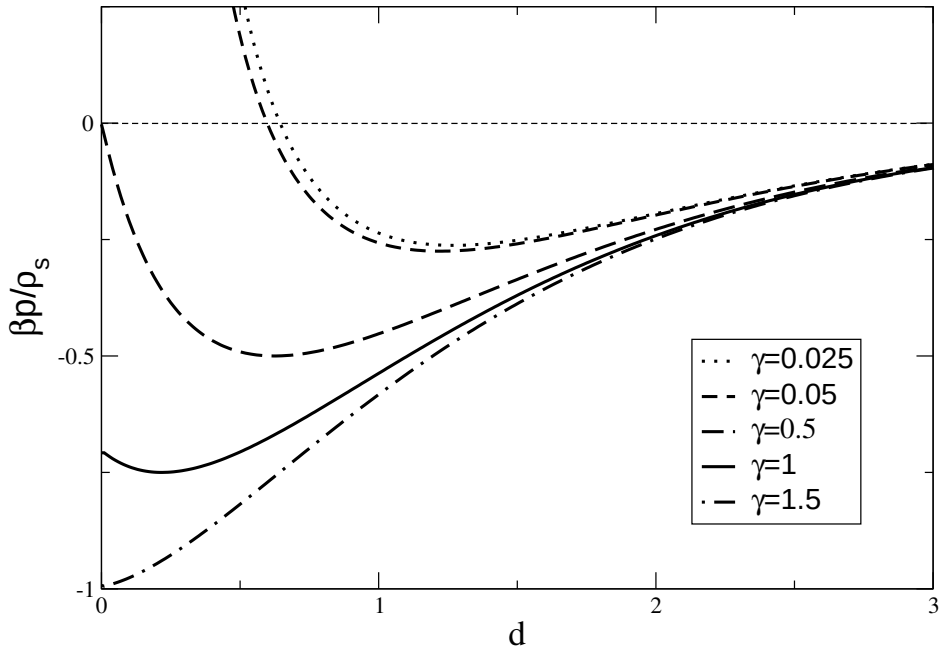

Figure 2.10: Reduced disjoining pressure as a function of the separation d for oppositely charged surfaces with reduced surface charge densities $f_L = 1$ and $f_R = -0.5$ and thickness $h = 1$. Note that the attraction reduces with decreasing ratio of dielectric constants γ (see text).

What are typical values for γ? In the case of lipid bilayers, with a thickness of the order of 10nm, such as those encountered in biological matter, the dielectric constant is estimated to be of the order of $\varepsilon^{obj} \simeq 2.0 - 2.5$ (see e.g. [56]). For such systems, when immersed in an aqueous solvent with a dielectric constant of about $\varepsilon^{solv} \simeq 78$, we obtain $0.025 \lesssim \gamma \lesssim 0.032$. On the other hand, in the case of colloidal gibbsite platelets such as those used in the experiments reported in [57], with a typical thickness of 15nm and a dielectric constant of the order of $\varepsilon^{obj} \simeq 2.0 - 3.0$, immersed in liquid toluene with a dielectric constant of the order of $\varepsilon^{solv} \simeq 2.2$, we obtain $0.9 \lesssim \gamma \lesssim 1.36$. In addition, in the case of silica platelets ($\varepsilon^{obj} \simeq 3.8$) immersed in toluene one would have $\gamma \simeq 1.7$. With these typical values for γ in mind we repeated the calculations of the disjoining pressure as a function of d for several thicknesses h, for the parameters also used in Fig.2.3, but now for $\gamma = 1.5, 0.5, 0.05$ and 0.025. Note that these parameters are such that the linear theory applies. The result is shown in Fig.2.9; note that the index-matched case $\gamma = 1$ was already shown in Fig.2.3. The first observation is that in the small-γ regime, i.e. in the membrane-in-water regime $\gamma \leq 0.05$, there is hardly a difference between objects of finite or infinite thickness, whereas in the opposite large-γ regime, i.e. in the platelet-in-toluene regime where $\gamma \simeq 1.5$, the increased attraction with decreasing thickness is even stronger than we found for $\gamma = 1$. In other words, the original Gouy-Chapmann model as e.g. proposed in [40] is indeed appropriate to describe the interactions of biological membranes in water since the finite membrane thickness plays a minor role, essentially

due to strong image charge effects as we have found here. Conversely, in the case of oppositely charged colloidal platelets in toluene-like solvents one cannot ignore the finite thickness of the platelets, since the attractions are significantly stronger for thinner platelets. These results are corroborated by Fig.2.10, where we plot the reduced disjoining pressure as a function of the separation distance for oppositely charged membranes with finite-thickness $h = 1$ and different values of γ, again for the parameters of Fig.2.3. One checks that the attractions are weakest for small γ's, although finite-thickness enhanced attractions are still observed for $\gamma \gtrsim 0.5$ for the parameters considered.

2.5 Conclusion

In this chapter we extended the Gouy-Chapman model for interactions between planar double layers so as to take the finite thickness of the charged surfaces into account, *i.e.* instead of two planar double layers we actually consider a system of four double layers in the geometry depicted in Fig.2.1. This geometry is relevant for interacting charged membranes, but also for e.g. colloidal platelets, dispersed in an electrolyte with a fixed Debye length. For a variety of boundary conditions (fixed surface charge, fixed surface potential, and surface charge regulation), we calculated within linear Poisson-Boltzmann theory the disjoining pressure p as a function of the separation d and the thickness h. For index-matched oppositely charged membranes or platelets, we find an enhancement of the surface charge density regime for which the force is attractive, both for fixed surface charge as well as for charge regulating surfaces. The enhanced force is most pronounced at separations of the order of a few Debye lengths or less, in particular if the membrane thickness and the separation are both of the order of a few Debye lengths or less. If the interacting objects have a different dielectric constant (ε^{obj}) than that of the solvent (ε^{solv}), such that image charge effects become relevant, we find that the enhanced attractions between thinner objects become even stronger if $\gamma \equiv \epsilon^{obj}/\epsilon^{solv} > 1$, and weaker otherwise. Given a typical membrane thickness of the order of nanometers, given a similar Debye length for millimolar salt concentrations in water at room temperature, and given that $\gamma \ll 1$ for typical biological membranes in water, we can conclude that for these parameters the finite thickness of the membranes is not very important; the traditional Gouy-Chapman model gives reliable results for such cases. For typical colloidal platelets in apolar solvents such as toluene, such that $\gamma \gtrsim 1$, the finite thickness is, however, very relevant; the predictions of the traditional Gouy-Chapman model differ substantially from those of the presently discussed quartet of double layers. The underlying mechanism for the enhanced attractions between thin membranes is the lifting of the strict charge neutrality condition in the subsystem in between the two nearest surfaces of the two platelets, since charge can be "squeezed-out" towards the double layers at the other sides of the membrane. The disjoining pressure was found to be independent of the membrane thickness in the case of fixed-potential surfaces. We consider our results to be a stepping stone towards some further studies, e.g. of highly-charged finite-thickness dissimilar objects, where a full non-linear treatment of electrostatics is required as e.g. in Ref.[36, 39, 47]. A particular case is studied in detail in the next chapter, where we consider highly-charged finite-thickness objects with the same sign of charge.

3

Non-linear screening and charge relaxation

In this chapter we continue the study of the extended classical Gouy-Chapman model of two planar finite thickness parallel interacting double-layers introduced in chapter 2. This model describes in first approximation the force between colloidal particles explicitly considering their finite thickness. As discussed in chapter 2 on the basis of a linear model, the formation of two additional double layers on the other side of the plates due to this finite thickness, modifies the interaction force compared to the Gouy-Chapman case, in which the colloids are semi-infinite objects. In this chapter we calculate this interaction force and some other size-dependent properties using a mean field level of description, based on the *non-linear* Poisson-Boltzmann (PB) equation. We show that in the case of finite-size colloidal particles, this equation can be set in a closed form depending on the geometrical parameters and on the value of the charge on the colloidal particles surface. The corresponding linear (Debye-Hückel) theory and the well-known results for semi-infinite colloidal particles are recovered from this solution after taking appropriate limits. We use a density functional corresponding to the PB level of description to show how in the case when the total colloidal charge is fixed, it redistributes itself on their surfaces to minimize the free energy of the system depending on the afore mentioned parameters. We study how this charge relaxation affects the colloidal interactions.

3.1 Introduction

Electrostatic forces play a remarkable role in the stabilization and phase behavior of colloidal suspensions. Thus, it is not surprising that understanding the interaction among charged colloidal particles across an intervening electrolyte solution has been an important goal for colloid science since the pioneering work by Verwey and Overbeek [4].

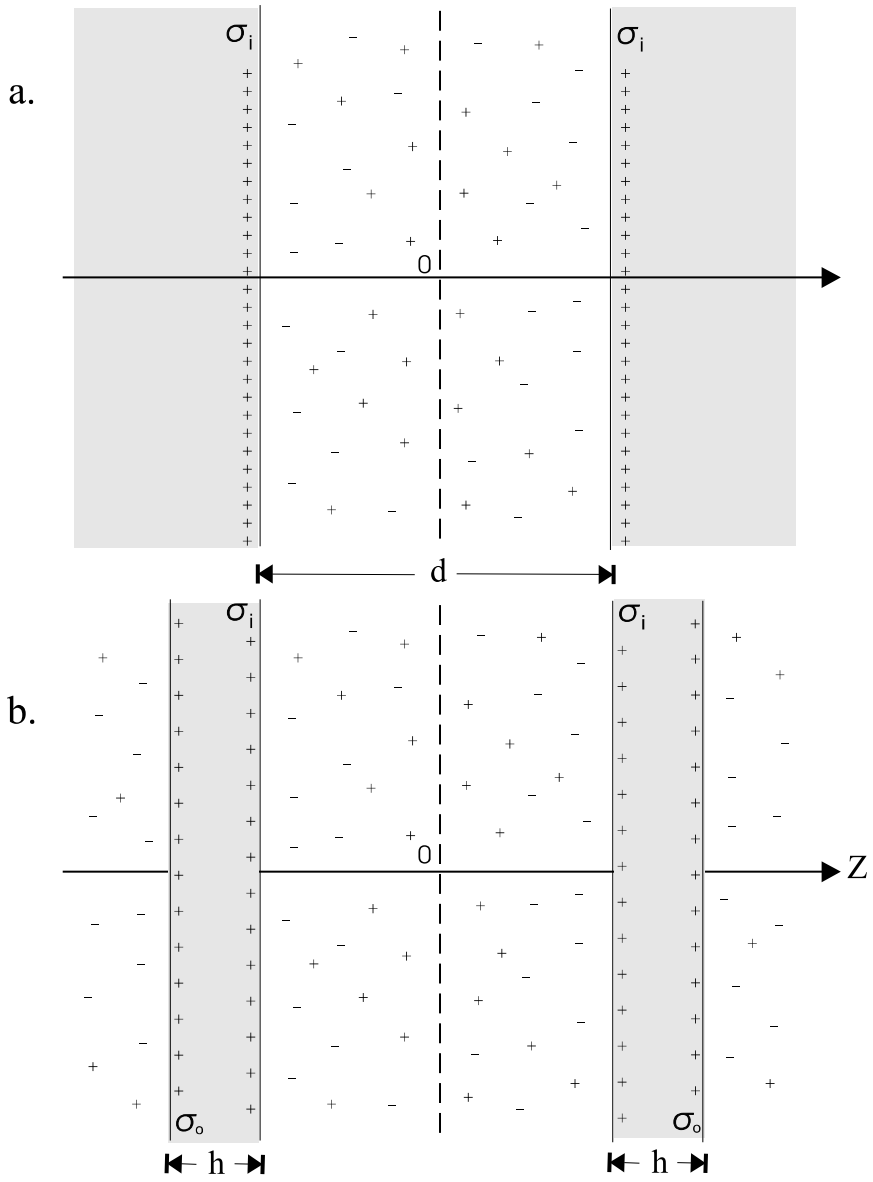

Figure 3.1: a) Two parallel double-layers. b) Four double-layers as a model for colloidal interactions. Here the finite size of the colloids is taken into account.

Poisson-Boltzmann theory (PB) allows a mean field calculation of these interactions at a nonlinear level. The corresponding linearized description, Debye-Hückel theory (DH), is exact in the asymptotic limit of infinite dilution and low charged colloidal particles, when the electrostatic interactions are weak compared to the thermal energy. DH theory fails to correctly describe quantitatively the thermodynamic properties of many colloidal suspensions, and nonlinear PB equation must be employed, often by using numerical computations.

Nonetheless, the PB equation admits analytical solutions in some non-trivial cases. An important example is that in which two parallel infinite double-layers interact. In this case the geometry is dictated by two planar objects (colloidal particles) which are infinite

in the directions parallel to their surface and semi-infinite in one direction perpendicular to their surface, and carrying a surface charge σ. The region between the semi-infinite objects is filled with a symmetric electrolyte, as illustrated in figure 3.1a. The force between the colloids is mediated by the diffuse layers surrounding their surface. PB theory allows the calculation of this force as well as the free energy of interaction, through the determination of the mean local electrostatic potential in the region filled with electrolyte [4]. The planar geometry is relevant for colloidal spheres in the case that the Debye length of the electrolyte is much smaller than the radius of the spheres (such that the curvature effects are small). It is also relevant for the understanding of colloidal clay platelets and their interactions. An important aspect of these clay platelets is their finite thickness h which can easily be of the same order as the Debye length and which could therefore affect the plate-plate interactions.

The geometry to be considered in this chapter is depicted in figure 3.1b, showing the finite thickness of the platelets and hence two inner surfaces (with charge density σ_i) and two outer surfaces (with charge density σ_o). Since the plates are completely immersed in electrolyte, double-layers form at both sides of the colloidal particles. The presence of charge on the outer surfaces induces the redistribution of ions in the electrolyte, and diffuse layers of charge appear in the vicinity of each region in contact with the colloids. In other words, the finite size of the colloidal particles allows the formation and interaction of four double-layers instead of two. It is clear that in this case, the force between the colloidal particles depends not only on their relative separation d but also on their thickness h.

In the traditional model of two interacting double layers [4], the initial studies supposed a fixed surface charge density or a fixed potential at the surfaces. But there have been several studies in which the surface charge of the colloidal planes is not fixed, but a charge regulation mechanism can occur [36, 58], due to an ion adsorption-desorption equilibrium of the colloidal surface groups. When the finite-thickness of the colloids is taken into account, as in our model (see figure 3.1b), there is another kind of charge regulation that can take place. The total charge of each colloid can be fixed but the amounts of charge on the inner and outer surfaces can vary in order to minimize the thermodynamic grand potential of the system. We call this mechanism "charge relaxation". Such mechanism can take place, for instance, in metallic colloids or electrodes, where the charges are free to move and rearrange themselves around the colloid surface. This charge relaxation also affects the force between the colloidal particles. In this chapter, we study quantitatively these finite-size effects in the case of two equally charged colloids immersed in a symmetrical electrolyte, in the framework of PB theory. The present nonlinear study already accounts for charge renormalization effects [59–62].

In section 3.2 we specify the model and introduce a suitable density functional. In section 3.3, the nonlinear PB equation is solved. We show that for the geometry of figure 3.1b, the solution of the PB equation can be set in a convenient analytical closed form, which depends only on the geometrical parameters h and d and on the total surface charge density σ of the colloids. The linear DH potential is obtained from the analytical solution by taking appropriate limits. In section 3.4, we minimize the density functional to calculate the fraction of charge on the inner and outer surfaces, as a function of the afore mentioned parameters, when charge relaxation is allowed. Results are discussed in section 3.5 and conclusions are given in section 3.6.

3.2 The model

We consider four infinite parallel planes located at $z_1 = -d/2 - h$, $z_2 = -d/2$, $z_3 = d/2$ and $z_4 = d/2 + h$, with surface charge densities σ_1, σ_2, σ_3, σ_4 respectively. The regions $z_1 < z < z_2$ correspond to the interior of the left colloid, and $z_3 < z < z_4$ to the interior of the right colloid. The regions outside the colloids are filled with an electrolyte solution of dielectric constant ϵ, at temperature T. Inside the colloids there is no electrolyte present but there is a medium with the same dielectric constant as the electrolyte solution to avoid electrostatic image effects. The system is assumed to be in contact with a monovalent salt reservoir of salt density ρ_s such that the electrolyte has screening length $l_D = \kappa^{-1} = (8\pi\lambda_B\rho_s)^{-1/2}$, with $\lambda_B = e^2/(k_BT\varepsilon)$ the Bjerrum length, where e is the elementary charge, k_B Boltzmann constant, and ε the electric permittivity of the solvent. In what follows, all lengths will be conveniently given in units of the Debye length, namely $D = \kappa d, H = \kappa h$ and $x = \kappa z$. For simplicity we consider the case when $\sigma_1 = \sigma_4 = \sigma_o$ and $\sigma_2 = \sigma_3 = \sigma_i$ as illustrated in figure 3.1b. Note that with these conditions the system possesses mirror symmetry with respect to the plane at $x = 0$, sketched with dashed lines.

The thermodynamic and statistical properties of the system are characterized by the dimensionless grand potential density functional $\omega[\rho] \equiv \kappa\beta\Omega[\rho]/(2A\rho_s)$ where A is the area of the planes and Ω is the grand potential density functional. $\omega[\rho]$ is given by

$$\omega[\rho] = \omega_{id}[\rho] + \frac{1}{4\rho_s}\int dx\rho(x)\phi(x) + 2f(\chi\log\chi + (1-\chi)\log(1-\chi)). \tag{3.1}$$

The first term in the right hand side is the ideal gas entropic contribution of the ions in the solution,

$$\omega_{id}[\rho] = \frac{1}{2\rho_s}\sum_{\alpha=\pm}\int dx\rho_\alpha(x)\left(\log\left(\frac{\rho_\alpha(x)}{\rho_s}\right) - 1\right), \tag{3.2}$$

where $\rho_+(x)$ and $\rho_-(x)$ are the number density profiles of the positive and negative salt ions respectively. The second term of (3.1) accounts for the electrostatic energy, with $\phi(x) = e\psi(x)/k_BT$ the reduced electrostatic potential (ψ is the electrostatic potential), and the total number charge in the system defined as

$$\rho(x) = \rho_+(x) - \rho_-(x) + \frac{\kappa}{e}\sum_{j=1}^{4}\sigma_j\delta(x - x_j). \tag{3.3}$$

The last term in (3.1) is of entropic origin and takes into account the fact that the surface charge ions on the colloids are indistinguishable. In the mean field framework used here, it is simply the free energy of the surface charges of the colloid treated as an ideal gas localized in the surfaces: $2(4\pi\lambda_B/(e\kappa))(\sigma_i\log(\sigma_i/\sigma) - \sigma_i + \sigma_o\log(\sigma_o/\sigma) - \sigma_o)$, where $\sigma = \sigma_i + \sigma_o$ is total charge density on a colloid. Since σ is fixed we can omit $-\sigma_i - \sigma_o$ from this expression, which in (3.1) has been rewritten in terms of the fraction of charge $\chi = \sigma_i/\sigma$ in the inner surface with respect to the total charge density on a colloid and $f = 4\pi\lambda_B\sigma/(e\kappa)$ which is the ratio of the Debye length $l_D = 1/\kappa$ and the Gouy-Chapman length $\Lambda = e/(4\pi\sigma\lambda_B)$. The latter is the decay length of the counterion distribution in the vicinity of an infinite charged plane with bare surface charge density σ in the salt free limit $\rho_s \to 0$.

Minimization of the density functional (3.1) with respect to the ion density profiles $\rho_{\pm}(x)$ gives the equilibrium density profiles in terms of the average local potential. In the mean field approach the reduced local electric potential $\phi(x)$ is the solution of the nonlinear Poisson–Boltzmann equation

$$\frac{d^2\phi}{dx^2} = \sinh\phi \qquad \text{in the outside} \tag{3.4}$$

$$\frac{d^2\phi}{dx^2} = 0 \qquad \text{in the inside} \tag{3.5}$$

with the boundary conditions that ϕ is a continuous function of x and

$$\phi'(\tfrac{D}{2}^-) - \phi'(\tfrac{D}{2}^+) = f_i \tag{3.6a}$$

$$\phi'((\tfrac{D}{2}+H)^-) - \phi'((\tfrac{D}{2}+H)^+) = f_o \tag{3.6b}$$

$$\lim_{|x|\to\infty} \phi'(x) = 0 \tag{3.6c}$$

with $f_i = 4\pi\lambda_B\sigma_i/(e\kappa)$, $f_o = 4\pi\lambda_B\sigma_o/(e\kappa)$ as explained before. The functional (3.1) evaluated for the equilibrium profiles gives the equilibrium dimensionless grand potential. Further minimization of the latter quantity with respect to the parameter $\chi = \sigma_i/\sigma$ allows to find the fraction of charge on each surface, when charge relaxation is allowed. This will be discussed in section 3.4. The DH level of description can be obtained by expanding (3.1) to second order in the density and linearizing (3.4) for $|\phi| \ll 1$. It can also be obtained from the nonlinear solution as will be discussed next.

3.3 Solution of Poisson-Boltzmann equation

3.3.1 The Nonlinear PB Equation

Due to the mirror symmetry it is sufficient to consider $x \geq 0$ since the potential is an even function of x: $\phi(x) = \phi(-x)$. Also, without loss of generality, we consider positively charged colloids, i.e. $f_i > 0$. The solution of the PB equation in the region $-D/2 < x < D/2$ with the boundary conditions $\phi(0) = \phi_0$ and $\phi'(0) = 0$ is well-known. There are several different but equivalent expressions for this solution [4, 36, 38, 55]. Multiplying both sides of Eq. (3.4) and using the identity $2\phi'(d^2\phi/dx^2) = d(\phi')^2/dx$ a first integration of the PB equation can be performed. Using the boundary condition at $x = 0$ we have

$$\phi'(x)^2 = 4\left(\sinh^2\frac{\phi(x)}{2} - \sinh^2\frac{\phi_0}{2}\right). \tag{3.7}$$

From this equation we see that $\sinh^2\frac{\phi(x)}{2} > \sinh^2\frac{\phi_0}{2}$, thus $|\phi(x)| > |\phi_0|$. We deduce that $\phi(x)$ does not change its sign. Furthermore with the choice $f_i > 0$, we have $\phi(x) \geq \phi_0$, and then $\phi'(x) \geq 0$.

Integrating once again with respect to x and defining $t = \sinh(\phi/2)$, the integral of (3.7) can be set in the form

$$x = \int_{\sinh(\phi_0/2)}^{\sinh(\phi(x)/2)} \frac{dt}{\sqrt{(t^2+1)(t^2-\sinh^2(\phi_0/2))}}. \tag{3.8}$$

One recognizes an elliptic integral of the first kind [63], defined as

$$F(\theta,k)=\int_0^\theta \frac{d\alpha}{\sqrt{1-k^2\sin^2\alpha}}, \tag{3.9}$$

and hence we have

$$x=\frac{1}{\cosh(\phi_0/2)}F\left(\arccos\frac{\sinh(\phi_0/2)}{\sinh(\phi(x)/2)},\frac{1}{\cosh(\phi_0/2)}\right). \tag{3.10}$$

An inversion yields

$$\sinh\frac{\phi(x)}{2}=\frac{\sinh(\phi_0/2)}{\mathrm{cn}(x\cosh(\phi_0/2),k)}, \tag{3.11}$$

where cn is the Jacobian cosine amplitude. The modulus $k=1/\cosh(\phi_0/2)$ of the elliptic functions will not be explicitly indicated in the following to lighten the notation. To take the finite thickness of the colloidal particles into account, we match this expression with the solutions in the regions $D/2<x<D/2+H$ and $D/2+H<x$. We get

$$\phi(x)=\phi_1(x)=2\sinh^{-1}\left[\frac{\sinh(\phi_0/2)}{\mathrm{cn}(x\cosh(\phi_0/2))}\right] \qquad \text{for } 0\le x\le D/2 \tag{3.12}$$

$$\phi(x)=\phi_2(x)=a\left(x-\frac{D}{2}\right)+\phi_1(D/2) \qquad \text{for } D/2\le x\le D/2+H \tag{3.13}$$

with the dimensionless electric field inside the colloids given by

$$a=2\sinh(\phi_0/2)\,\mathrm{sc}\left(\frac{D}{2}\cosh\frac{\phi_0}{2}\right)-f_i, \tag{3.14}$$

where $\mathrm{sc}(u,k)=\mathrm{sn}(u,k)/\mathrm{cn}(u,k)$ with $\mathrm{sn}(u,k)$ the Jacobian sine amplitude [23, 63]. For the outside region $x>D/2+H$ we find

$$\phi(x)=\phi_3(x)=2\ln\frac{1+Ce^{-x}}{1-Ce^{-x}} \qquad \text{for } D/2+H\le x, \tag{3.15}$$

with

$$C=\tanh(\phi_2(\tfrac{D}{2}+H)/4)e^{\frac{D}{2}+H}. \tag{3.16}$$

For a fixed ϕ_0 equations (3.12), (3.13) and (3.15) give the exact analytic form of the mean field within the Poisson-Boltzmann theory. To completely specify the spatial dependence of ϕ, we still need to determine its value at the origin ϕ_0. For this we use the boundary conditions (3.6) to get

$$\frac{f_o+f_i}{2}=\sinh\left[\frac{aH}{2}+\sinh^{-1}\left(\frac{\sinh(\phi_0/2)}{\mathrm{cn}(\frac{D}{2}\cosh\frac{\phi_0}{2})}\right)\right]+\sinh(\phi_0/2)\,\mathrm{sc}\left(\frac{D}{2}\cosh\frac{\phi_0}{2}\right) \tag{3.17}$$

with a given by eq. (3.14).

For given values of the parameters f_i, f_o, H and D, equation (3.17) can be easily solved numerically for ϕ_0 [64]. In combination with (3.12) to (3.16) it gives the exact mean field as a function of f_i, f_0, and the geometrical parameters H and D. An interesting feature of $\phi_1(x)$ as given in (3.12) is that if we consider the prolongation of the function ϕ_1 in eq. (3.12), for any value of x, from the general properties of the elliptic function cn, we notice that ϕ_1 is a periodic function of x with period $4K$, where $K = F(\pi/2, k)$. For $x > 0$, it has a first pole at the first positive zero of cn, at $x = K/(\cosh(\phi_0/2))$. Physically, the potential should be bounded. This means that for a given separation D, ϕ_0 satisfies

$$D < D_{\max} = \frac{2K}{\cosh(\phi_0/2)}. \tag{3.18}$$

The case $D = D_{\max}$ corresponds to a situation where the surface charge $\sigma_i \to +\infty$. Eq. (3.18) serves as a guide to choose the initial value for ϕ_0 in the numerical resolution of (3.17), or in a direct numerical integration of the Poisson–Boltzmann equation (3.4).

3.3.2 The Linear Regime: Debye–Hückel Theory

We can recover the results from the linear Debye–Hückel theory by taking the limit $\phi_0 \ll 1$. In that limit the modulus of the elliptic functions $k \to 1$. Using $\mathrm{cn}(u, 1) = 1/\cosh u$, we have $\phi_1(x) = \phi_0 \cosh x$ for $\phi_0 \ll 1$, which is the solution of the linear problem in the region $0 \le x \le D/2$. Similarly, using $\mathrm{sn}(u, 1) = \tanh u$ we have

$$a = \phi_0 \sinh(D/2) - f_i, \tag{3.19}$$

and equation (3.17) reduces to a linear equation which can be easily solved for ϕ_0. The result is

$$\phi_0 = \frac{f_o + (1 + H) f_i}{e^{D/2} + H \sinh(D/2)}. \tag{3.20}$$

The last equation in combination with (3.19) and the expression for $\phi_1(x)$, determines also the potential in the region $D/2 \le x \le D/2 + H$, namely, $\phi_2(x) = a(x - D/2) + \phi_1(D/2)$. Finally, linearizing (3.15) and (3.16) we get $\phi_3(x) = [aH + \phi_1(D/2)]e^{D/2+H}e^{-x}$. It is an easy exercise to show that the same expressions can be obtained with the DH approximation taken ab initio. For that, it is enough to take functions of the form $\phi_1(x) = Ae^x + Be^{-x}$, $\phi_2(x) = a(x - D/2) + \phi_1(D/2)$ and $\phi_3(x) = Ce^{D/2+H}e^{-x}$. Using the boundary conditions and the continuity of the potential, a system of coupled linear equations for the constants A, B, C and a is obtained. The solution coincides with the exact nonlinear solution in the limit of small potentials.

3.4 The Equilibrium Grand Potential

As mentioned before, the total charge on the colloids is assumed to be fixed, but eventually different fractions of charge can move between the inner and outer surfaces. We took this into account in the density functional (3.1) by fixing the total charge on the colloids instead of the surface charge on the inner and outer surfaces separately, through the

introduction of the charge fraction χ. The functional (3.1) evaluated at the equilibrium density profile gives, for fixed χ, the grand potential of the system. Further minimization of the latter quantity with respect to χ allow us to find the fraction of charge on each surface that minimizes the equilibrium grand potential. The grand potential is obtained by inserting the expressions (3.12), (3.13) and (3.15) into the density functional (3.1). The explicit calculation involves well-known quadratures of the Jacobian elliptic functions, in particular

$$\int \frac{du}{\mathrm{cn}^2(u,k)} = \frac{\mathrm{sc}(u,k)\,\mathrm{dn}(u,k) - E(\mathrm{am}(u,k),k)}{1-k^2} + u, \tag{3.21}$$

where $\mathrm{dn}(u,k)$ is the Jacobian delta amplitude, $E(x,k)$ the elliptic integral of second kind and $\mathrm{am}(u,k)$ the Jacobian amplitude [23, 63]. After some calculations we obtain

$$\begin{aligned}\omega &= 2\phi(D/2)\sinh(\phi_0/2)\,\mathrm{sc}(D/2k) - 8\cosh(\phi_0/2)\,\mathrm{sc}(D/2k)\,\mathrm{dn}(D/2k)\\ &\quad +8E(\mathrm{am}(D/2k),k)\cosh(\phi_0/2) - 2D\sinh^2(\phi_0/2)\\ &\quad +2\sinh(\phi(\tfrac{D}{2}+H)/2)\phi(\tfrac{D}{2}+H) - 16\sinh^2(\phi(\tfrac{D}{2}+H)/4)\\ &\quad +f[2\chi\ln\chi + 2(1-\chi)\ln(1-\chi) + \chi\phi(D/2) + (1-\chi)\phi(\tfrac{D}{2}+H)].\end{aligned} \tag{3.22}$$

Notice that $k = 1/\cosh(\phi_0/2)$, that $\phi(x)$ can be evaluated from (3.12), (3.13), (3.15), and that ϕ_0 is the solution of (3.17) and thus depends on χ. For given values of H, D and f we determine the value of χ that minimizes the grand potential (3.22) numerically [64].

The DH level of description is obtained from the linear density functional corresponding to (3.1). In this case the dimensionless grand potential reads

$$\omega = f[2\chi\ln\chi + 2(1-\chi)\ln(1-\chi) + \chi\phi(D/2) + (1-\chi)\phi(\tfrac{D}{2}+H)] \tag{3.23}$$

where ϕ is given by the expressions derived in section 3.2. Although equations (3.22) and (3.23) are a bit involved, the grand potential has the familiar repulsive form as that for semi-infinite colloids. This is illustrated in figure 3.2, where the linear and nonlinear results are compared for the case $f = 10$ and $\chi = 0.5$. Some consequences of the size-dependence of the potential will be discussed in the next section.

3.5 Results

3.5.1 Charge relaxation

Let us first consider the aforementioned effect of charge relaxation, in which charges can move between the inner and outer colloidal surfaces. We shall refer to this as the annealed case, in contrast to the case in which equal amounts of charge are fixed ("quenched") on the inner and outer surfaces. Notice that in the quenched case $\chi = \sigma_i/\sigma = 0.5$. In figure 3.3, the charge fraction χ is plotted as a function of the colloid separation D for different colloidal thicknesses. We observe that for inter-colloidal separations of the order of the Debye length, a fraction of charge moves to the outer surface. This effect substantially increases with increasing values of the parameter f, as we can conclude from the inset, which shows the fraction of charge at $D \to 0$. Notice that for increasing f, the values of χ at contact tend faster to zero. Thus, the effect of increasing f is similar to what we observe in the main plot when H is increased, namely, a more pronounced

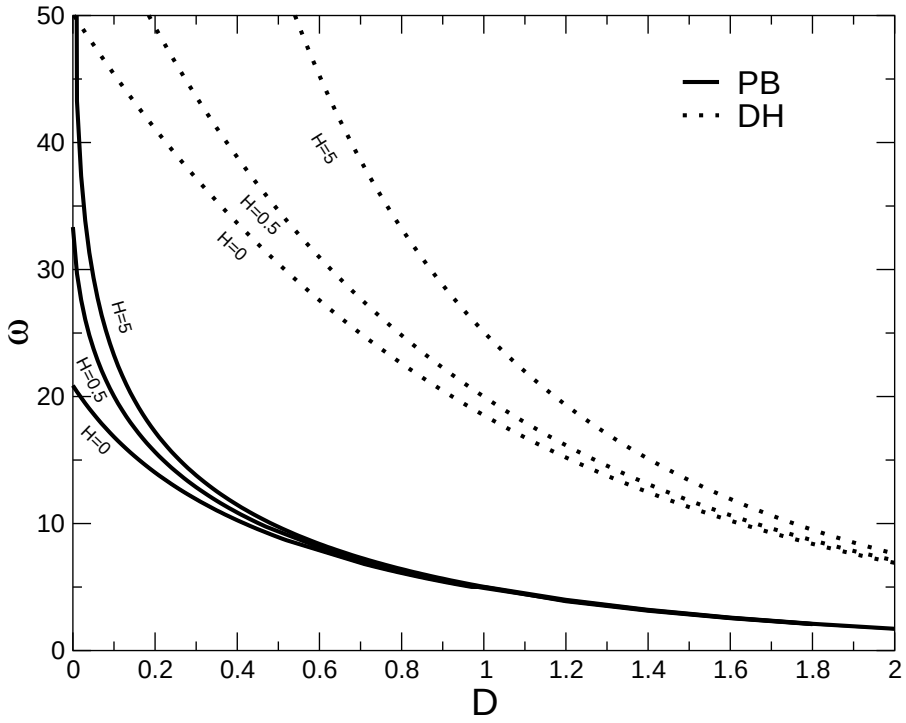

Figure 3.2: Non-linear (PB) and linear (DH) based equilibrium grand potential as a function of the dimensionless separation distance D for two interacting finite-size planes and different dimensionless thicknesses H. In this plot $\chi = 0.5$ and $f = 10$.

relaxation of charge toward the outer surface. Notice that this effect already disappears at colloidal separations of the order of two times the Debye length, at which a small difference with the quenched case is observed. It also worth to mention the fact that in the main plot, no substantial change is observed when the thickness is increased from $H = 5$ to $H = 10$. In fact, for a given value of $H \neq 0$, when the thickness varies from $H = 5$ to $H = \infty$, the charge fraction χ does not change beyond 3% . For a colloidal thickness of a few Debye lengths, the distance to the outer surface is already too large to affect the fraction of charge that migrates as we vary the distance between the colloids.

3.5.2 Electrostatic potential

In figure 3.4 we plot the electrostatic potential $\phi(x)$ for $x > 0$ in the quenched case, obtained by equations (3.12-3.15) using the methods described in section 3.3. The dotted line represents the corresponding linear DH mean potential. Even though for $f \ll 1$ both theories coincide, DH theory fails to quantitatively predict the local value of the mean field for $f \gtrsim 1$. For example, for $H \to 0$, (3.20) reduces to $\phi_0 = (f_i + f_o)e^{-D/2}$, thus, the total charge density $\sigma_i + \sigma_o$ is concentrated in a plane of infinitesimal width and

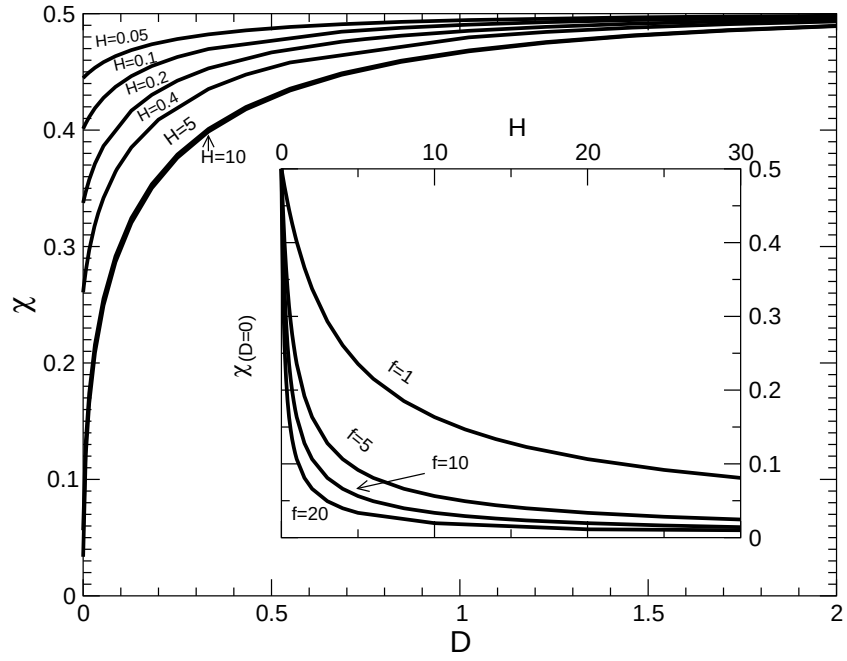

Figure 3.3: Fraction of surface charge density on the inner plates χ as a function of colloid separation for different colloidal sizes for $f = 10$. In the inset we see how $\chi(D \to 0)$ changes with varying H, for different values of f.

the potential at the plane of symmetry decreases exponentially with respect to the plates separation. In the limit $H \to \infty$ we have $\phi_0 = f_i/\sinh(D/2)$, this expression diverges for $D \to 0$ whereas eq. (3.17) predicts a finite value for this quantity. In figure 3.5, we compare the electrostatic potential in the quenched case with that in the annealed case. Notice that as charge moves from the inner to the outer surface, the potential at the first decreases while it increases at the latter. In other words relaxation of charge reduces the potential difference between the inner and outer surfaces. This effect is stronger for larger f in accordance with figure 3.3.

3.5.3 Force between the colloids

The force between the plates per unit area is given by the disjoining pressure p, defined in terms of the grand potential through the relation $\beta p/(2\rho_s) = -\partial\omega/\partial D$. Alternatively, taking into account the fact that the electrostatic pressure of the system must balance the hydrostatic pressure, it can be written in terms of the mean field ψ as [4]

$$p = k_B T(n(x) - 2\rho_s) - \frac{\varepsilon}{8\pi}\left(\frac{d\psi}{dx}\right)^2 + \frac{\varepsilon}{8\pi}\left(\frac{d\psi}{dx}\right)^2_{D\to\infty} \tag{3.24}$$

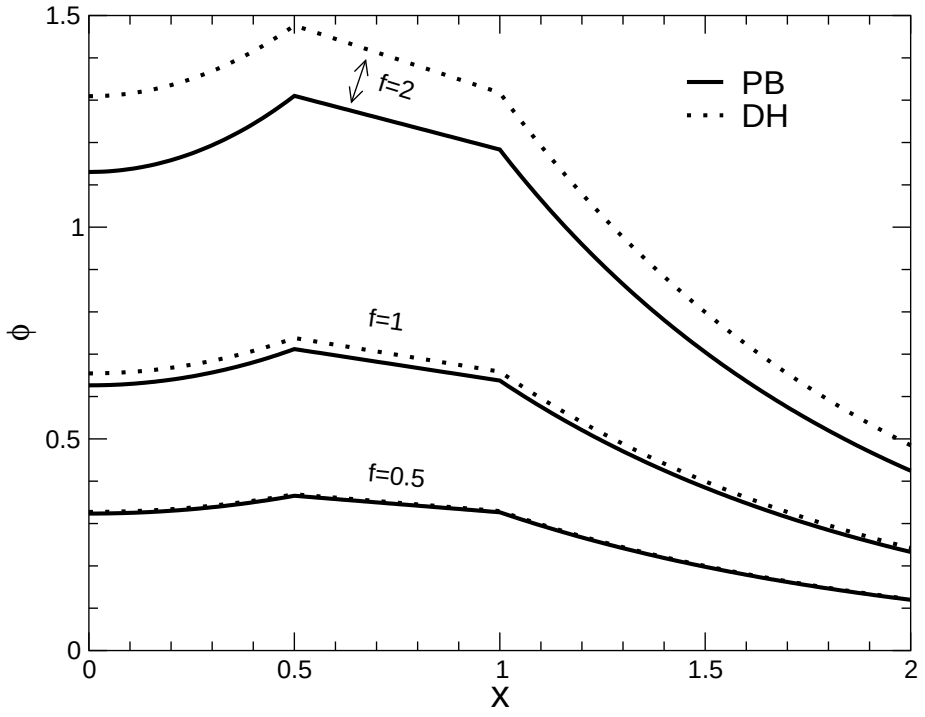

Figure 3.4: Average local electrostatic potential for $D = 1$, $H = 0.5$ and $\chi = 0.5$ (quenched case) for different values of the dimensionless parameter f. Notice that the linear DH results are asymptotically exact in the region $f \ll 1$, but fail to quantitatively predict the correct local mean field for $f \geq 1$.

where $n(x) = \rho_+(x) + \rho_-(x)$ is the total density of microions at x. It is easy to show that within PB theory, this quantity gives the same value for any position x. In particular evaluating at $x = 0$ we get

$$\beta p = 2\rho_s(\cosh\phi_0 - 1), \tag{3.25}$$

which implies that the force between the colloids is completely determined by the value of the mean electrostatic potential at the plane of symmetry. This feature allow us to find this quantity directly from the numerical solution of equation (3.17). In figure 3.6 we plot the dimensionless pressure as a function of the colloidal separation, for different values of the thickness H for the quenched and annealed cases. Although the last two give obviously the same curve for $H = 0$, a substantial difference is observed for small, nonzero, colloidal thicknesses. On the other hand, for $H = 10$ and larger, the inter-colloidal force turns out to be almost independent of the thickness for the same reasons discussed before in the context of charge relaxation. All the curves tend asymptotically to zero in the limit of infinite colloidal separation. In the DH limit $\beta p = 2\rho_s(\cosh\phi_0 - 1) \simeq \rho_s\phi_0^2$. Using (3.20) we obtain $\beta p = \rho_s f_i^2/\sinh^2\left(\frac{D}{2}\right)$ for $H \to \infty$. Again, in the limit

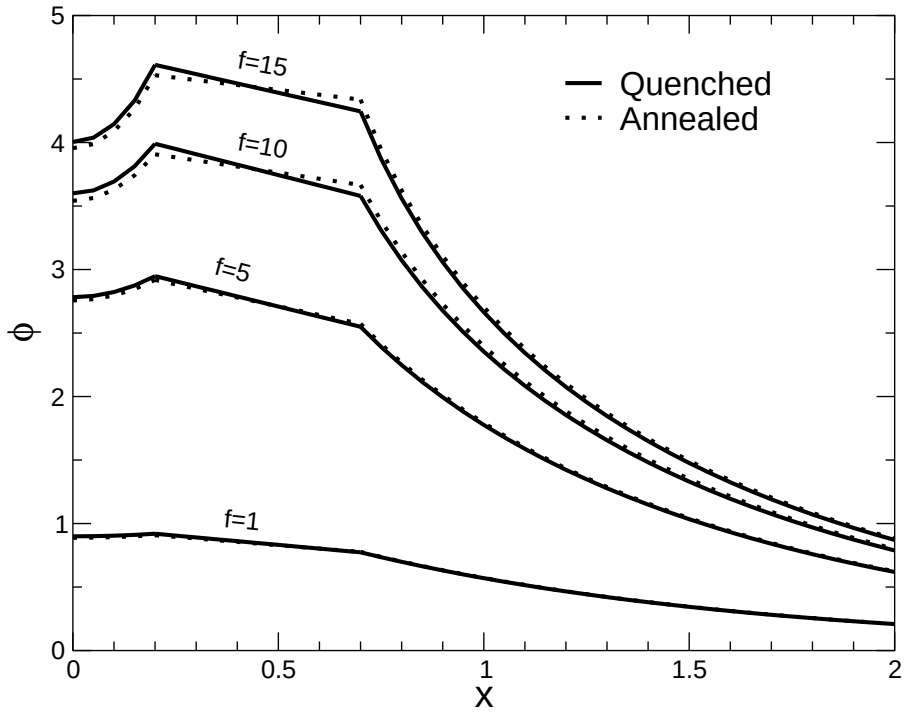

Figure 3.5: Comparison of the local electrostatic potential $\phi(x)$ for the quenched and annealed cases. The geometric parameters are same as in figure 3.4. Moderate difference is only observed for $f \gg 1$ in accordance with figure 3.3.

$D \to 0$, the linear theory predicts divergent behavior for the pressure, while the full nonlinear theory gives a finite value for this quantity.

3.5.4 Average charge density between the colloids

Using Poisson's equation $\phi''(x) = -\rho(x)/(2\rho_s)$, we compute the ratio $\langle Q \rangle$, the average ion charge density between the two colloidal particles, compared to the charge density on the inner faces of the colloids:

$$\langle Q \rangle = \frac{e}{\kappa\sigma_i} \int_0^{D/2} \rho(x)dx = \frac{1}{f_i}\left(\phi'(0) - \phi'(\tfrac{D}{2}^-)\right) = -\frac{\phi'(\tfrac{D}{2}^-)}{f_i}. \tag{3.26}$$

This quantity is shown as a function of the inter-colloidal distance for different values of H in figure 3.7. When the distance between the finite-width colloids is shortened, charge can be squeezed out of the region between the colloids. This is not possible for semi-infinite colloids, since in that case there is no place for the charge to be squeezed out. Then $\langle Q \rangle = -1$ for all D as shown in figure 3.7. The inset shows the squeezing of charge when we decrease the thickness for fixed separation D. For $H = 0$ the quenched and

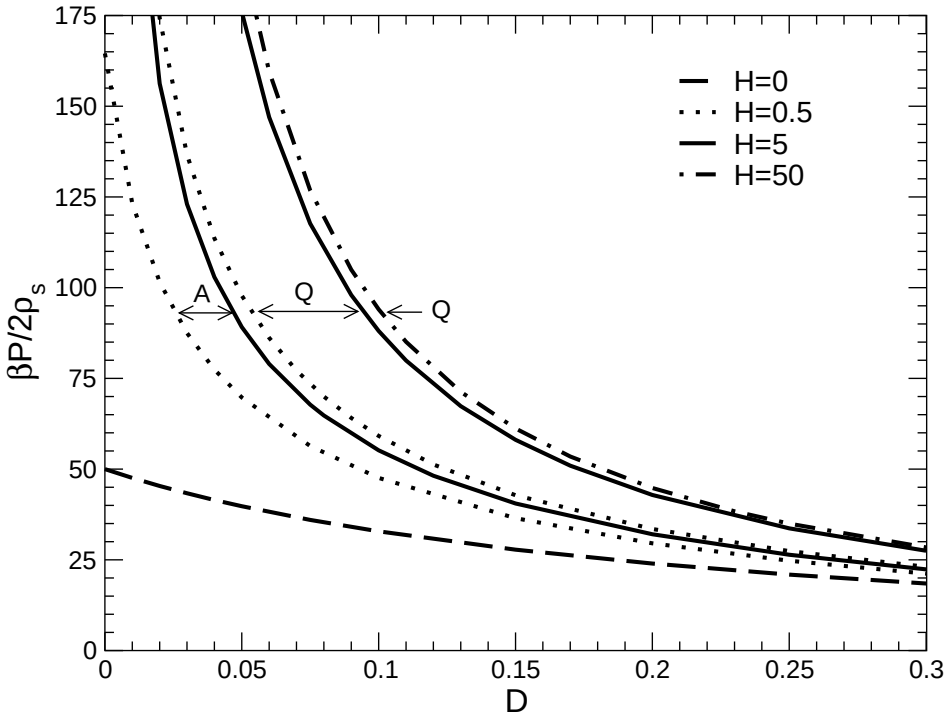

Figure 3.6: Dimensionless force per unit area between the colloids for $f = 10$. This quantity is always positive, indicating repulsion between the colloids, and tends to zero as the separation between the colloids increases. The plots for the quenched and annealed cases are labelled with Q and A respectively.

annealed cases coincide. One expects that Q is closer to -1 in the annealed case than in the quenched case, since the surface charge can follow the squeezed-out ionic charge by migration to the outer surface. This is indeed shown by our numerical results as shown in figure 3.8. However, for very small separations, $D \approx 10^{-2}$ this effect is reversed, as can be seen in figure 3.7, where $\langle Q \rangle$ is closer to -1 in the quenched case. Note that this effect occurs for rather small values of the separation distance. In a model that accounts for the finite-size of the ions this effect is presumably absent.

3.6 Conclusion

The system consisting of two planar interacting double-layers, used as a model of colloidal interactions in an electrolyte when the curvature of the macromolecules is negligible, has been extended in a twofold fashion: (i) the finite width of the colloids is taken into account, such that the system consists actually of four double layers, and (ii) the inner and outer surface charge of each of the two colloids can be either quenched to an equal value

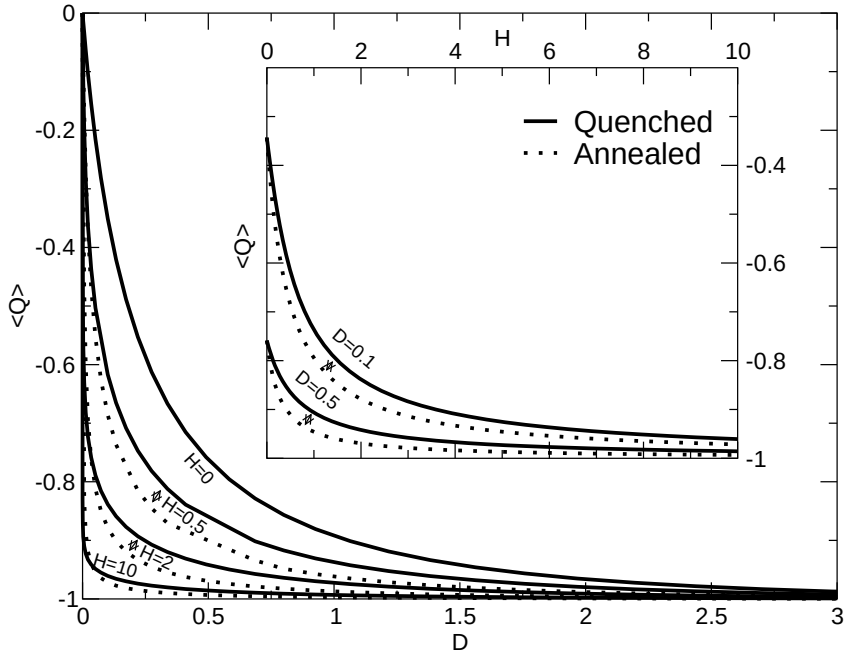

Figure 3.7: Average charge density in the region between the colloids for $f = 10$. When $H \to \infty$ charge of sign opposite to that on the colloidal surface is present in the middle region to neutralize the charge on the colloids. When H is finite, part of that charge is squeezed out of the middle region as the colloids are driven to a closer relative position. The inset shows the squeezing of charge when we decrease the thickness for fixed separation D.

or annealed such that charge relaxation (with a fixed total charge) is possible. For both these extensions we solve the nonlinear Poisson-Boltzmann equation, and we calculate the disjoining pressure as a function of the separation of the two colloids, the thickness of the colloids, and the total surface charge density. In the annealed case we also study the fraction of the surface charge at the inner and outer surface.

An interesting effect that occurs at finite colloid thickness is that the electrolyte charge in between the two colloids needs not exactly balance the charge on the inner colloidal surfaces (fig. 3.7), since part of the compensating charge may be "squeezed-out" to the outer double layers (the total system is charge neutral of course). The resulting charge imbalance in the inner region due to the squeezing-out effect may be as large as 20% at a colloid separation of 1 Debye length if the colloidal thickness vanishes, up to 80% if the separation is ten times smaller, where the relative effect is a bit more pronounced for the quenched case. For colloids with a thickness equal to the Debye length the relative imbalance in the inner region reduces to about 5% and 30% for the same two separations, respectively, i.e., yet very significant. For separations much larger than the Debye length the squeezing effect diminishes, as the two plates actually decouple and retain effectively their left-right symmetry.

These finite-thickness induced changes in the double layer structure at plate-plate sep-

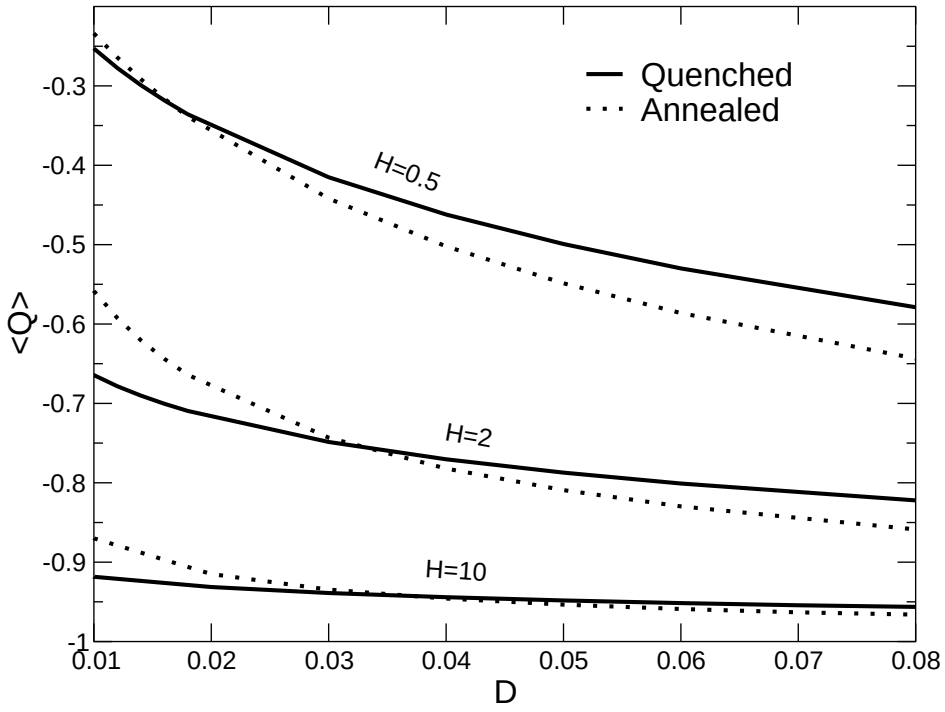

Figure 3.8: Average charge density (see text) in the region between the colloids for $f = 10$.

arations of the order of the Debye length or less also significantly affect the disjoining pressure. Our numerical results for the dimensionless charge density $f = 10$, which for an aqueous system with an electrolyte concentration of 1mM corresponds to a surface charge density of about 1 elementary charge per few nm^2, shows a decrease of the disjoining pressure by about 10% (5%) for the quenched (annealed) charge density at a separation of 1 Debye length when the thickness varies from infinity to zero. The reduction of the disjoining pressure is a factor of 3 (2) for quenched (annealed) surface charges upon decreasing the thickness from infinity to zero if the separation is ten times smaller than the Debye length. These data also indicate that the squeezing effect has a substantially larger effect on the reduction of the disjoining pressure for quenched than for annealed surface charges. Note, however, that a vanishing plate thickness yields identical disjoining pressures for quenched and annealed surface charged, since then the inner and outer surface charge cannot be distinguished physically.

We thus conclude that the finite thickness of the plates reduces the disjoining pressure considerably at separations shorter than about the Debye length (see fig. 3.6) due to the displacement of electrolyte charge from the inner to the outer region of the plates, and that this effect is stronger for quenched than for annealed charges. The present study can be extended to include more complicated and more realistic charge-relaxation and charge-

regulation mechanisms, and more complicated geometries, such as spheres treated, e.g., within the Derjaguin approximation.

Part II

Colloidal mixtures

4

The polydisperse cell model

In this chapter we propose a model for the calculation of renormalized charges and osmotic properties of mixtures of highly charged colloidal particles. The model is a generalization of the cell model and the notion of charge renormalization as introduced by Alexander and his collaborators (*J. Chem. Phys.* **80**, 5776 (1984)). The total suspension is partitioned into as many different cells as there are components in the mixture. The radii of these cells are determined self-consistently for a given set of parameters from the solution of the non-linear Poisson-Boltzmann equation with appropriate boundary conditions. This generalizes Alexander's model where the (unique) Wigner-Seitz cell radius is fixed solely by the colloidal particles packing fraction. We illustrate the technique by considering a binary mixture of colloids with the same sign of charge. The present model can be used to calculate thermodynamic properties of highly charged colloidal mixtures employing linear theories, while taking the effect of non-linear screening into account.

4.1 Introduction

Typical charge-stabilized colloidal suspensions consist of mesoscopic particles and ions, immersed in a solvent which to a good approximation can be considered as a continuous medium, characterized by a dielectric permittivity ϵ. The microscopic ions form a diffuse layer around the colloidal surfaces, with a typical thickness of the order of the Debye length of the electrolyte κ^{-1}, and with a net charge that compensates the charge of the colloidal surface. As a consequence, the effective colloidal interactions are screened: instead of the bare Coulomb interaction $Z^2e^2/\epsilon r$ between two colloidal spheres of radius a and charges Ze a distance r apart in the solvent, standard linear Poisson-Boltzmann theory predicts a screened coulomb interaction $Z^2e^2 \exp(2\kappa a)(1+\kappa a)^{-2} \exp[-\kappa r]/\epsilon r$ between the colloids [3, 4]. However, it is well-known that this relatively simple picture needs modification in the case of highly charged colloids, where the strong electrostatic

coupling between the colloids and their counterions induces the accumulation of the latter close to the colloid-surface. This condensation phenomenon cannot be described by a linearized Poisson-Boltzmann approach, and requires the full nonlinear Poisson-Boltzmann theory for a proper description [76]. However, the simplicity of the linear theories can be retained by the use of the concept of charge renormalization, which considers each colloid and its condensed counterion shell as a single entity, carrying a net effective charge which is usually smaller than the bare (structural) charge Z of the colloid. This so-called renormalized charge, Z^{ren}, characterizes the long-distance behavior of the screened electric potential created by the colloid and its condensed microion polarization cloud, and the effective colloidal pair interaction for large enough separation takes the linear screening form, but with Z replaced by Z^{ren}.

The concept of charge renormalization, and also its relatives such as dressed-ion theory [77], is very well-developed by now for *monodisperse* colloidal suspensions [76, 78–80]. The traditional theory by Alexander *et al.* is based on a cell model, in which a suspension of N colloidal spheres in an electrolyte of volume V is approximated by N identical spherical cells of volume V/N, each containing a single colloid in the center and co- and counterions such that each cell is neutral. The simple spherically symmetric geometry allows for a straightforward numerical solution of the nonlinear Poisson-Boltzmann equation in the cell, from which Z^{ren} follows directly [76, 78–80]. Although such an approach based on cells is most justified for colloidal crystals, the concept of charge renormalization has proved to be very useful for fluid-state suspensions, e.g. in describing the structure factor [81] or the electrophoretic mobility [82].

Much less is known about charge renormalization in the case of colloidal *mixtures* or *polydisperse* colloidal suspensions. In recent years such mixtures of charged colloids have generated a lot of interest, for instance because of their ability to form a plethora of crystal phases [83, 84] or the occurrence of fluid-fluid demixing phenomena [85]. Moreover, in the presence of external fields colloidal mixtures show a richer behavior than monodisperse systems. For instance, oppositely charged colloids can exhibit lane formation in an electric field [86–88], while sedimentation in the earth's gravity field can generate layers of colloids with equal mass-per-charge [89] or a "colloidal Brazil nut effect" in which a layer of heavier colloids floats on top of a layer of lighter ones [90]. Given the success of the cell model and of the concept of charge renormalization for the calculation of thermodynamic properties of monodisperse highly charged colloidal suspensions, and in view of the recent interest and advances in the synthesization of colloidal mixtures, it is desirable to extend the cell model to the polydisperse domain. The aim of this chapter is to introduce such a generalized cell model and to study some of its features, in particular the dependence on the composition of the mixture.

The outline of this chapter is as follows. In section 4.2 we introduce the model. In section 4.3 we discuss the particular case of a binary mixture. We calculate saturation curves for the renormalized charges, osmotic properties, and the radii of the cells as a function of composition, screening length and total colloid density. Discussion and some general remarks are presented in section 4.4, followed by conclusions in section 4.5.

4.2 Model

Let us begin by considering two species of spherical colloids with charges $Q_a = Z_a e$, $Q_b = Z_b e$ and radius a and b, respectively, where e is the proton charge and where we assume that the colloids possess charges of the same sign, i.e., $Z_a Z_b > 0$. Let N_a and N_b denote the total number of colloids of type a and those of type b, respectively. The colloidal mixture occupies a volume V and the colloids are immersed in a medium that is in osmotic equilibrium with a salt reservoir with screening length $\kappa^{-1} = (8\pi\rho_s\lambda_B)^{-1/2}$ where $2\rho_s$ is the salt concentration in the reservoir. As usual we define the Bjerrum length $\lambda_B = \beta e^2/\varepsilon$, with ε the dielectric constant of the solvent and $\beta = 1/(k_B T)$, with T the temperature and k_B the Boltzmann constant. The average number densities of colloids are defined by $\rho_a = N_a/V$ and $\rho_b = N_b/V$ and their respective volume fractions are $\eta_a = 4\pi a^3\rho_a/3$ and $\eta_b = 4\pi b^3\rho_b/3$. The composition of the mixture is characterized by the molar fraction $x = N_a/(N_a + N_b)$ which in the case of equisized colloids can be written as $x = \eta_a/\eta$ with $\eta = \eta_a + \eta_b$ the total packing fraction of the suspension.

Following the usual cell model approximation we consider the Wigner-Seitz cell of each colloidal particle as a sphere concentric with the spherical colloid. However, due to the difference in size and charge of each species, there is no a priori reason to assume that the cells corresponding to each species are of equal size. Therefore, we suppose that the Wigner-Seitz cells of the colloids of type a have a radius R_a and those of the colloids of type b have radius R_b, which are in principle different and to this point unknown.

Let $\phi_a(r) = \beta e\psi_a(r)$ be the reduced electric potential inside a cell of type a, with $\psi_a(r)$ the electric potential at a radial distance r from the center of the colloid. Accordingly, we define $\phi_b(r) = \beta e\psi_b(r)$ the reduced electric potential inside a cell of type b. In the mean-field approximation, the electric potential inside each cell is the solution of the Poisson–Boltzmann equation

$$\Delta\phi_a(r) = \kappa^2 \sinh\phi_a(r) \tag{4.1a}$$

$$\Delta\phi_b(r) = \kappa^2 \sinh\phi_b(r) \tag{4.1b}$$

together with the boundary conditions

$$r\frac{d\phi_a}{dr}\bigg|_{r=a} = -Z_a\lambda_B/a\,; \qquad r\frac{d\phi_b}{dr}\bigg|_{r=b} = -Z_b\lambda_B/b \tag{4.2}$$

$$\frac{d\phi_a}{dr}\bigg|_{r=R_a} = 0\,; \qquad \frac{d\phi_b}{dr}\bigg|_{r=R_b} = 0, \tag{4.3}$$

which are obtained from direct application of Gauss' law at the colloid surface (Eq. (4.2)), and at the boundary of the cell (Eq. (4.3)). The latter equation accounts for the electroneutrality of each cell. These equations completely determine the electrostatic potential inside each cell. However, the radius of each cell, R_a or R_b, remains undetermined, so far. These are determined by the following relations:

$$\eta_a\frac{R_a^3}{a^3} + \eta_b\frac{R_b^3}{b^3} = 1\,, \tag{4.4}$$

which expresses the fact that the Wigner-Seitz cells fill the accessible volume V, and

$$\phi_a(R_a) = \phi_b(R_b)\,, \tag{4.5}$$

which is a consequence of the continuity of the electric potential, and the fact that cells of different species can be in contact with each other. The system of differential and algebraic equations (4.1), (4.2), (4.3), (4.4) and (4.5) is a complete set to determine the unknown parameters and functions R_a, R_b, $\phi_a(r)$ and $\phi_b(r)$. The numerical solution of this system of equations can be obtained with a generalization of the elegant algorithm for a monodisperse colloidal suspension proposed in Ref. [78].

The generalization to a mixture of $M > 2$ colloidal species with radii r_i, packing fractions η_i and charges Z_i, is performed by introducing M different types of cells of radii R_i ($i = 1, 2, ..., M$), in which the Poisson–Boltzmann equation (4.1) with boundary conditions (4.2) and (4.3) is to be solved. To fix the values of the M radii of the cells, the equivalent of Eq. (4.4) is

$$\sum_{i=1}^{M} \eta_i \frac{R_i^3}{r_i^3} = 1. \tag{4.6}$$

Additionally, we have $M-1$ independent equations of continuity for the electric potential at the cell boundaries of the form

$$\phi_i(R_i) = \phi_1(R_1)\,. \tag{4.7}$$

for $i = 2, ..., M$. This completes the system of equations for the electric potentials and the radii of the cells.

4.2.1 Renormalized charge

The renormalized charge, defined using Alexander's prescription [76], is obtained by comparing the nonlinear solution of the Poisson–Boltzmann equation with its linearized solution, where the linearization is performed with respect to the value of the potential at the boundary of the cell. Following Ref. [78], and restricting the analysis to a binary mixture for the sake of simplicity, let us define $\tilde{\phi}_i(r) = \phi_i(r) - \phi_0$, for each cell $i = a, b$, with $\phi_0 = \phi_a(R_a) = \phi_b(R_b)$. Supposing that $\tilde{\phi}_i$ is small, it satisfies the linearized Poisson–Boltzmann equation

$$\Delta\tilde{\phi}_i(r) = \kappa_{\rm PB}^2(\tilde{\phi}_i(r) + \gamma_0) \tag{4.8}$$

with $\kappa_{\rm PB}^2 = \kappa^2 \cosh\phi_0$ and $\gamma_0 = \tanh\phi_0$, and the boundary conditions $\tilde{\phi}_i(R_i) = 0$ and $\tilde{\phi}_i'(R_i) = 0$. The solution of the linearized problem is

$$\tilde{\phi}_i(r) = \gamma_0\Big[-1 + \frac{e^{\kappa_{\rm PB}(r-R_i)}(\kappa_{\rm PB}R_i + 1)}{2\kappa_{\rm PB}r} + \frac{e^{\kappa_{\rm PB}(R_i-r)}(\kappa_{\rm PB}R_i - 1)}{2\kappa_{\rm PB}r}\Big]\,. \tag{4.9}$$

The linear potential $\tilde{\phi}_i(r)+\phi_0$, the behavior of which approximates the nonlinear solution $\phi_i(r)$ near the cell boundary, is created by an effective or renormalized charge $Z_i^{\rm ren} = r_i^2\tilde{\phi}_i'(r_i)/\lambda_B$ where r_i is the colloid radius ($r_a = a$, $r_b = b$ for $i = a, b$ respectively). Explicitly,

$$Z_i^{\rm ren}\frac{\lambda_B}{r_i} = \frac{\gamma_0}{\kappa_{\rm PB}r_i}\Big[(\kappa_{\rm PB}^2R_ir_i - 1)\sinh(\kappa_{\rm PB}(R_i - r_i)) + \kappa_{\rm PB}(R_i - r_i)\cosh(\kappa_{\rm PB}(R_i - r_i))\Big]\,. \tag{4.10}$$

As mentioned before, a convenient numerical algorithm to compute the renormalized charges can be formulated on the basis of the method introduced in Ref. [78]: we impose a value ϕ_0 for the common value of the electric potential at the cell boundaries. Solving numerically the system of equations (4.1)-(4.5) allows us to determine the radius of the cells R_a and R_b and the bare charges Z_a and Z_b corresponding to the value ϕ_0 of the potential at the boundaries of the cells. Finally, using Eq. (4.10) we compute the corresponding renormalized charges $Z_a^{\rm ren}$ and $Z_b^{\rm ren}$. The osmotic properties of the suspension can also be determined by this procedure as discussed below.

4.2.2 Thermodynamic properties

In the mean field approximation, the grand potential per cell (ω_a or ω_b) is given by (see e.g. Ref [91])

$$\beta\omega_i = \frac{1}{8\pi\lambda_B}\int\limits_{r_i\le r\le R_i} |\nabla\phi_i(r)|^2\, d\mathbf{r} + \int\limits_{r_i\le r\le R_i}\sum_{\alpha=\pm}\left[\rho_i^\alpha(r)(\ln\frac{\rho_i^\alpha(r)}{\rho_s}-1)\right] d\mathbf{r} \quad (4.11)$$

where the ionic density profiles inside each cell are given by

$$\rho_i^\pm(r) = \rho_s e^{\mp\phi_i(r)}. \quad (4.12)$$

The integration is performed in the cells excluding the volume occupied by the colloid, i.e., $r_i < r < R_i$. Using Gauss' law, Eqs (4.2) and (4.3), this can be written as

$$\beta\omega_i = \frac{Z_i}{2}\phi_i(r_i) + 4\pi\rho_s\int_{r_i}^{R_i} dr\, r^2\left[\phi_i(r)\sinh\phi_i(r) - 2\cosh\phi_i(r)\right]. \quad (4.13)$$

The total grand potential of the system is

$$\Omega = N_a\omega_a + N_b\omega_b + \boldsymbol{F}_a^{id} + \boldsymbol{F}_b^{id}, \quad (4.14)$$

where $\beta\boldsymbol{F}_i^{id} = N_i[\ln(\rho_i\Lambda_i^3)-1]$ accounts for the colloidal particles entropy, with Λ_i and N_i the thermal length of colloids of species i and their number respectively. The electrostatic contribution to the pressure p can be obtained deriving Ω with respect to the volume V at constant chemical potential. Introducing the osmotic pressure $\Pi = p - p_{res}$ with p_{res} the pressure in the electrolyte reservoir, the final result can be expressed in terms of the potential at the boundary of the cells ϕ_0 in the form

$$\frac{\beta\Pi}{\rho} = 1 + \frac{2\rho_s}{\rho}(\cosh\phi_0 - 1) \quad (4.15)$$

with $\rho = \rho_a + \rho_b$ the total number density of colloids. The l.h.s. of Eq (4.15) defines the osmotic compressibility factor which equals one in the dilute limit. In the next section we apply the model formulated above to study charge renormalization and osmotic properties in a colloidal binary mixture.

4.3 Colloidal binary mixture

Let us consider a colloidal mixture consisting of two species of colloids. In order to reduce the number of parameters, we will assume that the colloids have the same radius, i.e., $a = b$ and we will express all lengths in units of this quantity. In addition, the Bjerrum length will be fixed to $\lambda_B/a = 0.0022$ which is a typical value for a suspension of colloidal particles in water. The remaining free parameters are (i) the bare charge of species a: Z_a, (ii) the bare charge of species b: Z_b (iii) the total packing fraction: η, (iv) the composition of the mixture: x, and (v) the concentration of electrolyte as given by the parameter κa, where κ^{-1} is the screening length of the electrolyte reservoir. Notice that the screening parameter κ is *different* from κ_{PB} as defined after equation (4.8), the latter corresponding to the electrolyte concentration *at the cell boundary*.

4.3.1 Renormalized charges

Let us start our analysis by considering the behavior of the renormalized charges of the binary mixture as a function of the structural charges. Fig.4.1 shows the renormalized charge for each species when the bare charge of one of the species is fixed while that of the other species is changed. In Fig.4.1a the structural charge of species b is fixed to $Z_b\lambda_B/a = 5$ while Z_a varies. In Fig.4.1b we fixed $Z_a\lambda_B/b = 10$ and vary the bare charge of species b. Two different compositions are considered, $x = 0.05$ and $x = 0.95$, and two screening lengths $\kappa a = 0.1$ and $\kappa a = 1$. The remaining parameters are fixed to $\eta = 0.1$, $\lambda_B = 0.72$nm and $a = b = 326$nm. In Fig.4.2 a similar study is performed, this time for a larger total packing fraction of the mixture $\eta = 0.3$. A first observation following Figs.4.1 and 4.2 is that the dependence of $Z_i^{\rm ren}$ is similar to the behavior found in monodisperse systems: as the bare charges Z_i increases, the corresponding renormalized charges Z_i^{ren} grows. The growth is only linear for small values of the varying structural charges. For larger values of $Z_i\lambda_B/a$ the increment becomes highly non-linear (compared to the dashed lines corresponding to $Z_i^{ren} = Z_i$) and saturates towards a value much smaller than the structural charge for $Z_i\lambda_B/a \gg 1$. Notice that the saturation values of the charges depend not only on the total packing fraction but also on the composition of the mixture. The influence of the electrolyte concentration on the saturation curves, on the other hand, is relatively small, as compared to the effect produced by a drastic change in composition or total packing fraction of the mixture. In particular, in Fig.4.2 the curves corresponding to $\kappa a = 1$ and $\kappa a = 0.1$ are indistinguishable. For the packing fractions considered in these examples, reducing the electrolyte concentration manifests itself in a slight reduction of the saturation values in all cases.

The concentration of colloidal particles in suspensions can be adjusted and measured in a wide range of packing fractions, therefore, it is interesting to analyze to what extent the general behavior of the renormalized charges described above depends on this quantity. In Fig.4.3 we consider the scaled renormalized charges corresponding to a total packing fraction varying over several decades. The bare charges of species a and b are fixed by $Z_a\lambda_B/a = 10$ and $Z_b\lambda_B/a = 5$ respectively. The figure shows curves obtained for different electrolyte concentrations as fixed by the parameter κa. Several values of $x = \eta_a/\eta$ are represented by different types of lines. For $\kappa a \gtrsim 1$ and $\eta \lesssim 0.01$ varying either the electrolyte concentration, the total packing fraction, or the composition of the mixture has a small effect on the values of the renormalized charges. For $\eta \gtrsim 0.01$

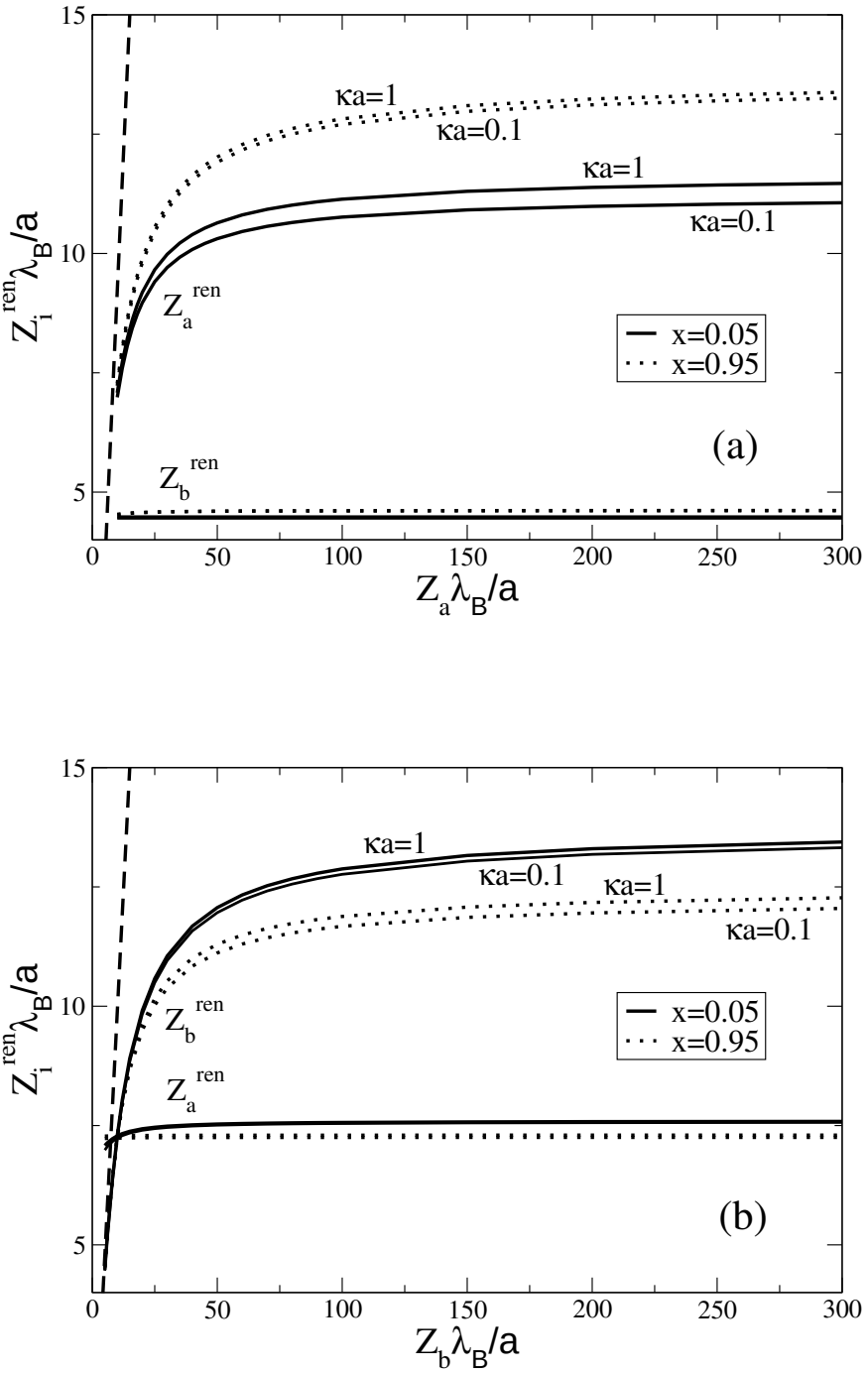

Figure 4.1: Renormalized charges $Z_a^{ren}\lambda_B/a$ and $Z_b^{ren}\lambda_B/a$ for a binary mixture with: (a) fixed bare charge $Z_b\lambda_B/a = 5$ and varying bare charge $Z_a\lambda_B/a$ and (b) fixed bare charge $Z_a\lambda_B/a = 10$ and varying bare charge $Z_b\lambda_B/a$ for $\lambda_B = 0.72$nm and $a = b = 326$nm. The total packing fraction is fixed to the value $\eta = 0.1$. Different electrolyte concentrations and compositions are considered as pointed by the legends. For the sake of comparizon, the dashed line shows the linear dependence corresponding to the case $Z_i^{ren} = Z_i$.

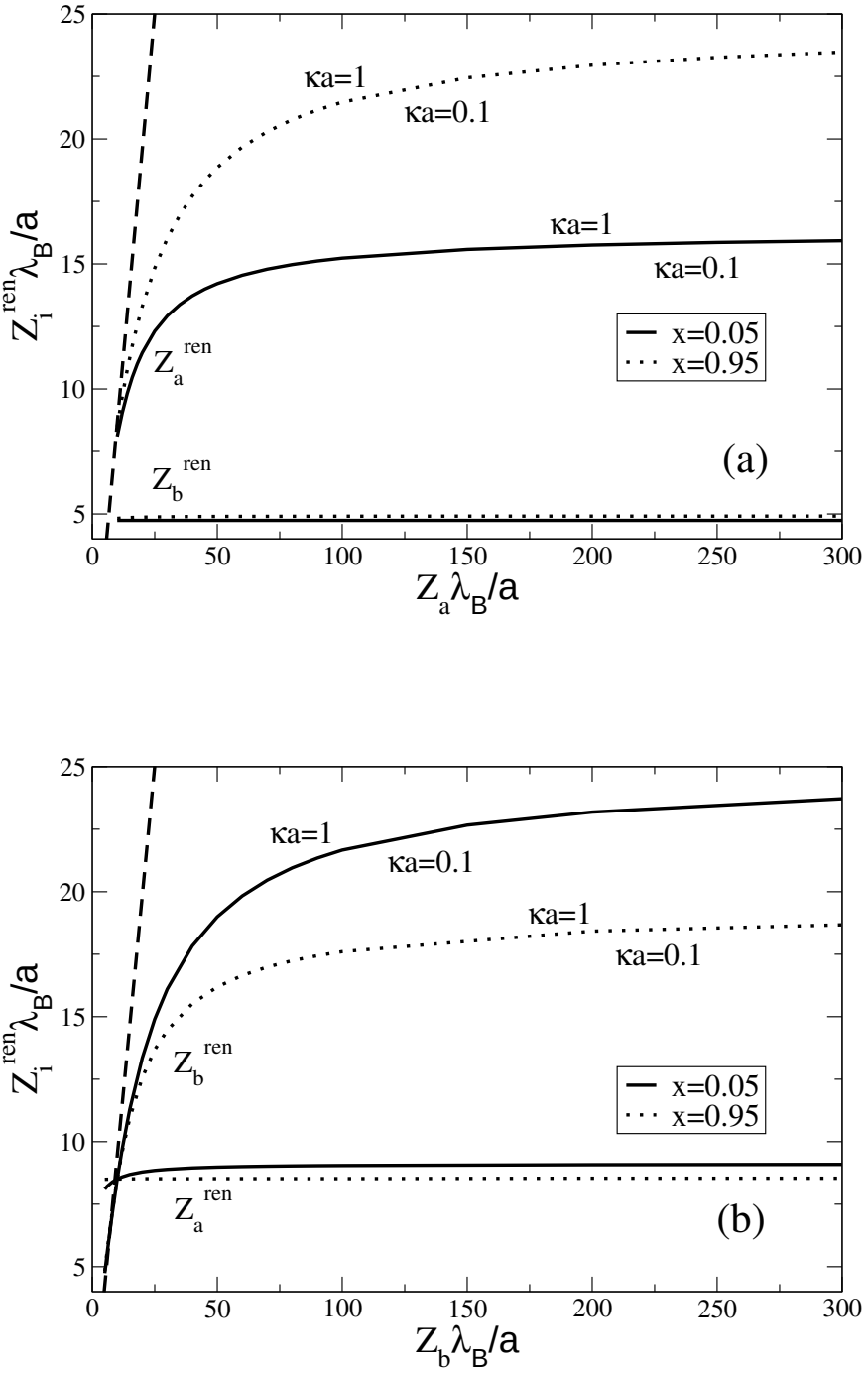

Figure 4.2: Renormalized charges for a binary mixture as given in Fig.4.1. Here we consider a higher value of the total packing fraction, $\eta = 0.3$.

varying the composition of the mixture causes the charge renormalization curves to split into several branches. This effect is also present for smaller total packing fractions in the extremely low electrolyte concentration curve corresponding to $\kappa a = 0.1$. In the latter case, the values of the renormalized charges are much more sensitive to variations of the total packing fraction, which increases after reaching a minimum at about $\eta = 0.015$. At total packing fractions $\eta \gtrsim 0.2$ all the curves show the same qualitative behavior and tend to merge into lines of similar slope.

In Fig.4.4 we show the effect of variations of the composition of the mixture on the scaled renormalized charge of species a. We observe that $Z_a^{ren}\lambda_B/a$ varies linearly with changing x between the corresponding values of a pure species$-a$ system, i.e., $x = 1$ and a pure species$-b$ system, i.e., $x = 0$. Similar curves are obtained for $Z_b^{ren}\lambda_B/a$. The slope of the renormalized charge curves is slightly larger for small electrolyte concentration and is practically zero for $\kappa a = 2$. For the larger packing fractions (triangles), the general tendency is that the renormalized charges increase with x. For smaller packing fractions and low electrolyte concentration (squares in Fig.4.4a), this tendency is reversed in correspondence with the behavior observed in Fig.4.3a.

4.3.2 Osmotic properties

In Fig.4.5 we show the compressibility factor (Eq. (4.15)) as a function of the total packing fraction, corresponding to the four different electrolyte concentrations considered in Fig.4.3. Different types of lines illustrate the effect of varying the compositions of the mixture. In general, adding particles of species with the larger charge increases the compressibility factor. This effect is particularly notable at high packing fractions. At low packing fractions the pressure reduces to the value of the reservoir pressure and the compressibility factor decays towards the ideal gas value, i.e., $\beta\Pi/\rho = 1$. It is interesting to observe the strong effect of varying the electrolyte concentration: following the sequence from Fig.4.5a to Fig.4.5d one notices that the compressibility factor decreases by about two orders of magnitude for $\eta < 0.1$. This diminishing in the compressibility factor is a consequence of the decreased range of the repulsions. Moreover, for low electrolyte concentrations the compressibility factor rapidly grows as a function of the total packing fraction. This effect is intensified by increasing the concentration of the highest charged species, species a in this particular case study. For higher electrolyte concentrations, Fig.4.5d, the rate of change of the compressibility factor is reduced and it assumes smaller values as comparison with Fig.4.5a shows, i.e., the system becomes ideal-like in the dilute regime, as a consequence of the screening of the strong repulsive electrostatic forces. This can be seen more clearly from the osmotic equation of state shown in Fig.4.6 for several electrolyte concentrations. In Fig.4.6a, corresponding to extremely low screening, the osmotic pressure assumes large values and the suspension is expected to be in a crystal-like phase. After increasing the screening constant, the osmotic pressure assumes values close to zero which means that the excess pressure due to electrostatic interactions reduces to the reference pressure in the reservoir.

4.3.3 Cell radii

In Fig.4.7 we plot the cell radii (expressed in units of the colloidal radius a) as a function of the charge of one of the species while the charge of the other species is fixed (see

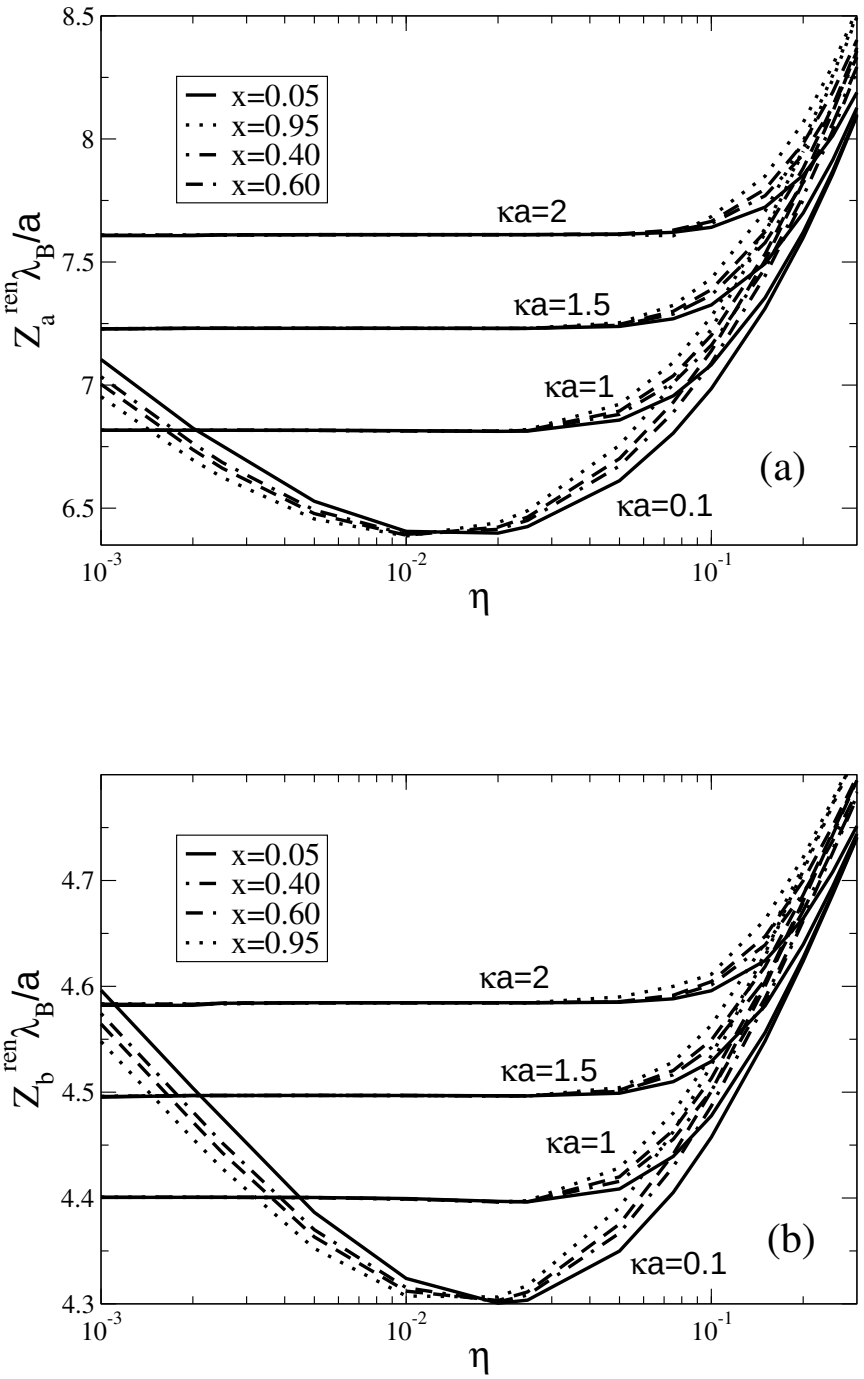

Figure 4.3: Renormalized charges $Z_a^{ren}\lambda_B/a$ and $Z_b^{ren}\lambda_B/a$ for a binary mixture with bare charges $Z_a\lambda_B/a = 10$ and $Z_b\lambda_B/a = 5$ as a function of the total packing fraction η. Different electrolyte concentrations as fixed by the parameter κa are shown. The values of the remaining parameters are typical for colloidal suspensions, namely $\lambda_B = 0.72$nm and $a = b = 326$nm. Different types of lines correspond to distinct compositions of the mixture as indicated by the legends.

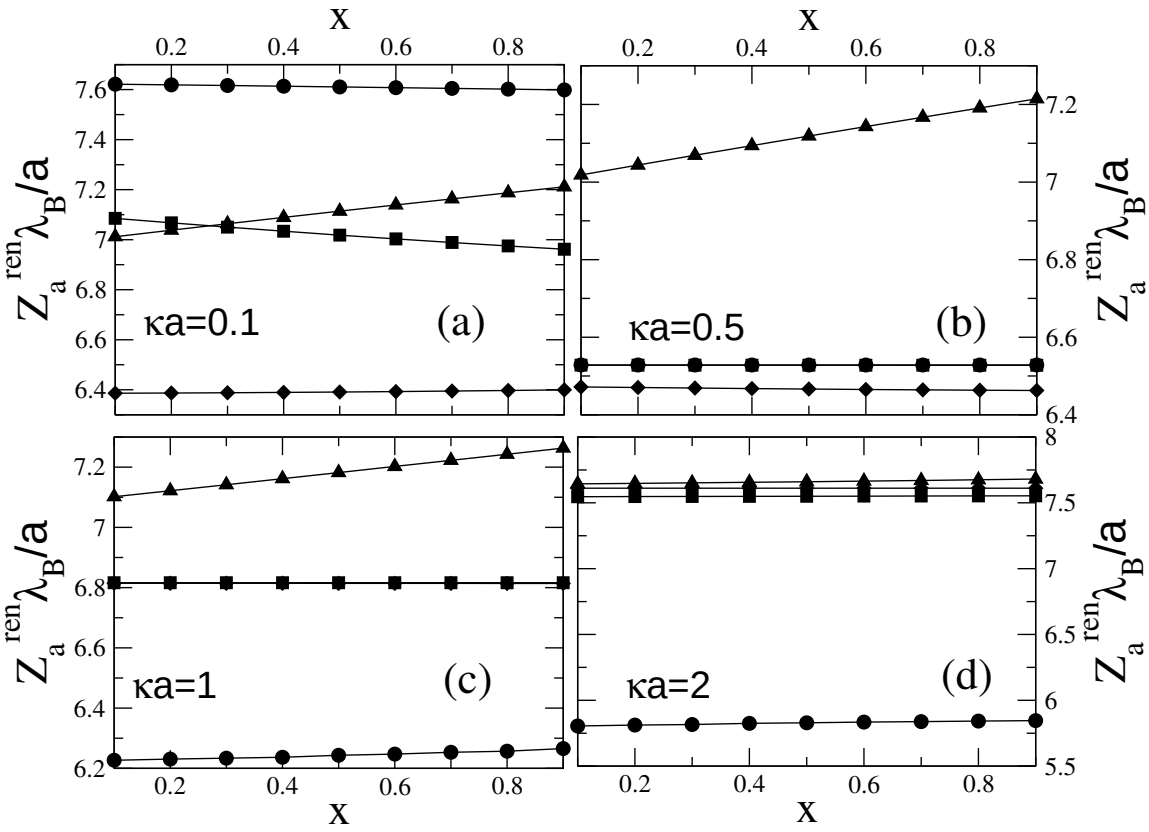

Figure 4.4: Renormalized charge $Z_a^{ren}\lambda_B/a$ as a function of the composition $x = \eta_a/\eta$ for different salt concentrations for the parameters $b = a$, $Z_a\lambda_B/a = 10$, and $Z_b\lambda_B/a = 5$. We consider different values of the total packing fraction, namely $\eta = 10^{-4}$, (circles), $\eta = 10^{-3}$, (squares), $\eta = 10^{-2}$ (diamonds), and $\eta = 10^{-1}$ (triangles). Notice that some sets of data superimpose themselves in (b) and (c).

details in the caption). In general, as one of the radii increases the other radius decreases to satisfy the constraint of fixed total packing fraction as expected from Eq. (4.4). The form in which this occurs depends on the colloid charges and compositions as well as on the other physicochemical parameters in the model. A small total packing fraction leads to larger cell radii, as we notice by comparing Figs.4.7a and 4.7c to Figs.4.7b and 4.7d. Notice also that in the latter case for small values of $Z_b\lambda_B/a$ we have $R_a/R_b > 1$. After the charge of species b is increased, the inequality quickly inverts i.e., the volume of the cells surrounding the now highly charged particles of species b surpasses that of species a. Finally, it is worth to notice the fact that beyond some value of $Z_i\lambda_B/a$ the radii of the cells become almost charge independent, reflecting the fact that the renormalized charges have reached their saturation value. In the light of the previous case study, we now proceed to discuss in more detail some general features of the polydisperse cell model.

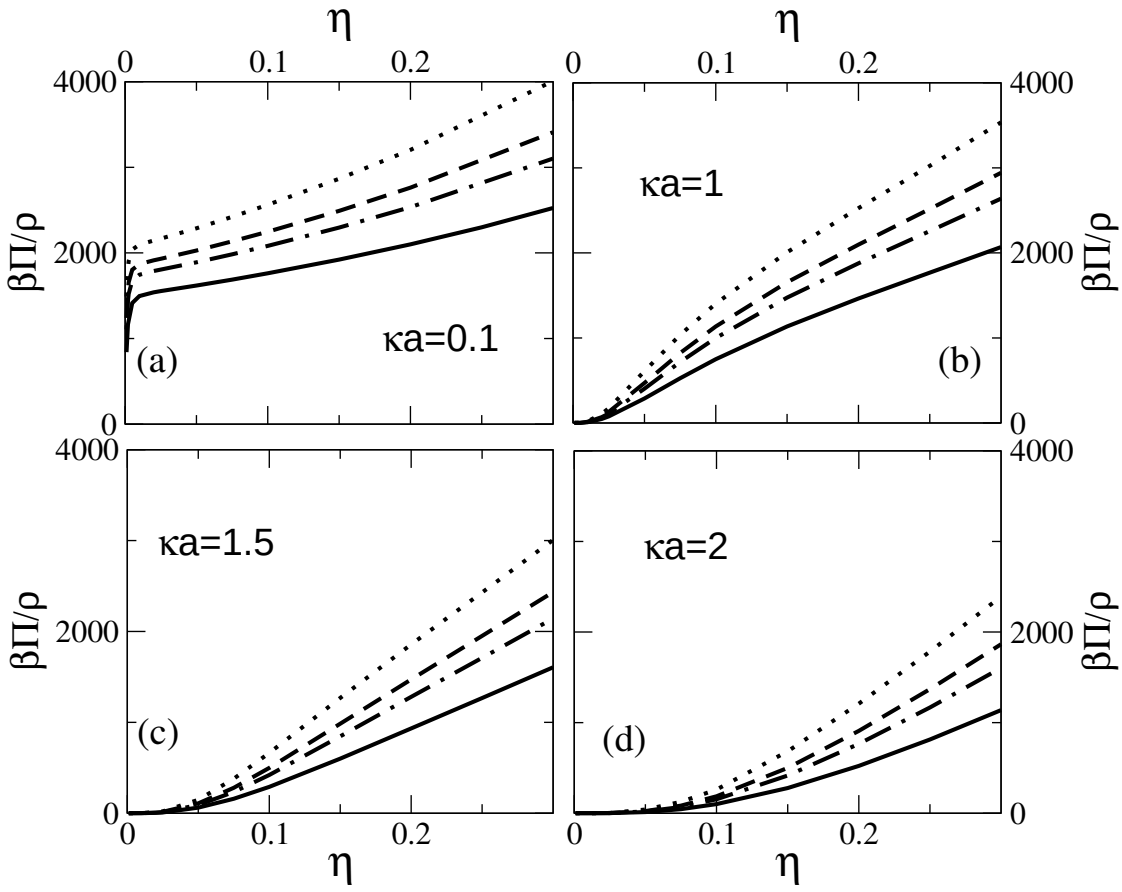

Figure 4.5: Compressibility factor as obtained from Eq. (4.15) as a function of the total packing fraction for different electrolyte concentrations. The line-type convention for different compositions the same as in Fig.4.3.

4.4 Discussion

Physically, the charge renormalization process results from the accumulation of ions in the vicinity of a highly charged object immersed in an electrolyte. Therefore, the relevant parameter to compute their interactions is not the bare charge but the effective (renormalized) charge that takes into account this non-linear screening effect. As shown in Fig.4.1, the behavior of the renormalized charges for polydisperse systems at the level of PB theory is reminiscent of that of their monodisperse counterpart: the renormalized charges saturate to finite values when the structural charges becomes sufficiently large. The saturation values can be orders of magnitude smaller than the structural charges. As a consequence of this non-linear screening effect, a very charge asymmetric colloidal mixture behaves electrostatically like a much more charge symmetric system. For instance, from Fig.4.2b one can notice that a colloidal binary mixture with charges $Z_a\lambda_B/a = 10$ and $Z_b\lambda_B/a = 300$ behaves *effectively* as a mixture with $Z_a^{ren}\lambda_B/a \simeq 7.5$ and $Z_b^{ren}\lambda_B/a \simeq 13$, so that the ratio $Z_a/Z_b = 0.03$ changes to $Z_a^{ren}/Z_b^{ren} = 0.58$ which corresponds to a much more charge symmetric effective mixture. On the other hand, for small values of the structural charges, $Z_i^{ren} \simeq Z_i$. As a consequence, expressions for

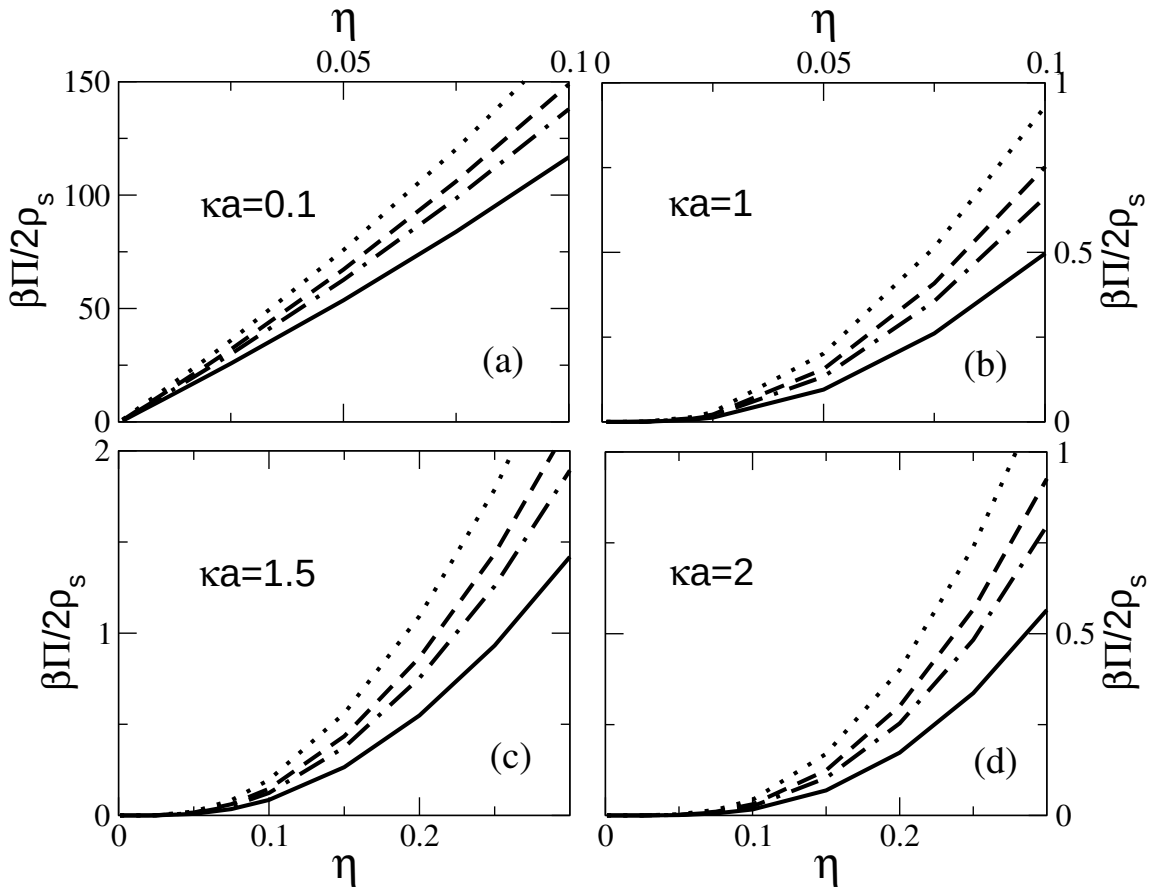

Figure 4.6: Osmotic pressure as a function of the total packing fraction for different electrolyte concentrations. The line-type convention is the same as in Fig.4.3.

the effective interaction potentials derived from linear theories, e.g., DLVO theory, are expected to be sufficient to describe the thermodynamic properties of the suspension, at least in the regime where pairwise additivity is expected [92, 93].

The saturation values of the renormalized charges depend on the physicochemical parameters: the electrolyte concentration, total colloids density, the dielectric constant of the solvent and the composition of the mixture. Increasing the electrolyte concentration has the effect of enhancing the value of the renormalized charges. This effect induces two competing tendencies in the screened interaction potential. On the one hand the spatial extent of the double-layer reduces, on the other the amplitude of the interactions increases. This tendency is inverted in the case of weak screening and total colloids packing fraction smaller that about 5% (see Fig.4.3). The balance of these two non-linear screening features is affected by the composition of the mixture and is expected to have consequences on, e.g., the phase diagrams of mixtures of highly charged macroions computed by using Yukawa-like potentials, the omission of such non-linear screening effects, as accounted by Z_i^{ren}, may lead to unphysical results as demonstrated by several authors (See e.g. [94, 95]).

In the context of the cell model for monodisperse systems, it is assumed that due to entropic reasons, the colloidal particles tend to occupy the maximum space possible

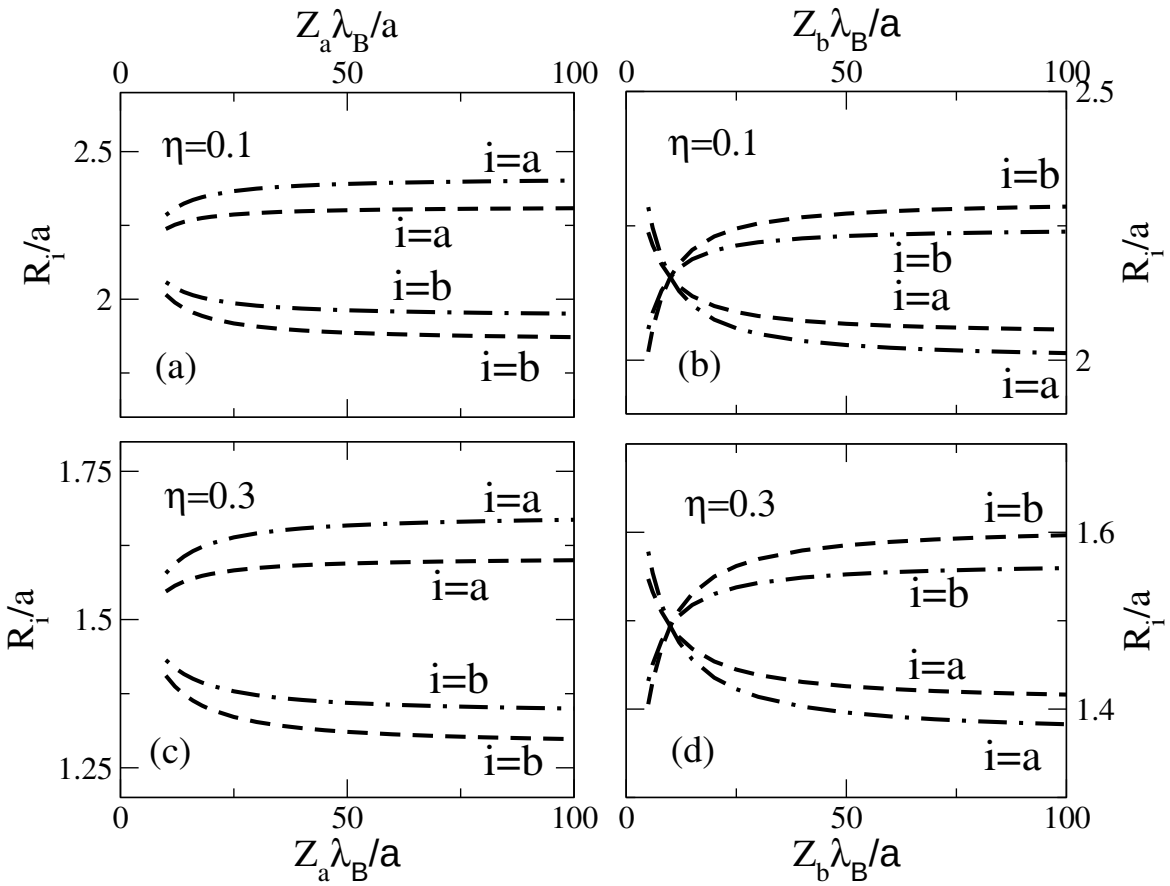

Figure 4.7: Radii of the cells R_a and R_b surrounding particles of type a and b respectively expressed in units of the colloids radius $a = b = 326$nm. In (a) and (c) the bare charge of type-a particles varies while $Z_b\lambda_B/a = 5$ is kept fixed. In (b) and (d) the bare charge of type-b particles varies while $Z_a\lambda_B/a = 10$ remains unchanged. Two different total packing fractions are considered as pointed by the legends and the values $\lambda_B = 0.72$nm and $\kappa a = 1$ are used in all figures. The line-type convention is the same as that in Fig.4.3.

inside the solvent. Therefore, it is feasible to factorize the suspension into spherical cells, each of them housing a colloidal particle in its center. The radius of such cells is then chosen in such a fashion that the cells fill all the suspension, namely $R/a = \eta^{-1/3}$. In other words, the packing fraction alone determines the size of the cells. In contrast, in the polydispense cell model, the radii of the cells depend not only on the total packing fraction and the composition of the mixture according to Eq. (4.4), but also on the relative charges of the species through the boundary conditions expressed by Eqs. (4.3) and (4.5). In other words, the volumes of the cells are not only determined by fixing the total packing fraction, but adapt themselves in order to satisfy the boundary conditions which impose the cells to be electrically neutral, the potential to be continuous at the cells boundaries and the cells to fill the whole volume accessible to the colloidal particles. The resulting cells are independent units regarding electrostatic interactions in virtue of their neutrality. Therefore, the grand potential of the entire suspension can be easily calculated as the sum of the grand potential of individual cells. This facilitates enormously the calculation

of thermodynamic response functions, in particular the osmotic pressure, according to the contact theorem, (see e.g., Ref. [3]), can be obtained directly from the value of the electrostatic potential at the cell boundary as explained before. The value of the potential at the cell boundary depends on the size of the cell, which has a radius depending on the parameters, and in particular, on the composition of the mixture.

Experimentally, in spite of the recent advances in electrophoretic techniques [96], it is difficult to precisely measure the values of renormalized charges in colloidal suspensions. Therefore, it would presumably be intricate to collect experimental evidence of, e.g., the splitting of the charge renormalization curves in Fig.4.3, even at the highest packing fractions. Osmotic properties are nevertheless relatively easy to probe experimentally e.g., in sedimentation-diffusion equilibria [97],[98]. In that sense the present formalism provides a reasonably simple and numerically robust scheme for the calculation of the osmotic equation of state and compressibility factors in a wide range of parameters. As illustrated in the case study of the binary mixture, these osmotic properties are non-trivially dependent on the mixture composition, which is illustrated by the fact that the relatively small change in the values of the corresponding renormalized charges shown in Fig.4.3, *do not* necessarily imply a mild change in the response functions: the former are obtained from changes in the slope of the potential at the colloidal particles surfaces as given by the solution of the linearized PB equation (see Eq. 4.10), whereas the latter depend on the value of the potential at the cell boundary (Eq. 4.15). The screening parameter, however, plays a much more important role in the osmotic properties than the relative composition of the mixture, and may cause, for instance, the osmotic pressure to vary over several orders of magnitude.

It is worth mentioning the fact that in the polydisperse cell model we restricted our attention to colloids of the same sign of charge. The reason is that one can impose on physical grounds the condition that each cell surrounding a colloid is charge neutral, i.e., $\phi_i'(R_i) = 0$ for $i = 1, ..., M$. It is not obvious that such a condition can be imposed for oppositely charged colloids, as the potential may change sign in between the colloids while the electric field does not vanish anywhere. The attractive or repulsive nature of the interactions between the cells is obtained straightforwardly from the signs of the potentials; potentials opposite in sign can still lead to colloidal repulsions [99]. A second limitation related to the cells electroneutrality is also present in Alexander's formulation: as a consequence of the restriction of the theoretical analysis to a single cell per colloidal component, all information on correlations between the colloids is lost. This may lead to unphysical ideal-gas-like values for the osmotic pressure in highly screened suspensions [100]. Care has to be exercised in drawing conclusion from cell models in this regime.

An important feature of charge renormalization is the fact that increasing the electrolyte concentration leads to higher values of the renormalized charges simultaneously reducing the extension of the double-layer [79, 80]. These two non-linear screening features are neglected in linear theories, such as the DLVO model, where the (structural) charge is in principle independent of the screening parameter. These artifacts of the linearization procedure can be cured by using the renormalized values of the charges within the linear schemes, which can in principle be achieved for example by using the analytical solution of the Ornstein-Zernike equation for a mixture interacting via a DLVO-like potential within Mean Spherical Approximation, by replacing $Z_i \rightarrow Z_i^{ren}$. A second alternative is provided by the variational treatment of DLVO-like potentials based on the Gibbs-Bogoliubov inequality, which uses the Laplace transforms of the pair correlation

functions to estimate the free energy of the system though a numerical optimization problem (see e.g., Refs. [101, 102]). This alternative is extremely suitable for the calculation of phase diagrams by e.g., using Maxwell constructions, providing a simple alternative for the study of phase behavior of highly charged colloidal mixtures while fully taking into account non-linear effects.

4.5 Conclusion

In this chapter we proposed a simple model which allows to study the thermodynamic properties of mixtures of highly charged macroions suspended in an electrolyte. The model is a generalization of the well-known cell model for colloids, and incorporates the notion of charge renormalization as introduced by Alexander and collaborators [76]. In contrast to the one-component cell model, where the radius of the cells is fixed by the packing fraction of colloids, in the polydisperse cell model the radii of the cells depend on the physicochemical parameters through the boundary conditions utilized to solve the non-linear Poisson-Boltzmann equation in the cell geometry. The radii of the cells play the role of parameters that enforce the constraint that the cells fill the entire volume occupied by the colloidal mixture and have to be determined within the numerical solution of the non-linear differential equations. We presented a method to perform such a calculation based on the algorithm of Ref. [78], which also allows to determine thermodynamic response functions and renormalized charges within a clear and efficient numerical scheme. We presented a detailed example of such an analysis in the case of a colloidal binary mixture, where we studied the effect that several physicochemical parameters have on the values of the saturation curves for the renormalized charges and osmotic properties of the suspension. In general, the ion condensation phenomenon that leads to charge renormalization has the effect of making the mixture more "electrostatically symmetric", in the sense that the ratio of the renormalized charges is much closer to one than that of the structural charges. Increasing the concentration of the species with the greatest charge keeping the total packing fraction fixed, raises the osmotic pressure. An important limitation of the present model, which is actually shared by all Poisson-Boltzmann-based models, is the fact that ion-ion correlations are neglected. This oversimplification of the problem may lead not only to quantitative but also to qualitative modifications to the saturation curves: the renormalized charge may exhibit a maximum followed by a decrease of Z_i^{ren} with Z_i increasing (see e.g., Ref. [103–105]). In some cases this can lead to a weakening of the interactions as calculated on the basis of the renormalized charges, which may eventually turn electrostatic repulsions into attractions. In the case of 1:1 electrolytes, such ion-ion correlations are relatively unimportant and the present Poisson-Boltzmann model is expected to provide a reasonably good description of highly charged colloidal mixtures.

5

Volume terms for colloidal mixtures

The presence of electrolyte makes an approach to the study of statistical thermodynamical properties of charge-stabilized colloids based on simulations of the Primitive Model computationally unfeasible. In this chapter, a theoretical analysis is performed instead by using the semi-grand canonical ensemble in the framework of density functional theory in the Debye-Hükel limit. A general expression is derived for the effective interaction potential for polydisperse colloidal systems with added electrolyte. In the particular case of deionized systems we re-encounter deviations from the Yukawa mixture behavior expected from a DLVO-like theory reported in the literature (A. Torres et al., *Phys. Rev. E.* **77**, 1 (2008)) and discussed later in chapter 7, due to many-body effects. Increasing the ionic strength attenuates many-body effects. Under these conditions the model with pairwise Yukawa potentials gives quantitatively accurate results.

5.1 Introduction

We have seen already that colloidal suspensions are extremely asymmetric mixtures of (sub)-micron-sized colloidal particles and sub-nanometer sized anions, cations, and solvent molecules. Treating all these species on an equal footing is often impractical, if not impossible, due to large differences in size and charge, such that the number of solvent molecules and screening ions exceeds the number of colloids by many orders of magnitude. It is therefore natural and often necessary to regard these complex mixtures as effective one-component systems of the colloidal component only, with medium-induced effective colloidal interactions. In the determination of such effective interaction potentials it is common to invoke the screening principle and replace the Coulomb potential by a pairwise screened potential, without much concern about the legitimacy of such an approximation or its range of validity in terms of the system's parameters, such as the colloidal charge or ionic strength. This is in general a risky procedure, since the long range

of the stabilizing electrostatic interactions gives the system a strong many-body character, and it is difficult to estimate a priori to what extent the interactions can be split into separate pair contributions.

A more rigorous approach to the problem of colloidal interactions can be taken in the spirit of McMillan-Mayer theory [17–19], as explained in Sec. 1.4. Let us consider for the sake of this introduction a monodisperse colloidal system consisting of N charged colloidal particles with coordinates $\mathbf{R}^N$ (the polydisperse case will be discussed in Sec 5.2), and N_+ positive and N_- negative mobile point-like ions of charge $\pm e$. The colloidal particles are immersed in a solvent which is considered to be a structureless medium at temperature T characterized by a dielectric constant ε. As discussed in Sec. 1.4, the free energy of the suspension can be calculated by integrating the effective Boltzmann factor, over all possible configurations of colloids, namely

$$e^{-\beta F} = \mathbf{Tr} e^{-\beta W_N(\mathbf{R}^N)}, \tag{5.1}$$

where $\mathbf{Tr}$ is the classical canonical trace over the colloidal particles coordinates*, where $W_N(\mathbf{R}^N)$ is the $N-$body potential of mean force. In order to use this scheme in practice, one has to be able to calculate the $N-$body potential of mean force $W_N(\mathbf{R}^N)$ explicitly. This is in general a formidable task. Approximation schemes can be developed by considering a sequence of systems consisting of $n = 0, 1, 2, \cdots, N$ colloidal particles, so that one can formally write

$$W_N(\mathbf{R}^N) = W_0 + \sum_{k=1}^{N} w_1(\mathbf{R}_k) + \sum_{k<l}^{N} w_2(\mathbf{R}_k, \mathbf{R}_l) + ..., \tag{5.2}$$

where w_n represents the n-body potential and where the dots represent the three-body and higher order terms. In Eq.(5.2) W_0 is the contribution of the (homogeneous) medium without a single colloidal particle, and $w_1(\mathbf{R})$ its excess due to a single colloid at position $\mathbf{R}$. In a homogeneous solvent, and without an external field acting on the colloidal particles, $w_1(\mathbf{R})$ is a constant independent of $\mathbf{R}$, hence the second term of Eq.(5.2) reduces to Nw_1. The effective pair-potential $w_2(\mathbf{R}, \mathbf{R}') \equiv W_2 - (W_0 + 2w_1)$ is the difference of the potential of mean force in the presence of two colloids at $\mathbf{R}$ and $\mathbf{R}'$ and that at infinite separation. Similar reasonings can be used to define the three-body potential, etc. Typically this scheme is truncated beyond the pair-level, i.e., one assumes that $w_n \equiv 0$ for $n \geq 3$. For many situations this is an excellent approximation, since the typical size of the colloids usually exceeds the typical correlation length of the medium, such that triplet "overlaps" are statistically insignificant. However, the assumption of pairwise additivity of $W_N(\mathbf{R}^N)$ is not at all expected to be accurate in the case of a suspension of charged colloids at vanishingly low salt concentrations [106]. In that case the correlation length of the medium is the Debye length, which for deionized water at room temperature can be as large as a micron and even larger in less polar solvents. Note that the typical range of the effective interactions is of the order of the correlation length ξ of the medium, as this is the length scale over which the medium is affected by the presence of a colloid [107], [108].

The cavalier next step has often been to assume pair wise additivity of the colloidal

*i.e., $\mathbf{Tr} = \frac{1}{N!\Lambda^{3N}} \int d\mathbf{R}^N$

interactions. The $N-$body potential of mean force then reads

$$W_N(\mathbf{R}^N) = \sum_{i<j}^{N} v^{eff}(\mathbf{R}_i, \mathbf{R}_j), \tag{5.3}$$

where $v^{eff}(\mathbf{R}_i, \mathbf{R}_j)$ is obtained from linear mean field theory, which yields a screened Coulomb potential (see Eq. (1.25)) as discussed in Sec 1.4. Many properties have been studied with this type of effective Hamiltonians, such as crystallization [109, 110], osmotic equations of state [111], and sedimentation profiles [112, 113], mostly in good agreement with experimental results. However, not all experimental observations are in qualitative agreement with DLVO theory. For example, there is evidence of "gas-liquid" coexistence of charged colloids at low salt concentration [114–120], which cannot be explained by the purely repulsive DLVO potential. It has been also shown that equilibrium sedimentation profiles are not always described correctly within DLVO theory at low salinity [106].

Alternatives to the scheme of calculating successive n-body potentials for charged colloids numerically were formulated in Refs. [22, 70–73], and are based on a linear treatment of electrostatic correlations. A direct effect of this linearization scheme is that $w_n \equiv 0$ for $n \geq 3$, i.e., the system *seems* to be pairwise additive. In fact, ignoring the $n \geq 3$ terms in eq. (5.2) is consistent with DLVO theory as regards the phase behavior of the suspension. The reason is that $W_0 = -p_0 V$ and $N w_1$ are linear in V and N and hence merely shift the pressure and the colloidal chemical potential by a constant. Here p_0 is the pressure of the suspending medium without colloids. However, since the linearization is performed about the self-consistently determined average ion densities and the average so-called Donnan electrostatic potential, which depend on the colloid density, one finds an $N-$body potential of mean force of the form

$$W_N(\mathbf{R}^N) = W_1(\rho_c) + \sum_{i<j}^{N} W_2(R_{ij}, \rho_c), \tag{5.4}$$

where $R_{ij} = |\mathbf{R}_i - \mathbf{R}_j|$. Notice that the linearization schemes are such that the $\{\mathbf{R}\}$-dependence of w_n for $n \geq 3$ in Eq.(5.2) is replaced by a dependence on the number density of the colloidal particles ρ_c of W_1. Therefore, the effective interaction potential includes averaged many-body terms. In what follows we shall refer to the model based on (5.4) as the effective model (EM). The additional density-dependent, coordinate-independent terms account for phenomena observed in primitive model (PM) simulations, where the colloids and microions are considered explicitly [106, 121]. The explicit form of the EM has direct thermodynamic consequences, as one finds from Eq. (5.4) that the free energy F of the whole suspension is now of the form $f(\rho_c) \equiv F/V = W_1(\rho_c)/V + f_2(\rho_c)$ with $f_2(\rho_c)$ the free energy density of a system of N particles in a volume V interacting with a potential energy given by the second term in the r.h.s of (5.4). Given that the phase behavior and the (osmotic) equation of state of the suspension depend on the curvature of $f(\rho_c)$ w.r.t. ρ_c, one directly sees that a nontrivial ρ_c-dependence of $W_1(\rho_c)$ and/or $W_2(R_{ij}, \rho_c)$ affects the thermodynamics of the system.

The purpose of this chapter is to calculate W_1 explicitly for a *polydisperse* system of charge-stabilized colloids in the presence of additional electrolyte, i.e., in the non-deionized case. The resulting $N-$body potential is an efficient alternative to PM simulations, which are computationally unworkable, specially when it is necessary to consider

a large range of parameters. Our alternative to these simulations is a theoretical approach using the semi-grand canonical ensemble, where the effect of added salt is taken into account only effectively, i.e., the ion degrees of freedom are averaged out. This formalism allows to calculate the explicit form of W_1 and W_2 for added salt. In chapter 7 we will use this expression in combination with Monte Carlo simulations of a fluid with interaction potential in the form of Eq. (5.4) to obtain thermodynamic properties, i.e., isothermal compressibility and sedimentation-diffusion profiles. We will use the latter as a suitable tool to study the effects of ionic strength on the effective many-body interactions by considering its consequences at the thermodynamic level.

5.2 Effective interaction potential for multi-component systems

In this section we derive an effective model of a system with M colloidal components, which includes implicitly the effect of added salt. For this model we will obtain averaged many-body colloid-colloid interactions. Below we discuss the main steps in the calculation of the effective interaction potential, deferring the details to the appendix. We consider a system consisting of M different species, each of them consisting of N_r colloidal particles so that $N = \sum_{r=1}^{M} N_r$ is the total number of particles in the system. The colloidal particles have coordinates $\mathbf{R}^N \equiv \{\mathbf{R}^{N_1}, ..., \mathbf{R}^{N_M}\}$ and are characterized by their radius a_r (diameters σ_r), their charge eZ_r, with e the proton charge, and their number densities $\rho_r = N_r/V$. The composition of the mixture is specified in terms of the molar fractions $x_r = \rho_r / \sum_{r=1}^{M} \rho_r$. The interior of the colloidal particles is assumed to be a medium of the same dielectric constant as that of the ion solution in order to avoid image charge effects (index-matched suspension). In addition, there are N_+ positive and N_- negative mobile point-like ions of charge $\pm e$. It is convenient to describe this system as being in equilibrium with a bulk salt reservoir with total number density ρ_s for either type of ions, separated by a membrane permeable for everything but the colloids. The system is therefore open with respect to the ions.

In order to calculate the $N-$body potential of mean force corresponding to the multi-component system defined above within a mean field approximation, we determine the grand potential density functional $\Omega(\mathbf{R}^N)$ introduced in Eq. (1.16), as the minimum of a suitable density functional $\hat{\Omega}[\tilde{\rho}_+(\mathbf{r}), \tilde{\rho}_-(\mathbf{r})](\mathbf{R}^N)$ with respect to variations of the ion density profiles $\tilde{\rho}_+(\mathbf{r})$ and $\tilde{\rho}_-(\mathbf{r})$. Notice that the grand potential completely determines the effective Boltzmann factor through (1.16), since the set of colloid-colloid interactions $U_{cc}(\mathbf{R}^N) = \sum'_{p,q}{}^{M} \sum'_{i,j}{}^{N_M} u_{ij}^{pq}$ is known, namely, a multi-centered sum of hard-sphere interactions with diameter $a_p + a_q$ with a Coulomb tail of the form $u_{ij}^{pq} = e^2 Z_p Z_q / \varepsilon |\mathbf{R}_i^p - \mathbf{R}_j^q|$, where $\mathbf{R}_i^r$, refers to the position of the colloidal particle i of a given species r with $i = 1, ..., N_r$. The primes in the summations indicate the fact that double-counting should be avoided. For low colloid concentrations and not too high colloid charges, a good approximation for such a density functional is given by

$$\hat{\Omega}[\tilde{\rho}_+(\mathbf{r}), \tilde{\rho}_-(\mathbf{r})](\mathbf{R}^N) = \sum_{\pm} \hat{\Omega}_{id}[\tilde{\rho}_\pm(\mathbf{r})] + \frac{e^2}{2} \int d\mathbf{r} d\mathbf{r}' \frac{\tilde{\rho}(\mathbf{r})\tilde{\rho}(\mathbf{r}')}{\epsilon |\mathbf{r} - \mathbf{r}'|} + \sum_{\pm} \int d\mathbf{r} \tilde{\rho}_\pm(\mathbf{r}) U_\pm(\mathbf{r}, \mathbf{R}^N), \tag{5.5}$$

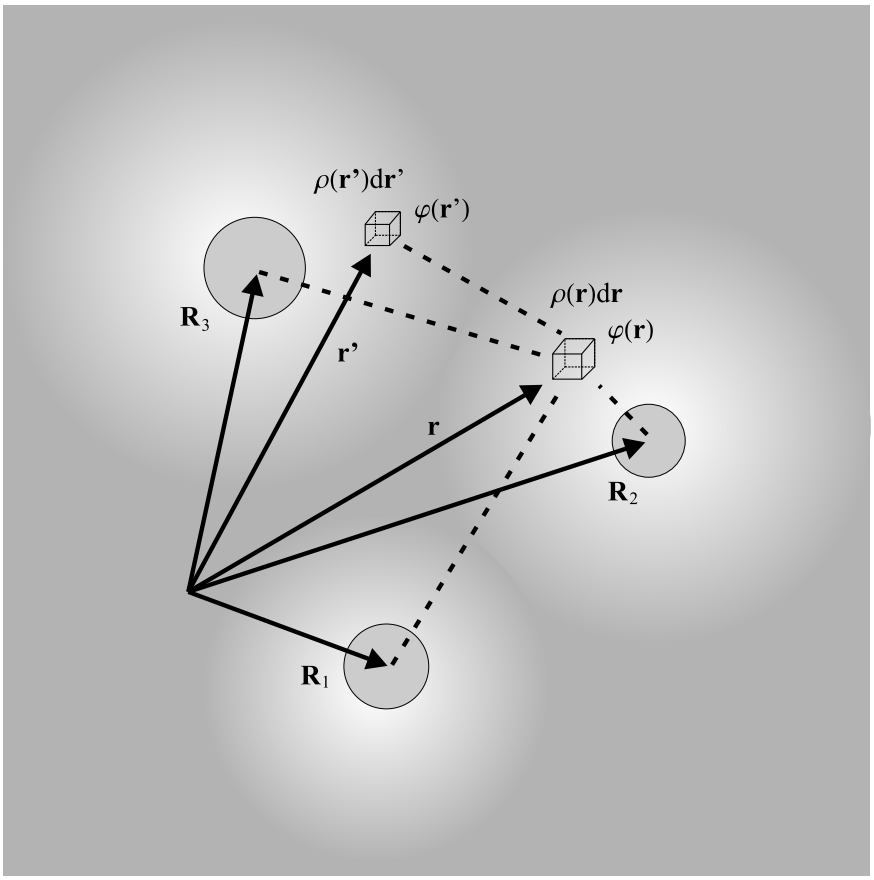

Figure 5.1: Schematic representation of the multicentered configuration of colloids which determines the inhomogeneous distribution of ions in space. The colloids are dressed by ion clouds which are distorted by the other dressed colloids.

where $\hat{\Omega}_{id}[\tilde{\rho}_{\pm}(\mathbf{r})] = k_B T \int d\mathbf{r} \tilde{\rho}_{\pm}(\mathbf{r}) \left(\ln\left(\tilde{\rho}_{\pm}(\mathbf{r})/\rho_s\right) - 1\right)$ are the entropic and chemical potential contributions of the microions and $e\tilde{\rho}(\mathbf{r}) \equiv e\left(\tilde{\rho}_{+}(\mathbf{r}) - \tilde{\rho}_{-}(\mathbf{r})\right)$ is the local charge concentration at point $\mathbf{r}$. The integrand in the second term on the r.h.s. of (5.5) is half the electrostatic interaction energy of two differential charge elements $e\rho(\mathbf{r})d\mathbf{r}$ and $e\rho(\mathbf{r}')d\mathbf{r}'$ separated by a distance $|\mathbf{r} - \mathbf{r}'|$ as illustrated in Fig. 5.1. The third term accounts for the energy of the ions in the external (colloidal) potential $U_{\pm}(\mathbf{r}, \mathbf{R}^N)$, which is the potential energy experienced by one ion at point $\mathbf{r}$ for a fixed configuration of colloids $\mathbf{R}^N$. The external potential determines the inhomogeneous density profiles $\rho_{\pm}(\mathbf{r})$ of the ions in the solution. Due to the difference in the range of the hard sphere $V_r^{hard}(\mathbf{r}, \mathbf{R}^N)$ and electrostatic contributions $V_r^{elec}(\mathbf{r}, \mathbf{R}^N)$ to the external field, it is convenient to write these separately as

$$U_{\pm}(\mathbf{r}, \mathbf{R}^N) = \sum_{r=1}^{M} \left\{ \pm V_r^{elec}(\mathbf{r}, \mathbf{R}^N) + \frac{2\bar{\rho}_{\mp}}{\bar{\rho}_{+} + \bar{\rho}_{-}} V_r^{hard}(\mathbf{r}, \mathbf{R}^N) \right\} \tag{5.6}$$

where the prefactor of the hardcore contribution is chosen for later convenience (see appendix and Ref. [143]). Correspondingly, the potentials characterizing the field due to a fixed configuration of colloidal particles can be written as sums of pair potentials

$V_r^{elec}(\mathbf{r},\mathbf{R}^N)=\sum_{r=1}^{M}\sum_{i=1}^{N_r} v_r\left(|\mathbf{r}-\mathbf{R}_i^r|\right)$ and $V_r^{hard}(\mathbf{r},\mathbf{R}^N)=\sum_{r=1}^{M}\sum_{i=1}^{N_r} \omega_r\left(|\mathbf{r}-\mathbf{R}_i^r|\right)$ consisting of Coulomb and hard-sphere pair interactions respectively (see appendix. Eqs. (5.13) and (5.14)). After expansion to quadratic order of the ideal-gas part $\hat{\Omega}_{id}[\tilde{\rho}_{\pm}(\mathbf{r})]$ with respect to the average ion density $\bar{\rho}_{\pm}$, two Euler-Lagrange equations determine the equilibrium density profiles $\rho_{\pm}(\mathbf{r})$ that minimize the density functional (5.5), namely

$$\left.\frac{\delta\beta\tilde{\Omega}[\tilde{\rho}_{+}(\mathbf{r}),\tilde{\rho}_{-}(\mathbf{r})]}{\delta\tilde{\rho}_{\pm}(\mathbf{r})}\right|_{\tilde{\rho}_{\pm}(\mathbf{r})=\rho_{\pm}(\mathbf{r})}=0. \tag{5.7}$$

The resulting equilibrium profiles can be inserted back into the functional (5.5) in order to determine the equilibrium grand potential, i.e, $\Omega[\rho_{+}(\mathbf{r}),\rho_{-}(\mathbf{r})](\mathbf{R}^N)$. After some algebra explained in the appendix, we find that the $N-$body potential of mean force can be written as

$$W_N(\mathbf{R}^N)=W_1(\gamma)+\sum_{p,q}^{M}{}'\sum_{i,j}^{N_p,N_q\prime} v_2^{pq}(R_{ij}^{pq},\gamma) \tag{5.8}$$

where $R_{ij}^{pq}=\left|\mathbf{R}_i^p-\mathbf{R}_j^q\right|$. The expression on the r.h.s. of (5.8) depend on the $3M+2$ parameters $\gamma\equiv\{a_r,Z_r,\rho_r,\rho_s,\lambda_B\}$. In the appendix we show that the second term on the r.h.s of (5.8) corresponds to the potential energy of a system of M chemical species interacting through a density dependent interaction potential, consisting of a hard-sphere part and a screened Coulomb tail:

$$\beta v_2^{pq}(R_{ij}^{pq},\gamma)=\begin{cases}\infty, & R_{ij}^{pq}<\sigma_{pq}\\ \dfrac{\Gamma_p\Gamma_q\lambda_B}{R_{ij}^{pq}}\exp\left(-\bar{\kappa}(\gamma)R_{ij}^{pq}\right), & R_{ij}^{pq}\geq\sigma_{pq}\end{cases} \tag{5.9}$$

with $\Gamma_r=Z_r e^{\bar{\kappa}(\gamma)a_r}/(1+\bar{\kappa}(\gamma)a_r)$, $\sigma_{pq}=(a_p+a_q)$ the contact distance between particles of species p and q, and $\lambda_B=e^2/\varepsilon k_BT$ the Bjerrum length. The screening length depends on the densities and charges of the species and on the ion concentrations in the reservoir through the parameters $y_r=Z_r\rho_r/2\rho_s$, and follows from

$$\bar{\kappa}^2(\gamma)=8\pi\rho_s\lambda_B\sqrt{Y^2(\{Z_r,\rho_r.\rho_s\})+K^2(\{a_r,\rho_r\})} \tag{5.10}$$

with $Y(\{Z_r,\rho_r.\rho_s\})=\sum_{r=1}^{M}y_r$ and $K(\{a_r,\rho_r\})=\exp\left[-\sum_{r=1}^{M}\eta_r/(1-\eta)\right]$ with $\eta_r=\pi\rho_r\sigma_r^3/6$ the packing fraction of species r and $\eta=\sum_{r=1}^{M}\eta_r$. Notice that y_r is by definition the ratio of the charge density of counterions of species r to the number density of ions in the reservoir (see appendix). The first term on the r.h.s. of (5.8) is a coordinate independent volume term. The explicit form of the latter includes the contribution of the free energy of each of the N colloidal particles in the presence of their own electrical double-layers as explained in the appendix. For the multi-component system under consideration here, we find

$$\begin{aligned}\beta W_1(\gamma) &= -\frac{1}{2}\frac{Y}{\sqrt{K^2+Y^2}}\sum_{r=1}^{M}Z_rN_r-\frac{1}{2}\sum_{r=1}^{M}\frac{\bar{\kappa}\lambda_B}{1+\bar{\kappa}a_r}Z_r^2N_r \\ &\quad+\frac{2K^2}{\sqrt{K^2+Y^2}}\sum_{r=1}^{M}\frac{\eta_r}{1-\eta}V+\sum_{\pm}\left(\bar{\rho}_{\pm}\ln\frac{\bar{\rho}_{\pm}}{\rho_s}-\bar{\rho}_{\pm}\right)V,\end{aligned} \tag{5.11}$$

where the dependencies on γ on the r.h.s. have been omitted in order to lighten the notation, and $\bar{\rho}_{\pm}$ are given by the relations

$$\frac{\bar{\rho}_{\pm}}{\rho_s} = \pm Y(\{Z_r, \rho_r.\rho_s\}) + \sqrt{Y^2(\{Z_r, \rho_r.\rho_s\}) + K^2(\{a_r, \rho_r\})}.$$

The effective potential, its corresponding free energy, and the thermodynamic properties derived from it, have some general interesting features which are not encountered in the traditional DLVO theory of colloidal interactions. Regarding the explicit form of the effective potential, we notice that although both terms on the r.h.s. of Eq. (5.8) depend on the thermodynamic state, only the second term depends explicitly on the colloidal coordinates. This term completely determines the structure and pair correlation functions of the suspension within this linear screening theory. In particular, the average of any quantity that only depends on the colloidal particle coordinates (or momenta) is unaffected by $W_1(\gamma)$. Regarding the free energy, it is clear that integration of the effective Boltzmann factor corresponding to the $N-$body potential of mean force as given in Eq. (5.8) over the colloidal coordinates leads to

$$F(\gamma) = W_1(\gamma) - k_B T \ln \mathbf{Tr} \exp\left[-\beta \sum_{p,q}^{M\ '} \sum_{i,j}^{N_p,N_q\ '} v_2^{pq}(R_{ij}^{pq}, \gamma)\right], \tag{5.12}$$

i.e., the free energy of the system consist of two contributions: (i) the contribution of the volume term (5.11) plus (ii) the contribution due to the free energy of a system interacting trough the hardcore plus density dependent Yukawa potential (5.9). Both contributions depend on the $3M+2$ parameters γ. Although at fixed density the volume term contribution to the free energy leaves the structure of the suspension unchanged, Eq. (5.12) shows that when the free energy density is considered as a function of the colloidal particle densities, as for example in the calculation of phase diagrams from a Maxwell construction, the contribution of the volume term can be important for the phase behavior depending on the values of the parameters. The influence of this term on the phase behavior of monodisperse systems has been studied in detail [67–69, 71, 75]. One of the difficulties in these kind of analyses is the calculation of the second term on the r.h.s. of (5.12). No exact solution for this problem is possible, nevertheless, an estimate for this term can be obtained by using the Gibbs-Bogoliubov (GB) inequality (see e.g., [10, 101, 122]). In the next section we study the thermodynamic consequences of the EM for the isothermal compressibility.

5.3 Results

The response functions, as obtained from the second partial derivatives of the free energy of the EM, lead to a behavior that differs from the DLVO predictions at low salt concentrations. In order to visualize this clearly, let us first consider a monocomponent system, $(M = 1)$, and study the osmotic isothermal compressibility $\chi_{tot}^{-1} = (\partial\beta\Pi/\partial\rho_1)_T$ with $\Pi = -(\partial F/\partial V)_{N_1,T,\rho_s} - 2\rho_s k_B T$ the osmotic pressure, by splitting it into two contributions, namely $\chi_{tot}^{-1} = \chi_{vol}^{-1} + \chi_{yuk}^{-1}$ where χ_{vol}^{-1} refers to the contribution due to the volume term whereas χ_{yuk}^{-1} is due to the Yukawa interactions. In Fig. 5.2 we plot the ratio $\chi_r = \chi_{vol}^{-1}/\chi_{tot}^{-1}$ as a function of the colloidal packing fraction. It has been obtained

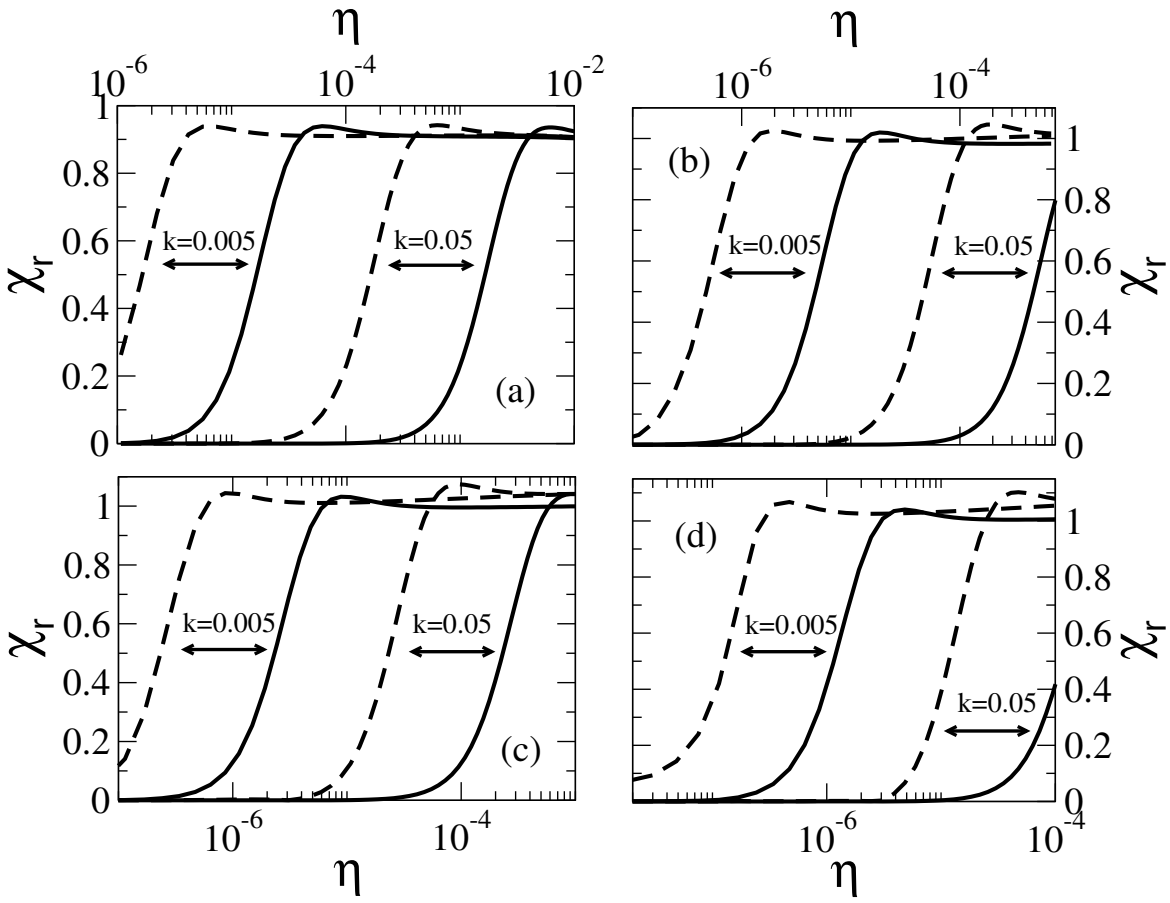

Figure 5.2: Relative contribution of volume terms to the isothermal compressibility for different salt concentrations for (a) $Z = 10$, (b) $Z = 50$, (c) $Z = 100$ and (d) $Z = 200$. The solid line corresponds to a dimensionless temperature (see text) $T^* = 400$ whereas for the dashed line $T^* = 40$. Different values of the parameter $k = \kappa\sigma$ are considered. The arrow shows the direction in which the curve is displaced when temperature is increased keeping $\kappa\sigma$ fixed.

from an approximation for the free energy based on the Gibbs-Bogoliubov inequality [101, 122] and on the volume term contribution (5.11). We consider situations at different ionic strengths as characterized by the product $k = \kappa\sigma = \sigma\sqrt{8\pi\lambda_B\rho_s}$. Let us first focus on the dashed line for $k = 0.005$ in Fig. 5.2(a). Two regimes are observed: at packing fractions smaller than about $\eta = 10^{-6}$ the contribution to the total compressibility due to χ_{vol}^{-1} is small. At higher packing fraction, the contribution to the isothermal compressibility due to many-body effects as contained in χ_{vol}^{-1} becomes important. Upon increasing the ionic strength, the Yukawa-dominated regime extends to higher packing fraction. For instance, Fig. 5.2(a) shows that in order to observe many-body effects for $k = 0.05$, the colloidal packing fraction has to be increased beyond 10^{-4} for $T^* = 40$. On the other hand, increasing the dimensionless temperature, defined as $T^* = \sigma/\lambda_B$, has the effect of increasing the Yukawa dominated regime up to higher packing fractions. In a deionized suspension, many-body effects are present at any colloidal packing fraction, and thermodynamic properties calculated on the basis of the Yukawa contribution to the effective potential only, become inaccurate [106]. In the case of added salt, many-body effects play

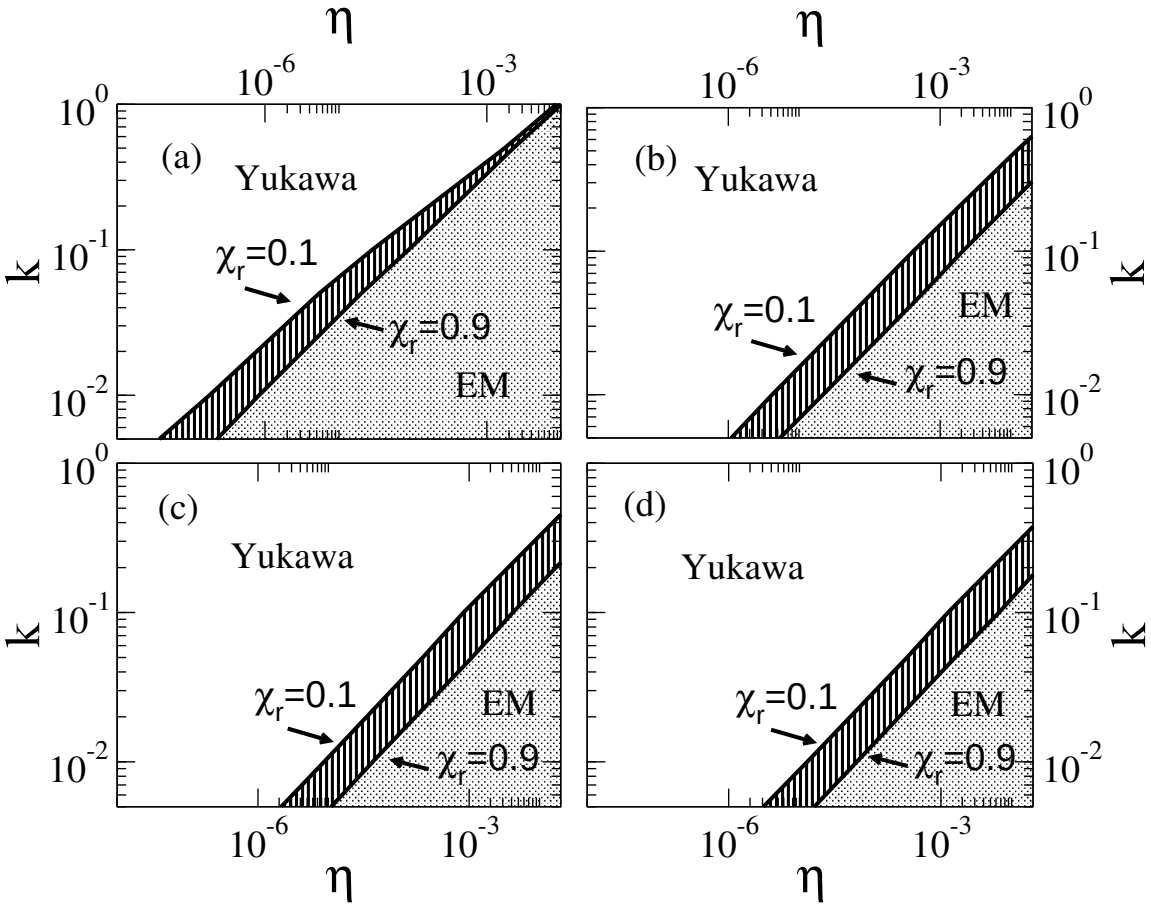

Figure 5.3: Parameter space illustrating the regions in which the Yukawa model (white area) and the EM (grey area) contribute predominantly to the (total) isothermal compressibility. Different values of the reduced temperature are considered, namely (a) $T^* = 40$, (b) $T^* = 1000$, (c) $T^* = 2000$ and (d) $T^* = 3000$. The solid line corresponds to the set of parameters for which $\chi_r = 0.1$ and $\chi_r = 0.9$ as indicated by the legends. The colloidal particles' charge has been fixed to $Z = 200$.

a minor role and the thermodynamic properties of dilute colloidal systems, as determined on the basis of a purely Yukawa potential, are in good agreement with simulations of the PM [113]. Increasing the charge of the colloidal particles has the effect of shifting the regime where volume terms are important towards lower packing fractions.

In order to visualize the regime of parameters for which the contribution χ_{vol}^{-1} to the (total) isothermal compressibility within the EM is relevant, we plot in Fig. 5.3 the parameter space (η, k) for different values of the reduced temperature T^* and for the colloidal particles charge fixed to $Z = 200$. The planes (η, k) are divided into two regions by an area bounded by the curves $\chi_r = 0.1$ and $\chi_r = 0.9$. For the set of parameters in the upper regions, the contribution of χ_{vol}^{-1} to χ_{tot}^{-1} is smaller than about 10% of the total isothermal compressibility of the system. Likewise, for the set of parameters in the lower region, the contribution of χ_{vol}^{-1} to the total isothermal compressibility is larger than about 90% of the value of χ_{tot}^{-1}. Fig. 5.3(a) considers the lowest temperature value for which the present linear theory is applicable according to the approximate criterium $Z\lambda_B/\sigma \lesssim 5$.

For lower values of the temperature, non-linear screening effects become important and proper charge renormalization schemes have to be implemented, in order to avoid artifacts in the thermodynamic properties that arise as a consequence of the misuse of the linear expressions outside of their range of applicability [75]. Increasing the temperature has the effect of shifting the crossover region towards the lower right corners of the plots, as can be observed from Figs. 5.3(a)-5.3(d), reducing the region of parameter space for which the volume term contributes significantly to the isothermal compressibility. The parameter space of typical colloidal suspensions in water ($\lambda_B = 0.72$nm), is similar to that illustrated in Fig. 5.3(d). In the latter case, the set of parameters for which χ_{vol}^{-1} is important corresponds to electrolyte concentrations such that $\kappa\sigma \lesssim 0.1$ or smaller depending on the packing fraction of colloidal particles. Such deionized conditions are difficult to obtain experimentally. In the case of colloidal particles suspended in ethanol, ($\lambda_B = 10.4$nm), $T^* = 183.2$. The corresponding parameter space is similar to that illustrated in Fig. 5.3(a). Notice that even in the case of ethanol whose dielectric constant is about one fourth that of water, the conditions for which volume terms contribute significantly to the isothermal compressibility are difficult to achieve experimentally. The parameters that correspond to most common colloidal suspensions lie thus in the regions well above the crossover area, where χ_{vol}^{-1} plays a small role. Given that experimental verifications of the present theory are difficult, Monte Carlo simulations of, e.g., the primitive model constitute an alternative method to test the theory. Such simulations are however computationally too expensive to study a large range of parameters. In part III of this thesis we will consider some examples of such an approach, and it will be shown that the present theory is in excellent agreement with simulations of the primitive model both in low and high salt concentration regimes.

5.4 Conclusions

For high or even moderate ionic strength, studies based on Monte Carlo simulations of the Primitive Model demand enormous amounts of processing time and become unfeasible. As an alternative, in this chapter we calculated the effective interaction potential for a multi-component colloidal system in the semi-grand canonical ensemble, where the system is considered to be in contact with an electrolyte reservoir. The effective interaction potential we obtained by this method consists of two parts: a Yukawa-like pairwise additive term with a screening length that depends on the colloid density and charges, and a volume term that is independent of the colloidal particle coordinates. Here we used those effective interactions to study the effect of ionic strength on the isothermal compressibility. We find that upon increasing the ionic strength or the temperature, many-body effects are attenuated. At ionic strengths typical of most colloidal suspensions at room temperature, and not too high values of the colloidal particle charge, many-body effects only contribute with a marginal correction to the thermodynamic properties and can be neglected. This constitutes supporting evidence in favor of the adequacy of the traditional pairwise additive DLVO-like theories as valid statistical thermodynamical models of colloidal suspensions under most common conditions.

The present studies are only valid in the linear regime, and modifications to the expressions have to be performed in order to account for non-linear effects by, e.g., proper charge renormalization schemes [76]. As regards simulations, the use of the effective po-

tential has a great computational advantage over simulations of the PM, where the ions are considered explicitly, so that even with not very high number of colloids, the total number of particles increases rapidly with enhanced colloidal charge. This is even more important in the case of non-deionized suspensions, where the effect of additional ions has to be taken into account. By using the effective potential it is possible to include more colloidal particles and therefore obtain better statistics with far less processing time. This will be illustrated in detail in part III of this thesis.

5.5 Appendix: Equilibrium Grand Potential

The purpose of this appendix is to explain in more detail how an explicit expression for the effective colloid-colloid interaction potential for non-deionized systems can be calculated in the semi-grand canonical ensemble, taking many-body interactions effectively into account. The idea is to determine the effective potential as the minimum of a suitable grand potential density functional. We stress that although this procedure allows to find an analytic expression for $W_1(\gamma)$, it is only valid in the linear screening regime. In order to permit the formulation of the linear theory, the potential inside colloidal particles of different species is supposed to assume a finite value $\pm v_r + \omega_r$ with v_r and ω_r determined after performing the required linearizations. With these considerations we define the pseudo-potentials introduced below Eq. (5.6) as

$$\beta v_r\left(|\mathbf{R}_i^r - \mathbf{r}|\right) = \begin{cases} \beta v_r & \text{for } |\mathbf{R}_i^r - \mathbf{r}| < a_r; \\ -\frac{Z_r \lambda_B}{|\mathbf{R}_i^r - \mathbf{r}|} & \text{for } |\mathbf{R}_i^r - \mathbf{r}| > a_r; \end{cases} \tag{5.13}$$

$$\beta \omega_r\left(|\mathbf{R}_i - \mathbf{r}|\right) = \begin{cases} \beta \omega_r & \text{for } |\mathbf{R}_i^r - \mathbf{r}| < a_r; \\ 0 & \text{for } |\mathbf{R}_i^r - \mathbf{r}| > a_r. \end{cases} \tag{5.14}$$

For a fixed configuration of colloids $\{\mathbf{R}_i\}$, the equilibrium local charge density $e\rho(\mathbf{r}) = e\left(\rho_+(\mathbf{r}) - \rho_-(\mathbf{r})\right)$ is related to the reduced electrostatic potential $\varphi(\mathbf{r}) = e\psi(\mathbf{r})/k_BT$, with $\psi(\mathbf{r})$ the local electrostatic potential, by the Poisson-Boltzmann equation

$$\Delta\varphi(\mathbf{r}) = -4\pi\lambda_B\rho(\mathbf{r}) - \sum_{r=1}^{M} \frac{Z_r\lambda_B}{a_r^2} \sum_{i=1}^{N_r} \delta\left(|\mathbf{R}_i^r - \mathbf{r}| - a_r\right), \tag{5.15}$$

where the last term on the r.h.s. accounts for the charge of the colloids assumed to be distributed uniformly on their surfaces. The solution of (5.15) is given in integral form by

$$\varphi(\mathbf{r}) = \lambda_B \int d\mathbf{r}' \frac{\rho(\mathbf{r}')}{|\mathbf{r} - \mathbf{r}'|} + \sum_{r=1}^{M} \beta V_r^{elec}(\mathbf{r}), \tag{5.16}$$

with $V_r^{elec}(\mathbf{r})$ defined below Eq. (5.6) with $v_r\left(|\mathbf{R}_i^r - \mathbf{r}|\right)$ given by Eq. (5.13). Note that $F^{elec}(\mathbf{r}) = -e\nabla\psi(\mathbf{r})$ is the *electrostatic* force experienced by a positive unit charge at any point $\mathbf{r}$ in the solution. By substituting the explicit form for the external potentials $U_\pm(\mathbf{r}, \mathbf{R}^N)$ defined in Eq. (5.6) into the grand potential Eq. (5.5), the latter can be written

as

$$\beta\Omega[\tilde{\rho}_+(\mathbf{r}),\tilde{\rho}_-(\mathbf{r})](\mathbf{R}^N) = \sum_{\pm}\beta\Omega'_{id}[\tilde{\rho}_\pm(\mathbf{r})] + \frac{1}{2}\int d\mathbf{r}\left(\varphi(\mathbf{r}) + \sum_{r=1}^{M}\beta V_r^{elec}(\mathbf{r})\right)\tilde{\rho}(\mathbf{r}) + \frac{2\bar{\rho}_+\bar{\rho}_-}{\bar{\rho}_+ + \bar{\rho}_-}\sum_{r=1}^{M}\int d\mathbf{r}\left[\frac{\tilde{\rho}_+(\mathbf{r})}{\bar{\rho}_+} + \frac{\tilde{\rho}_-(\mathbf{r})}{\bar{\rho}_-}\right]V_r^{hard}(\mathbf{r}) \quad (5.17)$$

where we made use of Eq. (5.16). In order to obtain an analytic expression for the effective colloid-colloid potential within a linear approximation, the integrand of $\hat{\Omega}_{id}[\tilde{\rho}_\pm(\mathbf{r})]$, defined after equation (5.5), is expanded up to second order about the overall† mean ion densities $\bar{\rho}_\pm = N_\pm/V$, which yields

$$\beta\Omega'_{id}[\tilde{\rho}_\pm(\mathbf{r})](\mathbf{R}^N) = \bar{\rho}_\pm\left(\ln\frac{\bar{\rho}_\pm}{\rho_s} - 1\right)V + \ln\frac{\bar{\rho}_\pm}{\rho_s}\int d\mathbf{r}\,(\tilde{\rho}_\pm(\mathbf{r}) - \bar{\rho}_\pm) \quad (5.18)$$

$$+\frac{1}{2\bar{\rho}_\pm}\int d\mathbf{r}\,(\tilde{\rho}_\pm(\mathbf{r}) - \bar{\rho}_\pm)^2\,. \quad (5.19)$$

After substitution of this expansion into the density functional (5.17) and evaluation of the functional derivatives (5.7), we obtain two Euler-Lagrange equations, namely

$$\ln\frac{\bar{\rho}_\pm}{\rho_s} + \frac{\rho_\pm(\mathbf{r}) - \bar{\rho}_\pm}{\bar{\rho}_\pm} \pm \varphi(\mathbf{r}) + \frac{2\bar{\rho}_\mp}{\bar{\rho}_+ + \bar{\rho}_-}\sum_{r=1}^{M}\beta V_r^{hard}(\mathbf{r}) = 0, \quad (5.20)$$

where $\rho_\pm(\mathbf{r})$ are the equilibrium ion density profiles. The first two terms in the l.h.s of Eqs. (5.20) originate from the entropic contribution Eq. (5.18), whereas the third and fourth terms include electrostatic and hard core contributions, respectively. The EL Eqs. (5.20) are two equations for the ion density profiles $\rho_+(\mathbf{r})$ and $\rho_-(\mathbf{r})$ involving the mean ion concentrations $\bar{\rho}_\pm$, the hard core contributions $V_r^{hard}(\mathbf{r})$ and the electrostatic potential $\varphi(\mathbf{r})$. The integral form of the PB equation, Eq. (5.16), provides an additional equation to this system. It is convenient to separate the hard core contribution from the local charge distribution $e(\rho_+(\mathbf{r}) - \rho_-(\mathbf{r}))$. This can be done by using the EL equations in the form of the linear combinations [143]

$$\frac{\rho_+(\mathbf{r})}{\bar{\rho}_+} + \frac{\rho_-(\mathbf{r})}{\bar{\rho}_-} = 2 - \left(\ln\frac{\bar{\rho}_+}{\rho_s} + \ln\frac{\bar{\rho}_-}{\rho_s}\right) - 2\sum_{r=1}^{M}\beta V_r^{hard}(\mathbf{r}) \quad (5.21)$$

$$\rho(\mathbf{r}) - \bar{\rho} = -(\bar{\rho}_+ + \bar{\rho}_-)\,(\varphi(\mathbf{r}) - \bar{\varphi})\,, \quad (5.22)$$

with $\bar{\rho} = \bar{\rho}_+ - \bar{\rho}_-$ and $\bar{\varphi} = V^{-1}\int d\mathbf{r}\varphi(\mathbf{r})$ the average (Donnan) potential and with $\varphi(\mathbf{r})$ replaced by v_r inside the colloidal particles. The advantage of such a choice of linear combinations of the density profiles will be evident soon. The equilibrium profiles can be inserted back into the functional (5.17) taking into account the expansion Eq. (5.18), in order to evaluate its equilibrium value $\Omega(\mathbf{R}^N) = \tilde{\Omega}[\rho_+(\mathbf{r}),\rho_-(\mathbf{r})](\mathbf{R}^N)$. By using the EL equations (5.20) in combination with the integral form of the PB equation (5.16) and the linear approximation of the entropic contribution to the grand potential Eq. (5.18), the calculation of the equilibrium value of the grand potential can be reduced to the evaluation

†Notice that $\bar{\rho}_\pm$ can be considered independent of the configuration of colloids, since deviations from these values are small in the thermodynamic limit.

of a single set of integrals involving the electrostatic external fields $V_r^{elec}(\mathbf{r})$. To show this we first insert the equilibrium profiles given by the Euler Lagrange equations (5.20) into the expansion for the entropic contribution to the grand potential Eq. (5.18) to obtain

$$\begin{aligned}\beta\Omega'_{id}[\rho_\pm(\mathbf{r})](\mathbf{R}^N) &= \bar{\rho}_\pm\left(\ln\frac{\bar{\rho}_\pm}{\rho_s}-1\right)V-\frac{1}{2}\ln\frac{\bar{\rho}_\pm}{\rho_s}\int d\mathbf{r}\,(\rho_\pm(\mathbf{r})-\bar{\rho}_\pm)\\ &\quad+\frac{1}{2}\int d\mathbf{r}\left[(\rho_\pm(\mathbf{r})-\bar{\rho}_\pm)\left(\mp\varphi(\mathbf{r})-\frac{2\bar{\rho}_\mp}{\bar{\rho}_++\bar{\rho}_-}\sum_{r=1}^{M}\beta V_r^{hard}(\mathbf{r})\right)\right]\end{aligned}$$

Using the previous result, the total ideal contribution to the equilibrium grand potential, approximated up to second order w.r.t. deviations of the local ion densities about their mean values $\bar{\rho}_\pm$ becomes

$$\begin{aligned}\sum_\pm\beta\Omega'_{id}[\rho_\pm(\mathbf{r})](\mathbf{R}^N) &= \sum_\pm\left(\bar{\rho}_\pm\ln\frac{\bar{\rho}_\pm}{\rho_s}-\bar{\rho}_\pm\right)V-\frac{1}{2}\int d\mathbf{r}\varphi(\mathbf{r})\rho(\mathbf{r})\\ &\quad+\frac{1}{2}\int d\mathbf{r}\varphi(\mathbf{r})\,(\bar{\rho}_+-\bar{\rho}_-)+\frac{2\bar{\rho}_-\bar{\rho}_+}{\bar{\rho}_++\bar{\rho}_-}\sum_{r=1}^{M}\int d\mathbf{r}\beta V_r^{hard}(\mathbf{r})\\ &\quad-\frac{1}{2}\sum_\pm\int d\mathbf{r}\left[(\rho_\pm(\mathbf{r})-\bar{\rho}_\pm)\left(\ln\frac{\bar{\rho}_\pm}{\rho_s}\right)\right]\\ &\quad-\frac{\bar{\rho}_-\bar{\rho}_+}{\bar{\rho}_++\bar{\rho}_-}\sum_{r=1}^{M}\int d\mathbf{r}\beta V_r^{hard}(\mathbf{r})\left(\frac{\rho_+(\mathbf{r})}{\bar{\rho}_+}+\frac{\rho_-(\mathbf{r})}{\bar{\rho}_-}\right).\end{aligned}$$

Using the fact that $\int d\mathbf{r}\,(\rho_\pm(\mathbf{r})-\bar{\rho}_\pm)=0$ (since $N_\pm=\int d\mathbf{r}\rho_\pm(\mathbf{r})$), and the fact that ions cannot penetrate the interior of the colloids, and therefore, any linear combination of $\rho_+(\mathbf{r})$ and $\rho_-(\mathbf{r})$, in particular $\rho_+(\mathbf{r})/\rho_+ + \rho_-(\mathbf{r})/\rho_-$ vanishes inside the colloids, we obtain

$$\begin{aligned}\sum_\pm\beta\hat{\Omega}_{id}[\rho_\pm(\mathbf{r})](\mathbf{R}^N) &= \sum_\pm\left(\bar{\rho}_\pm\ln\frac{\bar{\rho}_\pm}{\rho_s}-\bar{\rho}_\pm\right)V+\frac{1}{2}\bar{\rho}\bar{\varphi}V\\ &\quad-\frac{1}{2}\int d\mathbf{r}\varphi(\mathbf{r})\rho(\mathbf{r})+\frac{2\bar{\rho}_-\bar{\rho}_+}{\bar{\rho}_++\bar{\rho}_-}\sum_{r=1}^{M}\int d\mathbf{r}\beta V_r^{hard}(\mathbf{r}).\end{aligned}\tag{5.23}$$

Notice that the last term in (5.17) vanishes, since outside the colloidal particles the hard core contribution to the external potential $V_r^{hard}(\mathbf{r})$ equals zero, and inside the colloidal particles $\rho_+(\mathbf{r})/\bar{\rho}_+ + \rho_-(\mathbf{r})/\bar{\rho}_- = 0$ as explained above. Combining (5.23) with equation (5.17), the terms involving integrals of the form $\int d\mathbf{r}\varphi(\mathbf{r})\rho(\mathbf{r})$ cancel out, and the expression for the grand potential finally takes the form

$$\begin{aligned}\beta\Omega(\mathbf{R}^N) &= \frac{1}{2}\sum_{r=1}^{M}\int d\mathbf{r}\beta V_r^{elec}(\mathbf{r})\rho(\mathbf{r})+\frac{2\bar{\rho}_-\bar{\rho}_+}{\bar{\rho}_++\bar{\rho}_-}\sum_{r=1}^{M}\beta\omega_r\eta_r V\\ &\quad+\sum_\pm\left(\bar{\rho}_\pm\ln\frac{\bar{\rho}_\pm}{\rho_s}-\bar{\rho}_\pm\right)V+\frac{1}{2}\bar{\rho}\bar{\varphi}V,\end{aligned}\tag{5.24}$$

where we have used $\int d\mathbf{r}\beta V_r^{hard}(\mathbf{r}) = V\beta\omega_r\eta_r$. The calculation of the Grand Potential has been reduced to the calculation of the constants $\bar{\rho}_\pm, \bar{\varphi}$ and ω_r, and the evaluation of the set of integrals in the first sum in the r.h.s. of (5.24). These integrals represent the *electrostatic* energy of the ions in the presence of the field due to the colloids fixed at a given configuration. The set of electrostatic integrals can be evaluated in Fourier space by using the Parseval's identity $\int d\mathbf{r}\sum_{r=1}^{M} V_r^{elec}(\mathbf{r})\rho(\mathbf{r}) = \frac{1}{(2\pi)^3}\int d\mathbf{k}\sum_{r=1}^{M} V_r^{elec}(\mathbf{k})\rho(-\mathbf{k})$.

In order to perform the integrations, let us first calculate the explicit form of $V_r^{elec}(\mathbf{k})$ and $\rho(-\mathbf{k})$. With the aid of Eq. (5.22), the Fourier transform of $\rho(\mathbf{r})$ gives $\rho(\mathbf{k}) = D\delta(\mathbf{k}) - (\bar{\rho}_+ + \bar{\rho}_-)\,\varphi(\mathbf{k})$ with $D = (2\pi)^3\left[\bar{\rho} + (\bar{\rho}_+ + \bar{\rho}_-)\,\bar{\varphi}\right]$. On the other hand, after taking Fourier transform on both sides of (5.16) we obtain $\varphi(\mathbf{k}) = 4\pi\lambda_B\frac{\rho(\mathbf{k})}{k^2} + \sum_{r=1}^{M}\beta V_r^{elec}(\mathbf{k})$. Combining the last two results we obtain an expression for the local charge density in Fourier space, namely

$$\rho(\mathbf{k}) = \frac{k^2}{k^2+\bar{\kappa}^2}\left(D\delta(\mathbf{k}) - (\bar{\rho}_+ + \bar{\rho}_-)\sum_{r=1}^{M}\beta V_r^{elec}(\mathbf{k})\right), \tag{5.25}$$

with $\bar{\kappa}^2 \equiv 4\pi\lambda_B\,(\bar{\rho}_+ + \bar{\rho}_-)$. On the other hand, the Fourier transforms $V_r^{elec}(\mathbf{k})$ for each r, as calculated from the definition (5.13), read $\beta V_r^{elec}(\mathbf{k}) = \Theta(ka_r)\sum_j^{N_r} e^{i\mathbf{k}\cdot\mathbf{R}_j^r}$ with the structure factors $\Theta(ka_r) = -\frac{4\pi\lambda_B Z_r}{k^2(1+\bar{\kappa}a_r)}\left(\cos ka_r + \frac{\bar{\kappa}}{k}\sin ka_r\right)$, where we chose the value of the potentials $\beta v_r = \lambda_B Z_r/\left(1+\bar{\kappa}a_r\right)$ inside the colloidal particles, in order to recover the Debye-Hückel result for the local charge density in real space

$$\rho(\mathbf{r}) = \sum_{r=1}^{M}{}' \sum_{i=1}^{N_r\prime}\rho_i^r(\mathbf{r}) = \sum_{r=1}^{M}{}' \sum_{i=1}^{N_r\prime}\frac{Z_r\bar{\kappa}^2 e^{\bar{\kappa}a_r}}{4\pi(1+\bar{\kappa}a_r)}\frac{\exp[-\bar{\kappa}|\mathbf{r}-\mathbf{R}_i^r|]}{|\mathbf{r}-\mathbf{R}_i^r|}. \tag{5.26}$$

The term proportional to $D\delta(\mathbf{k})$ in Eq. (5.25) does not contribute to $\rho(\mathbf{r})$. Notice that with our choice of βv_r, for each colloidal particle i of species r the normalization conditions $\int_{|\mathbf{R}_i^r-\mathbf{r}|>a_r} d\mathbf{r}\rho_i^r(\mathbf{r}) = Z_r$ are satisfied. For given values of r, p and q, by using Parseval's relation together with equation (5.25) and the explicit form of $V_r^{elec}(\mathbf{k})$, the integrals in the first sum in the r.h.s. of (5.24) reduce to integrals in Fourier space of the form

$$\frac{D}{2(2\pi)^3}\int d\mathbf{k}\frac{k^2\Theta(ka_r)}{k^2+\bar{\kappa}^2}\delta(-\mathbf{k})\sum_j^{N_r} e^{i\mathbf{k}\cdot\mathbf{R}_j^r} - \frac{(\bar{\rho}_+ + \bar{\rho}_-)}{2(2\pi)^3}\int d\mathbf{k}k^2\frac{\Theta(ka_p)\Theta(ka_q)}{k^2+\bar{\kappa}^2}\sum_{i,j} e^{i\mathbf{k}\cdot\left(\mathbf{R}_i^p-\mathbf{R}_j^q\right)}, \tag{5.27}$$

where we notice that summations over components, i.e., over the indexes r, p and q, still have to be performed. From the first term in (5.27) we obtain

$$-\frac{D}{2(2\pi)^3}\frac{4\pi\lambda_B Z_r N_r}{1+\bar{\kappa}a_r}\frac{1+\bar{\kappa}a_r}{\bar{\kappa}^2} = -\frac{1}{2}\frac{\bar{\rho}Z_r N_r}{(\bar{\rho}_+ + \bar{\rho}_-)} - \frac{1}{2}\bar{\varphi}Z_r N_r. \tag{5.28}$$

The integrals in the second term of (5.27) lead to different possibilities depending on the values of the subindices. (i) For $p \neq q$, and any i, j, or $p = q$ and $i \neq j$ that is, for colloidal particles of different species or different colloidal particles of the same species, performing the integration the first sum if the r.h.s. of (5.24) yields

$$\sum_{p,q}^{M}{}' \sum_{i,j}^{N_p,N_q\prime}\frac{\lambda_B e^{-\bar{\kappa}R_{ij}^{pq}}}{R_{ij}^{pq}} - \sum_{p,q}^{M}{}' \sum_{i,j}^{N_p,N_q\prime}\frac{Z_p Z_q\lambda_B}{R_{ij}^{pq}}, \tag{5.29}$$

where Γ_r and R_{ij}^{pq} were defined after equation (5.9). (ii) For $p = q$ and $i = j$, the exponential factors in equation (5.27) vanish so that integration gives coordinate independent factors. By performing the integral and multiplying by the prefactors we obtain

$$-\frac{\bar{\rho}_+ + \bar{\rho}_-}{2(2\pi)^3}\left(\frac{4\pi\bar{\kappa}\lambda_B Z_r}{1+\bar{\kappa}a_r}\right)^2 2\pi^2\frac{1+\bar{\kappa}a_r}{\bar{\kappa}^3}N_r = -\frac{1}{2}\frac{\bar{\kappa}\lambda_B}{1+\bar{\kappa}a_r}Z_r^2 N_r. \tag{5.30}$$

After performing the summations over the different components, gathering the coordinate independent terms in Eqs. (5.24), (5.28) and (5.30) we obtain

$$\begin{aligned}\beta W_1(\gamma) \;\equiv\; & -\frac{1}{2}\frac{\bar{\rho}_+ - \bar{\rho}_-}{\bar{\rho}_+ + \bar{\rho}_-}\sum_{r=1}^{M} Z_r N_r - \frac{1}{2}\sum_{r=1}^{M}\frac{\bar{\kappa}\lambda_B}{1+\bar{\kappa}a_r}Z_r^2 N_r \\ & + \frac{2\bar{\rho}_-\bar{\rho}_+}{\bar{\rho}_+ + \bar{\rho}_-}\sum_{r=1}^{M}\beta\omega_r\eta_r V + \sum_{\pm}\left(\bar{\rho}_\pm \ln\frac{\bar{\rho}_\pm}{\rho_s} - \bar{\rho}_\pm\right)V.\end{aligned} \tag{5.31}$$

Notice that the last term on the r.h.s. of Eq. (5.28) is cancelled by the last term on the r.h.s. of Eq. (5.24) due to the electroneutrality condition $\bar{\rho}_+ - \bar{\rho}_- = \sum_{r=1}^{M} Z_r\rho_r$. Regarding the coordinate-dependent terms (Eq. (5.9)), we notice that the definition of the $N-$body potential of mean force $W_N = U_{cc}^{pq} + \Omega$ involves the direct colloid-colloid interactions U_{cc}^{pq}, so that the latter term is cancelled by the second term in Eq. (5.29), and after collecting terms we obtain the explicit form of equation (5.8).

Notice that in order to express W_1 as a function of $\gamma \equiv \{a_r, Z_r, \rho_r, \rho_s, \lambda_B\}$, a relation between the average ion densities $\bar{\rho}_\pm$ and the parameters $\{a_r, Z_r, \rho_r, \rho_s\}$ has to be determined. Multiplying both sides of Eqs. (5.20) by V^{-1}, integrating both sides over the total volume, and using the facts that $\int d\mathbf{r}\,(\rho_\pm(\mathbf{r}) - \bar{\rho}_\pm) = 0$ (since $N_\pm = \int d\mathbf{r}\rho_\pm(\mathbf{r})$) we obtain

$$\ln\frac{\bar{\rho}_\pm}{\rho_s} =_\mp \bar{\varphi} - \frac{2\bar{\rho}_\mp}{\bar{\rho}_+ + \bar{\rho}_-}\sum_{r=1}^{M}\beta\omega_r\eta_r. \tag{5.32}$$

Substituting this into Eq. (5.21) and given that ions cannot penetrate the interior of the colloids, and therefore, any linear combination of $\rho_+(\mathbf{r})$ and $\rho_-(\mathbf{r})$ vanishes inside the colloids so that $\rho_+(\mathbf{r})/\bar{\rho}_+ + \rho_-(\mathbf{r})/\bar{\rho}_- = 0$, we obtain

$$\sum_{r=1}^{M}\beta\omega_r\eta_r - \sum_{r=1}^{M}\beta V_r^{hard}(\mathbf{r}) + 1 = 0 \quad \text{inside the colloids,} \tag{5.33}$$

The values of the constants ω_r inside the colloids can be determined from Eq. (5.33) since inside any of the colloidal species, say species a, we have $\sum_{r=1}^{M}\beta V_r^{hard}(\mathbf{r}) = \beta\omega_a$, then from (5.33) we find that the value of the potential inside the colloids of species a is $\beta\omega = (1-\eta)^{-1}$, independent of r so that any species $r = 1, ..., M$ has the same hard-core value. Finally, using (5.32) to write the product $\bar{\rho}_+\bar{\rho}_-$ explicitly, we obtain a system of two coupled equations for the average ion concentrations in terms of the colloidal particles charges and concentrations

$$\bar{\rho}_+ - \bar{\rho}_- = \sum_{r=1}^{M} Z_r\rho_r; \;\; \bar{\rho}_+\bar{\rho}_- = \rho_s^2\exp\left(-2\sum_{r=1}^{M}\frac{\eta_r}{1-\eta}\right), \tag{5.34}$$

where the first equation in (5.34) is nothing but the electroneutrality condition, and the second follows immediately from Eq. (5.32). Solving for $\bar{\rho}_+$ and $\bar{\rho}_-$ we obtain

$$\begin{aligned} \frac{\bar{\rho}_\pm}{\rho_s} &= \pm\sum_{r=1}^{M}\frac{Z_r\rho_r}{2\rho_s} + \sqrt{\left(e^{-\sum_{r=1}^{M}\beta\omega_r\eta_r}\right)^2 + \left(\sum_{r=1}^{M}\frac{Z_r\rho_r}{2\rho_s}\right)^2} \\ &= \pm Y(\{Z_r,\rho_r,\rho_s\}) + \sqrt{Y^2(\{Z_r,\rho_r,\rho_s\}) + K^2(\{a_r,\rho_r\})} \end{aligned} \tag{5.35}$$

where $Y(\{Z_r,\rho_r.\rho_s\}) \equiv \sum_{r=1}^{M} Z_r\rho_r/2\rho_s$ and $K(\{a_r,\rho_r\}) \equiv \exp\left(-\sum_{r=1}^{M}\beta\omega_r\eta_r\right)$. The screening constant $\bar{\kappa}^2(\gamma) \equiv 4\pi\lambda_B\left(\bar{\rho}_+ + \bar{\rho}_-\right)$ can be written as

$$\bar{\kappa}^2(\gamma) = 8\pi\lambda_B\rho_s\sqrt{Y^2(\{Z_r,\rho_r,\rho_s\}) + K^2(\{a_r,\rho_r\})}. \tag{5.36}$$

By using the previous results in combination with the explicit form of $\beta\omega_r$ calculated above and Eq. 5.31, (after some trivial substitutions) one obtains Eqs. (5.10) and (5.11).

Part III

Colloidal Dispersions in External Fields

6

Sedimentation of charge-stabilized colloids

In this chapter sedimentation-diffusion equilibrium density profiles of suspensions of charge-stabilized colloids are calculated theoretically and by Monte Carlo simulation, both for a one-component model of colloidal particles interacting through pairwise screened Coulomb repulsions and for a three-component model of colloids, cations, and anions with unscreened-Coulomb interactions. We focus on a state point for which experimental measurements are available [C.P. Royall et al., J. Phys.: Cond. Matt. **17**, 2315 (2005)]. Despite the apparently different picture that emerges from the one- and three-component model (repelling colloids pushing each other to high altitude in the former, versus a self-generated electric field that pushes the colloids up in the latter), we find similar colloidal density profiles for both models from theory as well as simulation, thereby suggesting that these pictures represent different view points of the same phenomenon. The sedimentation profiles obtained from an effective one-component model by MC simulations and theory, together with MC simulations of the multi-component primitive model are consistent among themselves, but differ quantitatively from the results of a theoretical multi-component description at the Poisson-Boltzmann level. We find that for small and moderate colloid charge the Poisson-Boltzmann theory gives profiles in excellent agreement with the effective one-component theory if a smaller effective charge is used. We attribute this discrepancy to the poor treatment of correlations in the Poisson-Boltzmann theory.

6.1 Introduction

Colloidal particles with a mass density different from that of the dispersive medium sediment because of the gravitational force. At fixed temperature T, the resulting non-homogeneous equilibrium distribution is a consequence of the balance between energy

and entropy of the different chemical species involved. This equilibrium is characterized by measurable density profiles [97, 98]. In the case of sufficiently dilute suspensions those profiles obey the barometric law $\rho(x) \propto \exp(-x/L)$, with $L = k_B T/mg$ the gravitational length, m the buoyant mass, g the gravitational acceleration, k_B the Boltzmann constant, T the absolute temperature, and $\rho(x)$ the number density of colloids at altitude x. In dense systems, with non-negligible colloidal interactions, strong deviations from the barometric law have been observed, e.g. for colloidal hard-spheres at packing fractions up to and beyond the freezing point [97, 124]. More surprisingly (at least initially) were the strong deviations from the barometric law in rather dilute suspensions of highly charged colloids at low salinity [125]. The measured density profiles suggested an extreme reduction, by at least one order of magnitude, of the apparent mass of the colloids [98, 125]. This system was theoretically analyzed in terms of a three-component model of colloids and monovalent cations and anions, for which Poisson-Boltzmann (PB) theory in gravity revealed a self-consistent electric field that pushes up the colloids to high altitude against gravity, thereby reducing the apparent mass as observed experimentally [126]. However, another explanation was given more recently in Ref. [127], where hydrostatic equilibrium in a one-component system of colloids interacting through pairwise screened-Coulomb repulsion was considered. In the present chapter we investigate the relations between these two pictures in more detail by studying both models (colloid-cation-anion mixture and colloids-only system) by theory as well as Monte Carlo simulation. For the one-component approach we use a model based on effective pairwise screened-Coulomb interactions. The profiles are obtained from the solution of the hydrostatic equilibrium equation, that uses the isothermal compressibility obtained from the solution of the Ornstein-Zernike (OZ) equation with closure by the rescaled mean spherical approximation (RMSA) [15]. This approach is similar to that introduced in [127]. In this case, entropic and electrostatic effects are implicitly included in the structure of the suspension (see next section). Furthermore, we perform MC simulations for this model. Within the multi-component picture, we approach the problem using the Poisson-Boltzmann theory introduced in Ref. [126], which explains the non-barometric profiles in terms of a macroscopic electric field that appears as a consequence of a charge inhomogeneity. We also performed simulations of this system using the primitive model in gravity. These particular simulations require a substantial amount of CPU time since a considerable number of micro-ions has to be taken into account to mimic the substantial salt concentration in the suspension. We focus on a state point for which experimental information is available, and compare the profiles obtained from our theoretical and numerical approaches with published measurements [98].

The chapter is organized as follows. In section 6.2 we introduce the one-component model, the structure factor of the suspension determined through RMSA, and we discuss some details regarding the simulation technique of the one-component model. In section 6.3 we briefly revise the PB theory for sedimentation, introduce the primitive model under gravity and discuss some aspects of the simulations. Results and a discussion are presented in sections 6.4 and 6.5 respectively, where we compare the different theoretical and numerical results with experimental data. A summary and conclusions are gathered in section 6.6.

6.2 Effective One-Component Model

Let us consider a system consisting of charged spheres of diameter $\sigma = 2a$, mass M, and electric charge $-Ze$, in osmotic contact with a reservoir of 1:1 electrolyte with salt concentration $2\rho_s$. The solvent has mass density ρ_l and is characterized by an electric permittivity ϵ. Let us assume also that the dielectric constant of the spheres and the electrolyte are identical to avoid electrostatic image effects and Van der Waals forces between the spheres. We assume pairwise effective colloidal interactions, with an interaction Hamiltonian in the presence of gravity given by

$$H = \sum_{i=1}^{N} mgx_i + \sum_{i<j}^{N} v(r_{ij}). \tag{6.1}$$

Here the first term on the right-hand side is the potential energy of colloid i at height x_i measured from the bottom of the sample; $m = M - \rho_l \pi \sigma^3/6$ is the buoyant mass of the colloidal particles, and $v(r)$ is the familiar screened Coulomb potential plus a hard core given by

$$\beta v(r) = \begin{cases} \infty\,, & \text{if } r < \sigma, \\ \dfrac{Z^2 \exp(\kappa\sigma)}{(1+\kappa a)^2} \dfrac{\lambda_B}{r} \exp\left(-\kappa r\right), & \text{if } r \geq \sigma, \end{cases} \tag{6.2}$$

with $\beta = (k_B T)^{-1}$, where k_B is the Boltzmann constant and where $\lambda_B = \frac{\beta e^2}{\epsilon}$ is the Bjerrum length. $\kappa = \sqrt{8\pi\lambda_B \rho_s}$ is the inverse screening length, and r is the distance between centers of colloidal particles. Under isothermal conditions and for small density gradients, the osmotic pressure of the suspension depends only on the local number density of colloids $\rho(x)$. The latter is determined from the non-linear differential equation that follows from inserting $\rho(x)$ into the hydrostatic equilibrium equation $d\Pi(x)/dx = -mg\rho(x)$ with Π the osmotic pressure of the suspension with respect to the salt reservoir. This yields

$$\frac{d\rho(x)}{dx} + \frac{\chi_T(\rho(x))}{L}\rho(x) = 0, \tag{6.3}$$

where $\chi_T^{-1} = \left(\frac{\partial(\beta\Pi)}{\partial\rho}\right)_T$ is the isothermal compressibility of the bulk fluid and $L = k_B T/mg$ is the gravitational length. The equilibrium, sedimentation profiles can be obtained by solving (6.3) if the function $\chi_T(\rho)$ is known for the relevant density regime. In order to determine $\chi_T(\rho)$ we use the well-known Kirkwood-Buff relation $\chi_T = \lim_{q\to 0} S(q)$ with $S(q)$ the structure factor. For $S(q)$ we can use the expression obtained by by Hansen, Hayter and Penfold within the RMSA closure of the Ornstein-Zernike equation [15, 140]. By this procedure the sedimentation profiles are determined solely from the structure of the effective one-component bulk fluid. Notice that such a scheme was applied successfully to explain measured hard-sphere density profiles in Ref. [97]. For later comparison we also consider an alternative expression for $\chi_T(\rho)$, that is based on the Donnan equation of state as e.g. given in Ref. [126]. This yields

$$\chi_T^{-1} = 1 + \frac{Z^2\rho/2\rho_s}{\sqrt{1 + (Z\rho/2\rho_s)^2}}, \tag{6.4}$$

which features the high-density or low-salt limit $\chi_T(\rho) = 1 + Z$ for $Z\rho \gg 2\rho_s$, such that insertion into (7.1) yields $\rho(x) \propto \exp[-x/(Z+1)L]$, i.e. an effective gravitational length that is a factor $Z+1$ larger than that in the barometric law [126]. The remaining task in order to find the sedimentation profiles is to insert χ_T obtained within the RMSA approximation into (7.1) and to solve the non-linear equation numerically on an x-grid.

In addition we discuss standard Monte Carlo simulations of a system described by the interaction Hamiltonian (6.1) for the parameters $Z = 76$, colloid diameter $\sigma = 1.91\mu$m, Bjerrum length $\lambda_B = 10.4$ nm, screening parameter $\kappa\sigma = 1.2$ and average colloidal packing fraction $\overline{\eta} = H^{-1}\int_0^H \eta(x)dx = 0.0053$ with the height $H = 50.92\sigma$. These parameters are identical to those of the experimental system studied in Ref.[98], where $Z = 76$ stems from the best fit of the experimental density profile with a theoretical prediction based on the primitive model (see below). The dimensions of the rectangular simulation box are $10\sigma \times 10\sigma \times H$. We checked that the horizontal area was large enough to exclude finite-size effects. We employed periodic boundary conditions in the horizontal directions, in the vertical directions the system is bounded by hard walls that exclude the centers of colloids at $x < 0$ and $x > H$.

6.3 The Primitive Model in Gravity

As mentioned in the introduction, a different approach to study sedimentation profiles is to consider each chemical species separately, namely colloids (c), coions (-) and counterions (+). The interaction Hamiltonian of the system can be written as

$$H = H_{cc} + H_{ii} + H_{ci} + \sum_{i=1}^{N} mgx_i, \tag{6.5}$$

where the first three terms on the right-hand side include colloid-colloid, ion-ion and colloid-ion pairwise interactions, respectively, and the last term is the gravitational energy of the colloids introduced in equation (6.1); the ions are assumed to be massless. In this model, the electrostatic pair interactions are of the form

$$\beta v_{ij}(r) = \begin{cases} \infty\,, & \text{if } r < \sigma_{ij} = (\sigma_i + \sigma_j)/2, \\ Z_i Z_j \frac{\lambda_B}{r}\,, & \text{if } r \geq \sigma_{ij}, \end{cases} \tag{6.6}$$

with σ_k and Z_k the diameter and the charge number of species $k = \{c, +, -\}$, i.e. $Z_c = -Z, Z_+ = 1, Z_- = -1$, $\sigma_c = \sigma$ and $\sigma_+ = \sigma_- \ll \sigma$. The number of particles are denoted by N_k, i.e $N_c = N$ and $N_+ = N_- + ZN$ for charge neutrality reasons. This three-component model can be studied within Poisson-Boltzmann theory [126], which relates the density profiles $\rho(x), \rho_+(x), \rho_-(x)$ of the colloids cations and anions respectively, to the local electrostatic Donnan potential $\psi(x)$ through

$$\rho_\pm(x) = \rho_s \exp[\pm\phi(x)]; \tag{6.7}$$

$$\rho(x) = \rho_0 \exp[-x/L + Z\phi(x)]; \tag{6.8}$$

$$\phi''(x) = \kappa^2 \sinh\phi(x) + 4\pi\lambda_B Z\rho(x), \tag{6.9}$$

with $\phi(x)$ defined by the dimensionless combination $\phi(x) = e\psi(x)/k_BT$ and where ρ_0 is a normalization constant. Here a prime denotes a derivative w.r.t. x. Under appropriate

conditions, typically $Z^2\rho(x) \gg 2\rho_s$, it was found that $\phi(x)$ is a linear function of x in macroscopically large parts of the system, i.e. there is a constant electric field that lifts the colloids to higher altitudes than expected on the basis of their mass [126]. This result stems both from numerical solutions of (6.7)-(6.9) and from the "Laplace-Boltzmann" equation, where (6.9) is replaced by the local charge neutrality condition $\kappa^2 \sinh\phi(x) + 4\pi\lambda_B Z\rho(x) = 0$. Note that by combining the latter equation with (6.7) and (6.8) one recovers the hydrostatic equilibrium condition (6.3) with χ_T given by (6.4). On the other hand, the set of equations (6.7)-(6.9) can be solved numerically in order to determine the local electrostatic potential $\phi(x)$ together with the equilibrium profile $\rho(x)$ by an iterative procedure as pointed out in [126]. Such a procedure requires two boundary conditions, e.g. $\phi'(0) = \phi'(H) = 0$, where H is the height of the solvent meniscus.

A system described by the Hamiltonian (6.5) was simulated in a rectangular box of horizontal area $9\sigma \times 9\sigma$ and height $H = 50\sigma$. The vertical coordinate x is restricted to $x \in [0, H]$, and periodic boundary conditions are only applied in the horizontal plane and not in the vertical direction. In order to be as closely as possible to the experiments of Ref.[98], we considered colloids with charge $Z = 76$, diameter $\sigma = 1.910\mu$m, gravitational length $L = 2.41\sigma$, Bjerrum length $\lambda_B = 10.4$nm, and average colloidal packing fraction $\overline{\eta} = H^{-1}\int_0^H \eta(x)dx = 0.0053$ (with $H = 50\sigma$). The experimental screening parameter satisfies $\kappa\sigma = 1.2$. This state point is realized, with the present box size and shape, by the number of colloids N_c=12 and the number of positive and negative ions N_+ =13516 and N_- =12604, respectively. In order to take the long-range electrostatic interactions into account a combination of Ewald summation in a slab geometry with the lattice method proposed by Panagiotopoulos and Kumar [138] was employed. The parameters of the Ewald summation and lattice method are the same as those in reference [139]. Note that the large number of ions, which have to be included to represent the low but yet substantial screening parameter, makes the simulations extremely time consuming. A typical simulation consists of 10^5 MC cycles. A cycle consists of $0.9\mathcal{N}$ trials to move a randomly chosen colloid and $0.1\mathcal{N}$ trials to move a randomly chosen colloid or microion, with $\mathcal{N} = N + N_+ + N_-$ the total number of microions and colloids in the system. In a dense system of microions, a simple Monte Carlo move of a colloid would almost certainly result in an hard-core overlap with one of the microions. In order to avoid such overlaps a cluster move technique was used, where ions that overlap with the new colloid position are moved into the space left empty by the displaced colloid, more details on this technique can be found in Ref. [110, 137]. The percentage of accepted moves of each component (colloids and microions) was maintained at about 40%. To check if the system was equilibrated, the average altitude of the centers of mass of the colloids was monitored in the simulation; when the center of mass was not stable, further equilibration was performed before taking measurements. A final simulation with $2 \cdot 10^5$ MC cycles was performed to obtain averages.

6.4 Results

Figure 6.1 shows a first comparison of theoretical predictions based on the one-component and three-component model. We see several theoretical sedimentation profiles as a function of the altitude x, corresponding to colloids of diameter $\sigma = 1.91\mu$m, and three different salt concentrations characterized by screening parameters $\kappa\sigma = 0.8$, 1.2, and

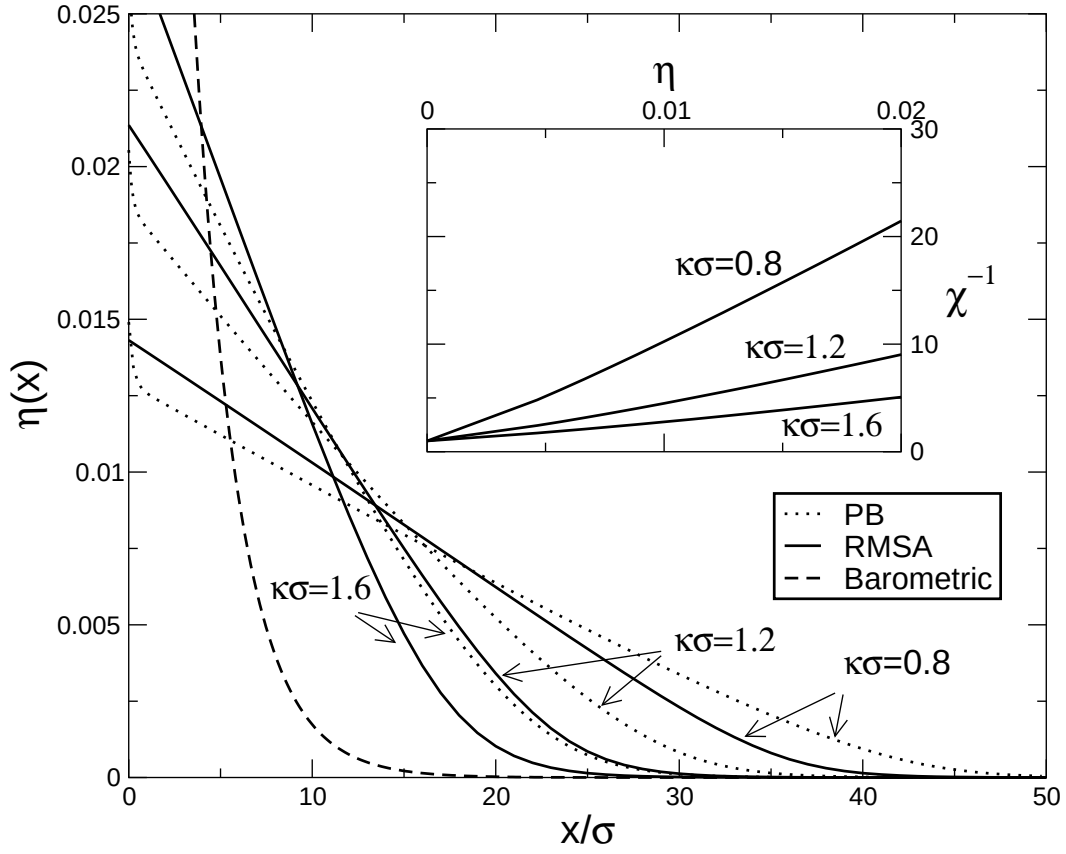

Figure 6.1: Colloidal sedimentation profiles based on hydrostatic equilibrium (7.1) calculated using the RMSA-based compressibility of the one-component Yukawa model, compared to those based on the multi-component PB theory (6.7)-(6.9), for the screening parameters $\kappa\sigma = 0.8, 1.2$ and 1.6. The colloidal charge is $Z = 76$, the colloid diameter $\sigma = 1.91\mu$m, the Bjerrum length is $\lambda_B = 10.4$ nm, the gravitational length $L = 2.41\sigma$, the average colloid packing fraction is $\overline{\eta} = 0.0053$, and the sample height is $H = 50\sigma$, as reported in Ref. [98]. The dashed curve is the barometric distribution with the same normalization. The inset shows the RMSA-based compressibility.

1.6. All profiles shown in Fig.6.1 are for the same gravitational length $L = 2.41\sigma$, average packing fraction $\overline{\eta} = 0.0053$, sample height $H = 50\sigma$, and Bjerrum length $\lambda_B = 10.4$nm. For each $\kappa\sigma$, the colloid density profile is calculated for both the effective one-component model based on the solution of the hydrostatic equilibrium equation (7.1) using the isothermal compressibility obtained from the RMSA closure, as well as from the multi-component PB theory described by equations (6.7)-(6.9). We also show, for the sake of comparison, the corresponding barometric profile obtained from (6.8) and (6.9) in the case of uncharged colloids ($Z = 0$), for the same normalization. The inset shows the compressibilities as a function of the colloid density, as obtained from the solution of the OZ equation within the RMSA closure. At zero density all the compressibility curves reduce to the ideal-gas compressibility, and with increasing colloid density the electrostatic repulsions manifest themselves as a reduction of χ_T: the weaker the screening, the

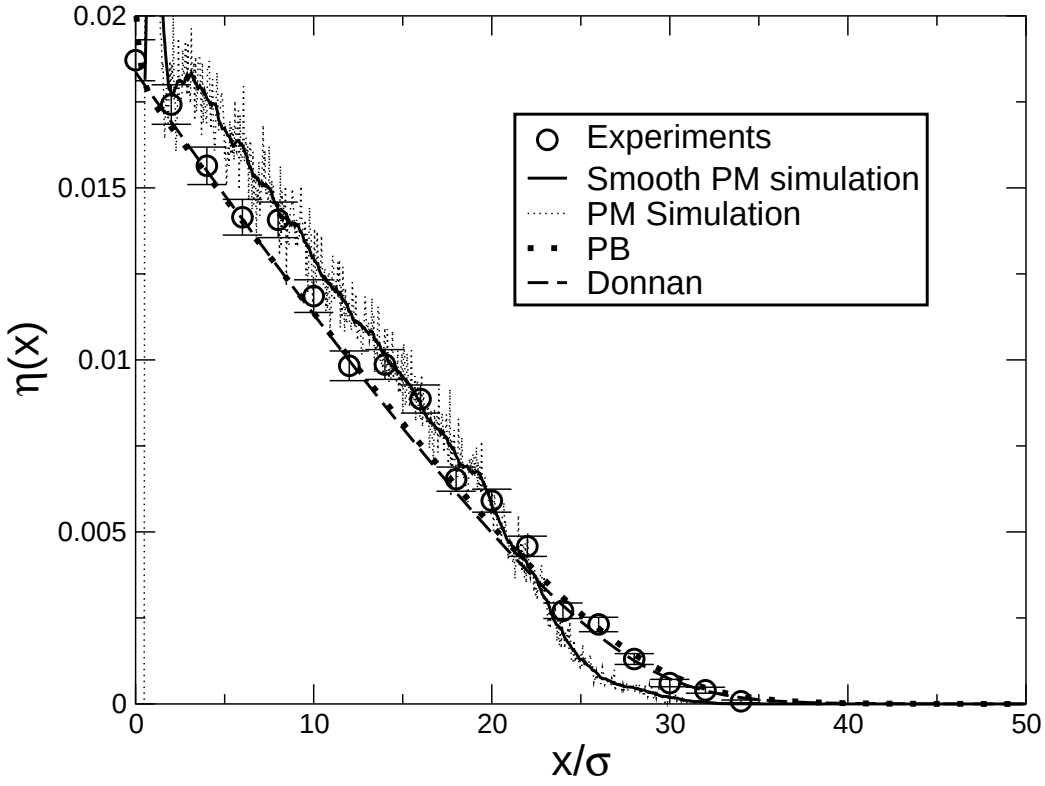

Figure 6.2: Colloidal sedimentation density profiles for colloidal charge $Z = 76$ stemming from multi-component PB theory (6.7)-(6.9), from the Donnan compressibility (6.4) combined with hydrostatic equilibrium (7.1), and simulations of the Primitive Model in gravity, for the parameters of Fig.6.1 and $\kappa\sigma = 1.2$. The symbols denote the experimental measurements from Ref.[98].

stronger the effective colloidal interactions. We note that each one-component Yukawa system yields steeper density profiles than those of the corresponding three-component model, for all $\kappa\sigma$ considered here, i.e. the one-component systems have a relatively small average altitude and a relatively low density at higher altitudes. We will argue in more detail below that the source of the difference between the one- and three-component predictions is mainly due to the poor representation of the colloid-colloid correlations in the three-component PB theory.

Figure 6.2 shows the experimentally measured density profile of Ref. [98] compared to density profiles as obtained from the multi-component models: the three-component PB theory of equations (6.7)-(6.9) and simulation of the primitive model in gravity as introduced in section 6.3. In spite of the fact that the primitive model simulation was equilibrated during about one year CPU, the level of noise in the raw data is still quite high. Therefore also a smoothed curve of the simulated profile is shown to facilitate comparisons. The difficulty in obtaining good statistics in this particular simulation is due

to the fact that the total number of colloids in the system is exceedingly small ($N_c = 12$), whereas the total number of particles in the system is rather large (26132), most of them salt ions needed to achieve the required screening parameter condition. That the Donnan-based density profile is accurate when compared to the experiments is *only* due to the fact that the experimental value $Z = 76$ * stems from a fit to PB theory [98], which is equivalent to the Donnan equation of state in the local neutrality "Laplace-Boltzmann" limit as explained below Eqs.(6.7)-(6.9). In other words, $Z = 76$ is close to a best fit to the Donnan equation of state.

In figure 6.3 we see a first comparison of the sedimentation profile obtained experimentally with sedimentation profiles calculated using the effective one-component models: simulation of the Yukawa system and the RMSA approach of section 6.2. We also include the profiles obtained from the multi-component PB theory for the sake of comparison. The contrast between the simulations and the experimental curve seems to reveal a systematic deviation such that the simulated and RMSA profiles are actually somewhat too steep. Indeed, when we allow Z to be a fit parameter in the one-component Yukawa system, keeping all the other parameters equal, it turns out that $Z = 94$ gives best agreement of the one-component models with the experimental profile. It is tempting to conclude, therefore, that $Z = 76$ gives merely a best fit to the experiment within PB theory given by Eqs.(6.7)-(6.9), which (to a large extent) ignores colloid-colloid correlations, whereas inclusion of these correlations (as in the simulations of the primitive model and that of the Yukawa system, and in the RMSA-based theory) gives rise to a density profile that is systematically steeper in comparison with the experiment.

In figure 6.4 we show the resulting sedimentation profiles based on the Yukawa potential simulations and the RMSA closure for $Z = 94$. For comparison we also plot the multi component PB model for $Z = 94$ revealing a relatively poor agreement with the other curves. In this case the PB approach clearly fails to reproduce quantitatively the sedimentation profiles. On the other hand, the agreement of the experimental profile with the effective one-component models is good, except that as mentioned before, the simulated profile exhibits much more structure close to the hard-wall that represents the bottom of the sample in the simulations —this packing effect is not captured by the local-density approximation that underlies the hydrostatic equilibrium condition, and is not seen in the experiment because the actual sample extends beyond the plotted x-range.

In Fig.6.5 we show sedimentation profiles as obtained by simulations of the primitive model and of the Yukawa model, compared with those by the RMSA approach, all for $Z = 76$. The agreement is perhaps a bit less quantitative than one would have expected. One of the reasons that the density in the primitive model is considerably higher in $x/\sigma \in (10, 25)$ is due to the structure close to the hard wall at the bottom near $x = 0$, as shown in the inset of Fig.6.5, where the two Yukawa systems reveal a larger net adsorption than that of the primitive model, albeit for different reasons: the simulated Yukawa system shows a strong peak at $x = \sigma/2$ while the RMSA-based profile continues to be nonzero down to $x = 0$. Given that we imposed that $\bar{\eta}$ is identical in all cases, there must also be a region in space where the density in the primitive model exceeds the other two; the order of magnitude of the integrated differences over $x/\sigma \in (10, 25)$ is indeed similar to

*The measured density profile was fitted to the predictions of Poisson-Boltzmann theory, and it was concluded in Ref. [98] that the colloidal charge equals $-78e$. Here we concluded that $-76e$ gives the best fit within Poisson-Boltzmann theory, this difference is due to details of the fitting procedure and does not interfere with our arguments.

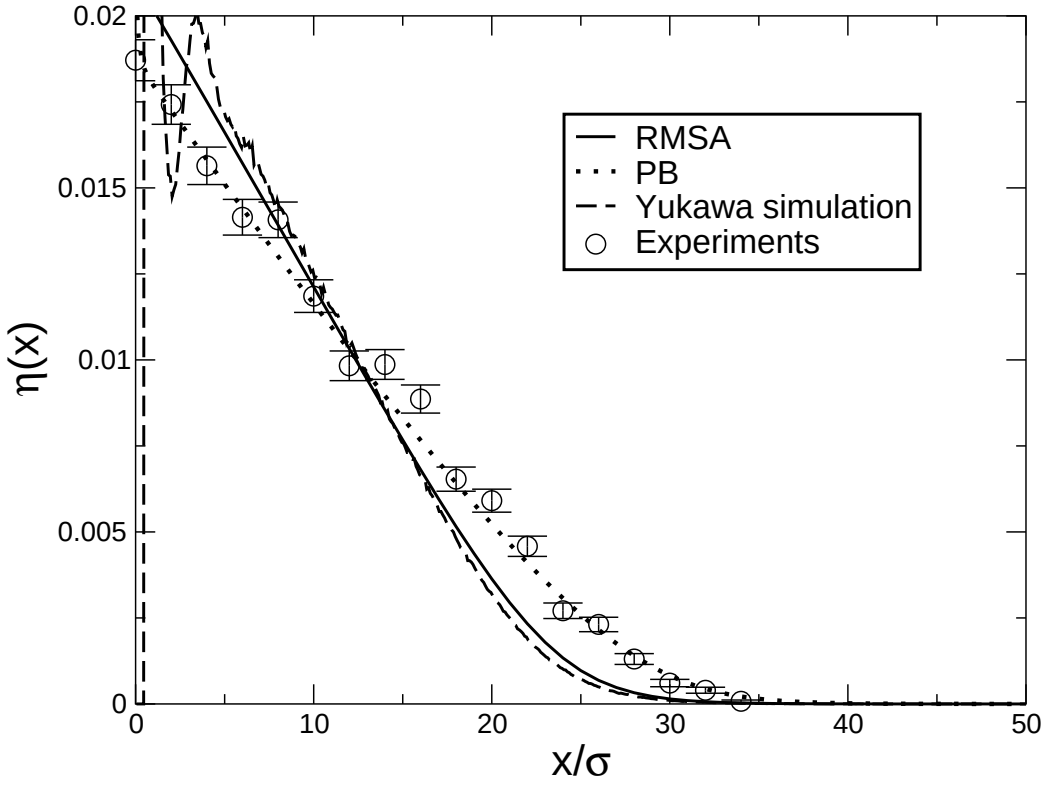

Figure 6.3: Sedimentation profiles of the effective one-component Yukawa model calculated using both RMSA and standard MC simulations, compared with the experimental measurements of Ref. [98] and the three-component PB theory, for $Z = 76$ and all other parameters as in Fig.6.2. Note the close agreement between the two Yukawa results, and their small but systematic deviation from the experiments and the PB theory.

the negative of that over $x/\sigma \in (0, 3)$. Another reason for these differences might be the poor statistics and slow equilibration of the primitive model simulations. Recall that the present data are based on about one year of CPU time, so considerable extensions and more checks are not easily obtained. This also prevented us from performing primitive model simulations for $Z = 94$.

6.5 Discussion

The first observation from Fig. 6.3 should be the gross agreement between the experiments and all calculated and simulated profiles. In all cases we have $\kappa\sigma = 1.2$, Bjerrum length $\lambda_B = 10.4$ nm, colloid diameter $\sigma = 1.91\mu$m, and gravitational length $L = 2.41\sigma$. The colloidal charge is taken as $Z = 76$, and the measured packing fractions are in

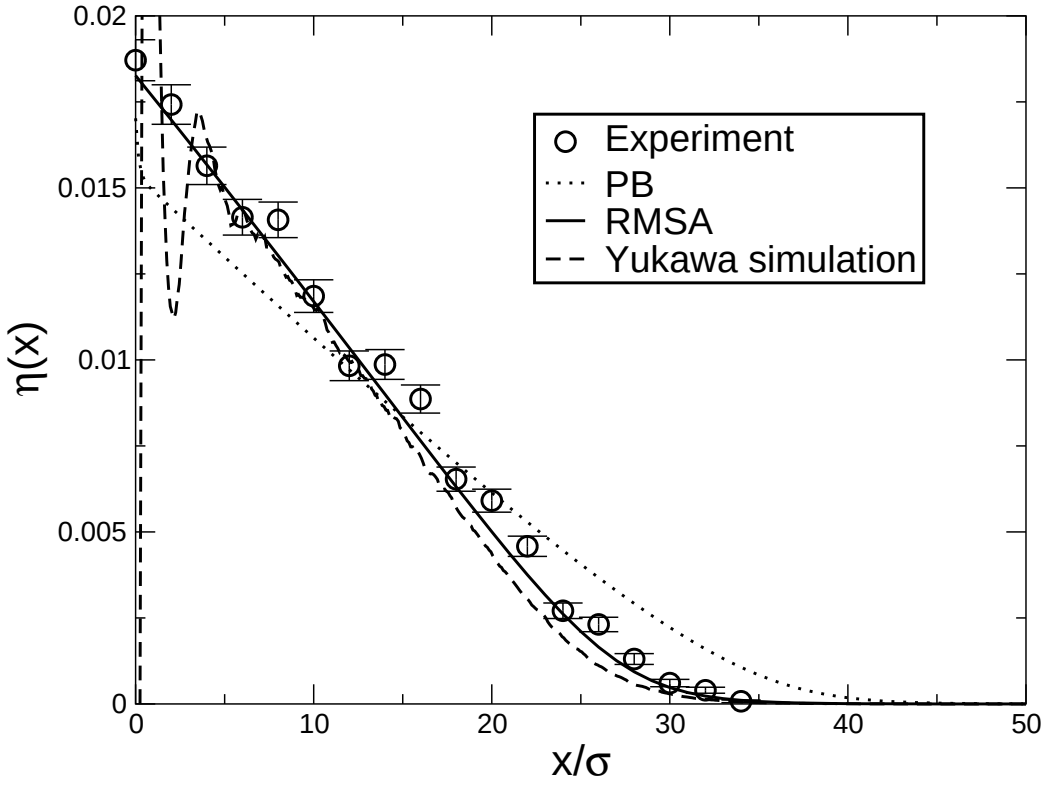

Figure 6.4: As Fig.6.3, but with $Z = 94$, such that the Yukawa model profiles (both RMSA and simulated) fit the experimental profile best. The PB profile is clearly less accurate now.

the range $0 < \eta(x) < 0.02$, where $\eta(x) = (\pi/6)\sigma^3\rho(x)$. This regime is such that $Z\rho(x)/2\rho_s < 0.17$ for all x, i.e. even at the highest density the ion concentration is dominated by the reservoir salt concentration $2\rho_s$, such that the screening constant is indeed essentially a constant independent of the height or density, as implicitly assumed in equation (6.2). A closer look, however, shows that even though the simulations and the RMSA result of the Yukawa system are very close to each other (except at the bottom where packing effects affect the simulations), they both deviate systematically from the experiment: the former two are too steep and have too low a density at higher altitudes. From the fact that the RMSA-based profile and that of the Yukawa simulations are so close to each other, one could conclude that they are mutually consistent and both accurate, and that their deviation from the experiment is mainly due to the present choice of $Z = 76$, which was based on the fitting to the PB theory of Eqs.(6.7)-(6.9). This fitting is not optimal due to the inadequacy of the present PB theory to account for correlations among the different species in the system. In particular, PB theory overestimates the colloid density at high altitudes for a given value of Z. For the present set of parameters this overestimate occurs for charges $Z \gtrsim 50$, whereas for smaller values of the colloid charge the agree-

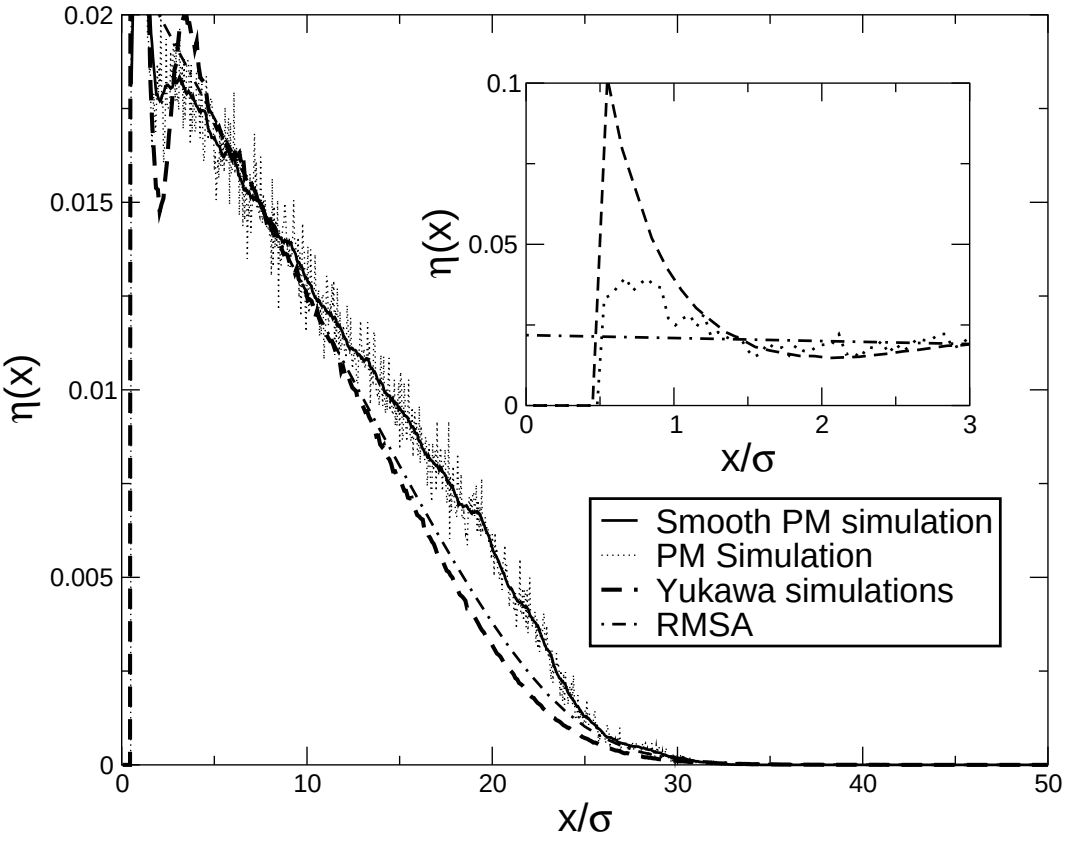

Figure 6.5: Sedimentation density profiles as obtained from simulations of the Primitive Model in gravity and simulations of the Yukawa fluid compared with the one-component RMSA model for colloidal charge $Z = 76$ and all other parameters as in Fig.6.2. The difference between the profiles can partly be attributed to the structural differences close to the bottom at $x = 0$ as shown in the inset, where the simulations reveal hard-wall induced structure that is not captured by the RMSA-based theory, and perhaps partly by slow equilibration and poor statistics in the simulations due to the small number of colloids.

ment between the profiles obtained from the PB and RMSA approaches is excellent. For the parameters of present interest, fitting the experimental density profile to that of the Yukawa system treated within the RMSA closure, we concluded that $Z = 94$ gives the best fit.

Given that a Yukawa system with a colloidal charge $Z = Z_{RMSA} = 94$ is best described within PB theory by a colloidal charge $Z = Z_{PB} = 76$, for the present system parameters, it is interesting to investigate the relation between Z_{RMSA} and Z_{PB} for other values of the colloid charge. In figure 6.6 we plot the ratio Z_{PB}/Z_{RMSA} for $0 < Z_{RMSA} < 200$, for three screening constants while all the other parameters are left unchanged. Figure 6.7 shows the corresponding density profiles for $\kappa\sigma = 1.2$ and $Z_{RMSA} = 200$, 94, and 40. One can conclude that for $Z_{RMSA} \lesssim 50$, PB theory reproduces the RMSA-Yukawa sedimentation profiles very accurately provided the colloidal charge Z_{PB} is reduced by up to 20% of Z_{RMSA}. Note that the average density here is

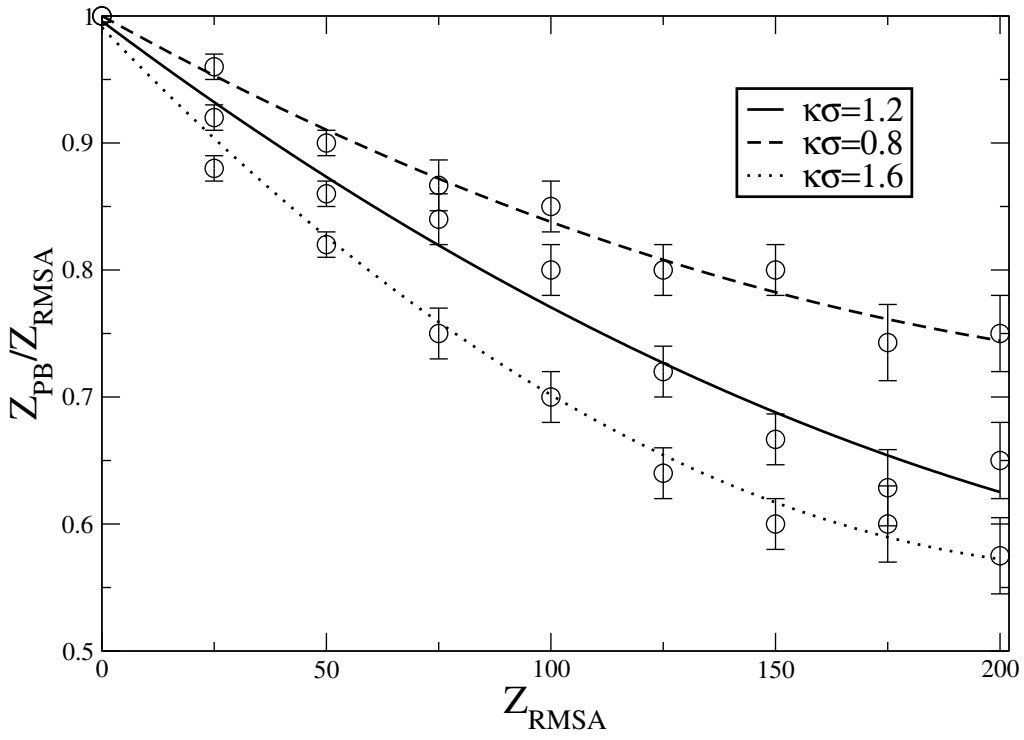

Figure 6.6: Ratio of the best-fitting colloidal charge $Z = Z_{PB}$ (see text) and that of the RMSA charge Z_{RMSA}, as a function $Z_{RMSA} \in (0, 200)$, with σ, λ_B, L, $\bar{\eta}$, and H as in Fig.6.1, for various screening parameters $\kappa\sigma$. Note that PB theory is increasingly better for lower colloidal charges and lower salt concentrations. The lines are mere guides to the eye.

low enough that the profile in the limit of $Z_{RMSA} \to 0$ becomes essentially barometric; at higher average packing fractions one also expects $Z_{PB}/Z_{RMSA} \neq 1$ in this limit, due to hard-core effects that are not accounted for properly in the PB theory. The required reduction of Z_{PB}/Z_{RMSA} with increasing $Z_{RMSA} > 50$ exceeds 20%, and, in addition, the quality of the best-fitting PB profile (quantified by the mean-squared deviation) becomes slightly less satisfactory as is reflected by the increase of the error bars in figure 6.6 with increasing Z_{RMSA}, this is also shown in figure 6.7.

The difference between Z_{RMSA} and Z_{PB} in the present system is of course considerable and significant, but not qualitative. The seemingly different mechanisms that underly the lifting of the colloids to higher altitudes than given by the barometric distribution, as predicted by the three- and one-component theory, should therefore be actually equivalent: the self-consistent electric field that is generated by a net charge-imbalance at the boundaries of the 3-component system such that the colloids are pushed upwards is merely another way of describing a pairwise screened-Coulomb repulsion that pushes the colloids apart to higher altitudes in a one-component model. This is in line with conclusions in

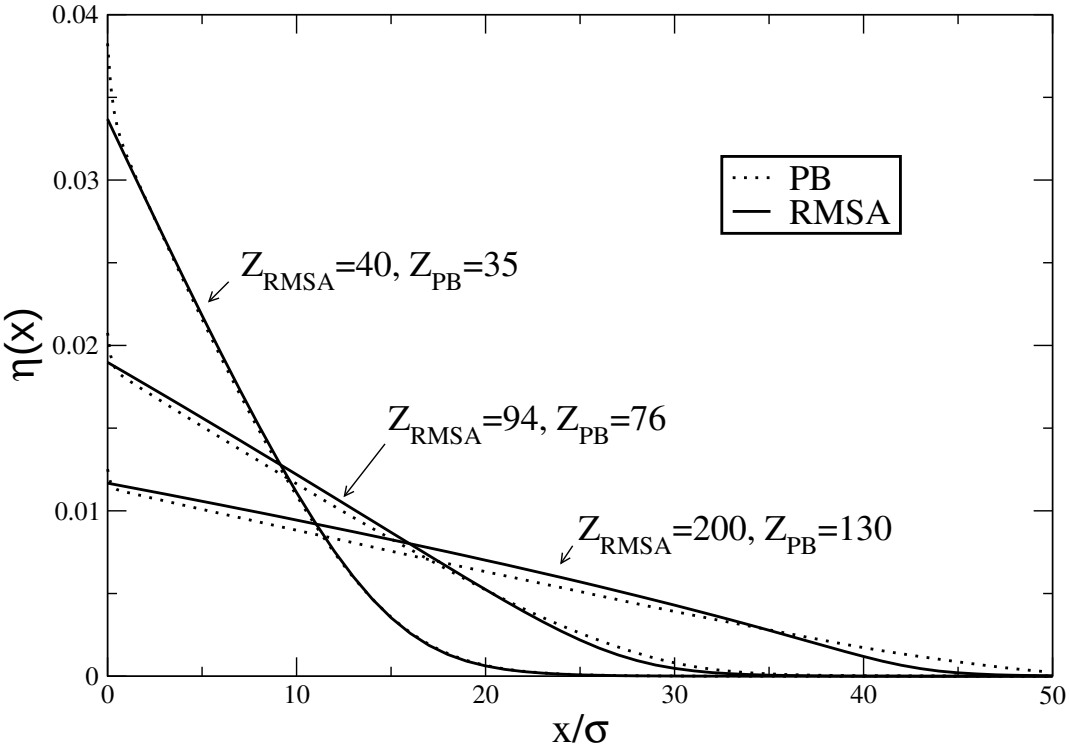

Figure 6.7: Sedimentation profiles obtained from RMSA theory compared to those of PB theory using the best-fitting Z_{PB} from Fig. 6.6, for $\kappa\sigma = 1.2$ and all the other parameters as in Fig.6.6. Note that the quality of the fit deteriorates slightly with increasing Z_{RMSA}.

Ref.[127].

We attribute the difference between the best fit for Z based on Poisson-Boltzmann theory and the other three methods (simulations of the primitive model, and simulations and RMSA theory of the one-component Yukawa system) to the poor account of correlations in the Poisson-Boltzmann theory. In principle, however, there could be other sources that cause such a difference, e.g. charge renormalization and hard-core exclusion effects for the screening ions. Charge renormalization due to nonlinear screening effects [76] is, however, *not* a candidate here to explain the difference for at least two reasons: (i) The actual bare charge is usually larger than the renormalized charge that appears in the prefactor of the screened-Coulomb interactions, whereas here the former seems to be smaller. (ii) The present parameters here are such that $Z\lambda_B/a < 1$, whereas charge renormalization is only substantial if this dimensionless combination exceeds about 5 or so [73, 76, 78]. A mechanism whereby the effective colloidal charge is increased was discussed in Refs. [144, 145], and is based on the hard-core exclusion of the screening ions at sufficiently high colloid packing fractions: the screening is therefore less effective, which appears as

an increase of the effective colloidal charge. However, applying the analysis of Ref.[145] to the present case gives only marginally larger values of the effective charge, by less than 1% at the highest density $\eta \simeq 0.02$. In other words, it appears that this effect cannot explain the difference between $Z = 76$ and $Z = 94$, leaving the poor account of colloid-colloid correlations in the Poisson-Boltzmann theory as the most plausible source of the difference.

It is interesting to inquire whether the one- and three-component models would also produce essentially the same sedimentation profiles for other sets of parameters than considered here, and whether the hydrostatic equilibrium condition (7.1) and the Poisson-Boltzmann theory (6.7)-(6.9) for the one-component and the three-component case, respectively, produce reliable profiles in all circumstances. In order to answer these questions we consider the regimes of extremely low and extremely high salt concentrations. First, the hamiltonian (6.1) for the effective one-component system is pairwise additive, which is expected to be a good approximation for the present parameter set where $\kappa\sigma > 1$ and $Z\rho/2\rho_s < 1$, i.e. the range of the interactions is smaller than the size of the particles and the background electrolyte concentration dominates the counterion concentration. At lower salt concentrations, such that $\kappa\sigma \ll 1$ and/or $Z\rho/2\rho_s > 1$, one would expect effective many-body interactions to become relevant [73, 134], such that (6.1) is not necessarily a reliable effective hamiltonian anymore. In such an extremely low-salt regime, which is realized in salt free systems, the Poisson-Boltzmann theory proved to be quantitatively accurate, at least in comparison with simulations [132, 147] at low Coulomb couplings. It is interesting to see if the pairwise one-component description is capable of describing the density profiles in this case. We wish to stress here that the possible break-down of the pairwise screened-Coulomb picture does *not* imply that the system can no longer be seen as a one-component system in hydrostatic equilibrium as described by (7.1) with a compressibility that follows from the Kirkwood-Buff relation $S(0) = \chi_T$: these relations remain valid (the former only within the local density approximation, but given the long screening length in the extremely low-salt regime this approximation is probably accurate). The breakdown would "merely" imply that it is not obvious how to calculate the compressibility or the structure factor without detailed knowledge of the effective hamiltonian. Second, let us consider the opposite high-salt regime such that $\kappa\sigma \gg 1$ and $Z\rho \ll 2\rho_s$. In this regime the electrostatic interactions are completely screened over distances much smaller than the colloidal diameter, such that the effective one-component system is essentially a (pairwise) hard-sphere system (for water at room temperature at least, where ion-ion correlations are not all that important). In this regime the one-component description based on (7.1) is far superior over the PB theory of Eqs. (6.7)-(6.9). This is directly seen by regarding the $Z = 0$ limit of equations (6.7)-(6.9), which reduce to $\phi(x) = 0$ and $\rho(x) = \rho_0 \exp[-x/L]$, i.e. the sedimentation profiles become barometric; the hard-core correlations are left-out completely from this theory. By contrast, the RMSA closure is, in this hard-core limit, equivalent to the Percus-Yevick closure, and in combination with (7.1) the density profiles of hard-sphere sedimentation equilibrium are well-described [97, 124]. Moreover, also in the present regime with $\kappa\sigma \simeq 1$ the one-component theory performs better.

6.6 Summary and Conclusions

In this chapter we have studied sedimentation equilibrium of charge-stabilized colloids at non-zero salt concentration. We compared experimental results with theoretical and simulated profiles obtained on the basis of two models. On the one hand we considered a multi-component model of point-like colloids, cations, and anions interacting with bare Coulomb potentials. For this model we considered a Poisson-Boltzmann theory of the three-component mixture and performed MC simulations using 12 colloidal particles and a total of about 26132 particles to guarantee the electroneutrality of the system. On the other hand we considered an effective one-component model of colloids interacting by an effective screened-Coulomb potential. For this model we employed a theory based on hydrostatic equilibrium, where the isothermal compressibility is given by the Kirkwood-Buff relation as obtained from the solution of the Ornstein-Zernike equation with the rescaled mean spherical approximation (RMSA) closure for the screened-Coulomb potential. For the effective one-component Yukawa model, we also performed simulations of sedimentation profiles.

The sedimentation profiles obtained from the one-component RMSA theory, simulations of the Yukawa system, and simulations of the primitive model are essentially consistent among themselves but differ from the results of the Poisson Boltzmann theory. The PB theory shows good agreement with the experiments only because the numerical value of the charge was estimated as to give the best fitting according to this theory. In fact, we have seen that PB theory actually overestimates the colloid density at high altitudes compared to the corresponding Yukawa system, for identical values of Z, at the parameters of interest here. Agreement between PB theory and Yukawa systems can be obtained by reducing the colloidal charge in the PB theory compared to that of the Yukawa model. For small values of the colloid charge, $Z \lesssim 50$ or so, the agreement between the resulting profiles obtained from the PB and RMSA approach is truly excellent, for larger charges up to say $Z = 200$ the agreement is still good though somewhat less quantitative as regards the functional form. The CPU time required for the simulation of the multi-component primitive model and the effective one-component Yukawa model varies between about one year in the former case and one hour in the latter. This shows that theory and simulations of sedimentation profiles on the basis of the effective one-component potential and the Poisson-Boltzmann theory (possibly with a reduced effective charge when colloid-colloid correlations are important) are considerably more efficient than primitive model simulations. In spite of the fact that we have only considered a particular case study, this is presumably true in general, with the Yukawa model probably more accurate when $\kappa\sigma \gtrsim 1$ while PB theory could be more accurate or efficient when $\kappa\sigma \ll 1$.

7

Colloidal Brazil nut effect and breakdown of pairwise additivity

In this chapter we study effective colloidal interactions in deionized colloidal mixtures through sedimentation-diffusion equilibrium. * We use the coarse-grained effective model (EM) derived in chapter 5, and compare its density profiles with those of the computationally much more expensive primitive model (PM) of colloids and counterions under gravity. The EM, which contains not only standard pairwise screened-Coulomb interactions but also explicit many-body effects by means of a so-called volume term, can quantitatively account for all observed sedimentation phenomena such as lifting of colloids to high altitudes, segregation into layers in mixtures, and floating of heavy colloids on top of lighter ones. Without the volume term there is *no* quantitative agreement between PM and EM, even in the present high-temperature limit of interest, showing that deionized colloidal suspensions cannot be described by a pairwise Yukawa model.

7.1 Introduction

Sedimentation of suspended colloidal particles in the Earth's gravity field is often a nuisance that is to be avoided, e.g., by careful density matching of the colloidal particles with the solvent or by sending samples to outer space [148]. However, it has also become clear over the last decade or so that the study of the colloidal density profile $\rho(z)$ (with z the vertical height) in sedimentation-diffusion equilibrium can (efficiently) give quantitative information about the (osmotic) pressure $\Pi(\rho)$ of a bulk colloidal suspension at density ρ, and hence about the effective colloidal interactions [149–151]. In pioneering studies it was shown that this scheme, which is based on hydrostatic equilibrium, can quantitatively

*Notice that this chapter is self contained, i.e., independent of chapter 5 as regards the notations.

reproduce the known equation of state of hard spheres in the fluid phase [149, 150], and recent extensions show that this method also works for hard-sphere crystals and for sticky spheres [151]. In this chapter we exploit the close relationship between effective colloidal interactions and sedimentation-diffusion equilibrium for the case of (mixtures of) index-matched charged colloidal spheres suspended in a dielectric solvent with monovalent salt ions, as e.g. studied experimentally in Refs.[131, 152]. Sedimentation of charged colloids has turned out to be interesting in its own right, given the rich phenomenology that was found for such systems during the last few years, e.g. the existence (in a conducting medium) of a macroscopic electric field that pushes the colloids up to relatively large heights [127, 131, 152, 153] and the "colloidal Brazil nut effect" such that the heavier colloids can float on top of a layer of lighter ones [93, 156, 158]. In the regime of relatively high salt concentrations, where the ionic strength is dominated by the background electrolyte, these sedimentation phenomena have been explained by two different types of models, (i) by the multi-component primitive model (PM) of mesoscopic charged colloids with sub-nanometer-sized cations and anions in a continuum solvent [153, 156], and (ii) by the Yukawa model (YM) of colloids interacting solely by a pairwise repulsive screened-Coulomb potential [93, 127, 160]. Advantages of the YM are that both colloid-colloid correlations and colloid-ion correlations ("the double layer") are taken into account in the hydrostatic equilibrium calculations [93, 127], and that larger systems can be simulated due to the absence of explicit ions.

We will show that the state of affairs is quite different at vanishingly low ionic strength: our direct simulations of the PM in gravity are *not* in agreement with our simulations and calculations of the YM. Given the close relationship between sedimentation profiles and the equation of state of bulk systems [149–151], this disagreement between the PM and the YM actually points to the break-down of the YM in deionized bulk suspensions. We attribute this to many-body effects that become relevant at low salinity due to the long Debye length (which sets the interaction range in the YM). Instead of trying to improve the YM by extending it with triplet and higher order potentials, such as e.g. in Refs.[161–164], we focus here on the high-temperature linear screening regime and derive an explicit expression for the effective interaction Hamiltonian W of the form $W = W_1 + W_2$. This effective model (EM) is found to consist of the pairwise YM Hamiltonian W_2 and a so-called volume term W_1 that does *not* depend on colloidal coordinates but nontrivially on the colloid densities [165–167]. We will show that the EM under gravity is in quantitative agreement with the PM, thereby showing that the non-pairwise many-body effects can be captured efficiently and accurately by the volume terms.

7.2 Model

Let us consider an n-component suspension of colloidal species $i = 1, \cdots, n$ with charges $Z_i e$, radii a_i, and buoyant masses m_i, confined between the bottom of a macroscopic sample cell at $z = 0$ and the meniscus of the solvent at $z = H$. The colloidal chemical potentials μ_i are such that the average packing fraction $\bar{\eta}_i = \int_0^H dz \eta_i(z)/H$ of each species i is fixed, with $\eta_i(z) = (4\pi/3)a_i^3\rho_i(z)$ the packing fraction of species i at height z. The solvent is a continuum with dielectric constant ϵ at temperature T, such that its Bjerrum length reads $\lambda_B = e^2/(\epsilon k_B T)$. Here e is the elementary charge and k_B the Boltzmann constant. The system is globally charge neutral due to monovalent, massless, and point-

like counter ions. The gravitational potential that acts on the colloids is $m_i g z \equiv k_B T z/L_i$ for species i, with L_i its gravitational length. The interaction potential between any pair of particles (colloids and counterions) is the sum of a hard-core repulsion and an (unscreened) Coulombic interaction $\propto r^{-1}$, with r the center-to-center distance.

In the previous chapter and in an earlier publication [158] we presented some direct Monte Carlo (MC) simulations of this PM in gravity with added salt. Under such simulations are computationally extremely expensive and slow due to the large number of counterions per colloid and due to the long range of the Coulomb interactions. It would therefore be convenient if one could model the system as a colloids-only system by integrating over the ionic degrees of freedom, of course without losing quantitative agreement with the PM results. Following the local density approximation that underlies hydrostatic equilibrium [168], the equilibrium packing fraction profiles $\eta_i(z)$ should satisfy

$$k_B T \ln \eta_i(z) + \mu_{i,ex}\Big(\eta_1(z), \cdots, \eta_n(z)\Big) + m_i g z = \mu_i, \tag{7.1}$$

where the effective colloidal interactions enter through the excess (over ideal) chemical potentials $\mu_{i,ex}(\eta_1, \cdots, \eta_n)$ of species $i = 1, \cdots, n$ in a colloidal bulk mixture. Note that Eq.(7.1) is equivalent, for $n = 1$, to the hydrostatic equilibrium condition $d\Pi(z)/dz = -mg\rho(z)$ [168]. In order to be able to solve the n local equations (7.1) an explicit form is needed for $\mu_{i,ex}(\eta_1, \cdots, \eta_n)$, which we obtain here along the same lines described in chapter 5.

The first step in this scheme consists of considering an arbitrary non-overlapping fixed configuration of $N_1, \cdots, N_n$ colloids of species i in a bulk volume V, in osmotic contact with a neutral reservoir of monovalent ions at a density $2\rho_s$ —at the end of the calculation we will consider $\rho_s \to 0$ in order to describe the deionized limit. The ionic density profiles $\rho_\pm(\mathbf{r}) = \rho_s \exp[\mp\phi(\mathbf{r})]$ and the electrostatic potential $k_B T\phi(\mathbf{r})/e$ in the electrolyte in between the colloids follow from the Poisson-Boltzmann (PB) equation $\nabla^2\phi(\mathbf{r}) = \kappa^2 \sinh\phi(\mathbf{r})$, where $\kappa = (8\pi\lambda_B\rho_s)^{1/2}$ is the reservoir's inverse Debye screening length. By linearizing the PB equation about a self-consistent average potential $\bar{\phi}$, the PB equation can be solved and analytic expressions for $\phi(\mathbf{r})$ and $\rho_\pm(\mathbf{r})$ follow as in Ref.[169]; one also finds for the so-called Donnan potential $\bar{\phi} = \text{arc}\sinh[\rho_c/(2\rho_s)]$ with the counterion density $\rho_c = \sum_{i=1}^n Z_i\rho_i$. The effective colloid Hamiltonian follows as $W = W_1(\rho_1, \cdots, \rho_n, V) + W_2(\rho_1, \cdots, \rho_n, \{\mathbf{R}\})$ with the so-called volume term W_1 that is independent of the colloidal coordinates and the pairwise additive term W_2 of effective colloidal potentials of the screened-Coulomb form $v_{ij}(r) = Z_i^* Z_j^* k_B T \lambda_B \exp(-\bar{\kappa}r)/r$ between a pair of species i and j at separation $r > a_i + a_j$. Here $Z_i^* = Z_i \exp(\bar{\kappa}a_i)/(1 + \bar{\kappa}a_i)$, and $\bar{\kappa} = \kappa\sqrt{\cosh\bar{\phi}}$. In the limit $\rho_s \to 0$ one finds $\bar{\kappa} = \sqrt{4\pi\lambda_B\rho_c}$, i.e. only the counterions contribute to the screening, and $W_1 = Vw_1$ with

$$\frac{w_1}{k_B T} = \rho_c\big(\ln\frac{\rho_c}{\rho_s} - 1\big) - \frac{1}{2}\sum_{i=1}^n \rho_i\big(\frac{Z_i^2\bar{\kappa}\lambda_B}{1 + \bar{\kappa}a_i} + Z_i\big), \tag{7.2}$$

where we recognize the ideal-gas entropy of the counterions and the self-energy of the colloids. Note that the term $-\rho_c \ln\rho_s$ arising from the first term in the r.h.s. of Eq. (7.2), does not affect the thermodynamic properties and it is kept here for the sake of making the argument of ln dimensionless. Note also that Eq. (7.2) reduces, for $n = 1$, to the results

of Ref.[169]. With the explicit analytic form of the effective Hamiltonian $W = W_1 + W_2$ at hand we can take the next step in the calculation of $\mu_{i,ex}$. We calculate the excess free energy $F_{ex} = W_1 + Vf_2$ of the colloids-only system, with $Vf_2(\eta_1, \cdots, \eta_n)$ the excess free energy of the pairwise Yukawa fluid with Hamiltonian W_2. This is done here by using the Gibbs-Bogolyubov (GB) inequality, with a reference hard-sphere mixture with variational hard-core diameters d_i for species i, such that $f_2(\eta_1, \cdots, \eta_n)$ is the minimum of

$$f_{HS}(\{x\}) + 2\pi \sum_{i,j}^{n} \rho_i \rho_j \int_{d_{ij}}^{\infty} dr r^2 g_{ij}(r; \{x\}) v_{ij}(r), \tag{7.3}$$

where $x_i = (\pi/6)\rho_i d_i^3$ is the variational packing fraction of species i, f_{HS} is the hard-sphere mixture free-energy density as given in Ref.[170], $d_{ij} = (d_i + d_j)/2$, and $g_{ij}(r)$ are the reference hard-sphere radial distribution functions treated within the Percus-Yevick approximation. Note that expression (7.3) is explicitly known analytically [170], and its minimization with respect to the variational diameters was performed numerically.

The final step in the calculation of $\mu_{i,ex}$ stems from the thermodynamic identity $\mu_{i,ex} = \partial F_{ex}/\partial N_i$. This can be rewritten as $\mu_{i,ex} = \partial(w_1 + f_2)/\partial\rho_i$, and can be calculated numerically using Eqs.(7.2) and (7.3). Hence we can solve the hydrostatic equilibrium conditions (7.1) numerically on a z-grid. Moreover, we not only used the effective model (EM) described by $W = W_1 + W_2$ as an intermediate step in the calculation of $\mu_{i,ex}$, but we also perform direct MC simulations of the EM in the Earth's gravity field. In such MC calculations we actually test the accuracy of the variational GB procedure. The MC simulations using the EM are at least ten times faster than those of the equivalent PM for the values considered in this chapter, because of the absence of explicit ions. By comparing colloidal profiles of the PM and the EM one tests in fact the accuracy of our expressions for W. One should be aware, however, of a potential problem in MC simulations of the inhomogeneous EM, since both W_1 and the screening parameter $\bar{\kappa}$ of the pair potentials of W_2 depend on the colloidal densities, for which we take local densities in slices of a thickness H/N_H with typically $N_H = 200$ in the calculations presented below. Thus MC trial moves in which colloids are displaced from one slice to another involve acceptance probabilities that take both the positional change and the density change into account.

7.3 Results

7.3.1 Deionized systems

In order to reduce the parameter space we consider equal-sized colloids with common diameter $2a_i = 2a \equiv \sigma$ for $i = 1, \cdots, n$, Bjerrum length $\lambda_B = 0.004\sigma$, and sample height $H = 100\sigma$. The computational details of our PM simulations are given in Ref.[158]. Our EM and YM simulations are based on systems with about 1000-2000 colloids, equilibrated for about 10^6 MC cycles while averages are taken over 5×10^5 cycles (where 1 cycle contains on average 1 trial move for each particle).

In Fig.7.1 we consider a one-component case, $n = 1$. We find excellent agreement between PM simulations, EM simulations, and EM calculations based on the hydrostatic equilibrium condition (7.1), except perhaps close to the walls at $z = 0$ and $z = H$,

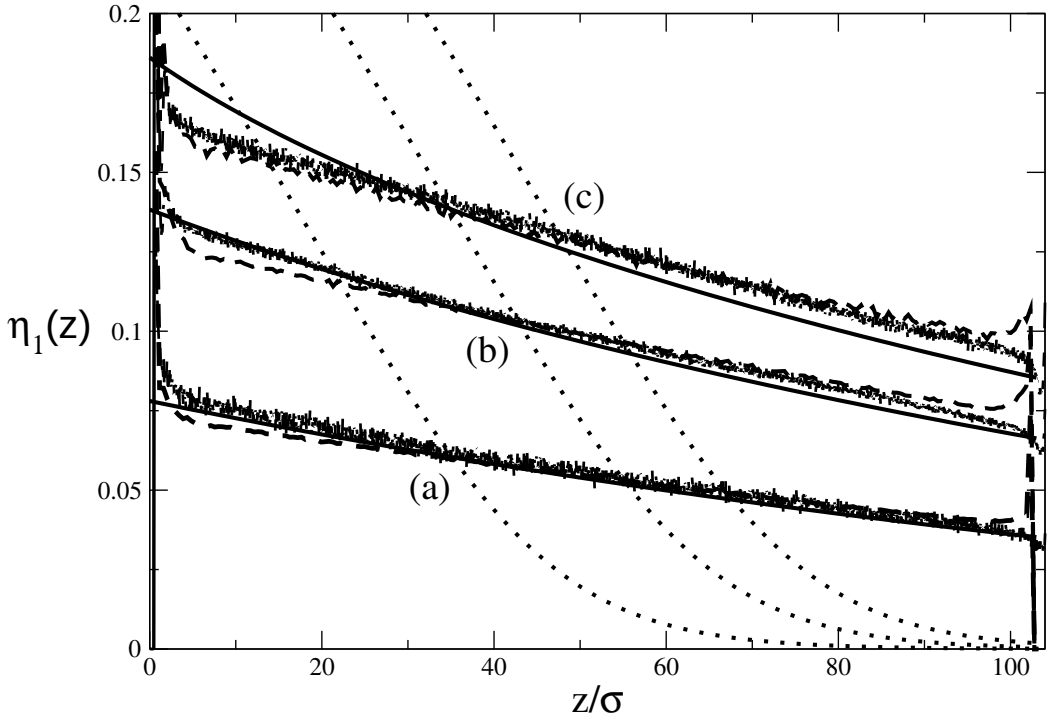

Figure 7.1: Packing fraction profiles $\eta_1(z)$ for deionized monodisperse suspensions of colloidal spheres with diameter σ, gravitational length $L_1 = 10\sigma$, charge $Z_1 = 10$, and sample height $H = 100\sigma$, for average packing fractions $\overline{\eta}_1 = 0.055$ (a), 0.099 (b) and 0.128 (c). The PM simulations (noisy curves, taken from [158]), the EM simulations (dashed curves), and the EM calculations based on hydrostatic equilibrium (solid curves) are all in good agreement, while the YM calculations (dotted curves) clearly differ. This indicates the importance of the volume term in the EM, and the accuracy with which it reproduces PM simulations.

where the local density approximation fails to describe the structure. Interestingly $\eta_1(z)$ is different (dotted curves) for the YM, i.e. the EM with its volume terms is qualitatively different from the YM. In fact one checks that the volume terms contain a net repulsive contribution here, as the actual profiles extend to higher altitudes than the pairwise ones. This can be traced back to the counterion ideal-gas contribution in Eq.(7.2), which is entirely omitted in the YM.

In Fig.7.2 we also show quantitative agreement between direct PM simulations, EM simulations, and EM calculations based on hydrostatic equilibrium, but now for density profiles of a two-component system, $n = 2$. Fig.7.2(a), (c), and (d) show a clear layering effect, in (a) the lighter ones are on top of the heavier ones, in (c) and (d) the order of the layers is reversed ("colloidal Brazil nut effect"), and (b) shows the crossover between these two regimes. Ignoring the volume terms in these systems yields profiles (not shown) that deviate from the actual ones in a fashion similar to that in Fig.7.1, again pointing at

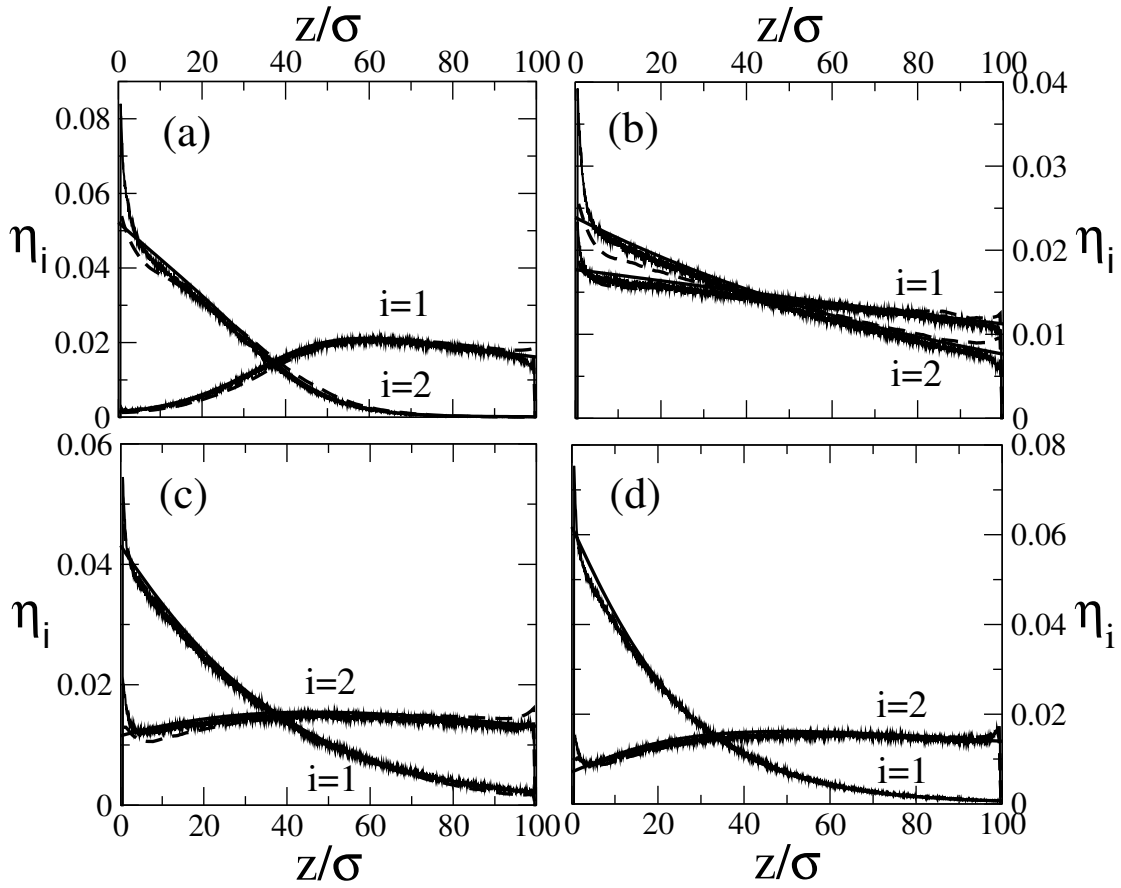

Figure 7.2: Sedimentation profiles for a deionized binary mixture of equal-sized colloids with diameter σ, gravitational lengths $L_1 = 10\sigma$ and $L_2 = 5\sigma$, average packing fractions $\overline{\eta}_1 = \overline{\eta}_2 = 0.0144$, colloidal charges $Z_1 = 10$ and (a) $Z_2 = 10$, (b) $Z_2 = 20$, (c) $Z_2 = 30$, and (d) $Z_2 = 40$. There is quantitative agreement, in all cases, between the PM simulations (noisy curves), EM simulations (dashed curves), and EM calculations based on hydrostatic equilibrium (solid curves).

the importance of w_1. This can be further quantified by considering the mean height

$$h_i = \frac{\int_0^H dz \eta_i(z) z}{H \overline{\eta}_i} \tag{7.4}$$

of species i, as shown as a function of Z_2/Z_1 in Fig.7.3 for the parameters of Fig.7.2. Fig.7.3 shows quantitative agreement between PM simulations (squares), EM simulations (circles), and EM hydrostatic equilibrium calculations (solid curves), while the pairwise YM calculations (dotted lines) and YM simulations (crosses) largely deviate from the other three curves. The mutual deviation between the calculations and the simulations of the YM is to be attributed to the approximate nature of the GB procedure that underlies the calculations. Clearly, Fig.7.3 points to the importance of the volume term, and to the accuracy with which the PM results are reproduced by the EM, in the present parameter regime at least.

Finally, in order to put the EM to a further test we consider a three-component mixture. The results, shown in Fig. 7.4, not only show both layering with increasing mass-per-

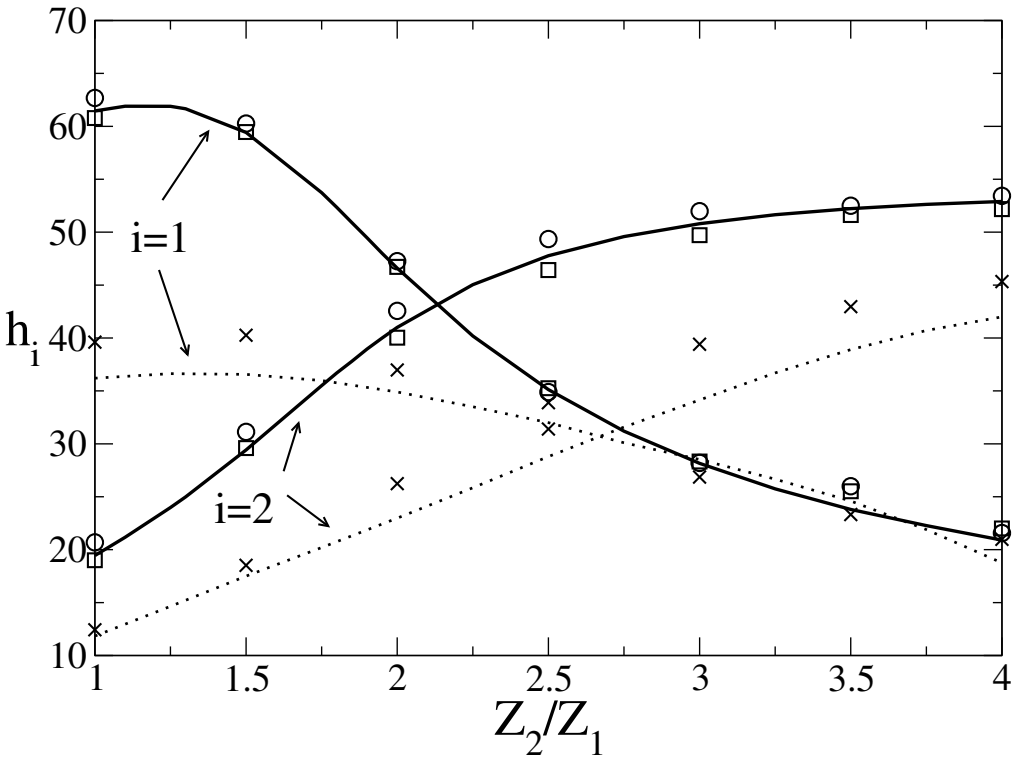

Figure 7.3: Mean height h_i (see text) as a function of the colloidal charge ratio Z_2/Z_1 for binary mixtures with the parameters given in Fig.2, showing mutual quantitative agreement between PM simulations (squares), EM simulations (circles), and EM calculations (solid curves). The mean height of the YM from simulation (crosses) and hydrostatic equilibrium calculations (dashed curves) cannot account for the PM results.

charge ($\propto Z_i L_i$) from bottom to top, but also the heavier species 1 floating on top of the lighter species 2 and 3. For these phenomena we find again good agreement between our (previously published [158]) PM simulations (noisy curves) and the EM simulations and calculations (dashed and solid curves, respectively) based on $W = W_1 + W_2$ derived above. Simulations of the pairwise YM (dot-dashed curves) are very accurate for species 3 but substantially off again for species 1 and 2.

7.3.2 The role of ionic strength

In Fig. 7.5 we show Monte Carlo simulations of sedimentation profiles for a binary mixture for different ionic strength. The solid line shows the sedimentation profiles as obtained by taking into account many-body contributions from $W_1(\rho_c)$, whereas the dashed lines are obtained on the basis of a Yukawa potential only, with density dependent screening length given by Eq. (5.10). Fig. 7.5a corresponds to a de-ionized system. Here we notice that the many-body effects captured in the volume term lead to differences between

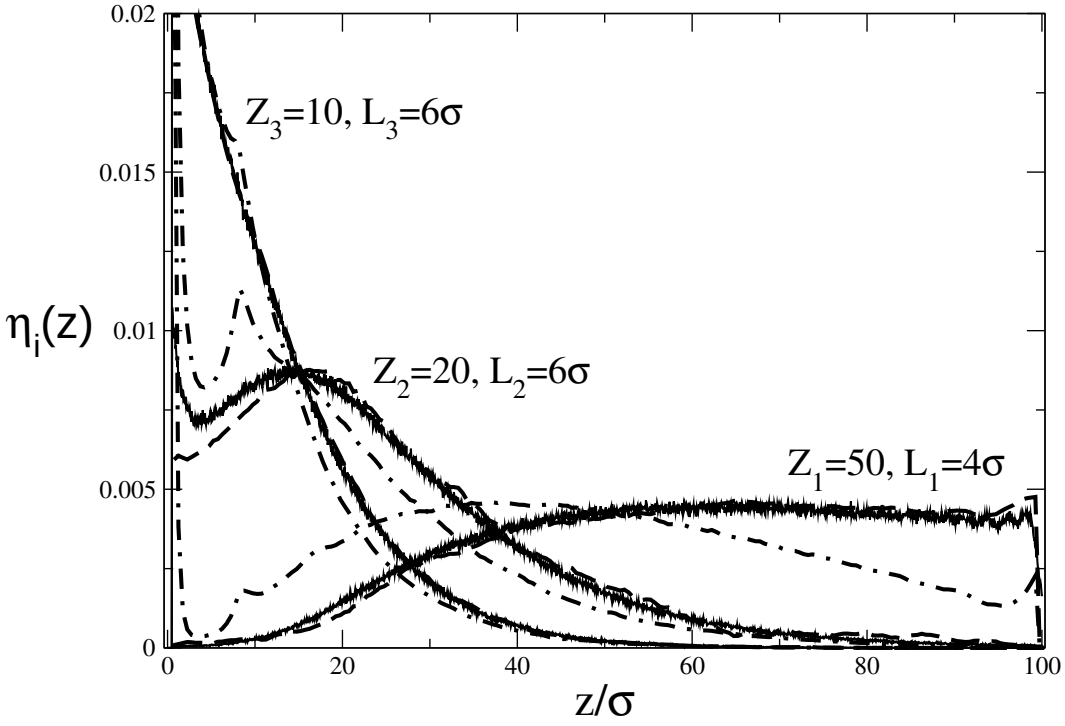

Figure 7.4: Sedimentation profiles of a deionized equimolar three-component colloidal system with average packing fractions $\overline{\eta}_i = 0.0031$, charges $Z_i = 50, 20, 10$, and gravitational lengths $L_i/\sigma = 4, 6, 6$ for the three species $i = 1, 2, 3$, respectively, as obtained from PM simulations (noisy curves) and EM simulations (dashed curves), and pairwise Yukawa simulations without volume term (dot-dashed curves).

these two models as reported in [106]. Upon increasing the ionic strength (Figs, 7.5b-7.5d), the effect of the volume term becomes less important. The Yukawa-dominated regime extends to higher packing fractions and dominates the equation of state for all local packing fractions in the profile, and therefore, the equilibrium distribution of the sedimentation profiles becomes that of a purely Yukawa fluid.

The simulations in Fig. 7.5 were performed in the NVT ensemble. In all cases the different species have the same diameter σ, but different charge Z_i and gravitational length L_i as explained in the caption. In order to account for the fact that the system is inhomogeneous in the $z-$direction, we divided the vertical dimension H into N_H =200 bins, and the local density after each Monte Carlo move of each bin was calculated. For simplicity we considered a density independent, i.e., an altitude independent screening length of the Yukawa contribution whereas the dependence on z of the volume term, as determined by the local density, was preserved. The intermolecular potential was truncated at distance r_c =9σ. With this cutoff it is ensured that in all cases the intermolecular potential at $r = r_c$ is less than $10^{-4}k_BT$. The effect of gravity is included by adding a term of

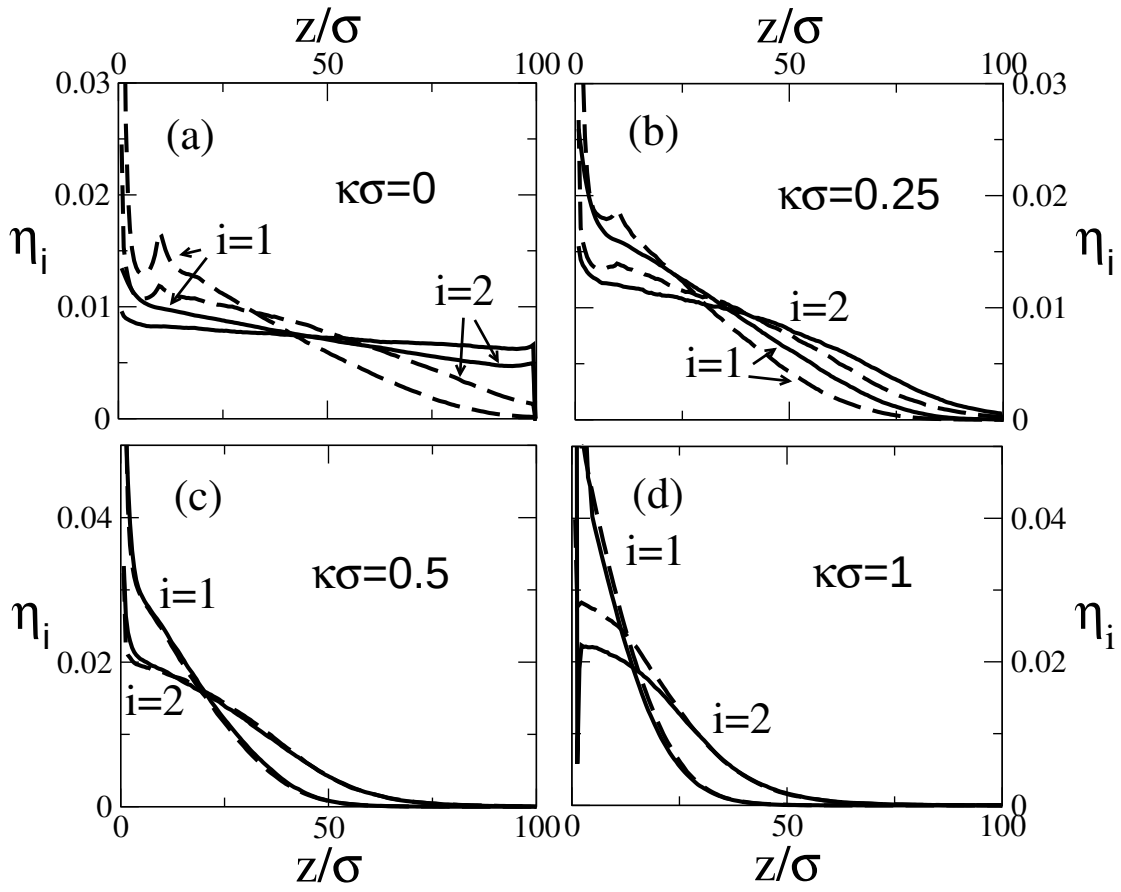

Figure 7.5: Sedimentation profiles $\eta_i(z)$ for binary mixtures for $Z_1 = 10$, $L_1 = 10\sigma$, $Z_2 = 20$, $L_2 = 1\sigma$, $\lambda_B = 0.004\sigma$ and $\overline{\eta}_1 = \overline{\eta}_2 = 0.0144$, for different values of the parameter $\kappa\sigma$ as indicated by the legends. Solids lines are simulations with EM model, dashed lines are simulations of the Yukawa model without many-body effects taken into account.

the form $\beta V_i = z/L_i$ in the interaction potential with $L_i = k_B T/m_i g$ the gravitational length, m the buoyant mass and g the gravitational acceleration. We used a total number of particles equal to 1860 for the binary mixtures in Fig. 7.5. A typical simulation consist on 10^6 MC cycles to equilibrate the system and $5 \cdot 10^5$ cycles to obtain the averages with a cycle consisting of N trials to move a randomly chosen particle.

In order to appreciate more clearly the dramatic effect of ionic strength in the averaged many-body effects included in $W_1(\rho_c)$, we plot in Fig. 7.6 the mean heights corresponding to several sedimentation profiles for a binary mixture at different ionic strengths as given by the parameter $\kappa\sigma$. In the same spirit of Ref. [90], where the so-called colloidal Brazil nut effect in binary mixtures was first reported, (see also Ref. [159]), we considered several colloidal charges as indicated by the legends. The solid lines represent MC simulations of the EM whereas the dashed lines were obtained by simulations considering only Yukawa interactions. It is clear from Fig. 7.6 that many-body effects in the mean heights of the sedimentation profiles diminish upon enhancing the ionic strength of the suspension. Notice that at ionic strengths such that $\kappa\sigma \gtrapprox 0.5$, the dashed and solid lines merge

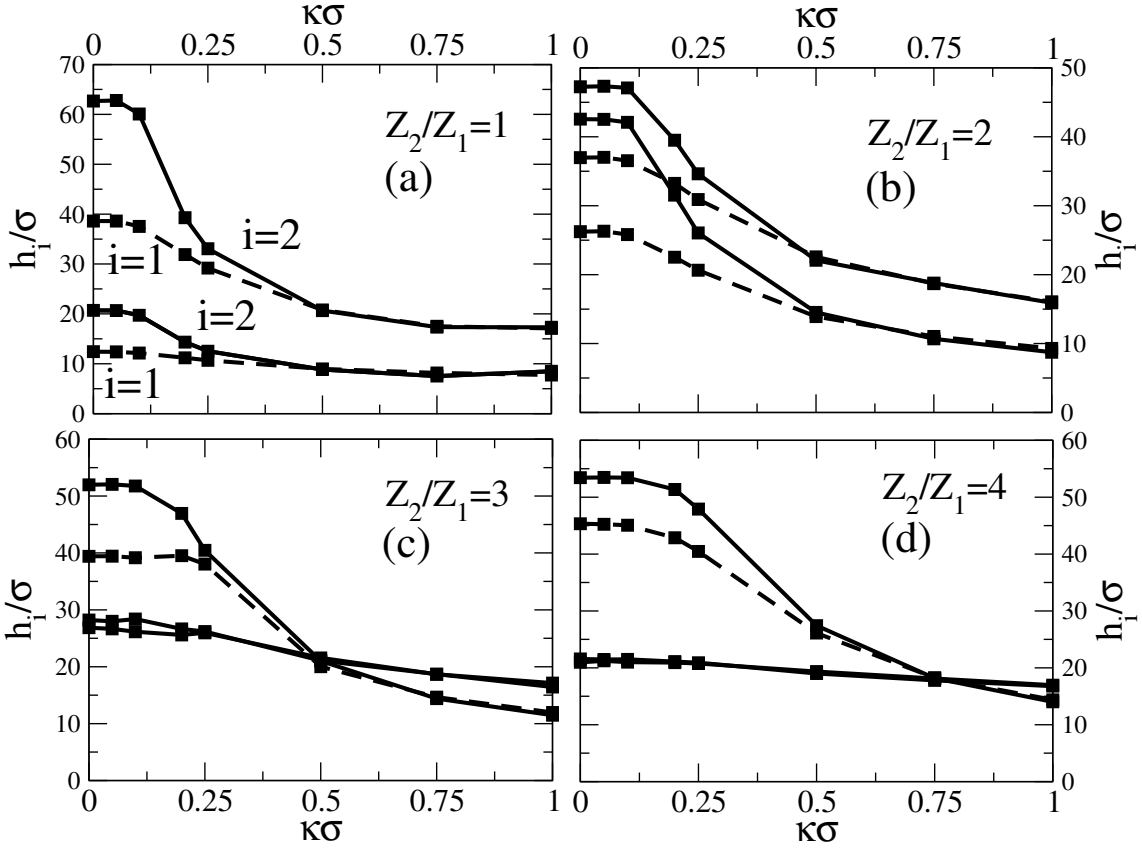

Figure 7.6: Mean heights (Eq. 7.4) for binary colloidal mixtures as a function of the screening parameter $\kappa\sigma$ for different values the ratio Z_2/Z_1 for the parameters $L_1 = 10\sigma$ and $L_2 = 5\sigma$, average packing fractions $\overline{\eta}_1 = \overline{\eta}_2 = 0.0144$ and Bjerrum length $\lambda_B = 0.004\sigma$. The solid lines interpolate points obtained by simulations of the EM including volume terms. The dashed lines interpolate points obtained by MC simulations of the Yukawa model.

into a single curve, i.e., the sedimentation profiles of a purely pairwise additive Yukawa system become indistinguishable from those of a many-body system as observed also in Fig. 7.5. Since the ionic strength of most colloidal suspensions is well above the approximate threshold $\kappa\sigma \approx 0.5$, it is expected that many-body effects contribute only with a marginal correction to the thermodynamic properties of most colloidal systems. This is certainly true at room temperature. In theory, it is possible to observe many-body effects by lowering the temperature even in non-deionized systems as explained in our discussion of Fig. 6.1, however, one has to go to extremely low temperatures at which any solvent at atmospheric pressure would freeze destroying the colloidal character of the system. These results constitute supporting evidence that statistical thermodynamic description of dilute colloidal suspensions based on the traditional pairwise additive DLVO-like models [65, 66] are accurate in majority of cases in spite of neglecting many-body effects, and that in they combination with proper charge renormalization schemes (see e.g. Refs. [76, 79, 80, 103]), constitute excellent models for the calculation of the thermodynamic

properties of most realistic colloidal suspensions.

7.4 Conclusions

We have explicitly shown that sedimentation-diffusion equilibrium and effective colloidal interactions in deionized suspensions cannot be described by the pairwise Yukawa model (YM) for the colloids, not even in the high-temperature limit of interest here. The effective model (EM) derived here, however, is in quantitative agreement with primitive model (PM) simulations. The main difference between the YM and the EM is the inclusion of ionic entropy and colloidal self-energy in the latter —these terms can be ignored at high salt concentrations but turn out to be crucial in deionized systems as we show here explicitly. The EM that we derived here is based on a linear screening theory, and should break down for $Z_i\lambda_B/a_i \gtrsim 5$ because then nonlinear screening effects such as charge renormalization become important [59, 171, 172]. Upon increasing the ionic strength or the temperature, many-body effects are attenuated. At ionic strengths typical of most colloidal suspensions and at room temperature, many-body effects only contribute with a marginal correction to the thermodynamic properties and can be neglected. This constitutes supporting evidence in favor of the adequacy of the traditional pairwise additive DLVO-like theories as valid statistical thermodynamical models of colloidal suspensions under common conditions. The parameters considered in this study are safely in the linear (high-temperature) regime since in all cases $\lambda_B/a_i < 0.01$ and $Z_i < 100$. Moreover, the EM simulations have great computational advantages over those of the PM, since they demand a simulation time of days rather than months.

References

[1] M. Baus and J.P. Hansen *Phys. Rep.* **59**, 1 (1980).

[2] D. C. Brydges and Ph. A. Martin, *J. Stat. Phys.* **96**, 1163 (1999).

[3] J. N. Israelachvili, *Intermolecular and Surface Forces: With Applications to Colloidal and Biological Systems*. Academic Press, (1985).

[4] E. J. W. Verwey and J. Th. G. Overbeek, *Theory of the stability of lyophobic colloids* Elsevier: Amsterdam, (1948).

[5] F. H. Stillinger and R. Lovett, *J. Chem. Phys.* **48**, 3858 (1968).

[6] F. H. Stillinger and R. Lovett, *J. Chem. Phys.* **49**, 1991 (1968).

[7] S. L. Carnie and G. M. Torrie, *Adv. Chem. Phys.* **56**, 141 (1987).

[8] J.-P. Hansen and H. Löwen, *Annu. Rev. Phys. Chem.* **51**, 209 (2000).

[9] E. H. Lieb and J. L. Lebowitz, *Adv. Math.* **9**, 316 (1972).

[10] J.-P. Hansen and I. R. McDonald, *Theory of Simple Liquids* B. Academic Press, London, (1986).

[11] J. P. Goedbloed and S. Poedts, *Principles of Magnetohydrodynamics* Cambridge University Press (2004).

[12] W. B. Russel, D. A. Saville and W. R. Schowalter, *Colloidal dispersions*. Cambridge University Press, (1989).

[13] J. L. Barrat and J.-P. Hansen, *Basic Concepts for Simple and Complex Fluids*. Cambridge University Press, (2003).

[14] P. Attard, *Adv. Chem. Phys.* **92**, 1 (1996).

[15] J.-P. Hansen and J.B. Hayter, *Molec. Phys.* **46**, 651 (1982).

[16] See, e.g., Prof. H. van Beijeren lecture notes on many-particle systems out of equilibrium to be found at http://www.phys.uu.nl/ vanbeije/script.pdf

[17] W. G. McMillan and J. E. Mayer, *J. Chem. Phys.* **13**, 276 (1945).

[18] C. Likos, *Phys. Rep.* **348**, 267 (2001).

[19] L. Belloni *J. Phys.: Condens. Matter* **12** R549 (2000).

[20] Y. Levin *Rep. Prog. Phys.* **65** 1577 (2002).

[21] L. Belloni, *Coll. Surf. A* **140**, 227 (1998).

[22] B. Beresford-Smith, D. Y. C. Chan and D. J. Mitchell, *J. Colloid Interface Sci.* **105**, 216 (1985).

[23] E. T. Whittaker and G. N. Watson, *A course of modern analysis*, Cambridge (1927).

[24] J. N. Israelachvili and G. Adams, *J. Chem. Soc. Faraday Trans. I.* **74**, 975 (1978).

[25] B. Derjaguin and L. Landau, *Acta Physicochim. URSS*. **14**, 633 (1941).

[26] G. Gouy, *J. Phys.* **9**, 457 (1910).

[27] D. L. Chapman, *Philos. Mag.* **25**, 475 (1913).

[28] S. Usui, *J. Coll. Int. Sci.* **44**, 107 (1973).

[29] J. Gragory, *J. Chem. Soc. Faraday II.* **69**, 1723(1973).

[30] S. Usui, *J. Coll. Int. Sci.* **51**, 44 (1975).

[31] S. L. Carnie and D. Y. C. Chan, *J. Coll. Int. Sci.* **161**, 260 (1993).

[32] E. S. Reiner and C. J. Radke, *J. Adv. Coll. Int. Sci.* **47**, 59 (1993).

[33] A. Hashidzume, A. Kawaguchi, A. Tagawa, A. Hyoda and K. T. Sato. *Macromolecules.* **39**, 1135 (2006).

[34] B. W. Ninham and V. A. Parsegian *J. Theor. Biol*. **31**, 405 (1971).

[35] J. Krozel and D. Saville, *J. Coll. Int. Sci.* **150**, 365 (1992).

[36] S. H. Behrens and M. Borkovec, *Phys. Rev. E.* **60**, 7040 (1999).

[37] V. A. Parsegian and D. Gingell *Biophys. J*. **12**, 1192 (1972).

[38] D. McCormack, S. L. Carnie and D. Y. C. Chan, *J. Colloid Interface Sci.* **169**, 177 (1995).

[39] D. Y. C. Chan, T. W. Healy, T. Supasiti and S. Usui. *J. Coll. Int. Sci.* **296**, 150 (2006).

[40] D. Ben-Yaakov, B. Yoram, D.S. Andelman and A. Safran, *Eurphys. Lett.* **79**, 48002 (2007).

[41] A. Bruce et al., *Molecular Biology of the Cell*, 4th edn, Taylor & Francis (2002).

[42] L. Koltover, T. Salditt, J. O. Rädler and C. R. Safinya *Science.* **281**, 78 (1998).

[43] K. Wagner, D. Harries, S. May, V. Kahl, J. O. Rädler, A. Ben-Shaul, *Langmuir.* **16**, 303 (2002).

[44] R. Bruinsma *Eur. Phys. J. B.* **10**, 175 (1999).

[45] D. Harries, R. Podgornik, V. A. Parsegian, E. Mar-Or and D. Andelman *J. Chem. Phys*. **124**, 124, 224702 (2006).

[46] E. Haleva, N. Ben-Tal, H. Diamant, *Biophys. J*. **86**, 2165 (2004).

[47] C. Russ, T. Heimburg and H. H. von Grünberg *Biophys. J*. **84**, 3730 (2003).

[48] A. Albersdörfer, T. Feder and E. Sackmann *Biophys. J.* **73**, 245 (1997).

[49] R. Bruinsma, A. Behrisch and E. Sackmann, *Phys. Rev. E.* **61**, 4253 (2000).

[50] G. Hed and S. A. Safran *Phys. Rev. Lett*. **93**, 138101 (2004).

[51] A. Torres, R. van Roij and G. Téllez, *J. Coll. Int. Sci.* **301**, 176 (2006).

[52] S. Ohki, *J. Coll. Int. Sci.* **37**, 318 (1971).

[53] A. Lau and P. Pincus, *Eur. Phys. J. B.* **10**, 175 (1999).

[54] S. Usui, *J. Coll. Int. Sci*. **97**, 247 (1984).

[55] M. N. Tamashiro and H. Schiessel, *Phys. Rev. E.* **68**, 066106 (2003).

[56] W. Huang and D. G. Levitt, *Biophys. J.* **17**, 111 (1977).

[57] F. M. van der Kooij and H. N. W. Lekkerkerker *J. Phys. Chem. B.* **102**, 7829 (1998).

[58] B. W. Ninham and V. A. Parsegian, *J. Theor. Biol.* **31**, 405 (1971).

[59] S. Alexander, P. M. Chaikin, P. Grant, G. Morales, P. Pincus, and D. Hone, *J. Chem. Phys.*, **80**, 5776 (1984).

[60] E. Trizac, L. Bocquet and M. Aubouy, *Phys. Rev. Lett.* **89**, 248301 (2002).

[61] L. Bocquet, E. Trizac and M. Aubouy, *J. Chem. Phys.* **117**, 8138 (2002).

[62] E. Trizac and Y. Levin, *Phys. Rev. E.*, **69**, 031403 (2004).

[63] I. S. Gradshteyn and I. M. Ryzhik, *Table of Integrals, Series, and Products* (Academic Press 1994).

[64] All the numerical resolutions (root finding and minimization) involving the Jacobian elliptic functions were performed using MATHEMATICA version 5.

[65] B. Derjaguin and L. Landau, *Acta Physicochim., URSS* **14**, 633 (1941).

[66] J. W. Verwey and J. T. G. Overbeek, *Theory of the Stability of Lyotropic Colloids* Elsevier, Amsterdam, (1948).

[67] R. van Roij and J.-P. Hansen, *Phys. Rev. Lett.* **79**, 3082 (1997).

[68] A. R. Denton, *J. Phys.: Condens. Matter.* **11**, 10061 (1999).

[69] R. van Roij, M. Dijkstra, and J. P. Hansen, *Physical Review E.* **59**, 2010 (1999).

[70] R. van Roij, M. Dijkstra and J.-P. Hansen, *Phys. Rev. E.* **59**, 2010 (1999).

[71] P. B. Warren, *J. Chem. Phys.* **112**, 4683 (2000).

[72] A. R. Denton, *Phys. Rev. E.* **67**, 011804 (2003).

[73] B. Zoetekouw and R. van Roij, *Phys. Rev. E.* **73**, 021403 (2006).

[74] D. Léger and D. Levesque, *J. Chem. Phys.* **123**, 124910 (2005).

[75] B. Zoetekouw and R. van Roij, *Phys. Rev. Lett.* **97**, 258302 (2006).

[76] S. Alexander, P. M. Chaikin, P. Grant, G. J. Morales, and P. Pincus, *J. Chem. Phys.* **80**, 5776 (1984).

[77] R. Kjellander and D.J. Mitchell *J. Chem. Phys.* **101**, 603 (1994).

[78] E. Trizac, L. Bocquet, M. Aubouy and H. H. von Grünberg, *Langmuir* **19**, 4027 (2003).

[79] E. Trizac, L. Bocquet, and M. Aubouy, *Phys. Rev. Lett.* **89**, 248301 (2002).

[80] M. Aubouy, E. Trizac, and L. Bocquet, *J. Phys. A: Math. Gen.* **36**, 5835 (2003).

[81] M. Quesada-Pérez, J. Callejas-Fernández and R. Hidalgo-Álvarez, *J. Coll. Interface Sci.* **206**, 354 (1998).

[82] P. Wette, H.J. Schöpe and T. *J. Chem. Phys.* **116**, 10981 (2002).

[83] A.-P. Hynninen and M. Dijkstra, *Phys. Rev. Lett.* **94**, 138303 (2005).

[84] A.-P. Hynninen, C.G. Christova, R. van Roij, A. van Blaaderen, and M. Dijkstra, *Phys. Rev. Lett.* **96**, 138308 (2006).

[85] J. Baumgartl, R.P.A. Dullens, M. Dijkstra, R. Roth, and C. Bechinger, *Phys. Rev. Lett.* **98**, 198303 (2007).

[86] M. Leunissen et. al., *Nature.* **437**, 235 (2005).

[87] J. Dzubiella et. al., *Phys, Rev. E.* **65**, 021402 (2002).

[88] M. Rex and H. Löwen, *Phys, Rev. E.* **75**, 051402 (2007).

[89] J. Zwanikken and R. van Roij, *Europhys. Lett.* **71**, 480 (2005).

[90] A. Esztermann and H. Löwen *Europhys. Lett.* **68**, 120 (2004).

[91] H. H. von Grünberg, R. van Roij, and G. Klein. *Europhys. Lett.* **55**, 580 (2001).

[92] L. Belloni, *J. Chem. Phys.* **123**, 204705 (2005).

[93] A. Torres, A. Cuetos, M. Dijkstra and R. van Roij, *Phys. Rev. E.* **75**, 041405 (2007).

[94] Y. Levin, M. C. Barbosa and M. N.Tamashiro, *Europhys. Lett.* **41**, 123 (1998).

[95] M. N. Tamashiro, Y. Levin and M. C. Barbosa, *Physica A.* **258**, 341 (1998).

[96] V. Lobaskin *et al.*, *Phys. Rev. Lett.* **98**, 176105, (2007).

[97] R. Piazza, T. Bellini and V. Degiorgio, *Phys. Rev. Lett.* **71**, 4267 (1993).

[98] C.P. Royall, R. van Roij and A. van Blaaderen, *J. Phys.: Cond. Matt.* **17**, 2315 (2005).

[99] A. Torres and R. van Roij, *Langmuir* **24**, 1110 (2008).

[100] M. Deserno and H. H. von Grünberg, *Phys. Rev. E.* **66**, 011401 (2002).

[101] T. Boublík, I. Nezbeda and K. Hlavatý, *Statistical thermodynamics of simple liquids and their mixtures*. Elsevier (1980).

[102] Y. Rosenfeld, *Phys. Rev. E.*, **54**, 2827 (1996).

[103] L. Belloni *Colloids Surfaces A.* **140**, 227 (1998).

[104] D. Leger and D. Levesque, *J. Chem. Phys.* **123**, 124910 (2005).

[105] M. Camargo and G. Téllez, *J. Chem. Phys.* **128**, 134907 (2008).

[106] A. Torres, A. Cuetos, M. Dijkstra and R. van Roij, *Phys. Rev. E.* **77**, 031402 (2008).

[107] C. Russ, M. Brunner, C. Bechinger, and H. H. von Grünberg, *Europhys. Lett.* **69**, 468 (2005).

[108] C. Russ, H. H. von Grünberg, M. Dijkstra, and R. van Roij, *Phys. Rev. E.* **66**, 011402 (2002).

[109] P. N. Pusey, W. van Megen, P. Bartlett, B. J. Ackerson, J. G. Rarity and S. M. Underwood, *Phys. Rev. Lett.* **63**, 2753 (1989).

[110] A.-P. Hynninen and M. Dijkstra, *J. Chem. Phys.* **123**, 244902 (2005).

[111] V. Reus, L. Belloni, T. Zemb, N. Lutterbach and H. Versmold, *Colloids Surf. A.* **151**, 449 (1999).

[112] L. Belloni, *J. Chem. Phys.* **123**, 204705 (2005).

[113] A. Torres, A. Cuetos, M. Dijkstra, and R. van Roij, *Phys. Rev. E.* **75**, 041405 (2007).

[114] K. Ito, H. Yoshida, and N. Ise, *Science.* **263**, 352 (1994).

[115] B. V. R. Tata, E. Yamahara, P. V. Rajamani, and N. Ise, *Phys. Rev. Lett.* **78**, 2660 (1997).

[116] N. Ise, T. Okubo, M. Sugimura, K. Ito, and H. Nolte, *J. Chem. Phys.* **78**, 536 (1983).

[117] A. E. Larsen and D. G. Grier, *Nature.* **385**, 230 (1997).

[118] B. V. R. Tata, M. Rajalakshmi, and A. K. Arora, *Phys. Rev. Lett.* **69**, 3778 (1992).

[119] T. Palberg and M.Wurth, *Phys. Rev. Lett.* **72**, 786 (1994).

[120] B. V. R. Tata and A. K. Arora, *Phys. Rev. Lett.* **72**, 787 (1994).

[121] P. Linse, *J. Chem. Phys.* **113**, 4359 (2000).

[122] Y. Rosenfeld, *Phys. Rev. E.* **54**, 2827 (1996).

[123] A. Cuetos, A.-P. Hynninen, J. Zwanikken, R. van Roij and M. Dijkstra. *Phys. Rev. E.* **73**, 061402 (2006).

[124] M.A. Rutgers, J.H. Dunsmuir, J.-Z. Xue, W.B. Russel and P.M. Chaikin. *Phys. Rev. B.*, **53**, 5043 (1996).

[125] A.P. Philipse and G.H. Koenderink. *Adv. Coll. Interface Sci.* **100-102**, 613 (2006).

[126] R. van Roij, *J. Phys.: Condens. Matter* **15**, S3569 (2003).

[127] L. Belloni, *J. Chem. Phys.* **123**, 204705 (2005).

[128] T. Biben, J.-P. Hansen and J.-L. Barrat, *J. Chem. Phys.* **98**, 7330 (1993).

[129] A.P. Philipse, *J. Phys.: Condens. Matter* **16**, S4051 (2004).

[130] M. Rasa, B.H. Erné, B. Zoetekouw, R. van Roij and A.P. Philipse. *J. Phys.: Condens. Matter* **17**, 2293 (2005).

[131] M. Rasa and A.P. Philipse *Nature.* **429**, 857 (2004).

[132] A.-P. Hynninen, R. van Roij and M. Dijkstra, *Europhys. Lett.* **65**, 719 (2004).

[133] T. Biben, J.-P. Hansen, *J. Phys. Condens. Matter* **6**, A345 (1994).

[134] C. Russ, H.H. von Grünberg, M. Dijkstra, and R. van Roij, *Phys. Rev. E.* **66**, 011402 (2002).

[135] G. Téllez, T. Biben, *Eur. Phys. J. E.* **2**, 137 (2000).

[136] G. Téllez, *J. Chem. Phys.* **106**, 8572 (1997).

[137] V. Lobaskin and K. Qamhieh, *J. Phys. Chem. B.* **107**, 8022 (2003).

[138] A.Z. Panagiotopoulos and S.K. Kumar, *Phys. Rev. Lett.* **83**, 2981 (1999).

[139] A. Cuetos, A.-P. Hynninen, J. Zwanikken, R. van Roij and M. Dijkstra, *Phys. Rev. E.* **73**, 061402 (2006).

[140] J.B. Hayter and J. Penfold, *Molec. Phys.* **42**, 109 (1981).

[141] E. Waisman, *Molec. Phys.* **25**, 45, (1973).

[142] H.L. Friedman and W. D. T. Dale, in *Modern Theoretical Chemistry 5.* (Plenum Press, 1977).

[143] R. van Roij, M. Dijkstra and J. P. Hansen, *Phys. Rev. E.* **59**, 2010 (1999).

[144] H. Löwen and G. Kramposthuber *Europhys. Lett.* **23**, 637 (1993).

[145] L. Belloni *J. Chem. Phys.* **85**, 519 (1986).

[146] P.M. Biesheuvel and J. Lyklema *J. Phys.: Condens. Matter* **17**, 6337 (2005).

[147] M. Dijkstra, J. Zwanikken and R. van Roij *J. Phys.: Condens. Matter* **18**, 825 (2006).

[148] A.E. Bailey *et al.*, *Phys. Rev. Lett.* **99**, 205701 (2007).

[149] R. Piazza *et al.*, *Phys. Rev. Lett.* **71**, 4267 (1993).

[150] M. Rutgers *et al.*, *Phys. Rev. B.* **53**, 5043 (1996).

[151] S. Buzzaccaro *et al.*, *Phys. Rev. Lett.* **99**, 098301 (2007).

[152] C.P. Royall *et al.*, *J. Phys.: Cond. Matt.* **17**, 2315 (2005).

[153] R. van Roij, *J. Phys.: Condens. Matt.* **15**, S3569 (2003).

[154] P.M. Biesheuvel, *J.Phys.: Condens. Matt.* **16**, L499 (2004).

[155] A.P. Hynninen *et al.*, *Europhys. Lett.* **65**, 719 (2004).

[156] A. Esztermann and H. Löwen, Europhys. Lett., **68**, 120 (2004).

[157] J. Zwanikken and R. van Roij, Europhys. Lett. **71**, 480 (2005).

[158] A. Cuetos *et al.*, *Phys. Rev. E.* **73**, 061402 (2006).

[159] M. Dijkstra, J. Zwanniken, and R. van Roij, *J. Phys.: Condens. Matter.*, **18**, 825 (2006).

[160] M. Dijkstra *et al. J. Phys.: Condens. Matter.* **18**, 825 (2006).
[161] C. Russ *et al.*, *Phys. Rev. E.* **66**, 011402 (2002).
[162] C. Russ *et al.*, *Europhys. Lett.* **69**, 468 (2005).
[163] A.P. Hynninen *et al.*, *J. Phys.: Condens. Matt.* **15**, S3549 (2003).
[164] A.P. Hynninen *et al.*, *Phys. Rev. E.* **69**, 061407 (2004).
[165] B. Beresford-Smith *et al.*, *J. Colloid Interface Sci.* **105**, 216 (1985).
[166] R. van Roij and J.-P. Hansen, *Phys. Rev. Lett.* **79**, 3082 (1997).
[167] P. B. Warren, *J. Chem. Phys.* **112**, 4683 (2000).
[168] T. Biben *et al.*, *J. Chem. Phys.* **98**, 7330 (1993).
[169] B. Zoetekouw *et al.*, *Phys. Rev. E.* **73**, 021403 (2006).
[170] T. Boublík *et al.*, *Statistical thermodynamics of simple liquids and their mixtures.* Elsevier (1980).
[171] E. Trizac *et al*, *Phys. Rev. Lett.* **89**, 248301 (2002).
[172] B. Zoetekouw *et al.*, *Phys. Rev. Lett.* **97**, 258302 (2006).